CARBORANE COMPOUNDS AS EFFICIENT LIGHT-DRIVEN IN OXIDATION CATALYSIS

Isabel Guerrero Troyano

Per citar o enllaçar aquest document:
Para citar o enlazar este documento:
Use this url to cite or link to this publication:
http://hdl.handle.net/10803/674733

http://creativecommons.org/licenses/by-nc-sa/4.0/deed.ca

Aquesta obra està subjecta a una llicència Creative Commons Reconeixement-NoComercial-CompartirIgual

Esta obra está bajo una licencia Creative Commons Reconocimiento-NoComercial-CompartirIgual

This work is licensed under a Creative Commons Attribution-NonCommercial-ShareAlike licence

Universitat de Girona

ICMAB
INSTITUT DE CIÈNCIA DE MATERIALS DE BARCELONA
EXCELENCIA SEVERO OCHOA
CSIC
CONSEJO SUPERIOR DE INVESTIGACIONES CIENTÍFICAS

Doctoral Thesis

Carborane compounds as efficient light-driven in oxidation catalysis

Isabel Guerrero Troyano

2022

Doctoral Thesis

Carborane compounds as efficient light-driven in oxidation catalysis

Isabel Guerrero Troyano

2022

Doctoral programme in Chemistry

Supervised by: Dra. M. Isabel Romero García

Prof. Francesc Teixidor i Bombardó

Tutor: Dra. M. Isabel Romero García

This manuscript has been presented to opt for the doctoral degree from the Universitat de Girona

Dra. M. Isabel Romero García, from the Universitat de Girona and Prof. Francesc Teixidor i Bombardó, from the Institut de Ciència de Materials de Barcelona,

WE DECLARE:

That the thesis *Carborane compounds as efficient light-driven in oxidation catalysis*, presented by Isabel Guerrero Troyano to obtain a doctoral degree, has been completed under our supervision.

For all intents and purposes, we hereby sign this document.

Dra. M. Isabel Romero García   Prof. Francesc Teixidor i Bombardó

Girona, 11th of January, 2022.

The work performed in the present thesis has been possible thanks to the funding of:

- Ministerio de Economía y Competitividad (MECO) through project: CTQ2015-66143-P
- Generalitat de Catalunya (AGAUR) through project: 2017-SGR-1720
- “Severo Ochoa” Program for Centers of Excellence in R&D 234 (SEV-2015-0496)
- Projecte de la Unió Europea H2020-LEIT-NMBP/0345, KARDIATOOL

  (Grant Nº -768686)

Agraïments

Per començar volia agrair als meus directors de tesi, Dra. Marisa Romero i Prof. Francesc Teixidor. Gràcies per donar-me l'oportunitat de gaudir d'aquesta experiència enriquidora, gaudint de la recerca en el món de la Química Inorgànica per fer el doctorat. Un camí que he emprès amb molta il·lusió. La confiança que heu dipositat en mi per portar a terme aquest projecte, ha sigut clau en el meu desenvolupament com a científica. Gràcies pel vostre esforç i dedicació, i per tot el que m'heu aportat durant tots aquests anys. Sembla ser ahir quan tu, Marisa, vas confiar en mi per conèixer més a fons la química inorgànica fent el TFG, experiència que em va fer descobrir la meva passió per la investigació científica.

A més vull expressar el meu agraïment a la Prof. Clara Viñas, per la seva valuosa ajuda constant i disponibilitat per tot el que he necessitat. La teva vocació científica ha sigut una inspiració per a mi.

També vull estendre la meva gratitud a la Dra. Rosario Núñez i el Dr. José Giner. Gràcies de tot cor Rosario per haver-me ajudat quan ho he necessitat, per haver-me escoltat i aconsellat en moments i situacions en què personalment he hagut de prendre decisions importants i a vegades complicades d'assumir.

Un agraïment molt especial i afectuós a la Dra. Montse Rodríguez. Mil gràcies per escoltar-me sempre. Espero poder gaudir sempre del teu consell en l'àmbit personal i científic.

També vull agrair al director de l'Institut de Ciència de Materials de Barcelona (ICMAB-CSIC) el Prof. Xavier Obradors per acollir-me al seu centre. A tot el personal d'administració i manteniment del centre per la seva professionalitat.

També vull agrair a tots els col·laboradors que han fet possible aquesta tesi. Al Servei de Ressonància Magnètica Nuclear de la UAB, i als Serveis Tècnics de

Recerca de la UdG: l’Anna Costa per les anàlisis elementals i els estudis basats en HPLC-MS, en Xavier Fontrodona per les estructures de raigs X, la Dra. Enriqueta Anticó per la seva ajuda amb l’ICP i el consells en cromatografia de gasos.

També vull agrair al Dr. Zsolt Kelemen per les seva important col·laboració i aportació en la realització dels càlculs TD-DFT, a l’Arpita Saha per la seva valuosa col·laboració i aportació en les nanopartícules magnètiques, a la Jewel Ann Maria Xavier per la seva eficient col·laboració en les nanopartícules magnètiques i la seva ajuda amb els estudis DLS portats a terme.

Durant més de quatre anys al grup de Inorganic Materials & Catalysis a l’ICMAB i al grup de Catàlisi i Sostenibilitat a la Universitat de Girona, he conegut a molt companys que m’han ensenyat molt amb les seves experiències científiques i la seva ajuda incondicional al laboratori. Als companys amb els quals vaig començar: Esther, Begoña, Isa, Flavia, Arpita, Abishek, Inés i Mahdi, i els que van arribar després: Lei, Joan, Miquel, Sohini, Zheng, M. José i especialment a Zsolt, Arpita i Jewel per les seves imprescindibles col·laboracions als articles als quals vam treballar.

I el més important de tot, no puc acabar sense agrair amb tot el meu amor al meu home, Pedro, que ha confiat sempre en mi i en el meu treball. Gràcies per fer possible tot el que somiat, has estat clau en aquesta aventura i m’has ajudat molt a construir aquest futur. A les meves filles, Marina i Daniela, per la seva paciència i el seu amor dia a dia i als meus pares que sempre vam pensar que jo ho aconseguiria.

A tots vosaltres mil gràcies de tot cor!

Al meu home Pedro i les meves
filles Marina i Daniela

List of publications

Publications related to the thesis content:

- *Metallacarboranes as photoredox catalyst in water.*

Isabel Guerrero, Zsolt Kelemen, Clara Viñas, Isabel Romero and Francesc Teixidor. *Chem. Eur. J.* **2020**, *26*, 5027-5036.

DOI: 10.1002/chem.201905395

- *Noncovalently Linked Metallacarboranes on Functionalized Magnetic Nanoparticles as Highly Efficient, Robust, and Reusable Photocatalysts in Aqueous Medium.*

Isabel Guerrero, Arpita Saha, Jewel Xavier, Clara Viñas, Isabel Romero and Francesc Teixidor. *ACS Applied Materials & Interfaces*. **2020**, *12* (50), 56372-56384.

DOI: 10.1021/acsami.0c17847

- *Aqueous Persistent Noncovalent Ion-Pair Cooperative Coupling in a Ruthenium Cobaltabis(dicarbollide) System as a Highly Efficient Photoredox Oxidation Catalyst.*

Isabel Guerrero, Clara Viñas, Xavier Fontrodona, Isabel Romero and Francesc Teixidor. *Inorg. Chem*. **2021**, *60*, 8898−8907.

DOI: 10.1021/acs.inorgchem.1c00751

- *A Stand-Alone Boron-Based Photoredox Catalyst Epoxidates Alkenes in Water at Extremely Low Catalyst Load.*

Isabel Guerrero, Clara Viñas, Isabel Romero and Francesc Teixidor. *Green Chem.* **2021,** *23*, 10123–10131.

DOI: 10.1039/D1GC03119H.

- *Ferrabis(dicarbollide), an Abundant Metal Photoredox Oxidation Catalyst in water.*

Isabel Guerrero, Clara Viñas, Isabel Romero and Francesc Teixidor. Submitted to ChemComm. **2021**.

Abbreviations

3c-2e	three centres-two electrons
Abs	absorbance
Anal. Found (Calc.)	analysis found (analysis calculated)
APMS	3-(2-aminoethylamino)propylmethyldimethoxy silane
APTES	(3-aminopropyl) triethoxy silane
APTMS	(3-aminopropyl) trimethoxy silane
Ar-	aromatic group
BNCT	boron neutron capture therapy
bpy	2,2’-bipyridine
cat	catalyst
cat*	excited state of the catalyst
Cc-M	carbon cluster metal
conv.	conversion
COSY	correlation spectroscopy
Cp	carboranyl ligand
CTAC	cetyl trimethyl ammonium chloride
CV	cyclic voltammetry
d	doublet
ddd	doublet of doublet of doublets
DLS	dynamic light scattering
DPV	differential pulse voltammetry
E	potential
e^-	electron
E^+	electrophile
$E_{1/2}$	half wave potential

EDX	energy-dispersive X-ray spectroscopy
EELS	electron energy loss spectroscopy
E_{pa}	anodic peak potential
E_{pc}	cathodic peak potential
ESI-MS	electrospray ionization mass spectrometry
ET	electron transfer
ε	extinction coefficient
Fc	ferrocene
FID	flame ionization detector
FT-IR	fourier transform infrared
GC	gas chromatography
HAT	hydrogen atom transfer
HDF	hydrodefluorination
HOMO	highest occupied molecular orbital
HPLC-MS	high-performance liquid chromatography-mass spectrometry
HRSEM	high-resolution scanning electron microscopy
HRTEM	high-resolution transmission electron microscopy
h*v*	light
J	coupling constant
LMCT	ligand to metal charge transfer
LUMO	lowest unoccupied molecular orbital
m	multiplet
m-	*meta-*
m/z	mass-to-charge ratio
MALDI-TOF	matrix assisted laser desorption/ionization-time of flight
MLCT	metal to ligand charge transfer

MNP	magnetic nanoparticles
MO	molecular orbital
MOFs	metal-organic frameworks
Ms	magnetic saturation
MSNP	magnetic silica nanoparticles
NEt_3	triethylamine
NHE	normal hydrogen electrode
nm	nanometer
NMR	nuclear magnetic ressonance
NTOs	natural transition orbitals
Nu^-	nucleophile
o-	*ortho-*
OAc	acetoxy group
ox.	oxidant
p-	*para-*
PCET	proton-coupled electron transfer
Ph-	phenyl group
PPh_3	triphenylphosphine
ppm	parts per million
py	pyridine
red.	reductant
RT	room temperature
s	singlet
SCE	saturated calomel electrode
select.	selectivity
SEM	scanning electron microscopy
SET	single-electron transfer

SPIONs	super paramagnetic iron oxide nanoparticles
STEM	scanning transmission microscopy
sub.	substrate
t	triplet
T	temperature
TBAH	tetra(n-butyl)ammonium hexafluorophosphate
TD-DFT	time-dependent density-functional theory
TEM	transmission electron microscopy
THF	tetrahydrofuran
TMAH	tetramethylammonium hydroxide
TMS	tetramethylsilane
TON	turnover number
trpy	2,2’:6’,2”-terpyridine
UV-*vis*	ultraviolet-visible spectroscopy
V	volt
vs	versus
X	halogen
X_{M}	metal electronegativity
XRD	X-Ray Diffraction
ʎ	wavelength
δ	chemical shift
ζ-potential	zeta-potential
v	frequency

Table of Contents

List of Figures XI

List of Tables XIX

List of Schemes XXI

Chapter I. Introduction 1

I.1. Introduction of elemental boron and boranes 3

I.2. Generalities of Boron clusters 3

I.2.1. Boranes 4

I.2.2. Carboranes. 4

I.2.3. Metallacarboranes 7

I.2.3.1 Physicochemical properties of metallacarboranes 9

I.3. Ruthenium complexes 12

I.3.1. Ruthenium polypyridyl aqua complexes 13

I.4. Homogeneous and heterogeneous catalysis. Supported Catalysts 15

I.4.1. Different immobilization strategies and supports 17

I.5. Catalytic oxidation reactions 19

I.5.1. Alcohol oxidation reactions 20

I.5.2. Epoxidation of alkenes 22

I.6. Catalysis and sustainability. 23

I.7. Principles of Photoredox catalysis 24

I.7.1. Mechanisms of photocatalysis 25

I.7.2. Different photocatalytic approaches 28

Chapter II. Objectives 47

Chapter III. Experimental section 53

III.1. Materials. 55

III.2. Preparations 55

III.2.1. Synthesis of metallacarborane compounds 55

III.2.2. Synthesis of ruthenium compounds 55

III.2.3. Preparations of heterogeneous systems 57

III.3. UV-visible studies from COSAN functionalized silica, Fe_3O_4 @SiO_2-NH_2 -H [COSAN], (MSNP-NH_2@**H**[**1**]) 58

III.4. Colloidal stability studies from Fe_3O_4 @SiO_2-NH_2 59

III.5. Computacional details from calculations 59

III.6. Crystallographic Data Collection and Structure.. 60

III.7. Photocatalytic oxidation studies 60

III.7.1. Photocatalytic oxidation of alcohols.. 60

III.7.1.1. Homogeneous phase... 60

III.7.1.2. Heterogenous phase 61

III.7.2. Photocatalytic oxidation of alkenes 62

III. 8. Additional Instrumentation and mesurements 63

Chapter IV. Results and discussion 67

IV.1. Metallacarboranes as Photoredox Catalysts in Water 69

IV.1.1. General strategy 70

IV.1.2. Computational study 72

IV.1.3. Photocatalytic oxidation of alcohols 76

IV.1.3.1. Photocatalytic oxidation of alcohols under common conditions 76

IV.1.3.2. Photocatalytic oxidation of alcohols under uncommon conditions... .86

IV.2. Non-covalently Linked Metallacarboranes on Functionalized Magnetic Nanoparticles as Highly Efficient, Robust and Reusable Photocatalysts in Aqueous Medium 89

IV.2.1. Catalyst Preparation, Structural and Spectroscopic Characterization. 90

IV.2.2. Photocatalytic Alcohol Oxidation 95

IV.3. Aqueous Persistent Noncovalent Ion-Pair Cooperative Coupling in a Ruthenium Cobaltabisorthodicarbollide System as a Highly Efficient Photoredox Oxidation Catalyst 105

IV.3.1. Synthetic Strategy, Structure, and Redox Characterization 106

IV.3.2. Photocatalytic Oxidation 117

IV.4. A Stand-Alone Cobaltabis (dicarbollide) Photoredox Catalyst Epoxidates Alkenes in Water at Extremely Low Catalyst Load 123

IV.4.1. Photocatalytic alkene oxidations 124

IV.4.2. Photocatalytic oxidations using catalyst load of 0.1 mol % 128

IV.4.3. Photocatalytic oxidations under lower catalyst load 131

IV.5. Ferrabis(dicarbollide), an Abundant Metal Photoredox Oxidation Catalyst in water 135

IV.5.1. Ferrabisorthodicarbollide: general properties 136

IV.5.2. Photocatalytic oxidation of alcohols 138

IV.5.3. Comparative overview of **Na[2]** vs **Na[1]** as photoredox catalysts in the oxidation of alcohols. 143

IV.5.4. Photocatalytic alkene oxidation 144

IV.5.4.1. Photocatalytic oxidations reducing catalyst loads. 150

IV.5.5. Comparative overview of photocatalytic oxidation of alkenes .**Na[2]** *vs* **Na[1]** 150

Chapter V. Conclusions 157

Chapter VI. References 165

ANNEX. Supporting Information 187

List of Figures

Figure I.1. The structural relationship between *closo*, *nido* and *arachno* polyhedral noted by Williams which were the motivation to develop the Wade's rules 5

Figure I.2. a) Structure of 1,2-$C_2B_{10}H_{12}$. (C in grey, B in pink and H in white). b) the dicarba-*closo*-dodecaborane with the numbering of the vertices. The nomenclature *o*-, *m*- and *p*- is referred to the relative position of the carbons 6

Figure I.3. Reactivity of the different vertices in the *o*-carborane 7

Figure I.4. Schematic representation of the synthesis from COSANE (M=Co) and FESANE (M=Fe). …………………. 8

Figure I.5. CV of **COSANE** (blue), **Cl_2-COSANE** (clear green) and **Cl_6-COSANE** (dark red) in CH_3CN+ 0.1M TBAH. All potentials *vs* Ferrocene .... ………………....11

Figure I.6. Comparison cyclic voltammetries of **COSANE** (orange) and **FESANE** (purple) in CH_3CN+ 0.1M TBAH. All potentials *vs* Ferrocene 12

Figure I.7. Schematic representation of different strategies for catalyst immobilization: a) adsorption, b) electrostatic immobilization, c) encapsulation, d) ionic liquid, and e) covalent binding. 17

Figure I.8. a) Magnetic nanoparticle. b) silica-coated magnetic nanoparticle 19

Figure I.9. Mechanism of oxidation of primary alcohols to carboxylic acids via aldehydes and aldehyde hydrates. [O]=oxidant reagent 20

Figure I.10. Epoxidation of alkene substrate and possible further transformations 22

Figure I.11. Photoinduced electron transfer (PET) 27

Figure I.12. Chemical structures of some polypyridyl complexes as photoredox catalyst 29

Figure I.13. Ruthenium polypyridyl complex: simplified molecular orbital depiction of $Ru(bpy)_3^{2+}$ photochemistry 30

Figure I.14. a) Electronic absorption spectrum of $[Ru(bpy)_3]^{2+}$ in acetonitrile solution at room temperature. The inset shows an expanded view of the metal-to-ligand charge transfer band. b) Representation of a MLCT state in $[Ru(bpy)_3]^{2+}$ 31

Figure I.15. a) Schematic general approach to improve productivity in visible-light photochemical reactions: adsorption of cationic photocatalyst on an oxide. This approach is applied to the synthesis of two commercially important terpenes: artemisinin (1) and rose oxide (2)...34

Figure I.16. a) Anionic structure of decatungstate POMs. b) Decatungstate Photocatalysis for oxidation of aliphatic alcohols, alkanes, and aromatic alcohols under aerobic conditions 35

Figure I.17. C-C bond cleavage reaction in different large alcohols using the catalyst depicted as 2e (on the right)...38

Figure II.1. Compounds used in this work 51

Figure IV.1. Metallacarboranes used in this work: $[3,3'-Co(1,2-C_2B_9H_{11})_2]^-$ (**$[1]^-$,** only the *trans* rotamer is shown) and its dichloro and hexachloro derivatives $[3,3'-Co(8-Cl-1,2-C_2B_9H_{10})_2]^-$ and $[3,3'-Co(8,9,12-Cl_3-1,2-C_2B_9H_8)_2]^-$, respectively. The green circles represent BCl units and the pink circles BH units 70

Figure IV.2. a) UV-Vis spectra of **Na[1]** in phosphate buffer solution, $1.3x10^{-4}M$ at pH 7.2. Inset: Magnification of the visible region of **Na[1]** in phosphate buffer solution, $2x10^{-3}M$ at pH 7.2. b) UV-visible spectra of carborane $Na[3,3'-Co(1,2-C_2B_9H_{11})_2]$ (black), $Na[3,3'-Co(8-Cl-1,2-C_2B_9H_{10})_2]$ (red) and $Na[3,3'-Co(8,9,12-Cl_3-1,2-C_2B_9H_8)_2]$ (blue) in acetonitrile solution, $1.3\ x10^{-4}$ M 71

Figure IV.3. Different rotamers of $[3,3'-Co(1,2-C_2B_9H_{11})_2]^-$ (**$[1]^-$**) 72

Figure IV.4. Charge-density difference map of the transition at 293 nm in case of the transoid structure. (The blue and red parts correspond to the regions in which electron density is increased and decreased after electron excitation, respectively). Isosurface value: 0.003......74

Figure IV.5. Representative ^1H NMR spectra of the reaction mixtures of the substrate (1-phenylethanol) and the corresponding oxidation product (acetophenone), dissolved in $CDCl_3$ at room temperature. i) 3h after irradiation, ii) 6h after irradiation, iii) 8h after irradiation after pH neutralization. The ^1H NMR spectra of 1-phenylethanol and acetophenone are included as control at the bottom and the top, respectively...76

Figure IV.6. Plot of yield as a function of time for the photoredox catalysis of 1-phenylethanol. Conditions: $Na[3,3'-Co(1,2-C_2B_9H_{11})_2]$ (0.08 mM), substrate (20 mM), $Na_2S_2O_8$ (40 mM), 5 ml 0.1M phosphate buffer solution at pH=7.2, light irradiation (2.2 W, λ ~253.7 nm) 78

Figure IV.7. Experimental MALDI mass spectrum of **Na[1]** a) before and b) after the photocatalytic oxidation of 1-phenylethanol. In b) The peak at m/z 324 corresponds to $[3,3'-Co(1,2-C_2B_9H_{11})_2]^-$, and that on the right to $[3,3'-Co(1,2-C_2B_9H_{11})(1,2-C_2B_9H_{11}O)]^-$. Simulated spectra for a) $[3,3'-Co(1,2-C_2B_9H_{11})_2]^-$ = 324.28 (m/z) and b) $[3,3'Co(1,2-C_2B_9H_{11})(1,2-C_2B_9H_{11}O)]^-$ = 340.28 (m/z)... 80

Figure IV.8. Suggested mechanism for the alcohol oxidation with **Na[1]** upon UV light irradiation 81

Figure IV.9. CV of **Na[1]** (blue), **$Na[Cl_2-1]$** (green) and **$Na[Cl_6-1]$** (brown) in CH_3CN+ 0.1M TBAH. All potentials *vs* Ferrocene 82

Figure IV.10. a) UV-vis spectra corresponding to the interaction of $MSNP-NH_2$ with 1 mM of **H[1]** in water. The inset photo shows the solution measured and the magnetic nanoparticles extracted using an external magnet at the bottom; b) Evolution of absorbance of a solution of 1 mM of **H[1]** in water with the addition of different amounts of $MSNP-NH_2$.............................92

Figure IV.11. UV-vis spectra at different time of extraction of the MNP. It shows that 10 minutes is sufficient for the extraction of all the MNP by an external magnet 93

Figure IV.12. IR spectra of $MSNP-NH_2$ (red) and $MSNP-NH_2$@H**[1]** (blue)..........................94

Figure IV.13. Plot of yield as a function of time for the photoredox catalysis of 1-phenylethanol using $MSNP-NH_2$@**H[1]** as catalyst. The blue curve shows the dependence of substrate yield with the reaction time in presence of $MSNP-NH_2$@**H[1]** catalyst. The red curve shows the dependence of substrate yield with the reaction time after the catalyst was removed at 4h. Conditions: $MSNP-NH_2$@**H**[**1**] (0,1µmol), substrate (0,1 mmol), $Na_2S_2O_8$ (0,2 mmol), 5 mL potassium carbonate solution at pH=7 ;light irradiation using a lamp with λ =300 nm. Sonication after 4 hours. 96

Figure IV.14. UV-vis spectra corresponding to a solution of 0.02 mM of **$[1]^-$** in 5 ml of water (yellow line). UV-visible spectra of the solutions after the oxidation of 1-phenylethanol by MSNP-NH_2@**H[1]** catalyst, throughout the different reuses 97

Figure IV.15. Plot of yield as a function of time for the photoredox catalysis of 1-phenylethanol using MNSP-NH_2@**H[1]** as the catalyst in the presence of 0,4 mM of cetyl trimethyl ammonium chloride (CTAC) as a surfactant. The blue curve shows the dependence of substrate yield on the reaction time after the catalyst was removed at 4h. Conditions: MNSP-NH_2@**H[1]** (0,1μmol), substrate (0,1 mmol), $Na_2S_2O_8$ (0,2 mmol), CTAC (2 μmol), potassium carbonate solution (5 mL) at pH=7; light irradiation using a lamp with λ =300 nm. 99

Figure IV.16. Yield values obtained throughout a number of successive reuses of catalyst MSNP-NH2@**H[1]** in the photooxidation of (a) diphenylmethanol (light purple) and 1-phenylethanol (dark purple); (b) cyclohexanol. Conditions: MNSP-NH_2@**H[1]** (0,1μmol), substrate (0,1 mmol), $Na_2S_2O_8$ (0,2 mmol), CTAC (2 μmol), potassium carbonate solution (5mL) at pH=7; light irradiation using a lamp with λ =300 nm, 4 h per run. 103

Figure IV.17. Crystal structure of complex **C5** 107

Figure IV.18. Packing displayed by **C5** 108

Figure IV.19. IR spectrum of **C4** 109

Figure IV.20. a) ^{1}H-NMR; b) ^{1}H{^{11}B}-NMR; c) ^{11}B{^{1}H}-NMR spectra of cobaltabis(dicarbollide) **C4** compound in acetone-d^6 111

Figure IV.21. a) UV-vis spectra of complex **C2’** (black line) and **C4** (dash dotted line) in phosphate buffer at 7.02 pH. b) UV-vis spectra of complex **C4** in CH_2Cl_2 (dotted line), phosphate buffer at 7.02 pH (dash-dotted line), and CH_3CN (solid line) 112

Figure IV.22. CV of **C4** in CH_2Cl_2 + 0.1 M TBAH *vs* Ag/AgCl 113

Figure IV.23. CV for complexes **C4** (red line) and **Na[1]** (blue line) registered in a phosphate buffer (pH= 7.12) *vs* Ag/AgCl. The right red and blue inserts show dI/dE to better appreciate the position of the couple Co^{IV}/Co^{III}. Further proof of this will be shown later when dealing with the **C4** precedents that we will henceforth call the **C4** history 114

Figure IV.24. a) DPV for complex **C4** registered in a phosphate buffer (pH= 7.12) *vs* Ag/AgCl. b) CV for complex **C4** registered in a phosphate buffer (pH= 7.12) *vs* Ag/AgCl 115

Figure IV.25. Proposed mechanism for alcohol photooxidation using **C4** 120

Figure IV.26. Plot of conversion as a function of time for the photoredox catalysis of styrene. Conditions: Na[3,3’-Co(1,2-$C_2B_9H_{11})_2$] (0.02 mM), styrene (20 mM), $Na_2S_2O_8$ (26 mM), 5 ml K_2CO_3 solution at pH=7, light irradiation (2.2 W, λ ~300 nm) 125

Figure IV.27. a) Plot of yield as a function of time and b) plot of the molar fractions (X_M) versus a time for the photoredox catalysis of styrene. Blue: styrene oxide; red: 1-phenyl-1,2-ethanediol; green: benzaldehyde; brown: benzoic acid; orange: styrene. Conditions: Na[3,3’-Co(1,2-$C_2B_9H_{11})_2$] (0.02 mM), styrene (20 mM), $Na_2S_2O_8$ (26 mM), 5 ml K_2CO_3 solution at pH=7, light irradiation (2.2 W, λ ~300 nm) 125

Figure IV.28. Plot of TON of styrene oxide as a function of pH. Conditions: Na[3,3’-Co(1,2-$C_2B_9H_{11})_2$] (0.02 mM), styrene (20 mM), $Na_2S_2O_8$ (26 mM), 5 ml of water, light irradiation (2.2 W, λ ~300 nm). TON = (mol of product)/(mol of catalyst) 126

Figure IV.29. Proposed mechanism for the alkene epoxidation in water, with **Na[1]** as photoredox catalyst upon UV light irradiation 130

Figure IV.30. Metallacarborane used in this work: $[3,3'\text{-Fe}(1,2\text{-}C_2B_9H_{11})_2]^-$ ($[2]^-$, only the *trans* rotamer is shown). The grey circles represent Cc-H units and the pink circles B-H units 136

Figure IV.31. Cyclic voltammetries of **Na[1]** (orange) and **Na[2]** (purple) in CH_3CN+ 0.1M TBAH. All potentials *vs* Ferrocene 137

Figure IV.32. a) UV-Vis spectrum of $Na[3,3'\text{-Fe}(1,2\text{-}C_2B_9H_{11})_2]$ **Na[2]** in acetonitrile (purple line) and in water (dashed line), $8.0\text{x}10^{-5}$ M. b) UV-visible spectra of $Na[3,3'\text{-Co}(1,2\text{-}C_2B_9H_{11})_2]$ **Na[1]** in acetonitrile (orange line) and in water (dashed line), $8.0\ \text{x}10^{-5}$ M 139

Figure IV.33. Experimental MALDI mass spectrum of **Na[2]**, a) before of photocatalytic oxidation of 1-phenylethanol The peak at m/z 321 corresponds to $[3,3'\text{-Fe}(1,2\text{-}C_2B_9H_{11})_2]^-$. b) Experimental MALDI mass spectrum after of photocatalytic oxidation of 1-phenylethanol. The peaks correspond to $[3,3'\text{-Fe}(1,2\text{-}C_2B_9H_{11})_2]^-$ $[1]^-$ and that on the to $[3,3'\text{-Fe}(1,2\text{-}C_2B_9H_{11})(1,2\text{-}C_2B_9H_{11}O)]^-$ $[2\text{-O}]^-$ = 336 (m/z), to $[3,3'\text{-Fe}(1,2\text{-}C_2B_9H_{11})(1,2\text{-}C_2B_9H_{11}O_2)]^-$ $[2\text{-}O_2]^-$=353 (m/z), $[3,3'\text{-Fe}(1,2\text{-}C_2B_9H_{11})(1,2\text{-}C_2B_9H_{11}O_4)]^-$ $[2\text{-}O_4]^-$=383 (m/z), $[3,3'\text{-Fe}(1,2\text{-}C_2B_9H_{11})(1,2\text{-}C_2B_9H_{11}O_6)]^-$ $[2\text{-}O_6]^-$=417 (m/z), $[3,3'\text{-Fe}(1,2\text{-}C_2B_9H_{11})(1,2\text{-}C_2B_9H_{11}O_7)]^-$ $[2\text{-}O_7]^-$=438 (m/z), $[3,3'\text{-Fe}(1,2\text{-}C_2B_9H_{11})(1,2\text{-}C_2B_9H_{11}O_8)]^-$ $[2\text{-}O_8]^-$=454 (m/z) 143

Figure IV.34. Plot of conversion as a function of time for the photoredox catalysis of styrene. Conditions: $Na[3,3'\text{-Fe}(1,2\text{-}C_2B_9H_{11})_2]$ (0.02 mM), styrene (20 mM), $Na_2S_2O_8$ (26 mM), 5 ml K_2CO_3 solution at pH=7, light irradiation (2.2 W, λ ~300 nm) 145

Figure IV.35. Plot of a) yield and b) molar fractions (Xi) *vs* time for the photoredox catalysis of styrene. Dark green line: styrene, line: styrene oxide, dashed line: 1-phenyl-1,2-ethanediol. Dash dotted line: benzaldehyde. Dotted line: benzoic acid. Conditions: $Na[3,3'\text{-Fe}(1,2\text{-}C_2B_9H_{11})_2]$ (0.02 mM), styrene (20 mM), $Na_2S_2O_8$ (26 mM), 5 ml K_2CO_3 solution at pH=7, light irradiation (2.2 W, λ ~300 nm) 148

Figure IV.36. a) Plot of yield in styrene oxide and 1-phenylethanediol as a function of time for the photoredox catalysis of styrene. Line: styrene oxide, dashed line: 1-phenyl-1,2-ethanediol. b) Plot of yield in benzaldehyde and benzoic acid as a function of time for the photoredox catalysis of styrene. Dash dotted line: benzaldehyde; dotted line: benzoic acid. Conditions: $Na[3,3'\text{-Fe}(1,2\text{-}C_2B_9H_{11})_2]$ (purple) or $Na[3,3'\text{-Co}(1,2\text{-}C_2B_9H_{11})_2]$ (orange)(0.02 mM), styrene (20 mM), $Na_2S_2O_8$ (26 mM), 5 ml K_2CO_3 solution at pH=7, light irradiation (2.2 W, λ ~ 300 nm) 152

Figure IV.37. Plot of the molar fraction (Xi) versus time for the photoredox catalysis of styrene. a) Using **Na[1]** as catalyst. Vermilion line: styrene, orange line: styrene oxide, dashed line: 1-phenyl-1,2-ethanediol, dash dotted line: benzaldehyde, dotted line: benzoic acid. b) Using **Na[2]** as catalyst. dark green line: styrene, purple line: styrene oxide, dashed line: 1-phenyl-1,2-ethanediol, dash dotted line: benzaldehyde, dotted line: benzoic acid. Conditions: $Na[3,3'\text{-Fe}(1,2\text{-}C_2B_9H_{11})_2]$ (purple) or $Na[3,3'\text{-Co}(1,2\text{-}C_2B_9H_{11})_2]$ (orange)(0.02 mM), styrene (20 mM), $Na_2S_2O_8$ (26 mM), 5 ml K_2CO_3 solution at pH=7, light irradiation (2.2 W, λ ~300 nm) 153

Figure SIV.1. Selected Kohn-Sahm orbitals of the different rotamers of $\mathbf{1}^-$ anion 189

Figure SIV.2. a) Representative ^{1}H NMR spectrum ($CDCl_3$) of the product benzaldehyde and the substrate benzyl alcohol, using $Na[3,3'\text{-Co}(1,2\text{-}C_2B_9H_{11})_2]$ as catalyst in the photooxidation reaction after 8 hours. Conditions: catalyst (0.08 mM), substrate (20 mM), $Na_2S_2O_8$ (40 mM) 5 ml 0.1M phosphate buffer solution at pH=7.2 light at 8 h of irradiation. b) ^{1}H NMR spectrum of pure commercial benzyl alcohol. c) ^{1}H NMR spectrum of pure commercial benzaldehyde 199

Figure SIV.3. a) Representative ^{1}H NMR spectrum ($CDCl_3$) of the product 4-methylbenzaldehyde and the substrate 4-methylbenzyl alcohol, using $Na[3,3'\text{-Co}(1,2\text{-}C_2B_9H_{11})_2]$ as catalyst in the photooxidation reaction after 8 hours. Conditions: catalyst (0.08

mM), substrate (20 mM), $Na_2S_2O_8$ (40 mM) 5 ml 0.1M phosphate buffer solution at pH=7.2 light at 8 h of irradiation. b) ^{1}H NMR spectrum of pure commercial 4-methylbenzyl alcohol. c) ^{1}H NMR spectrum of pure commercial 4-methylbenzaldehyde 201

Figure SIV.4. a) Representative ^{1}H NMR spectrum ($CDCl_3$) of 4-chlorobenzaldehyde and the substrate 4-chlorobenzyl alcohol, using Na[3,3'-Co(1,2-$C_2B_9H_{11}$)$_2$] as catalyst in the photooxidation reaction after 8 hours. Conditions: catalyst (0.08 mM), substrate (20 mM), $Na_2S_2O_8$ (40 mM) 5 ml 0.1M phosphate buffer solution at pH=7.2 light at 8 h of irradiation. b) ^{1}H NMR spectrum of pure commercial 4-chlorobenzyl alcohol. c) ^{1}H NMR spectrum of pure commercial 4-chlorobenzaldehyde 203

Figure SIV.5. a) Representative ^{1}H NMR spectrum ($CDCl_3$) of the product benzophenone and the substrate diphenylmethanol, using Na[3,3'-Co(1,2-$C_2B_9H_{11}$)$_2$] as catalyst in the photooxidation reaction after 8 hours. Conditions: catalyst (0.08 mM), substrate (20 mM), $Na_2S_2O_8$ (40 mM) 5 ml 0.1M phosphate buffer solution at pH=7.2 light at 8 h of irradiation. b) ^{1}H NMR spectrum of pure commercial diphenylmethanol. c) ^{1}H NMR spectrum of pure commercial benzophenone 205

Figure SIV.6. Representative chromatogram corresponding to the photooxidation tests of different alcohols performed with cobaltacarborane complex Na[3,3'-Co(1,2-$C_2B_9H_{11}$)$_2$]. Conditions: catalyst (0.08 mM), substrate (20 mM), $Na_2S_2O_8$ (40 mM) 5 ml 0.1M phosphate buffer solution at pH=7.2 light at 8 h of irradiation 206

Figure SIV.7. Representative ^{1}H NMR spectrum ($CDCl_3$) corresponding to the photooxidation of 1-phenylethanol, using Na[3,3'-Co(1,2-$C_2B_9H_{11}$)$_2$] as catalyst. Conditions: Na[3,3'-Co(1,2-$C_2B_9H_{11}$)$_2$] (0.002 mM), substrate (20 mM), $Na_2S_2O_8$ (40 mM), 5 mL potassium carbonate solution at pH=7. Light irradiation 8h 208

Figure SIV.8. ^{1}H NMR spectrum ($CDCl_3$) corresponding to the photooxidation of benzyl alcohol, using Na[3,3'-Co(1,2-$C_2B_9H_{11}$)$_2$] as catalyst. Conditions: Na[3,3'-Co(1,2-$C_2B_9H_{11}$)$_2$] (0.02 mM), substrate (20 mM), $Na_2S_2O_8$ (40 mM), 5 mL potassium carbonate solution at pH=7. Light irradiation 8h 208

Figure SIV.9. ^{1}H NMR spectrum ($CDCl_3$) corresponding to the photooxidation of 4-methylbenzylalcohol, using Na[3,3'-Co(1,2-$C_2B_9H_{11}$)$_2$] as catalyst. Conditions: Na[3,3'-Co(1,2-$C_2B_9H_{11}$)$_2$] (0.002 mM), substrate (20 mM), $Na_2S_2O_8$ (40 mM), 5 mL potassium carbonate solution at pH=7. Light irradiation 8h 209

Figure SIV.10. ^{1}H NMR spectrum ($CDCl_3$) corresponding to the photooxidation of 4-chlorobenzylalcohol, using Na[3,3'-Co(1,2-$C_2B_9H_{11}$)$_2$] as catalyst. Conditions: Na[3,3'-Co(1,2-$C_2B_9H_{11}$)$_2$] (0.002 mM), substrate (20 mM), $Na_2S_2O_8$ (40 mM), 5 mL potassium carbonate solution at pH=7. Light irradiation 8h 209

Figure SIV.11. ^{1}H NMR spectrum ($CDCl_3$) corresponding to the photooxidation of diphenylmethanol, using Na[3,3'-Co(1,2-$C_2B_9H_{11}$)$_2$] as catalyst. Conditions: Na[3,3'-Co(1,2-$C_2B_9H_{11}$)$_2$] (0.002 mM), substrate (20 mM), $Na_2S_2O_8$ (40 mM), 5 mL potassium carbonate solution at pH=7. Light irradiation 8h 210

Figure SIV.12. a) Representative ^{1}H NMR spectrum ($CDCl_3$) corresponding to the photooxidation of hexanol, using Na[3,3'-Co(1,2-$C_2B_9H_{11}$)$_2$] as catalyst. Conditions: Na[3,3'-Co(1,2-$C_2B_9H_{11}$)$_2$] (0.002 mM), substrate (20 mM), $Na_2S_2O_8$ (40 mM), 5 mL potassium carbonate solution at pH=7. Light irradiation 8h. b) ^{1}H NMR spectrum of pure commercial 1-hexanol. c) ^{1}H NMR spectrum of pure commercial Hexanoic acid 210

Figure SIV.13. a) Representative ^{1}H NMR spectrum ($CDCl_3$) corresponding to the photooxidation of 2-ethoxyethanol, using Na[3,3'-Co(1,2-$C_2B_9H_{11}$)$_2$] as catalyst. Conditions: Na[3,3'-Co(1,2-$C_2B_9H_{11}$)$_2$] (0.002 mM), substrate (20 mM), $Na_2S_2O_8$ (40 mM), 5 mL potassium carbonate solution at pH=7. Light irradiation 8h. b) ^{1}H NMR spectrum of pure commercial 2-ethoxyethanol 212

Figure SIV.14. a) Representative ^{1}H NMR spectrum ($CDCl_3$) corresponding to the photooxidation of cyclohexanol, using Na[3,3'-Co(1,2-$C_2B_9H_{11})_2$] as catalyst. Conditions: Na[3,3'-Co(1,2-$C_2B_9H_{11})_2$] (0.002 mM), substrate (20 mM), $Na_2S_2O_8$ (40 mM), 5 mL potassium carbonate solution at pH=7. Light irradiation 8h. b) ^{1}H NMR spectrum of pure commercial cyclohexanol 213

Figure SIV.15. a) Synthesis of Fe_3O_4 core (MNP) using co-precipitation method. b) Synthesis of Fe_3O_4 @SiO_2 core (MSNP) using co-precipitation method 215

Figure SIV.16. TEM images of a) MSNPs, b) Gaussian size graphs of MSNPs (9.34 nm), c) MSNPs-NH_2 (11.22 nm), and d) MSNPs-NH2@**H[1]** (14.17 nm) 215

Figure SIV.17. Hysteresis cycles recorded at room temperature (300 K) for MSNPs-NH_2 and MSNPs-NH_2@**H[1]** 216

Figure SIV.18. Stability of Fe_3O_4@SiO_2-NH_2 based on the measurement of the ζ-potential upon increasing amounts of dimethyl di-n-octadecyl ammonium chloride 217

Figure SIV.19. SEM images of MSNP-NH_2@**H[1]**, a) before the photooxidation of 1-phenylethanol and b) after twelve reuses 218

Figure SIV.20. a) Representative ^{1}H NMR spectrum ($CDCl_3$) corresponding to the photooxidation of 1-butanol, using MSNPs-NH2@**H[1]** as catalyst. Conditions: **[1]**$^-$ (0.02 mM), substrate (20 mM), $Na_2S_2O_8$ (40 mM), 5 mL potassium carbonate solution at pH=7. Light irradiation 8h. b) ^{1}H NMR spectrum of pure commercial 1-butanol. c) ^{1}H NMR spectrum of pure commercial butanoic acid 219

Figure SIV.21. a) Representative ^{1}H NMR spectrum ($CDCl_3$) corresponding to the photooxidation of Isobutyl alcohol, using MSNPs-NH2@**H[1]** as catalyst. Conditions: **[1]**$^-$ (0.02 mM), substrate (20 mM), $Na_2S_2O_8$ (40 mM), 5 mL potassium carbonate solution at pH=7. Light irradiation 8h. b) ^{1}H NMR spectrum of pure commercial Isobutyl alcohol. c) ^{1}H NMR spectrum of pure commercial Isobutiric acid 220

Figure SIV.22. a) Representative ^{1}H NMR spectrum (D_2O) corresponding to the photooxidation of diethylene glycol, using MSNPs-NH2@**H[1]** as catalyst. Conditions: **[1]**$^-$ (0.02 mM), substrate (20 mM), $Na_2S_2O_8$ (40 mM), 5 mL potassium carbonate solution at pH=7. Light irradiation 8h. b) ^{1}H NMR spectrum of pure commercial diethylene glycol. c) ^{1}H NMR spectrum of pure commercial diglycolic acid 222

Figure SIV.23. a) Representative ^{1}H NMR spectrum (acetone-d_6) corresponding to the photooxidation of 1,6-hexanediol, using MSNPs-NH2@**H[1]** as catalyst. Conditions: [1] (0.02 mM), substrate (20 mM), $Na_2S_2O_8$ (40 mM), 5 mL potassium carbonate solution at pH=7. Light irradiation 8h. b) ^{1}H NMR spectrum of pure commercial 1,6-hexanediol. c) ^{1}H NMR spectrum of pure commercial adipic acid...223

Figure SIV.24. Dihydrogen bonds C-H···H-B interactions between cationic and anionic moieties in **C5** 227

Figure SIV.25. a) ^{1}H{^{11}B}-NMR and b) ^{11}B{^{1}H}-NMR spectra of Ag[1] **C3** compound in acetone-d_6..227

Figure SIV.26. COSY NMR spectra of cobaltabis(dicarbollide) **C4** compound in acetone-d_6..228

Figure SIV.27. UV-visible of **Ag**[**1**], **C3**..229

Figure SIV.28. CV of **Ag[1] C3** in CH_3CN + 0.1 M TBAH *vs* Ag 229

Figure SIV.29. CV for complex **Na[1]** registered in a phosphate buffer (pH= 7.12) *vs* Ag/AgCl 230

Figure SIV.30. CV of complex **Na[1]** (1 mM) registered in a phosphate buffer (pH= 7.12) *vs* Ag/AgCl, before and after the addition of 1 mM of a) $CaCl_2$ and b) $ZnCl_2$. The blue and purple inserts show dI/dE to better appreciate the position of the couple Co^{IV}/Co^{III}. 230

Figure SIV.31. MALDI of **C4** after the photooxidation of 1-phenylethanol. $[3,3'\text{-Co}(1,2\text{-}C_2B_9H_{11})_2]^-$=324.1 (m/z) and $[3,3'\text{Co}(1,2\text{-}C_2B_9H_{11})(1,2\text{-}C_2B_9H_{11}O)]^-$ =340.1 (m/z) 231

Figure SIV.32. UV-Visible spectra of mixtures of **C2'**:**Na[1]** (1:1) (black line), (1:2) (dotted line) and **C4** (dash dotted line) at a)3 x 10^{-6} and b) 0.33 x 10^{-6} M 232

Figure SIV.33. DLS of catalytic mixture using a) **C4** as catalyst and b) **C2'** and **Na[1]** (1:2) as catalyst 233

Figure SIV.34. ESI-MS spectra of **C4**... 235

Figure SIV.35. HPLC/ESI-MS spectra from Oxidation of methyl oleate by **Na[1]** 237

List of Tables

Table I.1. Scheme of comparison among homogeneous, heterogeneous, and supported catalyst 16

Table IV.1. The main electronic transitions in the different rotamers of **[1]**$^-$ 73

Table IV.2. The overlap of hole and electron distribution 74

Table IV.3. The charge density difference maps of the different transitions. (The blue and red parts correspond to the region where electron density is increased and decreased after electron excitation, respectively. Isosurface value: 0.003) 75

Table IV.4. Oxidation tests of 1-phenylethanol performed with cobaltabis(dicarbollide) complex Na[3,3'-Co(1,2-$C_2B_9H_{11})_2$]. Conditions: catalyst (0.08-0.48 mM), substrate (20 mM), $Na_2S_2O_8$ (40 mM), 5 ml 0.1M phosphate buffer solution at pH=7.2, light irradiation for 3h........77

Table IV.5. Oxidation tests performed with **Na[1]**. Conditions: **Na[1]** (0.08 mM), substrate (20 mM), $Na_2S_2O_8$ (40 mM), 5 mL 0.1 M phosphate buffer solution at pH 7.2 light irradiation (2.2 W, ʎ=253.7 nm) for 6 and 8h. Yield values in the absence or in the presence of 40 mM NEt_3 79

Table IV.6. Oxidation tests performed with chlorinated cobaltabis(dicarbollide) complexes **Na[Cl_2-1]** and **Na[Cl_6-1]**. Conditions: catalyst (0.08 mM), substrate (20 mM), $Na_2S_2O_8$ (40 mM), NEt_3 (40 mM), 5 mL 0.1 M phosphate buffer solution at pH 7.2, light irradiation for 4, 6, and 8h. Percentage yields........85

Table IV.7. Oxidation tests on diphenylmethanol performed with **Na[1]**, **Na[Cl_2-1]**, and **Na[Cl_6-1]**. Conditions: catalyst (0.08 mM), substrate (20 mM), $Na_2S_2O_8$ (40 mM), 5 mL of an aqueous solution containing 40 mM of NEt_3 or K_2CO_3. Light irradiation for 6h 85

Table IV.8. Product set obtained from photooxidation of alcohols by **Na[1]**........87

Table IV.9. Photocatalytic oxidation of alcohols........100

Table IV.10. The substrate scope of photooxidation of alcohols by MSNP-NH2@**H[1]**.....102

Table IV.11. Potential values of complex **Na[1]**, corresponding to the couple Co^{IV}/Co^{III} after the addition of different concentrations of a) $CaCl_2$ and b) $ZnCl_2$........116

Table IV.12. Photooxidation tests performed with ruthenium cobaltabis(dicarbollide) complex **C4**........121

Table IV.13. Photooxidation tests performed with **C4** and **C2'** + **Na[1]**........119

Table IV.14. Photooxidation tests performed with **Na[1]** complex 127

Table IV.15. Comparative results of Photooxidation tests performed with **Na[1]** *vs* $[Ru(bpy)_3]^{2+}$complex 129

Table IV.16. Photooxidation of epoxides performed with **Na[1]** complex. Conditions: **Na[1]** (0.02 mM), epoxide (20 mM), $Na_2S_2O_8$ (26 mM), 5 mL potassium carbonate solution at pH=7........133

Table IV.17. Photooxidation tests performed with **Na[1]** complex 133

Table IV.18. Oxidation tests performed with ferrabis (dicarbollide) complex **Na[2]**. Conditions:

Na[2] (0.002 mM), substrate (20 mM), $Na_2S_2O_8$ (40 mM), 5 mL potassium carbonate solution at pH=7 .Light irradiation 4h 141

Table IV. 19. Products obtained from photooxidation of alcohols by **Na[2]**........ 142

Table IV. 20. Comparison product set obtained from photooxidation of alcohols by **Na[2]** *vs* **Na[1]** 144

Table IV.21. Photoepoxidation tests performed with **Na[2]** complex 146

Table IV.22. Comparative results of Photooxidation tests performed with **Na[2]** or **Na[1]** *vs* $[Ru(bpy)_3]^{2+}$complex 147

Table IV.23. Photooxidation of epoxides performed with **Na[2]** complex. Conditions: **Na[2]** (0.02 mM), epoxide (20 mM), $Na_2S_2O_8$ (26 mM), 5 mL potassium carbonate solution at pH=7........ 149

Table IV.24. Photooxidation tests performed with **Na[2]** complex 151

Table IV.25. Comparative overview about photooxidation tests performed with **Na[1]** *vs* **Na[2]** complexes 154

Table SIV 1.1. Natural Transition Orbitals (NTOs) of the different rotamers 190

Table SIV 1.2. The transitions which belong to the strong absorption band in the UV regions. Note that the OH and Cl group has the similar impact, which was in agreement with similar σ-electron withdrawing character........ 198

Table SIV 2.3. Stability of $Fe_3O_4@SiO_2-NH_2$ with different surfactants 216

Table SIV 3.4. Crystal Data for X-ray structure of complex **C5** 225

Table SIV 3.5. Selected bond lengths (Å) and angles (°) for **C5** complex 226

Table SIV 4.6. Photooxidation tests performed with **Na[1]** complex. Conditions: **Na[1]** (0.02 mM), substrate (20 mM), $Na_2S_2O_8$ (26 mM), 5 mL potassium carbonate solution at pH=7 236

Table SIV 5.1. Photooxidation tests performed with **Na[2]** complex. Conditions: **Na[2]** (0.02 mM), substrate (20 mM), $Na_2S_2O_8$ (26 mM), 5 mL potassium carbonate solution at pH=7 238

List of Schemes

Scheme I.1. PCET oxidation process characteristic of Ru-aqua complexes 13

Scheme I.2. Latimer diagrams of ruthenium polypyridyl complexes (a) without and with (b) a coordinated water molecule. V *vs* NHE, M=0.1 at pH=7 14

Scheme I.3. Mechanisms of Homogeneous Photocatalysis 26

Scheme I.4. Simplified molecular orbital diagram for an octahedral compound with π-acceptor ligands. The main types of electronic transitions typically observed in metal polypyridyl complexes are indicated by the arrows...32

Scheme I.5. a) The mononuclear complex $[Ru(L)(bpy)(bpz)]^{n+}$ ($L=Cl^-$,n=1) ($L=H_2O$, n=2) b) Main steps underlying the photocatalytic dehydrogenative oxidation of benzyl alcohol into benzaldehyde by the mononuclear complex $[Ru(H_2O)(bpy)(tppz)]^{2+}$.....................................33

Scheme I.6. Transition Cu-catalyzed synthesis of quinazolines using inexpensive CuCl as catalyst, without ligands/organic oxidants and reaction at room temperature being an environmentally benign and economically feasible reaction 36

Scheme I.7. On the top: $[Cu7(\mu_3\text{-}OH)_6(H_2O)_{10}]^{8+}$ cluster in complex surrounded by $DSDC^{4-}$ ligands, showing coordination geometries of the Cu(II) centres. On the bottom: Reaction conditions for the photooxidation of benzyl alcohol to benzaldehyde (t= 24 h) and benzoic acid (t= 60 h) 37

Scheme I.8. Cooperative photoredox catalysis in two separate complexes 41

Scheme I.9. Oxidation of lignin systems by merging palladium with photocatalysis 42

Scheme I.10. Organic-linker-connected photoredox catalyst and transition-metal catalyst for the oxidation of organic compounds 44

Scheme I.11. Bridging-ligand-connected photoredox catalysts and transition-metal catalysts for organic transformations 45

Scheme IV.1. The synthetic strategy used for a) the functionalization of MSNP with amine groups, $MSNP\text{-}NH_2$ and b) for the immobilization of H[COSAN], **H[1]**, $MSNP\text{-}NH_2$@**H[1]**........90

Scheme IV.2. Synthetic Strategy for the Preparation of Complexes **C4** and **C5** 106

Scheme IV.3. Oxidation of methyl oleate by **Na[1]** 131

Resum

A aquesta tesi presentem el funcionament de diferents metal·lacarborans com a catalitzadors fotoredox en l'oxidació de diferents alcohols i alquens aromàtics i alifàtics en medi aquós, utilitzant llum com a única font d'activació.

Amb la idea general anteriorment exposada, a la secció un del capítol IV, descrivim el comportament fotocatalític de diferents metal·lacarborans com, $Na[Co(C_2B_9H_{11})_2]$ **Na[1]** i els seus derivats clorats, $Na[3,3'\text{-}Co(8\text{-}Cl\text{-}1,2\text{-}C_2B_9H_{10})_2]$ **Na[Cl_2-1]** i $Na[3,3'\text{-}Co(8,9,12\text{-}Cl_3\text{-}1,2\text{-}C_2B_9H_8)_2]$ **Na[Cl_6-1]**. Aquests compostos van ser provats com a catalitzadors fotoredox a l'oxidació d'alcohols aromàtics i alifàtics en aigua a través de processos *single-electron transfer* (SET), mostrant alta eficiència que va poder ser a causa de l'alta solubilitat en aigua, el seu alt poder oxidant a causa del parell redox $Co^{IV/III}$ i la seva manca de fluorescència en l'excitació, entre altres propietats. En la major part dels experiments catalítics, va ser possible obtenir alts rendiments de 90-95% amb selectivitats superiors al 99%, utilitzant una concentració de catalitzador de 0.4 mol %. Reduint la càrrega del catalitzador a 0.01 mol %, es van obtenir alts rendiments, superiors al 99% en alguns casos. La reducció de concentració portada a terme, va permetre demostrar l'alta eficiència del catalitzador, aconseguint TON de 10000. Addicionalment, els metal·lacarborans van poder ser recuperats fàcilment mitjançant precipitació en afegir $[NMe_4]Cl$. Basat en els resultats obtinguts, és proposat un cicle per al procés catalític fotoredox.

Per altra banda, tenint en compte la importància dels avantatges de la reutilització i heterogeneïtzació del catalitzador pel seu ús en processos a gran escala, a la secció dos del capítol IV expliquem la seva heterogeneïtzació en nanopartícules magnètiques (MNPs) cobertes amb una capa de sílice, observant que l'activitat del catalitzador va ser preservada, a més de mostrar una fàcil separació magnètica i reciclabilitat. Les nanopartícules de sílice magnètiques amino funcionalitzades, enllaçades d'una manera no covalent a $H[3,3'\text{-}Co(1,2\text{-}C_2B_9H_{11})_2]$ (**H[1]**), anomenades $MSNPs\text{-}NH_2$@**H[1]**, són altament estables i no es produeix lixiviació del catalitzador fotoredox en aigua. L'estabilitat col·loïdal de MNPs en aigua ha sigut estudiada utilitzant diferents surfactants, ja que això suposa un gran problema en catàlisi. El sistema catalític heterogeni va ser estudiat per a la

fotooxidació d’alcohols, usant càrregues de catalitzador de 0.1 i 0.01 mol %. Els surfactants van ser introduïts per a prevenir l’agregació de MNP, i com a surfactant es va escollir el cetil trimetil clorur d’amoni (CTAC), amb el propòsit de donar estabilitat, sense impedir la fàcil separació magnètica. La reciclabilitat del sistema catalític va ser exitosa a través de 12 experiments catalítics, sense pèrdues de selectivitat i rendiment. El catalitzador cobaltabis(dicarballur) suportat en nanopartícules magnètiques recobertes de sílice ha demostrat ser un sistema robust, eficient i fàcilment reutilitzable per a la fotooxidació d’alcohols en aigua, resultant un sistema catalític heterogeni verd i sostenible.

A la secció tres del capítol IV descrivim la síntesi d’un sistema catalític fotoredox cooperatiu, $[Ru^{II}(trpy)(bpy)(H_2O)][3,3'-Co(1,2-C_2B_9H_{11})_2]_2$ (**C4**)**.** A aquest sistema, la part aniònica fotoredox es correspon amb el catalitzador cobaltabis(dicarballur) i la part catiònica correspon al catalitzador d’oxidació $Ru^{II}-H_2O$. Ambdues parts són enllaçades per interaccions no covalents que persisteixen inclús després de dissolució en aigua. Aquest fet suposa un pas endavant en la cooperativitat evitant els costosos enllaços covalents. A més, la recristal·lització de **C4** en acetonitril condueix a la substitució d’aigua per lligand acetonitril i a la formació del complex $[Ru^{II}(trpy)(bpy)(CH_3CN)][3,3'-Co(1,2-C_2B_9H_{11})_2]_2$ (**C5**), que és caracteritzat estructuralment. Un important acoblament electrònic entre les dues parts, $[Ru^{II}(trpy)(bpy)(H_2O)]^{2+}$ (**C2’**) i $[3,3'-Co(1,2-C_2B_9H_{11})_2]^-$ (**[1]**$^-$), va ser primerament detectat en estudis electroquímics en aigua. El parell redox $Co^{IV/III}$ va mostrar una diferència de 170 mV en aigua, quan **[1]**$^-$ posseeix sodi com a contraió davant a quan el complex de ruteni és el catió. El sistema cooperatiu permet demostrar la seva eficiència com a catalitzador per a l’oxidació fotoredox d’alcohols en aigua, a través de processos *proton-coupled electron transfer* (PCET), operant a temperatura ambient sota irradiació UV, utilitzant 0.005 mol % de catalitzador. És possible obtenir TON=20000, i cal assenyalar que **C4** demostra millor rendiment catalític que els compostos **C2’** i **Na[1]**, funcionant a les mateixes concentracions i proporcions de Ru/Co. A més es va proposar un mecanisme pel procés catalític fotoredox.

A la secció quatre del capítol IV es descriu a **Na[1]** com a catalitzador fotoredox efectiu per a l’oxidació d’alquens en aigua. Algunes característiques, descrites anteriorment, diferencien **Na[1]** del fotosensibilitzador conegut i àmpliament utilitzat, tris(2,2’-bipyridine)ruthenium (II) $[Ru(bpy)_3]^{2+}$, que a més participa en la transferència electrònica a través d’un mecanisme d’esfera externa. Una comparativa del rendiment catalític del complex de Ru(II) amb **Na[1]** per a la fotooxidació d’alquens va mostrar la manca o molt poca eficiència del fotosensibilitzador de ruteni. Amb una càrrega de catalitzador de 0.1 mol %, es van obtenir conversions entre el 65-97% en temps de reacció curts, amb selectivitat moderada vers l’epòxid corresponent, a causa de la formació de diols com a productes. La reducció de concentració del catalitzador, es va traduir en un augment important de la selectivitat vers l’epòxid, i es van obtenir alts valors de TON. Verifiquem que el cobaltabis(dicarballur) actua com a fotocatalitzador en l’epoxidació i en la hidroxilació d’alquens en aigua amb una proporció més alta per l’epoxidació que per la hidroxilació. Experiments preliminars de fotooxidació utilitzant oleat de metil com a substrat, van portar a la selectiva epoxidació del doble enllaç del substrat. Aquests resultats representen un prometedor punt de partida pel desenvolupament de mètodes pràctics pel processament d’àcids grassos insaturats, com ara la valorització de residus de greix animal utilitzant aquest catalitzador fotoredox sostenible.

Finalment, a la secció cinc del capítol IV hem investigat el comportament fotocatalític del ferrabis(dicarballur) $[3,3'\text{-Fe}(1,2\text{-C}_2\text{B}_9\text{H}_{11})_2]$ **Na[2],** en l'oxidació d'alcohols i alquens en aigua, utilitzant baixes càrregues de catalitzador. Els alcohols s'oxiden a compostos carbonílics, mostrant-se l’alta capacitat de **Na[2]** com a catalitzador fotoredox en aquests processos, aconseguint alts valors en rendiments, TON i selectivitat per la majoria dels substrats estudiats. A més va demostrar-se l’eficiència de **Na[2]** com a catalitzador fotoredox en l’epoxidació d’alquens, aconseguint valors de conversió i selectivitat elevats en els corresponents epòxids.

Hem establert una comparació amb el complex fotoredox cobaltabis(dicarballur) **Na[1]**, ja que **Na[2]** presenta característiques similars com la seva manca de fluorescència, alta solubilitat i comportament tensioactiu en medis aquosos. No obstant això, **Na[2]** presenta característiques avantatjoses com ara, **Na[2]** es basa en el metall de transició més abundant a l'escorça terrestre i el menor poder oxidant del seu parell redox $\text{Fe}^{IV/III}$. Aquest darrer fet porta a mostrar una major selectivitat i rendiment pels corresponents epòxids en temps de reacció curts, a més d’obtenir resultats comparables als obtinguts amb **Na[1]** en l’oxidació d’alcohols. En conseqüència tenim a les nostres mans un fotocatalitzador altament sostenible i verd.

Resumen

En esta tesis presentamos el funcionamiento de diferentes metalacarboranos como catalizadores fotoredox en la oxidación de diferentes alcoholes y alquenos aromáticos y alifáticos en medio acuoso, utilizando luz como única fuente de activación.

Con la idea general anteriormente expuesta, en la sección uno del capítulo IV, describimos el comportamiento fotocatalítico de diferentes metalacarboranos como, Na[Co($C_2B_9H_{11}$)$_2$] **Na[1]** y sus derivados clorados, Na[3,3'-Co(8-Cl-1,2-$C_2B_9H_{10}$)$_2$] **Na[Cl$_2$-1]** y Na[3,3'-Co(8,9,12-Cl_3-1,2-$C_2B_9H_8$)$_2$] **Na[Cl$_6$-1]**. Estos compuestos fueron probados como catalizadores fotoredox en la oxidación de alcoholes aromáticos y alifáticos en agua a través de procesos *single-electron transfer* (SET), mostrando alta eficiencia que pudo ser a causa de la alta solubilidad en agua, su alto poder oxidante debido al par redox $Co^{IV/III}$ y su falta de fluorescencia en la excitación, entre otras propiedades. En la mayor parte de los experimentos catalíticos, fue posible obtener altos rendimientos de 90-95% con selectividades superiores al 99%, utilizando una concentración de catalizador de 0.4 mol %. Reduciendo la carga del catalizador a 0.01 mol %, se obtuvieron altos rendimientos, superiores al 99% en algunos casos. La reducción de concentración llevada a cabo, permitió demostrar la alta eficiencia del catalizador, consiguiendo TON de 10000. Adicionalmente, los metalacarboranos pudieron ser recuperados fácilmente mediante precipitación al añadir [NMe_4]Cl. Basado en los resultados obtenidos, es propuesto un ciclo para el proceso catalítico fotoredox.

Por otro lado, teniendo en cuenta la importancia de las ventajas de la reutilización y heterogeneización del catalizador para su uso en procesos a gran escala, en la sección dos del capítulo IV explicamos su heterogeneización en nanopartículas magnéticas (MNPs) cubiertas con una capa de sílice, observando que la actividad del catalizador fue preservada, además de mostrar una fácil separación magnética y reciclabilidad. Las nanopartículas de sílice magnéticas amino funcionalizadas, enlazadas de una manera no covalente a H[3,3'-Co(1,2-$C_2B_9H_{11}$)$_2$] (**H[1]**), llamadas MSNPs-NH_2@**H[1]**, son altamente estables y no se produce lixiviación del catalizador fotoredox en agua. La estabilidad coloidal de MNPs en agua ha sido estudiada utilizando diferentes surfactantes, ya que esto supone un gran problema en catálisis. El sistema catalítico heterogéneo fue estudiado para la fotooxidación de alcoholes,

utilizando cargas de catalizador de 0.1 y 0.01 mol %. Los surfactantes fueron introducidos para prevenir la agregación de MNPs, y como surfactante se eligió cetil trimetil cloruro de amonio (CTAC), con el propósito de dar estabilidad, sin impedir la fácil separación magnética. La reciclabilidad del sistema catalítico fue exitosa a través de 12 experimentos catalíticos, sin pérdidas de selectividad y rendimiento. El catalizador cobaltabis(dicarballuro) soportado en nanopartículas magnéticas recubiertas de sílice ha demostrado ser un sistema robusto, eficiente y fácilmente reutilizable para la fotooxidación de alcoholes en agua, resultando un sistema catalítico heterogéneo verde y sostenible.

En la sección tres del capítulo IV describimos la síntesis de un sistema catalítico fotoredox cooperativo, $[Ru^{II}(trpy)(bpy)(H_2O)][3,3'-Co(1,2-C_2B_9H_{11})_2]_2$ (**C4**). En este sistema, la parte aniónica fotoredox se corresponde con el catalizador cobaltabis(dicarballuro) y la parte catiónica corresponde al catalizador de oxidación Ru^{II}-H_2O. Ambas partes son enlazadas por interacciones no covalentes que persisten incluso después de disolución en agua. Este hecho supone un paso adelante en la cooperatividad evitando los costosos enlaces covalentes. Además, la recristalización de **C4** en acetonitrilo conduce a la sustitución de agua por ligando acetonitrilo y a la formación del complejo $[Ru^{II}(trpy)(bpy)(CH_3CN)][3,3'-Co(1,2-C_2B_9H_{11})_2]_2$ (**C5**), que es caracterizado estructuralmente. Un importante acoplamiento electrónico entre las dos partes, $[Ru^{II}(trpy)(bpy)(H_2O)]^{2+}$ (**C2'**) i $[3,3'-Co(1,2-C_2B_9H_{11})_2]^-$ (**[1]**$^-$), fue primeramente detectado en estudios electroquímicos en agua. El par redox $Co^{IV/III}$ mostró una diferencia de 170 mV en agua, cuando **[1]**$^-$ posee sodio como contraión frente a cuando el complejo de rutenio es el catión. El sistema cooperativo permite demostrar su eficiencia como catalizador para la oxidación fotoredox de alcoholes en agua, a través de procesos *proton-coupled electron transfer* (PCET), operando a temperatura ambiente bajo irradiación UV, utilizando 0.005 mol % de catalizador. Es posible obtener TON=20000, y hace falta señalar que **C4** demuestra mejor rendimiento catalítico que los compuestos **C2'** i **Na[1]**, funcionando a las mismas concentraciones y proporciones de Ru/Co. Además se propuso un mecanismo para el proceso catalítico fotoredox.

En la sección cuatro del capítulo IV se describe a **Na[1]** como catalizador fotoredox efectivo para la oxidación de alquenos en agua. Algunas características, descritas anteriormente, diferencian **Na[1]** del fotosensibilizador conocido y ampliamente utilizado, tris(2,2'-bipyridine)ruthenium (II) $[Ru(bpy)_3]^{2+}$, que además participa en la transferencia electrónica a través de un mecanismo de esfera externa. Una comparativa del rendimiento catalítico del complejo de Ru(II) con **Na[1]** para la fotooxidación de alquenos mostró la falta o muy poca eficiencia del fotosensibilizador de rutenio. Con una carga de catalizador de 0.1 mol % se obtuvieron conversiones de entre el 65-97% en tiempos de reacción cortos, con selectividad moderada respeto el epóxido correspondiente, debido a la formación de dioles como productos. La reducción de concentración del catalizador, se tradujo en un aumento importante de la selectividad respecto al epóxido, y se obtuvieron altos valores de TON. Verificamos que el cobaltabis(dicarballuro) actúa como fotocatalizador en la epoxidación y en la hidroxilación de alquenos en agua, con una proporción más alta por la epoxidación que por la hidroxilación. Experimentos preliminares de fotooxidación utilizando oleato de metilo como sustrato, llevaron a la selectiva epoxidación del doble enlace del sustrato. Estos resultados representan un prometedor punto de partida para el desarrollo de métodos prácticos para el procesamiento de ácidos grasos insaturados, como la valorización de residuos de grasa animal utilizando este catalizador fotoredox sostenible.

Finalmente, en la sección cinco del capítulo IV hemos investigado el comportamiento fotocatalítico del ferrabis(dicarballuro) [3,3'-Fe(1,2-$C_2B_9H_{11})_2$], **Na[2],** en la oxidación de alcoholes y alquenos en agua, utilizando bajas cargas de catalizador. Los alcoholes se oxidan a compuestos carbonílicos, mostrándose la alta capacidad de **Na[2]** como catalizador fotoredox en estos procesos, consiguiendo altos valores en rendimientos, TON y selectividad para la mayoría de sustratos estudiados. Además se demostró la eficiencia de **Na[2]** como catalizador fotoredox en la epoxidación de alquenos, consiguiendo valores de conversión y selectividad elevados en los correspondientes epóxidos.

Hemos establecido una comparación con el complejo fotoredox cobaltabis(dicarballuro) **Na[1]**, ya que **Na[2]** presenta características similares como su falta de fluorescencia, alta solubilidad y comportamiento tensioactivo en medios acuosos. No obstante, **Na[2]** presenta características ventajosas como, **Na[2]** se basa en el metal de transición más abundante de la corteza terrestre y el menor poder oxidante de su par redox $Fe^{IV/III}$. Este anterior hecho lleva a mostrar una mayor selectividad y rendimiento por los correspondientes epóxidos en tiempos de reacción cortos, además de obtener resultados comparables a los obtenidos con **Na[1]** en la oxidación de alcoholes. En consecuencia tenemos en nuestras manos un fotocatalizador altamente sostenible y verde.

Abstract

In this thesis we present the performance of different metallacarboranes as photoredox catalysts in different aromatic and aliphatic alcohols and alkenes oxidation in aqueous media, using light as the only activation source.

With the above mentioned general idea, in section one of chapter IV, we describe the photocatalytic behavior of different metallacarboranes such as, Na[Co($C_2B_9H_{11}$)$_2$] **Na[1]** and their chlorinated derivatives, Na[3,3'-Co(8-Cl-1,2-$C_2B_9H_{10}$)$_2$] **Na[Cl$_2$-1]** i Na[3,3'-Co(8,9,12-Cl$_3$-1,2-$C_2B_9H_8$)$_2$] **Na[Cl$_6$-1]**. These compounds were tested, as photoredox catalysts in the oxidation of aromatic and aliphatic alcohols in water through *single-electron transfer* (SET) processes, showing high efficiency that could be due to the high solubility in water, their high oxidizing power of the $Co^{IV/III}$ redox couple, and their lack of fluorescence on excitation, among others properties. In the major part of the catalytic experiments, was possible to obtain high yields of 90-95% with selectivities greater than 99%, using a catalyst concentration of 0.4 mol %. By reducing the catalyst load to 0.01 mol %, high yields were obtained, greater than 99% in some cases. The reduction of concentration performed, allowed to demonstrate the high catalyst efficiency, achieving TON of 10000. Additionally, the metallacarboranes could be recovered easily by precipitation on addition of [NMe_4]Cl. Based on the results obtained, a cycle for the photoredox catalytic procedure is proposed.

On the other hand, taking into account about the importance and the advantages of the reutilization and heterogeneization of the catalyst for their use in a large-scale processes, in the section two of the chapter IV we explain about their heterogeneization on magnetic nanoparticles (MNPs) coated with a silica layer, noting that the catalyst activity was preserved, besides showing an easy magnetic separation and recyclability. The amino functionalized magnetic silica nanoparticles linked in a non-covalent manner to H[3,3'-Co(1,2-$C_2B_9H_{11}$)$_2$] (**H[1]**), named MSNPs-NH_2@**H[1]**, are highly stable and do not produce any leaching of the photoredox catalyst in water. The colloidal stability of the MNPs in water has been studied using different surfactants, since this supposes a huge issue in catalysis. The heterogeneous catalytic system was studied for the photooxidation of alcohols, using catalyst loads of 0.1 and 0.01 mol %. Surfactants were introduced to prevent the aggregation of MNPs, and cetyl trimethyl ammonium chloride (CTAC) was chosen as surfactant, with the aim of

providing stability, without hindering the easy magnetic separation. The recyclability of the catalytic system was successful through 12 catalytic experiments, without loss of selectivity and yield. The cobaltabis(dicarbollide) catalyst supported on silica-coated magnetic nanoparticles has proven to be a robust, efficient and easily reusable system for the photooxidation of alcohols in water, resulting in a green and sustainable heterogeneous catalytic system.

In section three of chapter IV we describe the synthesis of a cooperative photoredox catalytic system, $[Ru^{II}(trpy)(bpy)(H_2O)][3,3'\text{-}Co(1,2\text{-}C_2B_9H_{11})_2]_2$ (**C4**). In this system, the photoredox anionic part is corresponding to the cobaltabis(dicarbollide) catalyst and the cationic part corresponds to $Ru^{II}\text{-}H_2O$ oxidation catalyst. Both parts are linked by noncovalent interactions that persist even after water dissolution. This fact supposes a step ahead in the cooperativity avoiding costly covalent bonds. In addition, recrystallization of **C4** in acetonitrile leads to the substitution of water by acetonitrile ligand and the formation of complex $[Ru^{II}(trpy)(bpy)(CH_3CN)][3,3'\text{-}Co(1,2\text{-}C_2B_9H_{11})_2]_2$ (**C5**), which is structurally characterized. A significant electronic coupling between both parts, $[Ru^{II}(trpy)(bpy)(H_2O)]^{2+}$ (**C2'**) and $[3,3'\text{-}Co(1,2\text{-}C_2B_9H_{11})_2]^-$ (**[1]**$^-$) was first sensed in electrochemical studies in water. The $Co^{IV/III}$ redox couple displayed a difference of 170 mV in water, when **[1]**$^-$ has sodium as counterion versus when the ruthenium complex is the cation. The cooperative system allows demonstrating their efficiency as catalyst for the photoredox oxidation of alcohols in water, through *proton-coupled electron transfer* (PCET) processes, operating at room temperature under UV irradiation, using 0.005 mol % of catalyst. It is possible to obtain TON=20000, and it is worth noting that **C4** demonstrates better catalytic performance than **C2'** and **Na[1]** compounds**,** operating at the same concentrations and ratios of Ru/Co. Furthermore a mechanism for the photoredox catalytic process was proposed.

In section four of chapter IV we describe **Na[1]** as an effective photoredox catalyst for alkene oxidation in water. Some features, described above, differentiate **Na[1]** from the well-known and widely used photosensitizer tris(2,2'-bipyridine)ruthenium (II) $[Ru(bpy)_3]^{2+}$, which also participates in electron transfer through an outer sphere mechanism. A comparison of the catalytic performance of the Ru(II) complex with **Na[1]** for alkene photo-oxidation showed the lack or very low efficiency of the ruthenium photosensitizer. With a catalyst load of 0.1 mol % conversions between 65-97% have been obtained in short reaction times, with moderate selectivity for the corresponding epoxide, due to the formation of diols as products. The reduction of concentration of the catalyst was traduced in an important increase of the selectivity with respect the epoxide, and high TON values were obtained. We have verified that cobaltabis(dicarbollide), acts as photocatalyst in the epoxidation and hydroxylation of alkenes in water with a higher ratio for the epoxidation than for the hydroxylation. Preliminary photooxidation tests using methyl oleate as substrate, led to the selective epoxidation of the double bond of the substrate. These data represent a promising starting point for the development of practical methods for the processing of unsaturated fatty acids, such as the valorisation of animal fat waste by using this sustainable photoredox catalyst.

Finally, in section five of chapter IV we have investigated the photocatalytic behavior of the ferrabis(dicarbollide) [3,3'-Fe(1,2-$C_2B_9H_{11})_2$], **Na[2]** in the oxidation of alcohols and alkenes in water, using low catalyst loads. Alcohols are oxidized to carbonyl compounds, showing the high capacity of **Na[2]** as photoredox catalyst in these processes, achieving high yields, TON and selectivity values in the corresponding epoxides for the major part of the substrates studied. Furthermore, it was demonstrated the efficiency of the **Na[2]** as a photoredox catalyst in the alkene epoxidation, achieving high conversion and selectivity values in the corresponding epoxides.

We have stablished a comparison with the cobaltabis(dicarbollide) photoredox complex **Na[1]**, since **Na[2]** displays similar features as its lack of fluorescence, high solubility and surfactant behavior in aqueous media. However, **Na[2]** presents advantageous features such as, **Na[2]** is based in the most abundant transition metal in the earth's crust and the minor oxidizing power of its $Fe^{IV/III}$ redox couple. This last fact leads to display higher selectivity and performance for the corresponding epoxides in short reaction times, furthermore with the obtention comparable results to those obtained with **Na[1]** on alcohols oxidation. Consequently we have in our hands a highly sustainable and green photocatalyst.

Chapter I. Introduction

I.1. Introduction of elemental boron and boranes

The Boron element in periodic table belongs to the group 13 and it is the only one that does not have metallic character but being a metalloid, therefore it behaves like a semiconductor. With trivalent electronic configuration, it has an empty *p* orbital, which makes it a varied chemistry. Boron-containing compounds have been known for 4,000 years. Although the existence of boron and boron hydrides or boranes was known in 1878, but it was not until 1912 when the German chemist A. Stock prepared and characterized the first boranes.[1] The first correct structure of diborane (B_2H_6) was proposed by W. C. Price,[2] and H. C. Longuet-Higgins had introduced the concept of three-center two-electron bond (3c-2e),[3] based on the high chemical connectivity of boranes (B-H-B bridging bonds) that complies with the Lewis theory and that of molecular orbitals. Great advances were made in the field of boranes (pentaborane and decaborane) in times close to World War II, as fuels and energy sources for aviation.[4] From these times, boranes started to play an important role due to the properties of boron hydrides as an energy source, which generated various symposia and a great growth was experimented in this field. In 1976 W. N. Lipscomb received the Nobel Prize in Chemistry for his work about the structure of boranes and boron clusters.[5,6] In 1979 H. C. Brown also received the Nobel Prize with G. Wittig for his studies of boron hydrides and phosphorous compounds applied in the field of organic synthesis.[7] Furthermore, Lipscomb described polyhedral boron clusters as compounds with occupied orbitals and multicentric bonds in different resonant forms.[8] The last fact led them to be considered as superatomic, rather than electron deficient species.[9,10] Recently it has been demonstrated by Teixidor, Solà and Co. that borane compounds can be considered aromatic, obeying according to the Huckel rule.[11,12]

I.2. Generalities of Boron clusters

Elemental boron has the property of forming three-dimensional structures due to the catenation property that as well elemental carbon exhibits. Also, boron has 4 orbitals and 3 electrons of valence, which suppose the formation of more clusters than chains.[13] Boron clusters are classified into boranes, carboranes, and metallacarboranes. According to this classification, boranes are built up only of boron and hydrogen atoms, carboranes contain in addition carbon atoms and metallacarboranes also contain a metal in their structures.

I.2.1. Boranes

Borane compounds were discovered by Alfred Stock in 1912. Their molecular formula is $[B_nH_m]^{x-}$ and can be prepared by different synthetic routes from minerals such as borax.[14,15] The simplest of the boranes is BH_3 that dimerizes giving rise to diborane (B_2H_6), which is one of the most important boranes along with pentaborane (B_5H_9) and decaborane ($B_{10}H_{14}$). Between their properties, they are diamagnetic, with a colourless, white, or yellow appearance and can be neutral or anionic. Furthermore, from 5 boron atoms they form clusters. Within the family of boranes, *closo*-dodecaborate or $[B_{12}H_{12}]^{2-}$ stands out for its enormous stability,[16] its electronic properties (electronic delocalization throughout the cluster), chemical reactivity and magnetic properties.[17] All these properties have led it to be considered as a three-dimensional aromatic compound.[18,19]

I.2.2. Carboranes

There are a large number of boranes in which one or more of the boron vertexes have been substituted by heteroatoms such as C, N, O, Si, P, As, S, Se, Sb and or Te,[20,21] giving rise to a variety of compounds named Heteroboranes. The most studied among them are the carboranes in which one or two of the boron atoms have been replaced by carbon atoms. The empiric formula of these compounds is represented by $[C_nB_mH_{n+m+p}]^{x-}$, where *n* represents the number of C atoms in the vertices of the cluster, *m* is the number of B atoms in the cluster, p the number of bridging H and *x* the charge of the molecule.

In 1971 R. E. Williams classified the great variety of boranes in three groups: *closo*, *nido* and *arachno* (**Figure I.1**), based on these electronic requirements for boranes were studied as well by Wade, Mingos and Rudolph,[22,23] furthermore obey the classic Wade's rules,[24,22] which allow to predict the shape of the cluster considering the number of occupied vertices and the number of electron pairs required to form the cluster skeleton. With respect the classification made by Williams, if the number of electrons in the cluster is 2*n*+2, the compound shows a *closo* structure; if it is 2*n*+4, the compound will be *nido* and in the case of 2*n*+6 the cluster will be *arachno*, being *n, the* number of polyhedral vertexes (B atoms or different heteroatoms). The skeletal electron counts are made by considering that each B-H unit brings two electrons to the cluster, from the boron atom; each C-H or C-R unit gives three electrons from the carbon atom and each bridge hydrogen atom contributes with one electron to the cluster. With respect the structural relationship between closo, nido and arachno boranes as well as hetero-substituted boranes we can mention that, when a vertex of the *closo* is removed, we will obtain the *nido* structure and if a second vertex is removed the *arachno* cluster will be obtained. The boron clusters are electron deficient due to their characteristic molecular form and type of bond based on 3c-2e,[25] these properties provide to the cluster specific properties that cannot be found in their organic analogous.[26]

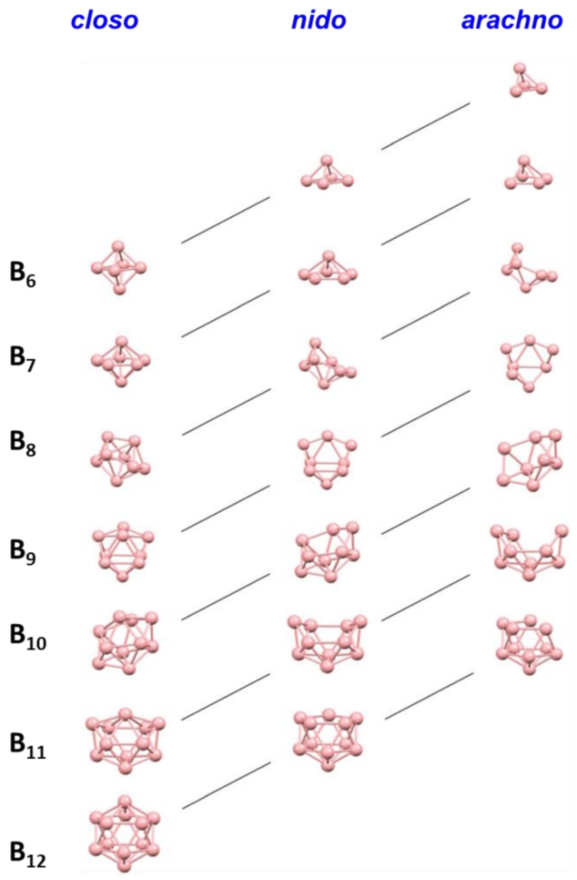

Figure I.1. The structural relationship between *closo*, *nido* and *arachno* polyhedral noted by Williams which were the motivation to develop the Wade’s rules. Figure adapted from ref 22a.

The most known and studied carboranes are those in which two atoms of boron have been replaced by two carbon atoms giving rise to dicarba-*closo*-dodecaboranes, with the empirical formula $C_2B_{10}H_{12}$, commonly named carboranes. The (**Figure I.2 a**) shows the ortho-carborane specie[27,28] with formula 1,2-$C_2B_{10}H_{12}$. The dicarba-*closo*-dodecaboranes, are the most studied of all the carboranes due to their properties as high thermal stability[26a,29] and chemical resistance.[30,31] These properties are a consequence of the electronic delocalization of the structure. In these compounds, the position of the carbon atoms determines the existence of three different isomeric forms, 1,2-dicarba-*closo*-dodecaborane or *o*-carborane, 1,7-dicarba-*meta*-dodecaborane or *m*-carborane and 1,12-dicarba-*para*-dodecaborane or *p*-carborane, that are showed in the following (**Figure I.2 b**).

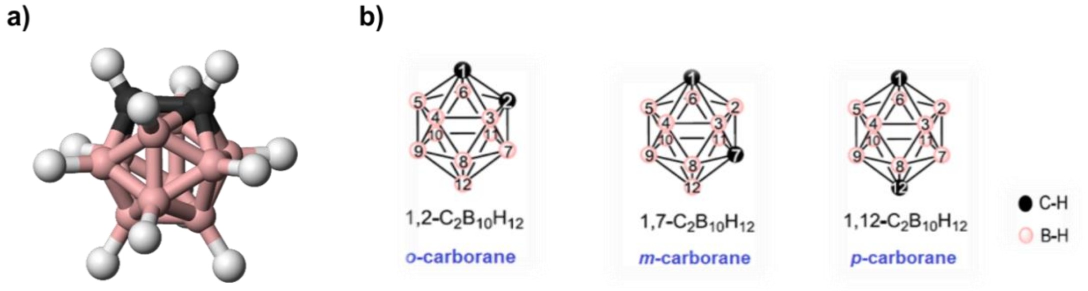

Figure I.2. a) Structure of 1,2-$C_2B_{10}H_{12}$. (C in grey, B in pink and H in white). b) The dicarba-*closo*-dodecaborane with the numbering of the vertices. The nomenclature *o*-, *m*- and *p*- is referred to the relative position of the carbons.

The *o*-carborane presents atoms with different electronegativities (C=2.5, B=2.0, H=2.2 at the Pauling scale). This fact affects the different reactivity of the vertices and the type of isomer.[32,33] Thus, the cluster has an electron-withdrawing character on the substituents attached along the carbons in the cluster and on the neighbouring atoms,[34,35] as is showed in the (**Figure I.3**). In carboranes the bonds (B-H), hydrogen atoms exhibit low polarity due to the low electronegativity of boron atom, thus, the B-H atoms exhibit almost no acidic character toward even the strongest proton acceptors as organolithium and Grignard reagents. However, the electron-delocalized of the o-carborane could be attacked by electrophile species. The boron atoms attached directly to the carbon atoms, see B3 and B6, present a positive charge density than the others, while the rest of eight BH vertices would react with electrophile species and the two vertices allow be attacked with nucleophile species. To functionalize the carborane species, the B(9) and B(12)positions followed by B(8)and B(10) are the most susceptible to the electrophilic attack on the cluster cage, thus, the halogenation reaction in these positions is possible to carry out[36].Halogenation in positions B(3) and B(6) was achieved years later.[37]

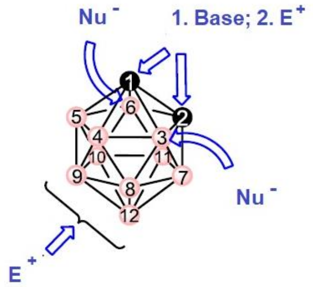

Figure I.3. Reactivity of the different vertices in the *o*-carborane.

I.2.3. Metallacarboranes

Due to steric and electronic properties of anionic carborane clusters, they have been used as ligands for formation of metallacarborane complexes. Metallacarborane compounds form a large family of carborane species that their structures allow one or more transition metals or lanthanides.[38,39] The most studied metallacarboranes have a sandwich structure and they are formed by two dicarbollide units as $[1,2\text{-}C_2B_9H_{11}]^{2-}$ with a central transition metal between the two units. Among the most used metals are Co(III), Co(II), Fe(II), Ni(III) and Au(III).

In 1965 was carried out the synthesis of the first metallacarborane,[40] using iron as the central atom, the $[3,3\text{-}Fe(1,2\text{-}C_2B_9H_{11})_2]^-$, named ferrabis(dicarbollide) or FESANE. Recently, C. Viñas and Co. have published a fast and very efficient green synthesis that does not require any solvent, which could facilitate the research over these compounds.[41]

Cobaltabis(dicarbollide)[42] $[3,3'\text{-}Co(1,2\text{-}C_2B_9H_{11})_2]^-$, also name COSANE, in which the two Cc carbon atoms of the cluster occupy adjacent positions, is the best representative example of metallabisdicarbollides. The latter has been the most widely studied and synthesized metallacarborane. The reason why COSANE is the most studied are diverse but undoubtedly lie in its thermal and chemical stability and simple synthesis. In its structure, the central cobalt atom has an oxidation state of +3 and the two dicarbollide ligands provide two negative charges each one (-4), yielding one global negative charge delocalized throughout the volume of the complex which contributes to the low charge density of it, distributed between the atoms in the compound.[43] This anionic specie shows other properties as high molecular volume, and low nucleophilic character.[44,45]

To synthetize the metallacarborane, the 1,2-dicarba-closo-dodecaborane could be deboronated partially under nucleophilic reaction in a selective manner over one of the boron atoms directly bonded to the carbon cluster, as mentioned above, because of the electronic impoverishment. Thus, the partial deboronation gives the anionic *nido* cluster [7,8-*nido*-$C_2B_9H_{12}$]$^-$ which has lost one B^+ fragment with respect the *closo* specie, having a pentagonal face (C_2B_3) with the hydrogen still present in the structure manly bonded over the B (10).[46] The next step consists in the extraction of the bridging H in [7,8-*nido*-$C_2B_9H_{12}$]$^-$ to form the dicarbollide dianionic cluster $[C_2B_9H_{11}]^{2-}$ using a strong base such as K[^{t}BuO], NaH or *n*-BuLi under anhydrous conditions.[47] **(First step in the Figure I.4).** Then, anhydrous $CoCl_2$ or $FeCl_2$ is added to form the form the cobalt or iron complexes, in each case, as is showed in the step of the (**Figure I.4**).[42]

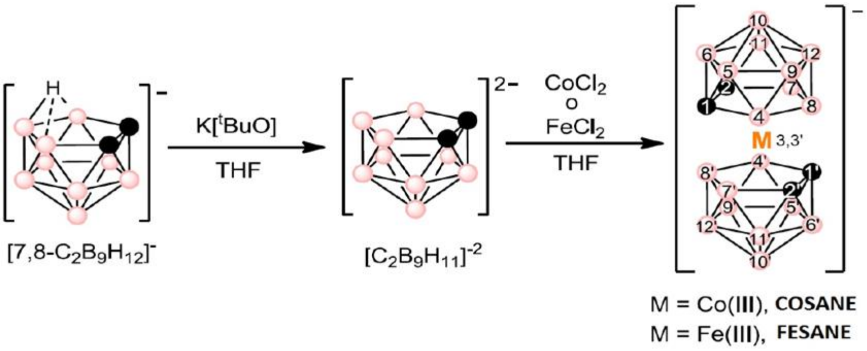

Figure I.4. Schematic representation of the synthesis from COSANE (M=Co) and FESANE (M=Fe).

I.2.3.1. Physicochemical properties of metallacarboranes

Initially, the investigations related to metallacarborane complexes were developed in a lot of applications with the purpose of introducing new functional groups into the molecules.[48] The development of new applications for the metallacarboranes supposed to study in more depth its physical-chemical properties, such as their self-assembly capacity, redox properties, being both the most important, and others like, low charge density, high molecular volume, high thermal and chemical stability, [49] hydrophobicity and limitation of the movement due to the geometry stiffness. In addition, other properties as low nucleophilic character and the possibility to establish di-hydrogen bridging bonds.[19,50,51,52] Metallacarboranes exhibit derivatization capacity similar or superior to that of organic compounds.[43a,53] The interactions in a supramolecular approach seem to be significant in the processes of electron transfer and therefore in the effectiveness of photocatalytic systems, which is the main objective of this thesis.[54]

It is important to highlight the solubility of the metallacarboranes.[38] The state of oxidation from metal that build up the metallacarborane influences the type of solubility of the molecule.[39] The neutrality or the ionicity of the compound will determine its solubility in organic or both aqueous and organic media, respectively.

Metallacarboranes are considered highly compact Θ-shaped molecules ready for stepwise substitutions at B that sequentially modify its redox potentials and maintain them reversible.[55] Teixidor et. al. described the monohalogenation of metallacarborane compounds. The study reveals the existence of intermolecular C_c-H…X-B hydrogen bonds building up two dimensional structures. The results showed that halogens (Cl, Br and I) are well hydrogen-bond acceptors in the bonding to boron atoms.[56] Other properties of metallacarboranes are, its nonlocalized negative charge spread all over the molecule,[43a,57] its possibilities to form hydrogen bonds such as C_c-H…O and C_c-H…H-B dihydrogen bonds, which have been proven to participate their self-assembly,[58] water solubility,[59] micelle and vesicle formation,[60] and derivatization capacity similar or superior to that organic compounds,[43a,61] all properties mentioned in the above section. They can be substituted either at carbon or boron atoms,[62] and in the last chemical element, regioselectivity at different ways of the cobalbis(dicarbollide) molecule.[63] In the metallacarboranes under study (COSANE and FESANE), the negative monocharged nature of the compounds play an important role in their solubility, depending on the nature of the cation, as well was previously mentioned.

The self-assembly property exhibited by the metallacarboranes, is a broad term that is extensive to surfactants, block copolymers, monolayers, nanoclusters, nanotubes and nanowires and larger building blocks.[64] Furthermore, it is abundant in many biological systems. Also, there are certain similarities between the self-assembly showed by metallacarboranes and surfactants.[65] Metallacarboranes, without classical amphiphilic topology but with an inherent amphiphilic character can behave similarly to classical surfactants. The differences in electronegativity between the atoms that build up the metallacarborane, the metal and the coordinating atoms of the ligands, (e.g., X_{Fe}-X_B= -0.21 in $[Fe(C_2B_9H_{11})_2]^-$ and X_{Co}-X_B= -0.16 in $[Co(C_2B_9H_{11})_2]^-$) are responsible for the ability to self-assemble and for the presence of different natures in the hydrogen atoms which influence the existence of hydrogen bridging bonds for the construction of supramolecular structures.

The part “$Co(C_2B_3)_2$” from the cobaltabis(dicarbollide) anion is similar to that of ferrocene “$Fe(C_5H_5)_2$”, showing similarities in the reversible electrochemistry,[66] but differentiating in the enhanced protection of the Co at cobaltabis(dicarbollides) by the canopy of boron hydrogen atoms.[67] These boron hydrogen atoms can suffer substitution reactions of electrophilic halogenation.[68] The better positions susceptible to be halogenated are in the order of B (8, 8’)>B (9,9’,12,12’)>B (10,10’), due to that these vertexes are richer in electrons.[69]

There are different types of oxidation state of metallacarboranes ($M^{IV/III}$, $M^{III/II}$ and $M^{II/I}$) with potential values that may change negatively or positively depending on the nature of the substituents attached to the clusters of metallacarborane. The redox potentials of a wide variety of metallacarboranes have been studied[70], although here we will study COSANE, FESANE and some chlorinated derivatives of COSANE in more detail, as they are the metallacarboranes used in this doctoral thesis.

Previous work has shown that cobaltabis(dicarbollide) anion can be modified by halogenations, [71] and it has the ability to produce a stepwise modulation of its redox potential by each B-X (X=halogen) added. Our group demonstrated that sequential substitution of B-H by B-X units gives an average $E_{1/2}$ shift, close to 0.13 V, to more positive values of potential. [72] This sequential process is exclusive from it structure. The shift induced by each Cl atom in cobaltabis(dicarbollide) is in average about +0.1 V, approximately to more positive values, as is showed in (**Figure I.5**).

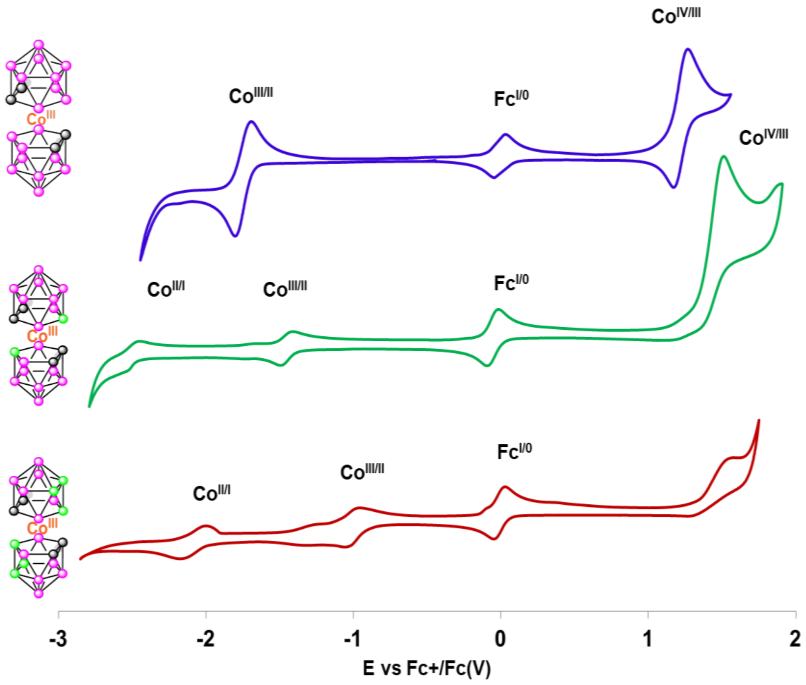

Figure I.5. CV of **COSANE** (blue), **Cl$_2$-COSANE** (clear green) and **Cl$_6$-COSANE** (dark red) in CH$_3$CN+ 0.1M TBAH. All potentials *vs* Ferrocene.

Comparing the E$_{1/2}$ redox potentials for the pure COSANE , that are -1.75 and -2.64 V *vs* Fc for the redox couples Co$^{III/II}$ and Co$^{II/I}$, respectively (for the Co$^{IV/III}$ the E$_{1/2}$ is 1.22 V *vs* Fc)[70] and the FESANE, the redox potential will be more positive. The ferrabisdicarbollide shows potentials of 0.76 and -0.78 V vs Fc for the redox couples Fe$^{IV/III}$ and Fe$^{III/II}$, respectively, as is showed in (**Figure IV.6**). The easy modulation of the redox potentials of metallacarboranes described, allow use them in different applications where the catalysis is one of them.

These metallacarborane complexes have been tested as catalysts in synthetic processes such as hydrogenation, hydroformylation, hydrosilylation, carbonylation, amination, alkylation, sulfonylation, the Kharasch reaction, polymerization, and ring opening metathesis polymerization.[73]

There is a wide history about the implication of metallacarborane complexes in catalysis in diverse areas, however there are no studies reported in the literature, about the photooxidation catalysis of organic compounds with metallacarboranes as catalyst.

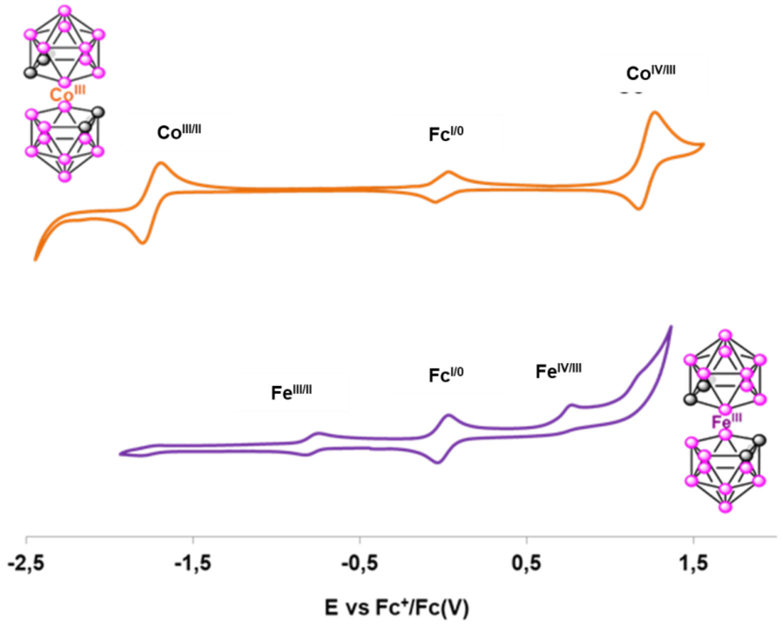

Figure IV.6. Comparison cyclic voltammetries of **COSANE** (orange) and **FESANE** (purple) in CH_3CN+ 0.1M TBAH. All potentials *vs* Ferrocene.

1.3. Ruthenium complexes

Ruthenium is a metal situated in the d group of the periodic table. The electronic configuration of this, allows the displaying of a wide range of oxidation states, from -2 to +8) in their complexes. The synthetic versatility of these in different oxidation states makes these complexes particularly interesting. Other characteristics are their high electron transfer capacity,[74] the robust character of their coordination sphere, their redox-active capacity, their easily available high oxidation states, their application as redox reagents in many different chemical reactions, and their ability to stabilize reactive species like oxo-metals[75] and metal-carbene complexes.[76]The robust character of their coordination sphere and the other properties mentioned before, make ruthenium complexes specifically advantageous for catalytic transformations, such as cyclopropanation,[77] isomerization,[78] metal-promoted radical reactivity,[79] oxidation,[80]addition,[81] hydrogen generation,[82] hydrogenation,[83] C-H and C-halogen bond activation[84] and olefin metathesis.[85] Furthermore, the wide utility of ruthenium complexes with heterocyclic N-donor ligands have been demonstrated due to their attractive spectroscopic, photophysical and electrochemical properties,[86] which led to important applications in different areas such as photosensitizers for photoactive conversion of solar energy,[87] molecular electronic devices and photoactive DNA cleavage agents for therapeutic goals.[88]

1.3.1. Ruthenium polypyridyl aqua complexes

Numerous publications about hexacoordinated ruthenium complexes containing polypyridyl ligands, like 2,2'-bypyridine (bpy) or 2,2':6',2"-terpyridine (trpy), have been reported, because of their ligand stability towards oxidation and their magnific coordinative capacity, enhanced by their chelating effect , giving a high stability to the formed complex. When an aqua ligand is directly attached to the ruthenium center, the redox properties of these complexes become particularly interesting. In that event, a proton-coupled-electron transfer (PCET) is possible, becoming the high oxidation states fairly accessible.[89] The successive oxidation form Ru(II) to Ru(IV) are accompanied by a sequential loss of protons and electrons favored by the increased acidity of the bonded aqua ligand. Hence, the initial Ru^{II}-OH_2 is oxidized to Ru^{IV}=O, passing through a Ru^{III}-OH specie (**Scheme I.1**).

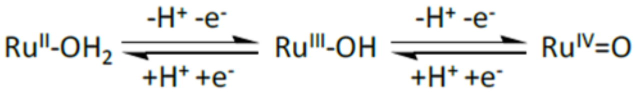

$$Ru^{II}\text{-}OH_2 \underset{+H^+ +e^-}{\overset{-H^+ -e^-}{\rightleftharpoons}} Ru^{III}\text{-}OH \underset{+H^+ +e^-}{\overset{-H^+ -e^-}{\rightleftharpoons}} Ru^{IV}{=}O$$

Scheme I.1. PCET oxidation process characteristic of Ru-aqua complexes.

The coordinated aqua ligand to the metal decreases the redox potential values due to the production of protons upon oxidation. This equilibrium is promoted by the successive deprotonation and the following electronic stabilization of the higher oxidation states by the oxocomplex formation, thanks to the more acidic character of the deprotonated aqua ligand. The Latimer diagrams allow comparing the basic trends of different polypyridyl ruthenium complexes (**Scheme I.2**), where the electronic configuration of each compound is important in redox processes due to the fact that a rising or loss of electrons takes place from $d\pi$ levels. In the case of ruthenium chloride complexes, the Ru(III/II) oxidation occurs at low potentials (0 V) however a rising in charge and oxidation state changes the Ru(IV/III) changes the Ru (IV/III) oxidation to greatly positive potentials (1.7 V). [90] When the chloride ligands are changed by pyridine and water ligands, the rising in charge and the changes in bonding rise the potential of the Ru^{III}-OH/Ru^{II}-OH_2 redox couple (from 0 to 0.67 V) in comparison to that corresponding to chloride complexes. [91]

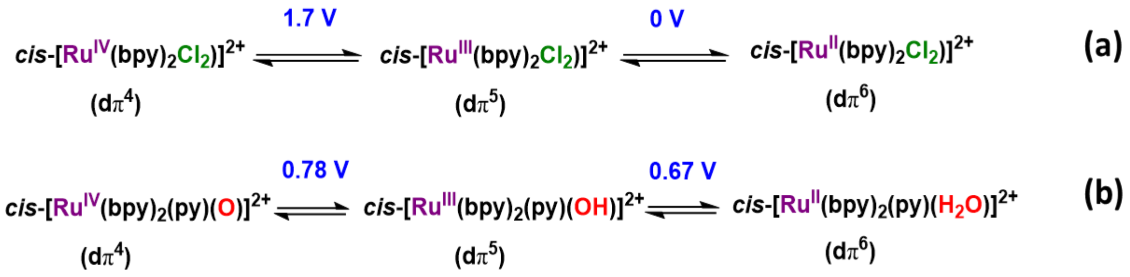

Scheme I.2. Latimer diagrams of ruthenium polypyridyl complexes (a) without and with (b) a coordinated water molecule. V *vs* NHE, M=0.1 at pH=7.

The reactivities of the oxocomplexes in ruthenium are related to different elements, affecting the values of half-wave potential, $E_{1/2}$, and the stability of the complex. One of the elements, are the modification of the ancillary ligands. The modulation of the reactivity by tuning their redox potentials, furthermore with the selectivity improvement of the catalysts, derived in a variety of studies oriented to the redox properties of the complexes, with a large number of ligands with different electronic and geometric nature.[92] There is a strong effect over Ru(IV/III) redox couples potentials in different complexes N-containing ligands. [93] The range of potentials for Ru(IV/III) and Ru(III/II) couples is important for the mechanism. Since the accessibility of both Ru^{III} and Ru^{II}, Ru^{IV} can act as a one-or two-electron oxidant. It is worth mentioning that oxocomplexes with a two-electron process is important due that the fact that this type of catalyst gives concerted reactions preventing a radical mechanism which allow the encouragement of unwanted secondary reactions.[94,95]

Due to these properties, polypyridyl ruthenium complexes with aqua ligands have been extensively employed in catalytic oxidation reactions of organic substrates by a

PCET process[96] or an oxygen transfer.[97] Furthermore, ruthenium polypyridyl aquo complexes participate in different oxidation reactions, like the epoxidation of alkenes, the cleavage of double bonds, the oxidation of alcohols and ethers and the oxidation of amines and amides among other catalytic processes. The orbital and energetic properties of $Ru^{IV}=O$ promote different manner to operate, like outer-sphere electron transfer, PCET, electrophilic ring attack, oxo transfer, hydride transfer and C-H insertion.

In this thesis we have taken advantage of catalytic capabilities of a $Ru\text{-}OH_2$, in a cationic form together with metallacarboranes, working in a cooperative manner, to carry out the photoredox oxidation catalysis of different alcohols and alkenes in water.

I.4. Homogeneous and heterogeneous catalysis. Supported Catalysts

The term Catalysis was coined by Berzelius more than 150 years ago and the current definition is: “A catalyst is a substance that increases the rate of approach to thermodynamic equilibrium of a chemical reaction without being consumed”.[98]

In general, the broad concept of Catalysis is shared by two topics homogeneous and heterogeneous catalysis. The first type of catalysis supposes that both catalyst and substrate are in the same phase; meanwhile in the second one is in a different phase (solid and liquid respectively). In the context of the last group, a supported catalyst consists in the immobilization of a homogeneous catalyst on the surface of an insoluble solid, a support. Furthermore, it can be considered as a heterogeneous catalyst. Currently, the development of these systems is subjected to strong ecological and economical demands for sustainability lead by a green chemistry approach for catalytic reactions. [99] The main differences between the types of catalyst are showed at the table **(Table I.1).**

Homogeneous catalysts have the advantage that they are well defined on a molecular level with well-defined active sites and speedily soluble inside the reaction medium. Such single-site catalysts are extraordinarily accessible to the substrates and frequently show high catalytic activity and selectivity, despite off to work under mild conditions. Therefore, there is an invariable energetic interaction among the active sites and the substrate. From the perspective of sustainability and industrial applicability, homogeneous catalysts are often expensive and generate further waste and their regeneration is difficult. In addition, the constitution of the catalyst by expensive noble metal and/or ligands makes the processes more expensive. Thus, the recyclability of the homogeneous catalysts supposes a crucial matter in the mark of sustainability of large-scale industrial production of fine chemicals, such as for enantioselective transformations in which the cost of the ligands frequently surpasses that of the metals used.[100] Therefore, despite their intrinsic advantages, homogeneous catalysts are used in less than 20 % of the industrially relevant processes.[101]

Table I.1. Scheme of comparison among homogeneous, heterogeneous, and supported catalyst.

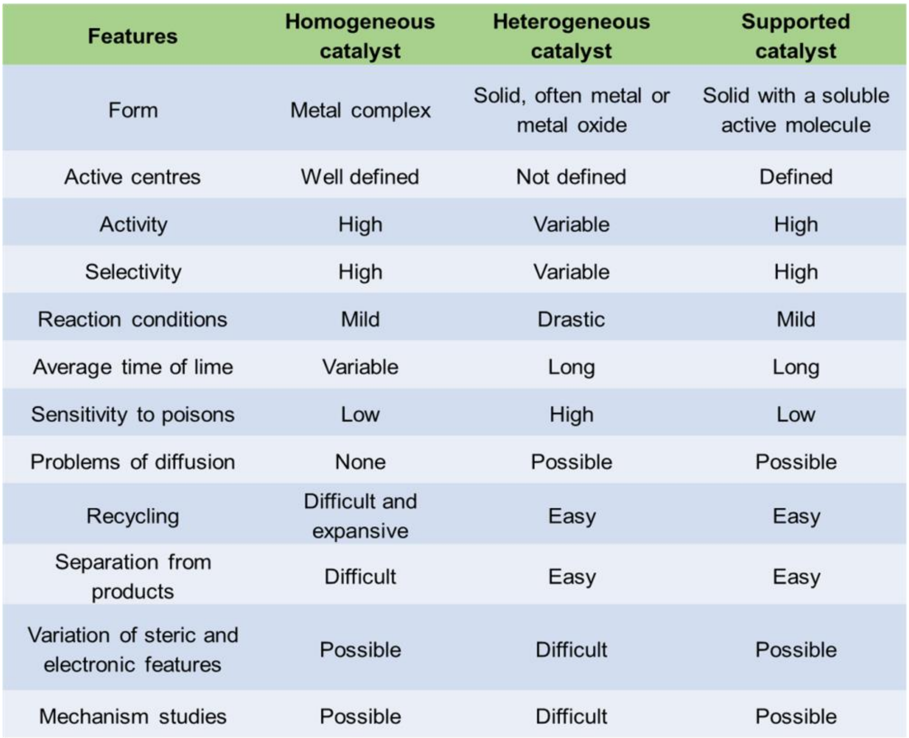

Features	Homogeneous catalyst	Heterogeneous catalyst	Supported catalyst
Form	Metal complex	Solid, often metal or metal oxide	Solid with a soluble active molecule
Active centres	Well defined	Not defined	Defined
Activity	High	Variable	High
Selectivity	High	Variable	High
Reaction conditions	Mild	Drastic	Mild
Average time of lime	Variable	Long	Long
Sensitivity to poisons	Low	High	Low
Problems of diffusion	None	Possible	Possible
Recycling	Difficult and expansive	Easy	Easy
Separation from products	Difficult	Easy	Easy
Variation of steric and electronic features	Possible	Difficult	Possible
Mechanism studies	Possible	Difficult	Possible

It is worth mentioning, that heterogeneous catalytic systems allow the simple product and catalyst separation, along with the recovery from the reaction medium, easy manipulation, and for their recycling. Moreover, they are frequently several active sites in catalysis that differ in activity and selectivity in the bulk commodity of the heterogeneous systems, which are challenging to probe on a molecular level. Furthermore, the synthetic procedures are concerted and therefore not necessarily reproducible. [102] Additionally, the situation of the actives sites in a microporous environment frequently causes diffusion control of the catalysed reaction and decreases the activity and selectivity of the system. Hence, the development of novel catalysts that combine the best attributes of each type of systems become an interesting and growing area in catalysis. These improved catalysts are named supported catalysts. [103] Based on the development of the studies made for this thesis we will focus on the grafting of homogeneous catalyst on a solid support with a high surface area, such (e.g. magnetic nanoparticles, MNPs), being a good approach.[104]

I.4.1. Different immobilization strategies and supports

The purpose of supported catalysts is to merge the advantages of homogeneous and heterogeneous catalysts such as: (1) great activity, selectivity and reaction rates contributed by the homogeneous catalysis, (2) simple catalyst recovery and sustained recyclability, as well as preparation of multifunctional catalysts contributed by the heterogeneous one. Between the different techniques described to immobilize catalysts into solid supports, the methods frequently used[98] **(Figure I.7)** are adsorption,[105] electrostatic immobilization,[106] encapsulation,[107] ionic liquid,[108] and covalent binding (anchoring).[109]

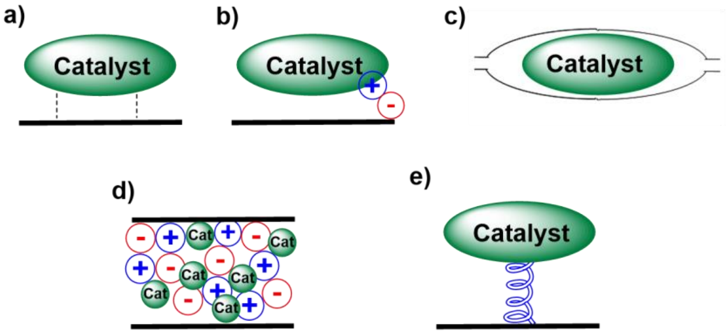

Figure I.7. Schematic representation of different strategies for catalyst immobilization: a) adsorption, b) electrostatic immobilization, c) encapsulation, d) ionic liquid, and e)covalent binding.

Between the different techniques used for the inmobilization of the catalyst the electrostatic inmobilization is a simple and quick approach to the formation of heterogeneous catalytic systems.

• Magnetic Nanoparticles and core-shell magnetic nanoparticles supports

Among the different types of existing supports, we will focus on magnetic nanoparticles and core-shell magnetic nanoparticle that will be the object of study in this doctoral thesis.

The definition of Nanoparticles (NPs) can be related to microscopic particles with a diameter of 1-100 nm.[110] They can be considered as a connection between homogeneous and heterogeneous catalysis, usually referring us to a kind of “quasihomogeneous “systems or in other words soluble heterogeneous systems.[111]

The nanoparticles are classified depending on their properties, shape and composition.[112] These materials are of significant interest due to the singular properties in compensation of the small sizes. The properties exhibited by these particles are different than that of the same materials in their bulk counterparts owing to the greater surface to volume ratio that they have. NPs have different shapes like spheres, rods, tetra-pods, wires, belts, rings disks etc. which aids in the attainment of interesting results in their properties. Depending on the overall shape of NPs, these can up to 3D.

Currently, magnetic nanoparticles (MNPs), as iron oxide nanoparticles, have emerged growing attention due the exclusive physical properties as the high surface, supermagnetism and low toxicity. All these properties spread the field of applications.[113] Different iron oxides are currently in use: iron (II) oxide (FeO), iron (III) oxide (Fe_2O_3) and iron (II, III) oxide (Fe_3O_4). In catalysis usually species as Ƴ-Fe_2O_3 or maghemite and Fe_3O_4 or magnetite are used. They are often referred to as SPIONs (Super Paramagnetic Iron Oxide Nanoparticles) as they show superparamagnetic properties due to their size. The synthesis of magnetic nanoparticles (MNPs) has been intensively developed for many technological[114] and medical applications.[115]

In the case of Fe_3O_4 materials, the simplicity of preparation, surface-functionalization and recycling from the solution by an external magnetic field make the Fe_3O_4 nanoparticles ideal for the separation of the reaction system and reuse of the catalyst supported on that.[116] Inside the groups of core-shell structured composites, silica-coated magnetic nanoparticles highlight in the field of catalysis due to their potential applications, furthermore with the fact that each nanoparticle is formed by a well-defined magnetic nucleus which is enclosed by a microporous silica shell and a broad surface are-to volume ratio and easy functionalization (**Figure I.8**). [117]

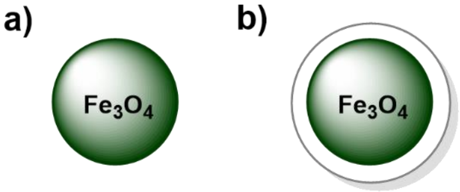

Figure I.8. a) Magnetic nanoparticle. b) silica-coated magnetic nanoparticle.

As we mentioned before, from the point of view of sustainability and industrial applicability, the anchoring of a homogeneous catalyst on a solid support with a high surface area, such magnetic nanoparticles (MNPs) suppose an advance. To avoid undesired oxidation and agglomerations, it is mandatory the suitable coating with a layer of material, as we mentioned before, leading to core-shell magnetic particles for their stabilization and where to link the actives sites. These materials combine the magnetic properties of the core with the possibility to further functionalize the surface.[118] Additionally, the application of an external magnetic field enables the removal of the particles in a simple way.[119]

Recently, core-shell multi-components have attracted serious attention due to their potential applications in a catalytic context.[120]

I.5. Catalytic oxidation reactions

During the last years a set of research are focused to imitate natural systems that carry out chemical transformations with magnific efficiency in the context of selectivity and energy consumption. Particularly, the oxidation of organic substrates has received an extraordinary interest.[121] Oxidation of organic substrates mediated by transition metals is a relevant process from an industrial point of view.[122] The high selectivity in the oxidation of starting materials is important for the industry, due to the aim for the production of oxygen-containing chemicals from fossil hydrocarbons preventing the complete conversion to carbon dioxide. To achieve selective oxidation is commonly a problem in the synthesis of fine chemicals, given that it is still challenging to cleanly add an alcohol function at the wanted position of a drug precursor similarly as enzymatic systems work. Many enzymes are present in nature acting as “biological catalysts” able of catalyzing oxidation reactions in living organism.[123] Metals in enzymes work in complex biochemical reactions and greatly specialized biological functions due to their capability to be in different oxidation states and several geometries. Despite biomimetic catalysts of iron[124] or manganese[125] are extensively studied, different studies with ruthenium have been published.[126]

I.5.1. Alcohol oxidation reactions

The oxidation of primary and secondary alcohols to, aldehydes, ketones and carboxylic acids is a fundamental reaction in organic synthesis.[127] Primary alcohols (R-CH_2-OH) can be oxidized either to aldehydes (R-CHO) or to carboxylic acids (R-CO_2H). The direct oxidation of primary alcohols to carboxylic acids normally proceeds via the corresponding aldehyde, which is transformed via an aldehyde hydrate (R-$CH(OH)_2$) by reaction with water before it can be further oxidized to the carboxylic acid (**Figure I.9**).

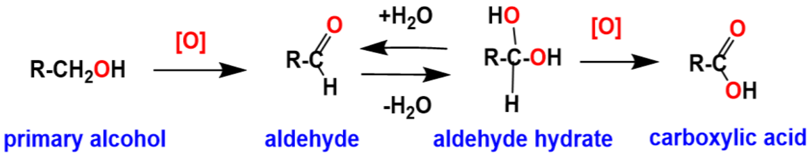

Figure I.9. Mechanism of oxidation of primary alcohols to carboxylic acids via aldehydes and aldehyde hydrates. [O]=oxidant reagent.

The conversion of alcohols to aldehydes or ketones is of great relevance, as have been shown by the number of publications.[128] This process has practical importance in the hydrogen-based energy technologies because the anodic liberation of protons and electrons can be coupled on a cathode for hydrogen fuel production in an integrated photochemical cell (**Equation I.1**).[129] In recent years, alternative methods for the selective oxidation of alcohols to aldehydes or ketones have been developed in the mark of green and environmentally acceptable processes.[130]

However, there are not many catalytic systems based on metals abundant in nature, as photocatalysts for the oxidation of alcohols, where the compound acts as catalyst and photosensitizer.

$$\mathbf{RCH(OH)R' \rightarrow RC(=O)R' + 2H^{+} + 2e^{-}} \qquad \textbf{Equation I.1.}$$

In the context of efficient systems supported on silica-coated magnetic nanoparticles for chemical alcohol oxidation, Rossi and coworkers[131] reported about the use of magnetically recoverable supports for the immobilization of gold nanoparticles (AuNP) as catalysts. The catalyst preparation is based on the immobilization of Au^{3+} on the surface of core-shell silica-coated magnetite nanoparticles, followed by metal reduction. The catalyst resulted to be active in the aerobic oxidation reactions, but less selective for the aldehyde product. Years after, Gawande, Sharma and coworkers[132] reported about a new and efficient manganese-based magnetic nanocatalyst developed through a covalent grafting of the manganese acetylacetonate complex onto amine-functionalized silica-coated iron-core nanoparticles and the resulting nanocatalyst was found to be efficient for selective and greener oxidation of organic halides and alcohols to desirable carbonyl compounds in terms of excellent yields with high turnover number. This catalytic protocol included effortless magnetic recovery, employment of H_2O_2 as the sole and green oxidant, and nontoxic solvents, that are mild reaction conditions, operating in shorter reaction times.

Safaei and coworkers[133] reported about the immobilization of a complex of iron(III) amine bis(phenolate) on silica-coated magnetic nanoparticles as a new magnetically recoverable catalyst (Fe_3O_4@SiO_2-APTES-FeL^{GDC}). The latter sustainable catalyst leads to the efficient oxidation of a wide range of alcohols and sulfides with excellent conversion and selectivity under mild conditions.

All these examples described in the literature are efficient systems supported on silica-coated magnetic nanoparticles for chemical alcohol oxidation; however, no examples of well-defined molecular photoredox catalysts supported on the previously mentioned MNPs have been described.

I.5.2. Epoxidation of alkenes

Olefin epoxidation has received considerable interest from both academics and industry. Epoxides constitute an important and versatile class of intermediates and building blocks to obtain more elaborated chemical products both in organic synthesis and in industrial production of bulk and fine chemicals.[134,135] Epoxides can be transformed into a variety of functionalized products (**Figure I.10**). For example reductions, rearrangements or ring-opening reactions with various nucleophiles give diols, aminoalcohols, allylic alcohols, ketones, etc.[136-139] Starting from alkenes four general methods are available: the Jacobsen-Katsuki epoxidation that uses a Mn catalyst and NaOCl or variations of these,[140,141] the Prilezhaev reaction uses commercially available m-CPBA,[142,143] the Sharpless epoxidation that uses *tert*-butyl hydroperoxide and is catalyzed by Ti(O*i*Pr)$_4$,[144,145] and the Shi epoxidation that uses oxone and a ketone as a catalyst to generate dioxirane.[146,147] Most of these processes have been studied by chemical catalysis in organic media by some of us.[148,149,150] A common characteristic is that all these reactions are carried out in organic solvents.

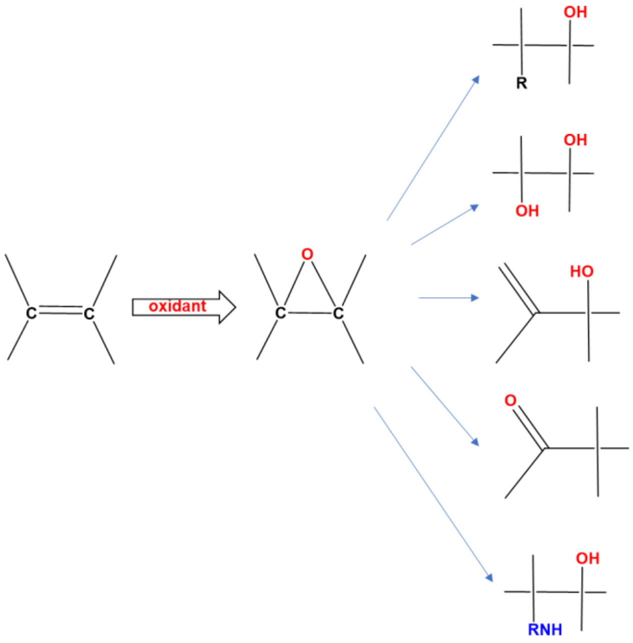

Figure I.10. Epoxidation of alkene substrate and possible further transformations.

In 2017, Romero, Teixidor and coworkers,[151] reported carboranyl-carboxylate complexes as precatalysts in epoxidation reactions, using peracetic acid as the oxidant. These studies are based on Mn or Co complexes, all containing the carboranylcarboxylic ($1\text{-}CH_3\text{-}2\text{-}CO_2H\text{-}1,2\text{-}closo\text{-}C_2B_{10}H_{10}$) ligand. This work highlights that the coordination of the carboranylcarboxylic ligand to the metal ions is important for the performance of the complexes as catalysts. In these studies, was demonstrated that the manganese complexes were more active in the epoxidation of different alkenes than the cobalt complex.

Currently, photochemical systems studied for the oxidation of substrates involve a photocatalyst[152] or a photocatalyst combined with a transition metal catalyst based on polypyridyl compounds.[153,154,155,156,157,158] In these, one compound acts as the light-harvesting antenna and the second metal complex is used as catalyst to activate a water molecule or an organic substrate by a proton coupled electron transfer mechanism (PCET) (vide infra). However, few examples of photochemical epoxidation of alkenes have been carried out with earth abundant metals.[159,160]

I.6. Catalysis and sustainability

Most of the homogeneous catalysts mentioned in the previous section for organic transformations, operate in organic media. Nevertheless, today, chemical processes and even at the industrial production level, are undergoing an intense transformation in order to meet sustainability criteria, where obsolete methods are renewed in accordance with the principles of green chemistry.[161] It is mandatory the use of compatible chemicals with human health and the environment, instead of that harmful and hazardous, and among these the solvent replacement is especially important since amounts of solvents are usually much larger than those of reagents and products.

In this context, new solvents should exhibit small environmental impact, no toxicity, and no volatility to meet the demands of sustainability. [162] Water has been much under-investigated as a solvent for chemical transformations basically because of poor solubility of organic molecules; however, water is the “ideal solvent” [163] being economic, non-toxic, non-inflammable and compatible with the environment. Substitution of organic solvent by water is desirable, but it becomes especially suited for those chemicals transformations in which water is one of the reagents.

Currently, one of the challenges is to design catalysts to improve the control on the activity and selectivity of the chemical processes, and in a parallel manner, they should be compatible and friendly with the environment. Light can be considered an ideal reagent for environmentally friendly, green chemical synthesis; unlike many conventional reagents, UVA, visible, and IR lights are nontoxic and generate no waste. There is consensus that solar energy combined with water is the best alternative energy source for the development of non-fossil-based fuels.[164] Hence, the development of photocatalytic methods and systems for organic transformations is an important challenge in this aspect.[165] The photoredox catalysis which uses the absorption of light radiation through a catalyst to generate reactive radicals that activate stable low-energy organic molecules through single-electron processes (oxidation or reduction) is a successful way of imitating nature in efficiency and sustainability.

I.7. Principles of Photoredox catalysis

Photoredox catalysis is an emerging methodology where light is used to alter the redox properties of compounds then accelerating chemical reactions by electron transfer between a photocatalyst and a substrate.[166] In particular, photoredox catalysis employs small quantities of a light-sensitive compound that, when excited by light, trigger single-electron transfer (SET) processes with substrates upon radiation.

The interaction of simple organic molecules with light is generally weak; however photocatalysts can absorb light with greater efficiency and converting the energy of an absorbed photon into chemical potential that can be used to transform organic substrates.

The photoredox catalysis facilitates access to highly reactive radical species under mild conditions that often cannot be generated using other non-photochemical strategies.

Mimic processes that occur in nature is one step forward in the development of a sustainable chemistry. In this sense, the photosynthesis is a source of inspiration for scientists; in this process, plants convert light energy into chemical energy.[167]

Then, photoredox catalysis that use the absorption of light radiation by a catalyst that generates reactive radicals and activates stable low-energy organic molecules through single-electron processes (oxidation or reduction), is a successful way of mimic nature in efficiency and sustainability.[167,168]

There is consensus that solar energy combined with water is the good alternative energy sources for the development of non-fossil-based fuels.[169] A great effort has been dedicated to catalysis activation of organic molecules.

Photoredox strategies have been used in diverse fields offering excellent benefits in terms of atom economy. So in the pharmaceutical industry, protocols for the direct and selective functionalization of drug-like scaffolds (amination, halogenation, and alkylation)[170] and late-state functionalization of biologically active heterocycles[171] have been developed. Another benefit of photoredox catalysis in the industrial production is the use of renewable resources, the reduced environmental impact and the energetically efficiency. An example could be the revalorization of bulk biomass and feedstock materials for the production of value-aromatic feedstock chemicals through the lignin of different plants,[167] or the easy functionalization of hydrocarbon feedstock as methane.[172]

These examples highlight the potential of photoredox catalysis for a circular chemistry, which aims is to replace today's linear 'take–make–dispose' approach with circular processes.

I.7.1. Mechanisms of photocatalysis

The interaction between an electronically excited photocatalyst and the substrate can result in the generation of diverse reactive intermediates. Then a photochemical synthesis could take place according to different mechanistic pathways (**Scheme I.3**).[173]

1. Photoinduced electron transfer, which involves one-electron oxidation or one-electron reduction of a substrate by the photocatalyst, occurring an outer-sphere reaction on the photoexcited metal centre. (path **i** and **ii**)
2. Photoinduced atom transfer, which an atom or group is transferred from the substrate to the photocatalyst, with the formation of a radical and an inner sphere reaction can takes place on the photoexcited metal centre. (path **iii**).
3. Photoinduced energy transfer, which electronically excited photocatalyst can activate the substrate via energy transfer to yield electronically excited species, (path **iv**).

The majority of photoinduced reactions occur through the first or second mechanisms; however there are few examples of reactions catalyzed through photoinduced energy transfer.

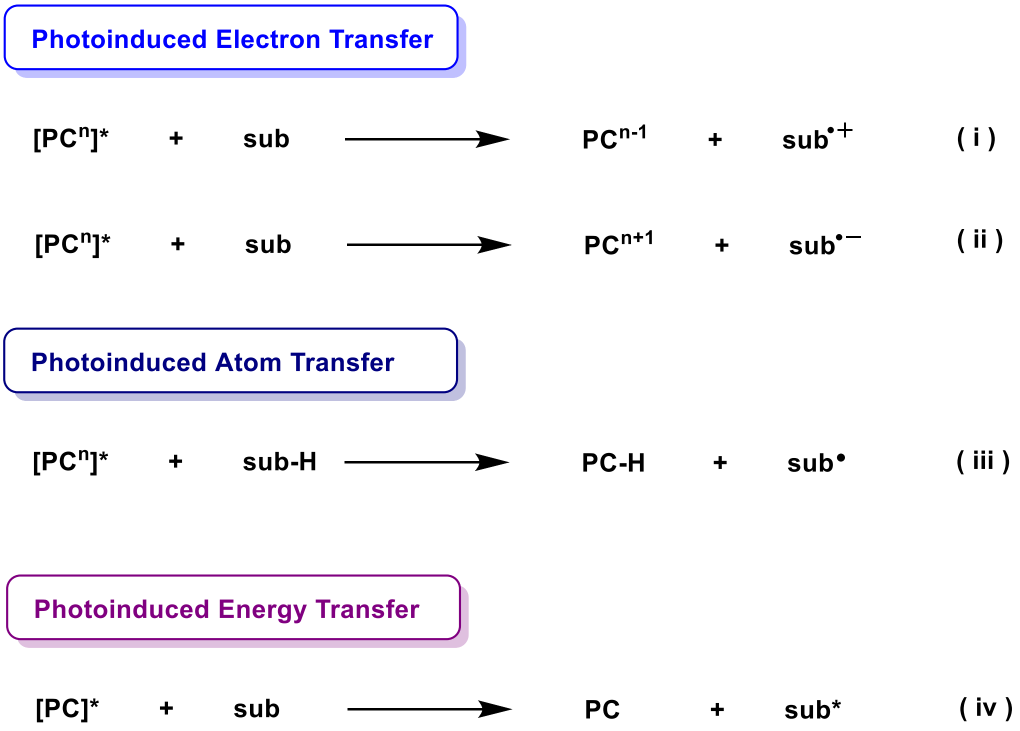
Photoinduced Electron Transfer
$[PC^n]^* + sub \longrightarrow PC^{n-1} + sub^{\bullet +}$ (i)
$[PC^n]^* + sub \longrightarrow PC^{n+1} + sub^{\bullet -}$ (ii)
Photoinduced Atom Transfer
$[PC^n]^* + sub\text{-}H \longrightarrow PC\text{-}H + sub^{\bullet}$ (iii)
Photoinduced Energy Transfer
$[PC]^* + sub \longrightarrow PC + sub^*$ (iv)

Scheme I.3. Mechanisms of Homogeneous Photocatalysis. Scheme extracted and modified from ref. 173.

Photoinduced promotion of an electron from the HOMO to the LUMO orbital, results in the formation of an electronically excited state that can formally be conceptualized as a charge-separated electron-hole pair. In a photoredox process the absorption of a photon results in the generation of an electronically excited state; this can undergo relaxation back to the ground state via a number of unimolecular emissive and non-emissive pathways at relatively rapid rates. The redox properties of the excited state, however, can lead to a fast electron transfer to an electron-deficient acceptor or oxidative quencher (A) or from and electron-rich donor or reductive quencher (D) compound. Regeneration of the photochemically active state requires a second electron transfer process from others donor or acceptor species. (**Figure I.11**) displays the mechanism.

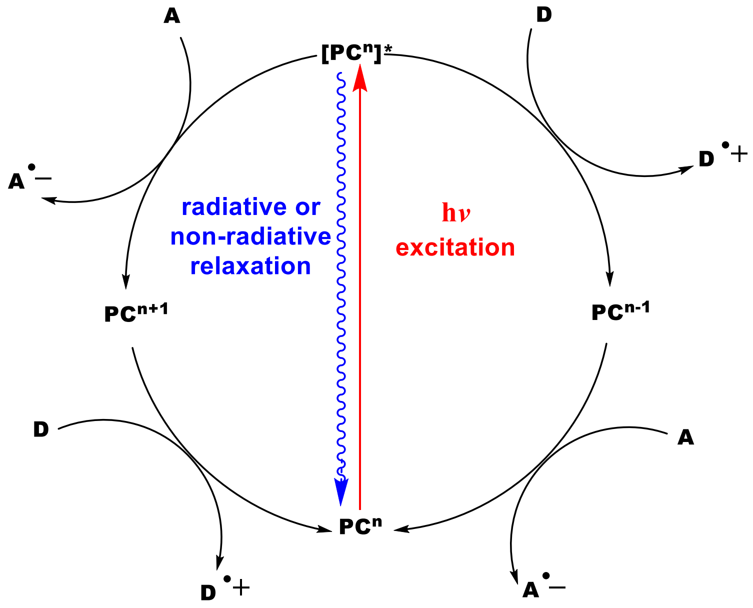

Figure I.11. Photoinduced electron transfer (PET). Figure extracted and modified from ref. 173.

It is important to outline the main points that need to be considered when choosing photocatalyst:

1) The photocatalyst must have a good absorption over a wide range of wavelengths that the other species in the reaction mixture do not absorb.

2) The yield of formation of the reactive excited state should be as high as possible. This concept is influenced both by intrinsic quantum yield of its formation (the efficiency with which the reactive excited state is formed upon photon absorption), as well as the absorption cross-section as measured by the compound's concentration and molar absorptivity.

3) The excited state lifetime must persist enough to undergo the desired reaction with the substrate.

4) The photophysics of the photocatalyst must be reversible (*i.e.,* no degradation in the absence of quencher). In electron transfer catalysis, the photocatalyst should exhibit reversible electrochemical behaviour. Both of these

characteristic are important to maintain the viability of the chromophore as part of the catalytic cycle.[174]

5) The excited-and ground-state redox potentials of the photocatalyst must provide for an exothermic reaction.
6) In an ideal form, the excited-state properties of the photocatalyst should be easily tuned through synthetic modifications to facilitate the adaptation of the excited-state reactivity of the photocatalyst to the reaction desired.

I.7.2. Different photocatalytic approaches.

Light induced reactions have become an important and powerful issue in metal-catalysed transformations. Photocatalysis can be systemized into three categories: A) photocatalysis that enables the transformation to occur either via redox- or atom transfer; the photocatalyst is not involved in the bond-forming /breaking event. The processes occur through an outer-sphere mechanism. B) Cooperative/dual photocatalysis, which synergistically combines the first strategy with a transition metal catalysis. C) The photocatalyst is a transition metal that enables the bond-forming/breaking event, and then the processes occur through an inner-sphere mechanism.

This introduction focuses on the development of A and B photoredox catalyst in relation to the oxidation of organic substrates.

A. Outer-sphere photoredox catalysis

Electron-transfer processes are initiated by the absorption of a photon by a chromophore, (*i.e.,* the photocatalyst). These systems take the advantage of the enhanced redox reactivity of the chromophore in it excited state to facilitate a reaction that would not proceed otherwise; in this direction, light provides the added energy needed to make the reaction thermodynamically viable.[175] The photoredox catalyst is able to transform the light into chemical energy and performs the selective molecule activation, simultaneously, by means of the mechanism of photoredox catalysis.

The most common photocatalysts are based in transition metal complexes; between them the more studied and employed are the polypyridyl ruthenium[176,177] and iridium[178] complexes (**Figure I.12**).

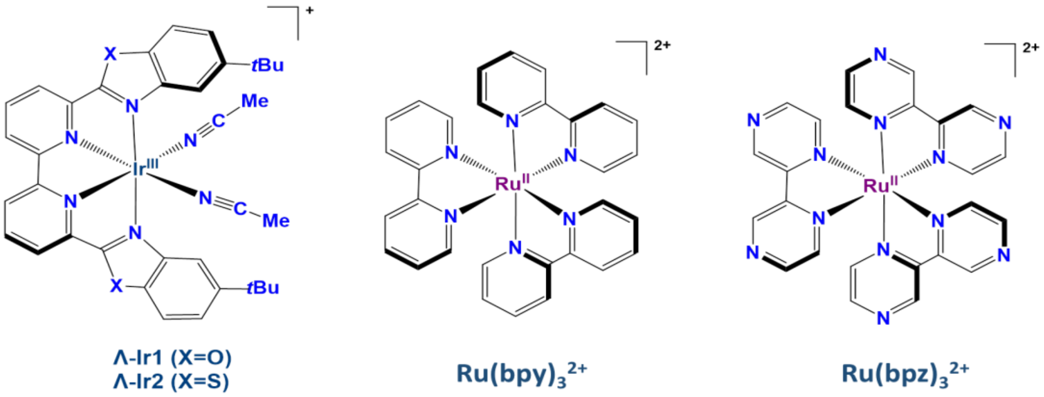

Figure I.12. Chemical structures of some polypyridyl complexes as photoredox catalyst. Figures reproduced from ref: 176,177,178.

For the complex tris(2,2'-bipyridine)ruthenium (II) upon absorption of a photon in the visible region, an electron is excited from one of the photoredox catalyst's metal-centered *d*-orbitals to a ligand-centered π* orbital,[179] thus this transition is termed a metal to ligand charge transfer (MLCT). During this process, exists a reductive and oxidative quenching cycle in which are produced $[Ru(bpy)_3]^+$, a strong reducing agent −1.76V *vs* Fc$^{+/0}$ in CH_3CN, and $[Ru(bpy)_3]^{3+}$, a strong oxidant (+0.85 V *vs* Fc$^{+/0}$ in CH_3CN), respectively [180]. The highly studied octahedral tris (2,2′-bipyridine)ruthenium(II) ($[Ru(bpy)_3]^{2+}$),[181] participates in electron transfer through an outer sphere mechanism, that implies that no major structural modification occurs upon ET. In the photoredox catalyst the ligand-centered π* orbital is lower in energy than the metal-centered e_g orbital. Upon irradiation, an electron is transferred from the t_{2g} orbital from the metal to the π* orbital from the ligand which after rapid intersystem crossing results in an excited triplet state, as is showed in (**Figure I.13**).[182]

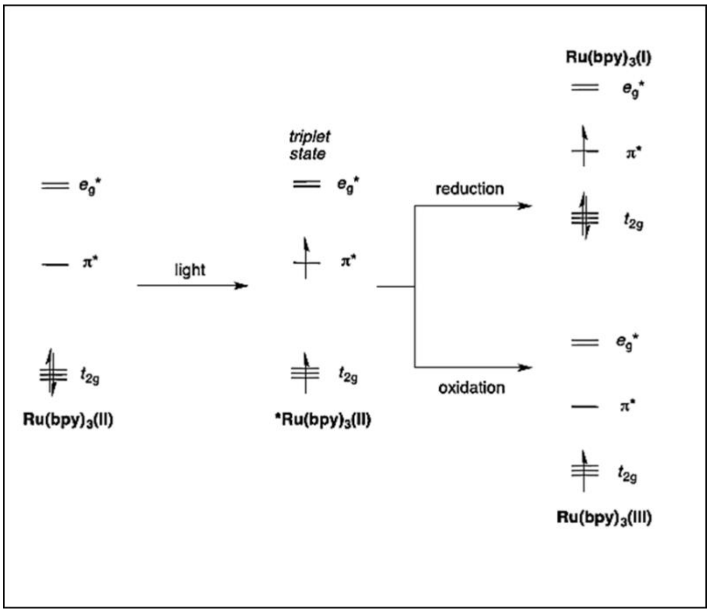

Figure I.13. Ruthenium polypyridyl complex: simplified molecular orbital depiction of $Ru(bpy)_3^{2+}$ photochemistry. Figure adapted from ref. 182.

The electronic absorption spectrum of $[Ru(bpy)_3]^{2+}$ shows (**Figure I.14 a**), an intense absorption at 285 nm that corresponds to a ligand-centered transition ($\pi_L \rightarrow \pi_L*$).[183] The band in the visible region (Λ_{max}=452 nm) corresponds to a metal-to-ligand charge-transfer (MLCT) transition. The energy of the MLCT band can be as the amount of energy necessary to reduce the ligand and oxidize the metal. This type of excited state can be though as the promotion of an electron from a metal-based orbital to one ligand like character. This transition is a simultaneous photo-induced oxidation of the metal center and the reduction of the ligand that gives a chemical specie as $[Ru^{III}(bpy^{\bullet -})(bpy)_2]^{2+}*$**(Figure I.14 b).**[184] Due to this spatial redistribution of electron density, this transition is responsible of better reactivity of the excited state with respect to what is observed in the ground state and makes the compounds a candidate to be a photoredox catalyst.

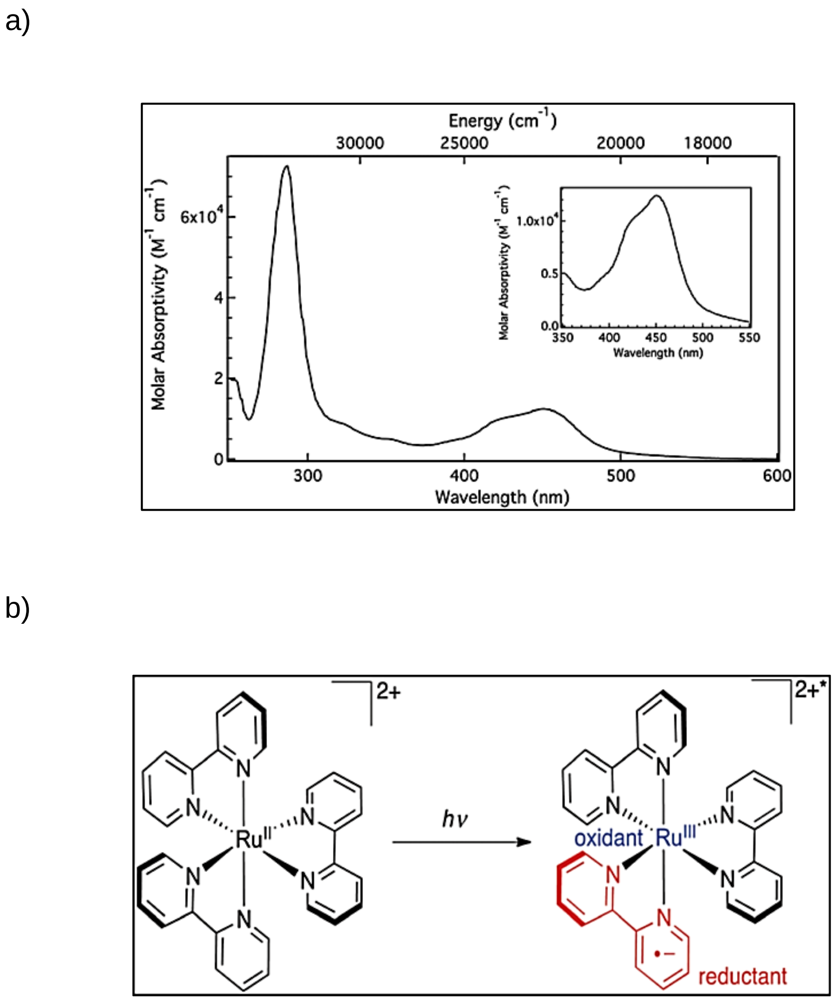

Figure I.14. a) Electronic absorption spectrum of $[Ru(bpy)_3]^{2+}$ in acetonitrile solution at room temperature. The inset shows an expanded view of the metal-to-ligand charge transfer band. b) Representation of a MLCT state in $[Ru(bpy)_3]_2^+$. Figures extracted from ref. 175.

Another features can be seen in the absorption spectrum of $[Ru(bpy)^3]^{2+}$, one at 330 nm and the other at 350 nm. Their origin could be due to ligand-field or “d-d” transitions within the d-orbital of the metal. These metal-centered transitions redistribute electronic density into orbitals that are antibonding with respect to the metal-ligand bonds and thus typically promote photodissociation.[185] A molecular orbital-based description of these various transitions is shown in **Scheme I.4**.

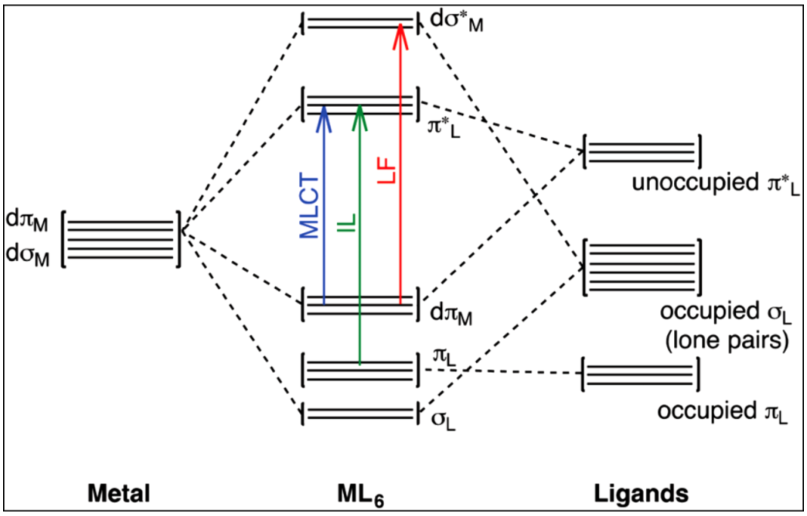

Scheme I.4. Simplified molecular orbital diagram for an octahedral compound with π-acceptor ligands. The main types of electronic transitions typically observed in metal polypyridyl complexes are indicated by the arrows. Scheme adapted from ref. 175.

In this sense, Cano-Yelo and Deronzier[186] reported about the feasibility of photo-oxidation by visible light of some alcohols to aldehydes, catalysed by Ru(II) polypyridyl complexes in presence of diazonium salts as quenchers and basic agents.

Rocha et al.[187] reported a ruthenium complex $[Ru(O)(bpy)(tppz)]^{2+}$(**Scheme I.5 a**), with π-accepting N-ligands. The oxo-complex is produced directly from a single metal-to-ligand charge-transfer (MLCT) photoexcitation of the Ru^{II}-aquo complex in aqueous media. This photoinduced path to 2-electron/2-proton activation of mononuclear catalyst is enabled by thermodynamic instability of the intermediate Ru^{III}-hydroxo species, which disproportionate into the Ru^{IV}-oxo and Ru^{II}-aquo states as was reported by the electrochemical tests in a wide range of pH. The proton-coupled multielectron photocatalytic capability of the complex in neutral solution, at room conditions, was demonstrated through the dehydrogenative oxidation of benzyl alcohol into benzaldehyde with selectivity >99 %. The mononuclear complex act as chromophore/catalyst and the overall photocatalytic cycle is showed in (**Scheme I.5 b**)

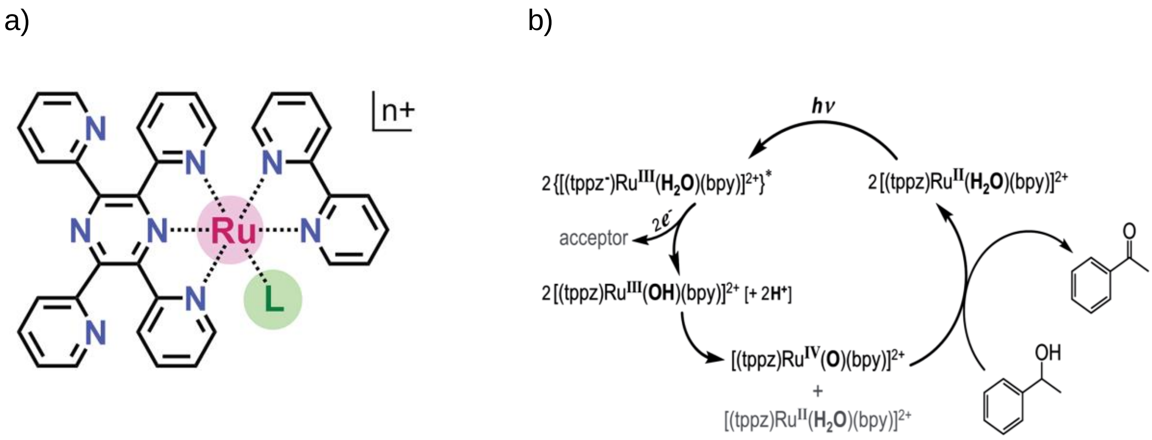
a)
b)
N
N
N
N
Ru
N
N
N
N
L
n+
hν
2{[(tppz·)Ru^III(H2O)(bpy)]2+}*
2[(tppz)Ru^II(H2O)(bpy)]2+
acceptor
2e⁻
2[(tppz)Ru^III(OH)(bpy)]2+ [+ 2H+]
[(tppz)Ru^IV(O)(bpy)]2+
+
[(tppz)Ru^II(H2O)(bpy)]2+
O
OH

Scheme I.5. a) The mononuclear complex [Ru(L)(bpy)(bpz)]$^{n+}$ (L=Cl$^-$,n=1) (L=H_2O, n=2) b) Main steps underlying the photocatalytic dehydrogenative oxidation of benzyl alcohol into benzaldehyde by the mononuclear complex [Ru(H_2O)(bpy)(tppz)]$^{2+}$. Scheme modified from ref. 187.

Z. Amara and co-workers published almost recently about the efficient immobilization by adsorption and photochemical reactivity of [Ru(bpy)$_3$]Cl$_2$ on silica in the context of photochemical oxidations with singlet oxygen ($^1O_2$), as is shown in (**Figure I.15**).[188] The adsorption of the latter ruthenium compound on unmodified silica particles provides opportunities in the intensification of photochemical oxidations with almost 10-fold increase in reactivity. This outstanding performance is attributed to noncovalent outer-sphere interactions between the substrate and the solid particles, because higher concentrations of reactive species are produced at the interface. This catalytic system was efficiently recycled and shows an up to 4-fold increase in stability, compared to its homogeneous counterpart.

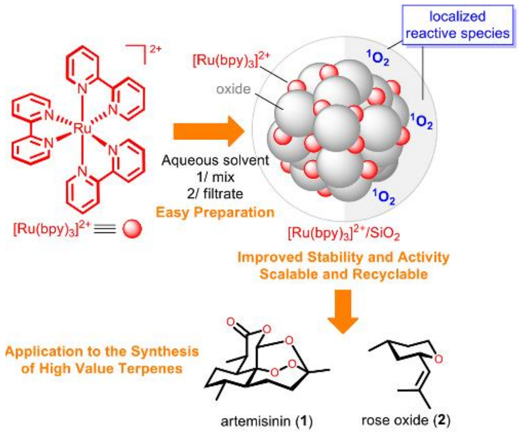
localized reactive species
$[Ru(bpy)_3]^{2+}$
oxide
$^1O_2$
$^1O_2$
$^1O_2$
Aqueous solvent
1/ mix
2/ filtrate
Easy Preparation
$[Ru(bpy)_3]^{2+}$ ≡
$[Ru(bpy)_3]^{2+}/SiO_2$
Improved Stability and Activity
Scalable and Recyclable
Application to the Synthesis of High Value Terpenes
artemisinin (1)
rose oxide (2)

Figure I.15. a) Schematic general approach to improve productivity in visible-light photochemical reactions: adsorption of cationic photocatalyst on an oxide. This approach is applied to the synthesis of two commercially important terpenes: artemisinin (1) and rose oxide (2). Figures extracted and modified from ref. 188.

As we have seen, photoredox catalysis with metal complexes as sensitizers and catalysts frequently relies on the use of precious metals like ruthenium or iridium. Recently, some progresses are made with respect the use of complexes made from earth-abundant elements in photoredox catalysis. In the context of photoredox catalysis oriented to the oxidation of substrates, metals as copper, tungsten or vanadium are reported in the literature.

Polyoxometalates (POMs) are metal oxide nanoclusters that can adopt a wide variety of structures.[189] These complexes are stable, have acid-base and redox properties, and have received much attention especially in the field of oxidation catalysis.[190] Therefore, POMs are attractive materials for application as photocatalysts. Upon irradiation with UV and /or near UV light takes place a intramolecular charge transfer from the O^{2-} based highest occupied molecular orbital (HOMO) to the W^{6+} based lowest unoccupied molecular orbital (LUMO), leading to the formation of photoexcited states that are highly reactive, as oxidizing agents, allowing them to be used for photocatalytic reactions. Photocatalytic oxidation of organic compounds such as alcohols, alkanes and alkenes can be carried out under aerobic conditions using UV-driven decatungstate photocatalysis, as is showed in (**Figure I.16**). The irradiation of decatungstate generates short-lived excited states that decay to form the reactive specie, which is responsible for the subsequent transformation of the organic substrates. Thus, the reaction of the excited catalyst may occur by HAT and /or SET.

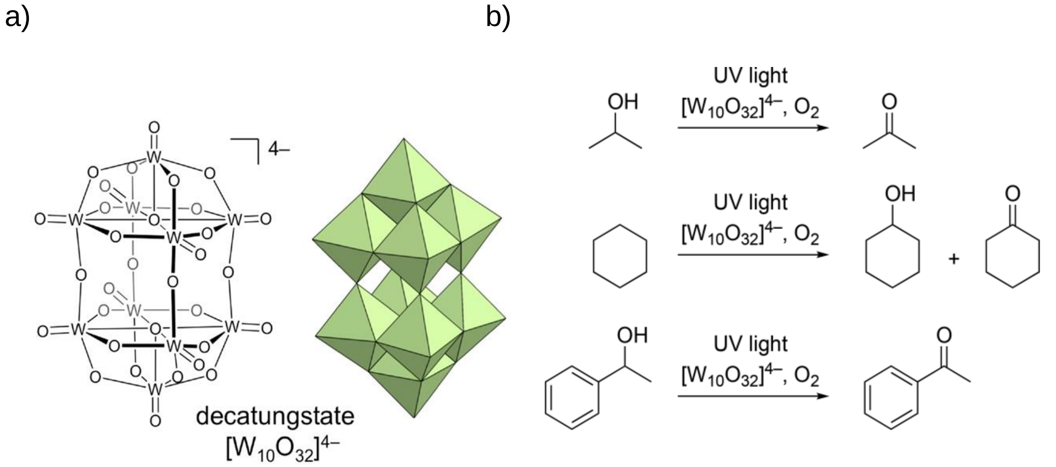

Figure I.16. a) Anionic structure of decatungstate POMs. b) Decatungstate Photocatalysis for oxidation of aliphatic alcohols, alkanes, and aromatic alcohols under aerobic conditions. Figures extracted and modified from ref. 190.

The first example of photoredox catalysis using copper (I) complex was reported by Sauvage et al.[191] The group reported the C-C coupling of benzylic bromides to form bibenzyl derivatives or benzyl aldehydes using $[Cu(dap)_2]Cl$ as the photocatalyst.

Owing to its abundance on the Earth and inexpensiveness, copper catalysts are particularly attractive for different organic processes, like C-H alkenylation, alkynylation, and amination of arenes via two-electron or single electron processes (SET).[192] K. C. Hwang and co-workers,[193] developed a visible light-induced photo-redox copper-catalyzed oxidative Csp^2-H annulation of amidines with terminal alkynes at room temperature to synthesize functionalized quinazolines, using O_2 as oxidant. Copper (I)-phenylacetylide catalyzed this reaction at room temperature, and it have been demonstrated the application of this method to the synthesis of anti-cancer compounds (**Scheme I.6**).

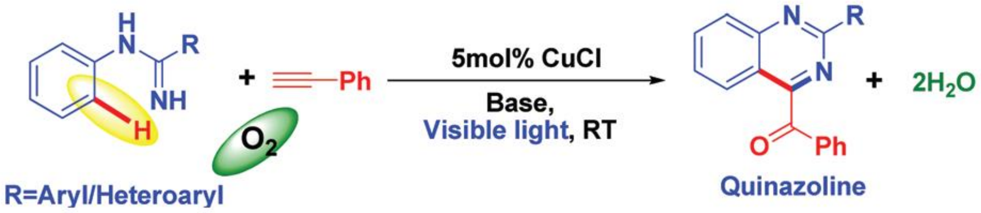

Scheme I.6. Transition Cu-catalyzed synthesis of quinazolines using inexpensive CuCl as catalyst, without ligands/organic oxidants and reaction at room temperature being an environmentally benign and economically feasible reaction. Scheme extracted from ref. 193**.**

X-D. Chen and coworkers[194] reported metal-organic frameworks (MOFs) copper-based as promising catalysts under the point of view of their environmental friendly features such as the use of renewable and sustainable energy of visible light and potential catalyst recyclability. The group developed potential heterogeneous photocatalysts, a family of three copper (II) coordination polymers bearing different Cu-O assemblies with ligands 4,4′-disulfo-[1,1′-biphenyl]-2,2′-dicarboxylate acid (H4DSDC), namely, $\{[Cu_7(DSDC)_2(OH)_6(H_2O)_{10}]\cdot xH_2O\}_n$, as is shown in (**Scheme I.7**). The polymer catalyzes the visible-light oxidation of alcohols at mild conditions using hydrogen peroxide as an oxidant, demonstrating a satisfactory efficiency. For this photoreaction, the extent of oxidation over aryl primary alcohols was fully controllable with time-resolved product selectivity, giving either corresponding aldehydes or carboxylate acids in good yields. It is worth mentioning, that the photocatalyst was able to be recovered quantitatively once the reaction was finished without any structure changes, and it could be recycled for catalytic use for at least five cycles with constant efficiency.

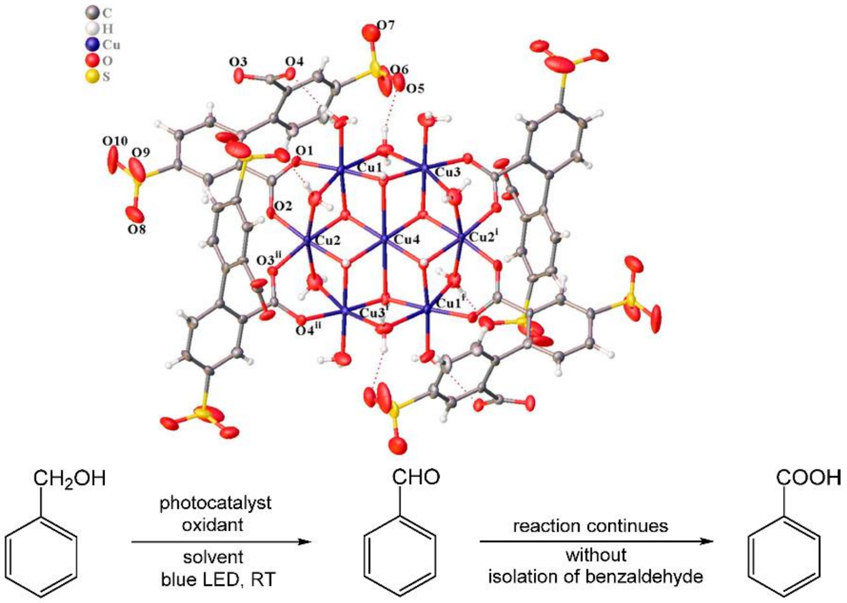
C
H
Cu
O
S
O7
O3
O4
O6
O5
O10
O9
O1
Cu1
Cu3
O2
O8
Cu2
Cu4
Cu2^{i}
O3^{ii}
Cu3^{i}
Cu1^{i}
O4^{ii}
CH$_2$OH
photocatalyst
oxidant
solvent
blue LED, RT
CHO
reaction continues
without
isolation of benzaldehyde
COOH

Scheme I.7. On the top: $[Cu7(\mu_3\text{-}OH)_6(H_2O)_{10}]^{8+}$ cluster in complex surrounded by DSDC^{4-} ligands, showing coordination geometries of the Cu(II) centres. On the bottom: Reaction conditions for the photooxidation of benzyl alcohol to benzaldehyde (t= 24 h) and benzoic acid (t= 60 h). Schemes modified and extracted from ref. 194.

H-S. Soo and co-workers[195] reported a vanadium photocatalyst for the transformation of hydroxyl-terminated polymers such as polyethylene glycol, the block co-polymer with polycaprolactone, and the non-biodegradable polyethylene into fuels and chemical feedstocks, such as formic acid and methyl formate (see, **Figure I.17**). This work integrates the benefits of the photoredox catalysis into environmental remediation and artificial photosynthesis. The cleavage and oxidation of the different aromatic alcohols yielded conversions > 95 % in most cases into different aldehydes, and hydroxylated derivatives using hydrogen atom transfer (HAT) as antioxidants to preserve the selectivity of the reaction over the production of the desired products when it was needed.

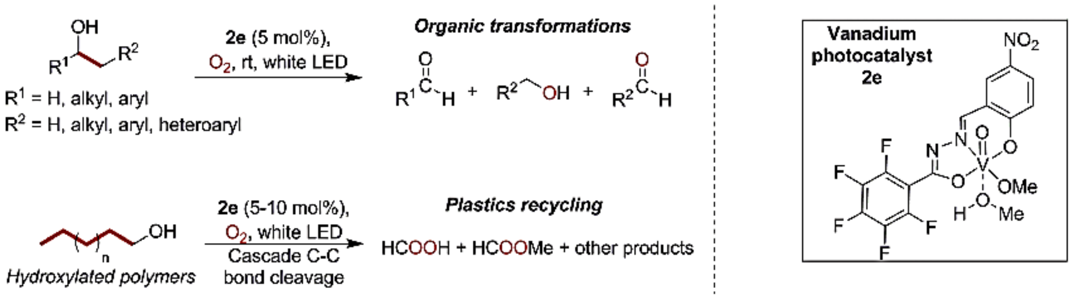
2e (5 mol%), O₂, rt, white LED
R¹ = H, alkyl, aryl
R² = H, alkyl, aryl, heteroaryl
Organic transformations
2e (5-10 mol%), O₂, white LED
Cascade C-C bond cleavage
Hydroxylated polymers
Plastics recycling
HCOOH + HCOOMe + other products
Vanadium photocatalyst 2e

Figure I.17. C-C bond cleavage reaction in different large alcohols using the catalyst depicted as 2e (on the right). Figure extracted and modified from ref. 195.

The use of *iron catalysts* in photochemistry has sprung up owing to their abundance, low price, nontoxicity, and novel properties, including the exhibition of ligand to metal charge transfer states. To date, there have been important progresses on the utilization of iron complexes in photoredox catalysis for organic transformations.[196]

In this direction an iron catalyst for visible-light-driven oxidation reactions was developed by Wolf and co-workers[197] for the photocatalytic oxygenation of alkyl benzenes delivering the desired ketones and carboxylic acids with high yields and selectivity. In this system, a tris(2-pyridylmethyl)amine iron complex was used to catalyze the disproportion of hydrogen peroxide produced in the reaction, which prevented the degradation of the vitamin B_2 derivative riboflavin tetraacetate (RFT) as well introduced on the reaction, owing to the low concentration of H_2O_2.

Selective oxidation of alkanes is an efficient method to synthesize alcohols and ketones.[198] Recently, iron (III) complexes were found to be efficient catalysts in photocatalytic oxidation reactions. Jiang, Quiao and co-workers[199] shows a tetrahalogenoferrate (III) complex as photocatalyst for the selective oxidation of alkanes. The method has been employed for the photooxygenation of benzylic $C(sp^3)$-H and the challenging aerobic oxidative transposition of vinyl halides, which allows a well chemoselective approach to carbonyl compounds in moderate to excellent yields.

Another iron complex $[(MeN_4Py)Fe^{II}(CH_3CN)]^{2+}$ was reported by Browne et al.[200] the complex catalyzed the oxidation of methanol to formaldehyde using molecular oxygen as oxidant under the irradiation at 365 nm at room temperature, achieving

TON=50 in the oxidation reaction.[201]

Cerium is among the earth-abundant elements (~$10^{1.5}$ atoms per 10^6 atoms of Si), with comparable abundance to copper, and cerium reagents have been widely used in synthetic and material chemistry, displaying a wide range of photocatalytic pathways for organic transformations. Related with the substrate oxidations, J.-J. Guo et al.[202] reported recently about the photocatalytic alkoxy radical-mediated transformations, based on a previous work reported by the same group.[203] Under redox-neutral conditions, in the presence of catalytic amounts of cerium trichloride and tert-butylammonium chloride, cyclic alcohols could be directly oxidized to aminated ketones via an alkoxy radical-mediated C-C bond scission and radical amination pathway. This protocol could be applied to the efficient and selective C-C bond functionalization of a wide range of cyclic alcohols. Hence, numerous secondary alcohols can also be cleaved and functionalized, under the catalytic conditions, to achieve the formation of cyclic ketones via direct oxidation.

B. Cooperative photoredox catalysts

Cooperative photoredox catalysis entails a new progress in this field and refers to a first catalyst that is photochemically active, while the second is redox-active in the absence of light.[204] This strategy allows multielectron photoredox catalysis with the help of a second redox catalyst, avoiding the single electron transfer (SET) imposed by the photoredox catalyst. The union in one single complex of a photoredox catalyst and a transition metal catalyst could result in higher efficiency and may lead to new selective light-induced organic transformations.

Inside the mark of cooperative photoredox catalysis oriented to photoredox oxidation reactions we will expose different examples classified in base on the nature of the system, thus, we can find different cooperative systems: i) based in two separate complexes in the reaction media (photoredox catalyst and transition metal catalyst); ii) based in one complex that contents both parts linked by an organic linker or iii) sharing a common bridging ligand or are directly connected.

B.1. Cooperativity in photoredox catalysis in two separate complexes.

Inside the mark of the formation of carbon-carbon bonds, the concept of cooperative photoredox catalysis operates well for selective oxygenation of organic molecules with a ruthenium or iridium complexes photoredox catalyst and transition-metal catalysts **(Scheme I.8).** The mechanism of two-electron transfer is commonly used for the transformation of one organic molecule, although a single-electron transfer is more frequent inside the mark of photoredox catalysis. Thus, the use of a catalyst based on transition-metals to accumulate two oxidation events generated by a photoredox catalyst to engender a high valence state , results in a good option for the oxidation of one molecule.

Fukuzumi, Nam and co-workers reported in 2011[205] about a cooperative effect between Mn complex (**m1**) and Ru-complex photoredox catalyst (**a**) **(equation 1, scheme I.8)** in different oxygenation reactions such as the epoxidation of alkenes and the hydroxylation of alkanes with water as the oxidant**.** The oxidative quenching of the excited Ru complex by $[Co^{III}(NH_3)_5Cl]^{2+}$ leads to a Ru^{III} specie, which can induce the oxidation of Mn^{III} to Mn^{IV}. Accompanied by the oxidation of water, i.e., PCET, the Mn^{IV} is oxidized by another Ru^{III} that leads to Mn^{V}-oxo specie, from which the oxygen atom transfers to the organic substrate, resulting in an oxidation product with high quantum efficiency. The selective oxygenation of sulfide using sodium persulfate as sacrificial electron acceptor have been done using a Fe complex (**m2),** [206] which works in a cooperative manner with the photoredox catalyst of ruthenium **(Scheme I.8 a) (equation 2, scheme I.8)**.

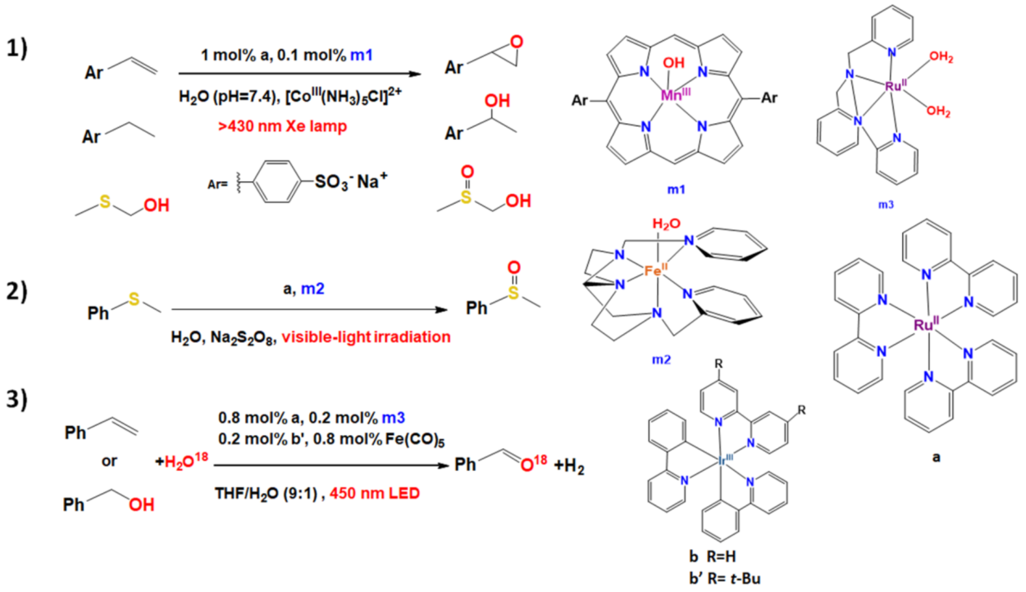

Scheme I.8. Cooperative photoredox catalysis in two separate complexes. Schemes extracted and modified from ref: 205, 206 and 207.

Zhao and co-workers,[207] demonstrated the coupled production of H_2 and oxygenation of a hydrocarbon carried out with two photoredox catalysis reactions working in concert. **(equation 3, scheme I.8)**. The oxidation catalyst **m3** to Ru^{IV}-oxo driven by Ru^{III}, generated by the oxidative quenching of Ru complex (**a**), performs the half-reaction of the oxygenation of the hydrocarbon; the reduction catalyst $Fe(CO)_5$ driven by Ir^{II} formed by the reductive quenching of Ir complex (**b'**) executes the reduction of protons. The electrons exchange of the two excited photoredox catalyst stabilizes the charge of the overall system.

More recently, Mn(V) nitride complex $[Mn(N)(CN)_4]^{2-}$ was reported as an efficient catalyst for visible-light induced oxidation of alkenes and alcohols in water using $[Ru(bpy)_3]^{2+}$as photosensitizer and $[Co(NH_3)_5Cl]^{2+}$ as a sacrificial oxidant. Alkenes were oxidized to epoxides and alcohols to carbonyl compounds, through proton-coupled electron transfer (PCET) processes.[208]

At the same time, Stephenson and co-workers reported about successful dual photoredox/Pd catalysis for the efficient oxidation of several lignin model substrates to their corresponding ketone in high yields, an oxidation mechanism is shown in (**Scheme I.9**).[209]

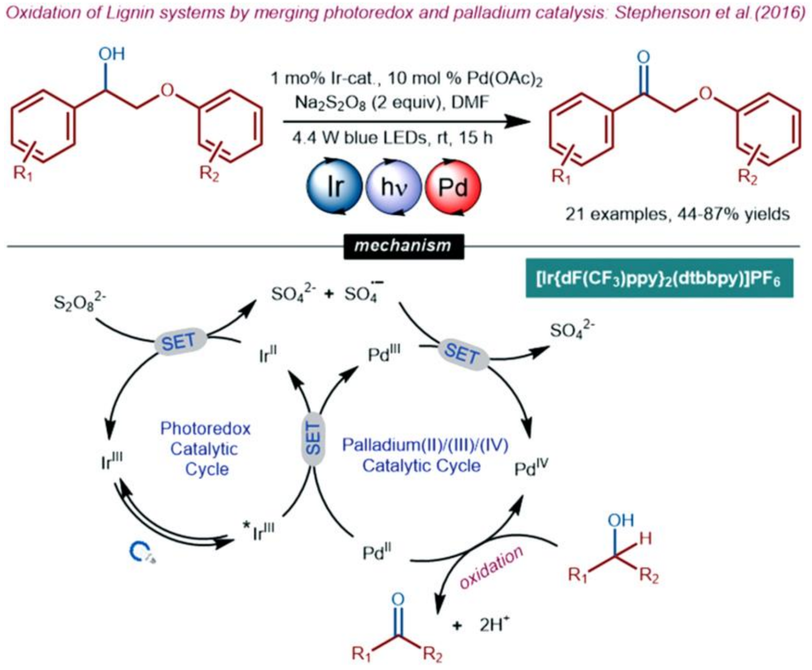
Oxidation of Lignin systems by merging photoredox and palladium catalysis: Stephenson et al.(2016)
OH
O
R1
R2
1 mo% Ir-cat., 10 mol % Pd(OAc)2
Na2S2O8 (2 equiv), DMF
4.4 W blue LEDs, rt, 15 h
Ir
hν
Pd
21 examples, 44-87% yields
mechanism
[Ir{dF(CF3)ppy}2(dtbbpy)]PF6
S2O8 2-
SO4 2- + SO4•-
SET
Ir II
Pd III
SO4 2-
Ir III
Photoredox Catalytic Cycle
Palladium(II)/(III)/(IV) Catalytic Cycle
Pd IV
*Ir III
Pd II
oxidation
H
+ 2H+

Scheme I.9. Oxidation of lignin systems by merging palladium with photocatalysis. Scheme extracted from ref. 209.

B.2. Cooperativity in photoredox catalysis in one complex.

The linking of a photoredox catalyst and a transition metal catalyst into one complex could to leave to an enhancement of the efficiency of the catalytic reaction or may be new activity for the selective visible-light-induced organic transformations.

In a general overview, two methods are reported about the linking of a photoredox catalyst and a transition-metal catalyst, in one, the photoredox catalyst and transition-metal catalyst are connected with an organic linker, where both parts can operate independently in their common roles; in the other, the central metal atom of the transition-metal catalyst share a common bridging ligand or an organic linker or simply are directly connected. The merging of two complexes in a unimolecular system, considering that the linker does not alter the electronic properties, supposes the prediction of additional findings in comparison with the separate complexes.

B.2.1. Photoredox and transition metal catalyst connected by organic linkers.

In this context, Rocha and coworkers[210] have described the selective oxidation of alcohols to aldehydes in aqueous media performed by some ruthenium dyads (**aa**) and (**ab**) using $[Co^{III}(NH_3)_5Cl]^{2+}$ as sacrificial oxidant (**equation 1, scheme I.10**). Fu and Chao in 2013,[211] reported that the Ru-Fe complex **ac** can perform the oxygenation of triphenyl phosphine in aqueous media. In contrast to the reaction pathway exposed in previous where $Na_2S_2O_8$ plays the role as the electron acceptor, the role of $[Co^{III}(NH_3)_5Cl]^{2+}$ as an electron acceptor is less ambiguous. It only results in the oxidative quenching of the excited Ru unit in the complex (**ac**) to produce Ru^{III} (**equation 2, scheme I.10**). Accompanied by PCET, the consecutive oxidation of Fe^{II} with two Ru^{III} produces Fe^{IV}-oxo, transferring the oxygen atom to triphenyl phosphine.

Numerous photocatalytic reactions have been well established today and photocatalytic oxidation of organic substrates as the selective oxidation of organic sulfides is of significant interest.[212] Oxidation of sulfides can generate sulfoxides that are an important class of compounds in organic synthesis and pharmaceuticals.[213] Many homogeneous photocatalytic systems have been developed for this transformation using metal complexes and organic dyes.[214]

Almost at the same time, Hamelin, Torelli and co-workers[215] in 2015 reported about the visible-light-induced aerobic oxidation of sulphides to sulphoxide, using O_2 rather than water as the terminal oxidant, by means of Ru-Cu complex (**ad**) **(equation 3, scheme I.10)**. The Ru-Cu complex (**ad**) oxidates sulphide, phosphine, and alkenes in an efficient manner. The reaction is performed by the reductive quenching of the Ru unit by triethanolamine (TEOA) to produce Ru^{I} specie. Electron transfer from Ru^{I} results in the recovery of the Ru unit and the reduction of Cu^{II} to Cu^{I}. The latter can activate O_2 for the oxidation of organic substrates.

In this type of oxidation reactions, the loading of catalysts is still relatively high. For instance, several chromophore-catalyst assemblies containing ruthenium(II)-based chromophore were studied for this purpose using water as an oxygen source.[216] However, these photocatalytic procedures displayed limited TON numbers. In addition, sacrificial reagents are needed, but in some dyes display low stability upon irradiation in the presence of O_2 and can lower the TON even more.[217] With all this in mind, M. Zhao et. al.[218] reported about a molecular chromophore-catalyst assembly containing a chromophore ruthenium (II) center (Ru^{II}_{chro}) and a catalytic coper (II) center (Cu^{II}_{cat}).

This bimetallic complex was used in the photocatalytic oxidation of sulfides without sacrificial reagent in the presence of dioxygen under blue light irradiation. The procedures allowed to obtain TON=32000.

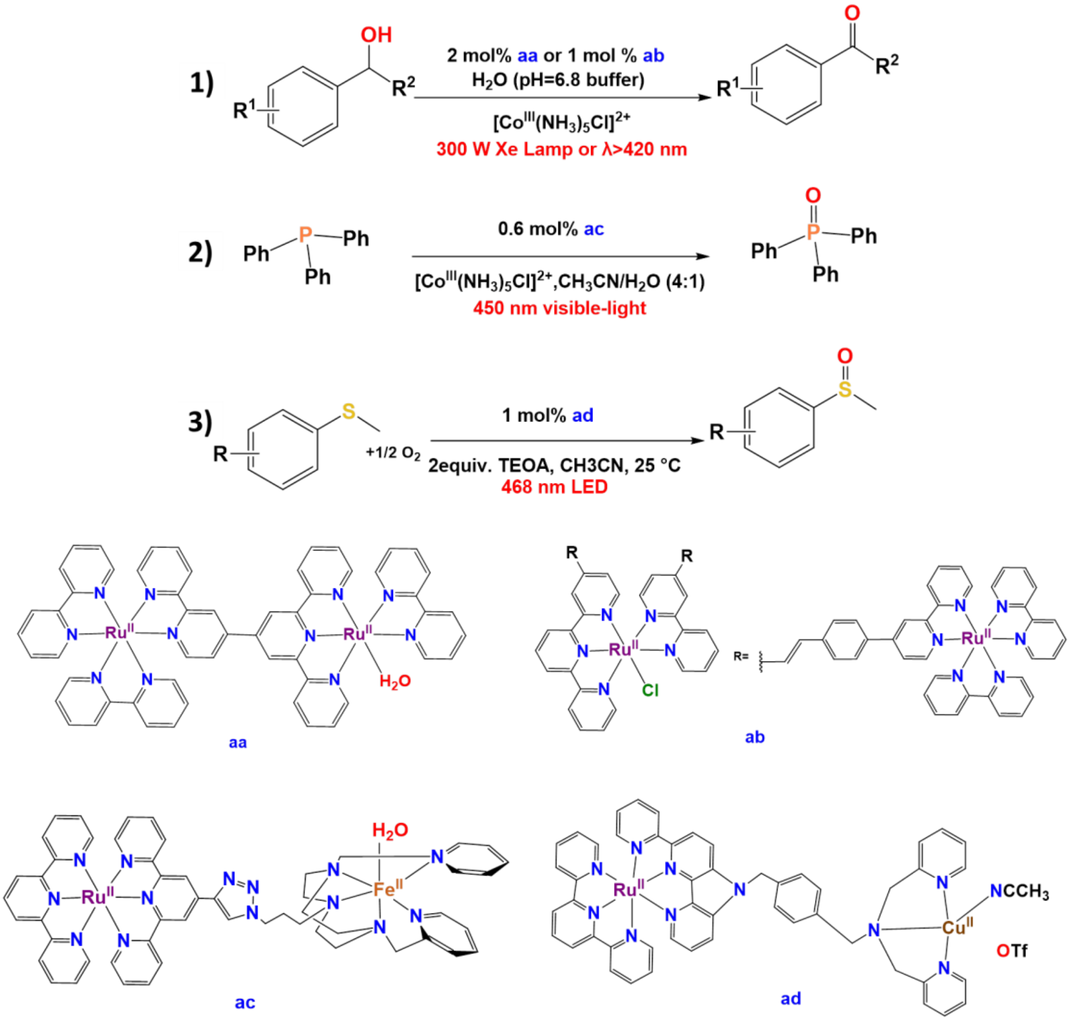
1)
OH
R1
R2
2 mol% aa or 1 mol % ab
H2O (pH=6.8 buffer)
[CoIII(NH3)5Cl]2+
300 W Xe Lamp or λ>420 nm
O
2)
Ph
P
Ph
Ph
0.6 mol% ac
[CoIII(NH3)5Cl]2+,CH3CN/H2O (4:1)
450 nm visible-light
3)
R
S
+1/2 O2
1 mol% ad
2equiv. TEOA, CH3CN, 25 °C
468 nm LED
RuII
H2O
aa
Cl
R=
ab
FeII
ac
CuII
NCCH3
OTf
ad

Scheme I.10. Organic-linker-connected photoredox catalyst and transition-metal catalyst for the oxidation of organic compounds. Scheme extracted and modified from ref: 210, 211, 212.

B.2.2. Photoredox and transition metal catalyst sharing a ligand.

As an alternative of an organic linker, a shared bridging ligand can connect the two functionalities together as well. The visible-light-absorbing unit, or a photoredox catalyst, and the bridging ligand and reactive central metal atom are the three interconnected components for a successful architecture that might upgrade existing discoveries or permit us to carry out novel tasks. The substitution of the electronic properties of the two central metal atoms with a shared bridging ligand is important.

Curiously, numerous reaction types that cannot be conducted with two separated complexes can be performed by through this paradigm of cooperative photoredox catalysis. The selective oxygenation of sulphides mentioned before, which can be performed with a mixture of a photoredox catalyst and a transition-metal catalyst, furthermore, can be performed with the Ru-Ru complex (**ag**), **(Scheme I.11) ,** where one Ru unit carry out the task of the redox catalyst.[219] The oxidative quenching of the excited Ru unit to Ru^{III} is accompanied by PCET to produce Ru^{IV}-oxo specie in the redox catalytic unit. The latter oxo specie confers the oxygen atom onto the sulphide to complete the oxidation reaction. The (**ag**) complex demonstrated to be more efficient than the bimolecular system.

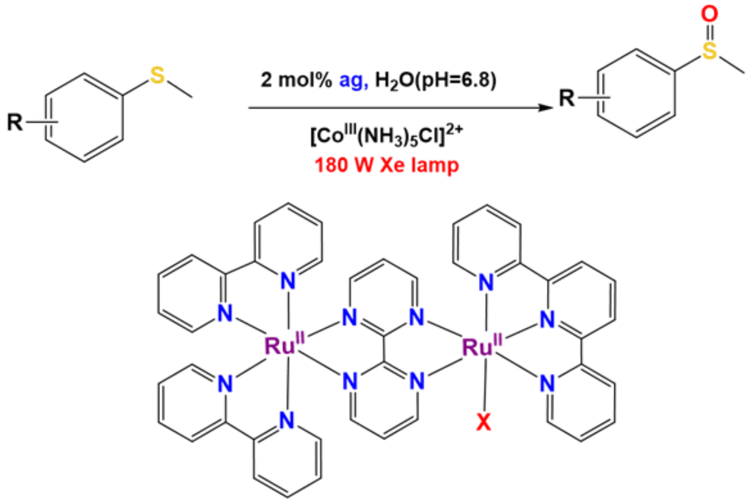

ag

Scheme I.11. Bridging-ligand-connected photoredox catalysts and transition-metal catalysts for organic transformations. Scheme extracted and modified from ref: 219.

Chapter III. Objectives

The main research lines of the groups where this PhD Thesis has been developed are, on the one hand, the evaluation of metallacarboranes compounds in diferent types of applications and, on the other hand, the study of transition metal compounds as catalysts and photocatalysts in oxidation reactions.

As it has been in the introduction chapter, metallacarboranes of the type cobaltabis*ortho*dicarbollide, which are the most representative of this group, are highly robust species able to withstand harsh conditions. Contrarily to some ruthenium compounds like $[Ru(bpy)_3]^{2+}$, the cobaltabis(dicarbollide) upon excitation no produces fluorescence. These properties motivated us to study the possible performance of metallacarboranes as a non-conventional photocatalyst. Metallacarboranes have never been used as part of a photocatalytic system, although they have been tested as catalyst in different synthetic processes. Metallacarboranes despite being purely inorganic molecules they have a substitution behaviour comparable or superior to organic frameworks, an important aspect that could introduce hybrid systems with new and interesting innovative features in photocatalysis.

On the other hand, one of the challenges of this century is to design improved active and selective catalysts respectful with environment. From a sustainable perspective, one of the ways that makes the reuse of catalysts and photocatalysts possible is their heterogeneization on solid supports. In this way, costs, toxicity and waste formation can be reduced.

For this purpose, the objectives of this thesis were the design of new systems based in metallacarborane compounds and their evaluation in photoredox oxidation catalysis of alcohols and alkenes, using a green methodology based in the use of water and light, together with the heterogeneization of these systems on the surface of magnetic nanoparticles.

On the basis of the above considerations , the specific objectives for this PhD thesis were:

- The synthesis and characterization of the cobaltabis*ortho*dicarbollide [Na.2,5 H_2O] [3,3'-Co(1,2-$C_2B_9H_{11}$)$_2$], **Na[1]**, and its dichloro [3,3'-Co(8-Cl-1,2-$C_2B_9H_{10}$)$_2$]$^-$ **[Cl$_2$-1]$^-$**, and hexachloro derivatives [3,3'-Co(8,9,12-Cl_3-1,2-$C_2B_9H_8$)$_2$]$^-$,**[Cl$_6$-1]$^-$** **(Figure II.1)** following the procedures described in the literature. We use sodium as counterion due to the high solubility of the corresponding metallabisdicarbollide in water.

- The computational studies through TD-DFT calculations, in order to get more detailed insight into the character of the electron transitions of $[3,3'\text{-Co}(1,2\text{-}C_2B_9H_{11})_2]^-$ and to know the type of charge transfer that takes place under excitations at 293 nm, which is the most intensive band in the UV spectrum.

- The study of the photocatalytic behavior of these compounds, in the photooxidation of alcohols in water, under different catalytic conditions, in some cases, under uncommon conditions from 0.01 to 0.1 mol% of catalyst. In all cases the metallabisdicarbollides perform two roles: photosensitizers and catalysts at once. Also, the study of the influence of lamp frequency on the efficiency of the catalysts.

- The study of the photoredox oxidation of alkenes in water by **Na[1]** and the optimization of conditions. For the purpose of comparison, we want to study the performance of the conventional photosensitizer tris(2,2′-bipyridine) ruthenium(II) ($[Ru(bpy)_3]^{2+}$), in the photoredox oxidation of alkenes, under the same catalytic conditions.

- The heterogenization of the homogeneous photoredox catalyst cobaltabis*ortho*dicarbollide **[1]**$^-$, on magnetic nanoparticles (MNP) coated with a silica layer functionalized with amine groups $Fe_3O_4@SiO_2\text{-}NH_2$ (MSNP-NH_2), and the full characterization of the functionalized supports to learn about their morphology and colloidal stability. The colloidal stability of the MNP in water will be studied using different surfactants, since this is a huge issue in catalysis. The immobilization is based in the formation of a hybrid material linked by ionic interactions between **[1]**$^-$ and the functionalized magnetic nanoparticles with amine groups, (MSNP-NH_2).

- The study of the performance of the cobaltabis*ortho*dicarbollide as a heterogeneous catalyst in the photooxidation of aromatic and aliphatic alcohols in aqueous media, even using small loadings of the catalyst and short catalytic times and the re-utilization of the corresponding supported catalyst.

- The design and synthesis of a cooperative photoredox catalytic System, $[Ru^{II}(trpy)(bpy)(H_2O)][(1,2\text{-}C_2B_9H_{11})_2Co]_2$ (**C4,** where trpy=terpyridine and bpy=bipyridine; where the photoredox metallacarborane catalyst **[1]**$^-$ and the oxidation catalyst $[Ru^{II}(trpy)(bpy)(H_2O)]^{2+}$ are linked by noncovalent interactions, together with their complete spectroscopic and electrochemical characterization.

- The study of their catalytic activity in the photooxidation of aliphatic and aromatic alcohols and alkenes, in aqueous media.

- The study of the photocatalytic behavior of the ferrabis*ortho*dicarbollide $[Na\cdot 2,5H_2O][3,3'\text{-}Fe(1,2\text{-}C_2B_9H_{11})_2]$, **Na[2]** in the oxidation of alcohols and alkenes in water, together with a comparative study of its efficiency compared to the previous compounds studied.

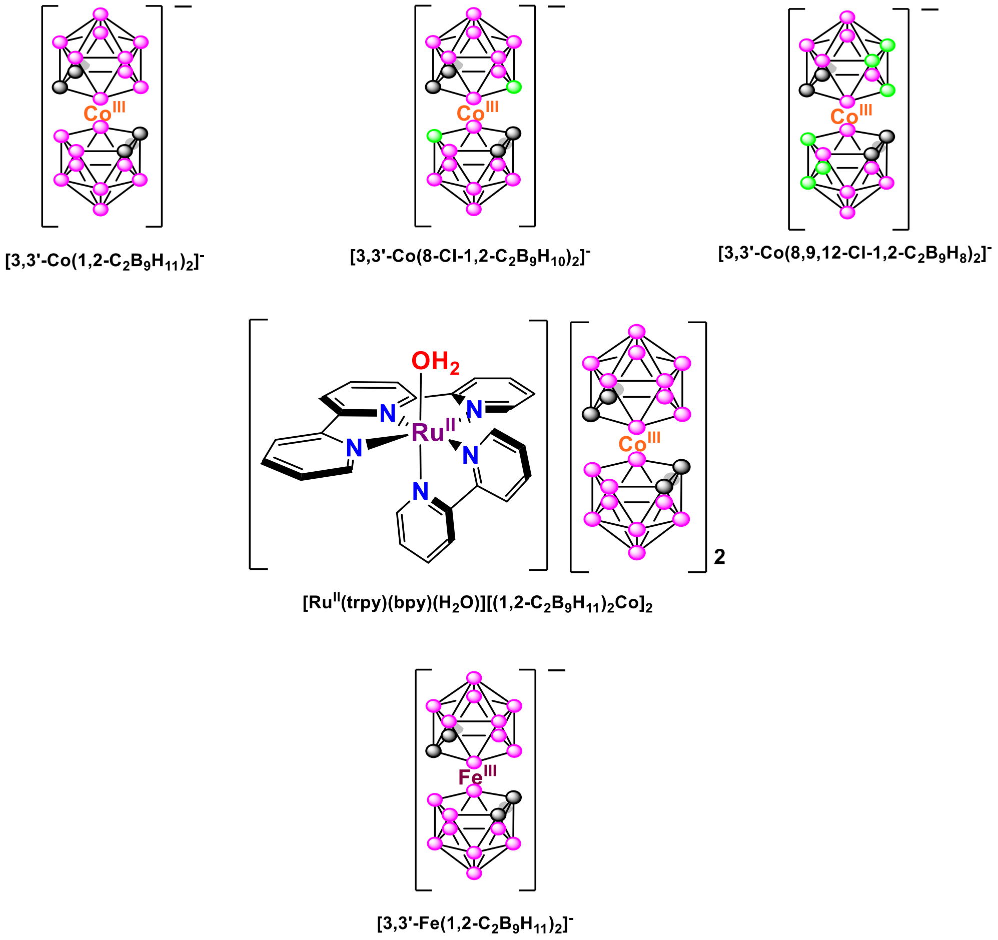

$[3,3'\text{-}Co(1,2\text{-}C_2B_9H_{11})_2]^-$

$[3,3'\text{-}Co(8\text{-}Cl\text{-}1,2\text{-}C_2B_9H_{10})_2]^-$

$[3,3'\text{-}Co(8,9,12\text{-}Cl\text{-}1,2\text{-}C_2B_9H_8)_2]^-$

$[Ru^{II}(trpy)(bpy)(H_2O)][(1,2\text{-}C_2B_9H_{11})_2Co]_2$

$[3,3'\text{-}Fe(1,2\text{-}C_2B_9H_{11})_2]^-$

Figure II.1. Compounds used in this work.

Chapter IV. Experimental section

III.1. Materials

All reagents used in the present work were obtained from Aldrich Chemical Co and Panreac Applichem and were used without further purification. Reagent grade organic solvents were obtained from SDS, and high-purity deionized water was obtained by passing distilled water through a Milli-Q water purification system.

All synthetic manipulations were performed under nitrogen atmosphere using vacuum line techniques.

III.2. Preparations

III.2.1. Synthesis of metallacarborane compounds

[Na·2.5H_2O] [3,3'-Co(1,2-$C_2B_9H_{11}$)$_2$] (**Na[1]**),[220] **[Na·2.5H_2O][3,3'-Co(8-Cl-1,2-$C_2B_9H_{10}$)$_2$] (Na[Cl_2-1]),**[221] **[Na·2.5H_2O][3,3'-Co(8,9,12-Cl_3-1,2-$C_2B_9H_8$)$_2$] (Na[Cl_6-1])**,[221,222] H[3,3'-Co(1,2-$C_2B_9H_{11}$)$_2$] (**H[1]**),[223] Ag[Co(1,2-$C_2B_9H_{11}$)$_2$] **Ag[1], C3**,[224] were synthesized from commercial Cs[Co(1,2-$C_2B_9H_{11}$)$_2$], **Cs[1]** and **[Na·2.5H_2O] [3,3'-Fe(1,2-$C_2B_9H_{11}$)$_2$]** (**Na[2]**)[47] was synthetized from ortho-*nido*-carborane compound. All the compounds were synthesized following the methods described in the literature.

III.2.2. Synthesis of ruthenium compounds

[$Ru^{III}Cl_3$(trpy)] **(C1),**[225] [Ru^{II}Cl(trpy)(bpy)]Cl **(C2),** [Ru^{II}(trpy)(bpy)(OH)$_2$](ClO_4)$_2$ or [Ru^{II} (trpy)(bpy)(OH)$_2$](PF_6)$_2$ both **(C2'),**[226] were synthesized following the methods described in the literature.

-Synthesis of **[Ru^{II}(trpy)(bpy)(H_2O)] [(1,2-$C_2B_9H_{11}$)$_2$Co]$_2$ (C4)**

A 90 mg sample of **C2** and 173 mg sample of **Ag[1]** were dissolved in 60 ml of acetone : water (1:1) and the resulting solution was refluxed for 3h. Then, AgCl was filtered off through a frit containing celite. The volume of the solution was reduced, and the mixture chilled in a refrigerator for 48 h. The orange dark precipitate was collected on a frit, washed with cold water and anhydrous ethyl ether and then vacuum-dried.

Yield: 134.69 mg(89.93%). Anal. Found (Calc.) for C_{33} H_{65} $B_{36}N_5Co_2ORu$ 1.5 H_2O . 2Et_2O : C, 37.04 (36.99); H, 6.24 (6.66); N, 5.19 (5.26). ^{1}H-NMR (acetone-d_6, 400 MHz): δ 9.87 (d, 1H, $^3J_{H-H}$ = 5.6 Hz, 1H, H1), 8.98 (d, 1H, $^3J_{H-H}$ = 8.1 Hz, 1H, H7), 8.91 (d, $^3J_{H-H}$ = 8.0 Hz, 2H, H17, H19), 8.76 (d, $^3J_{H-H}$ = 8.1 Hz, 2H, H14, H22), 8.64 (d, $^3J_{H-H}$ = 8.1 Hz, 1H, H4), 8.52 (t, $^3J_{H-H}$ = 8.1 Hz, 1H, H8), 8.43 (t, $^3J_{H-H}$ = 8.1 Hz, 1H, H18), 8.23 (t, $^3J_{H-H}$ = 7.1 Hz, 1H, H9), 8.16 (t, $^3J_{H-H}$ = 8.1 Hz, 2H, H13, H23), 8.04(d, $^3J_{H-H}$ = 5.6 Hz , 2H, H11, H25), 7.88 (t, $^3J_{H-H}$ = 8.4 Hz, 1H, H3), 7.55 (ddd, $^3J_{H-H}$ = 7.9 Hz, 8.0 Hz, $^4J_{H-H}$ = 1.3 Hz, 3H, H10, H12, H24), 7.17 (t, $^3J_{H-H}$ = 7.0Hz, 1H, H2), , 5.83 (s, 2H, Ru-OH_2), 3.98 (s, 8H, C_c-H). ^{1}H{^{11}B}-NMR (acetone-d_6, 400 MHz): δ 3.98 (s, 8H, C_c-H), 3.41 (s, 4B-H, B8, B8'), 3.16 (s, 4B-H, B10, B10'), 2.75(s, 8B-H, B4, B4', B7, B7'), 1.96 (s, 8B-H, B9, B9', B12, B12'), 1.68 (s, 4B-H, B6, B6'), 1.59 (s, 8B-H, B5, B5', B11, B11'). ^{11}B NMR (acetone-d_6, 128 MHz): δ 6.31 (d, 4B, J_{B-H} = 144.3 Hz, B-H), 1.13 (d, 4B, J_{B-H} = 143.5 Hz, B-H), -5.87 (m, 16B, B-H), -17.45 (d, 8B, J_{B-H} = 156.0 Hz, B-H), -22.90 (d, 4B, J_{B-H} = 165.3 Hz, B-H). ^{11}B{^{1}H}-NMR (acetone-d_6, 128 MHz): δ 6.33 (s, 4B, B8, B8'), 1.19 (s, 4B, B10, B10'), -5.87 (d, J_{B-B} = 95.4 Hz 16B, B4, B7, B4', B7', B9, B12, B9', B12'), -17.40 (s, 8B, B5', B11', B5, B11), -22.84 (s, 4B, B6', B6). ^{13}C{^{1}H}-NMR (acetone-d_6, 100 MHz): δ 159.42, 158.98, 153.69, 153.55, 150.66, 138.74, 138.46, 128.32, 127.91, 126.68, 126.50, 124.27, 124.17, 123.63 and 123.47 (C Ru trpy-bpy), 51.11 and 50.89 (C_c). IR (*v*, cm^{-1}): 3039, 2922, 2854, 2531, 1601, 1446, 1464,1384, 1095, 1016, 980, 884, 761. $E_{1/2}$ (CH_2Cl_2+ 0.1 M TBAH) Co$^{III/II}$, -1.37 V; Co$^{IV/III}$, 1.38 V; Ru$^{III/II}$, 0.70 V; Ru$^{IV/III}$, 1.06 V *vs* Ag. UV-*vis* (CH_2Cl_2,1.16x10^{-5} M): λ_{max} nm (ε, M^{-1} cm^{-1}) 279 (37297), 292 (42727), 325 (66493), 392 (9686), 477 (8362). ESI-MS (*m/z*): [M-Cosane-H_2O]$^+$ 814.4 (100%); [M-Cosane]$^+$ 831.4 (31%).

-Synthesis of **[Ru^{II}(trpy)(bpy)(CH_3CN)] [(1,2-$C_2B_9H_{11}$)$_2$Co]$_2$ (C5)**

[Ru^{II}(trpy)(bpy)(CH_3CN)] [(1,2-$C_2B_9H_{11}$)$_2$Co]$_2$ **(C5)**, was synthesized from [Ru^{II}(trpy)(bpy)(H_2O)] [(1,2-$C_2B_9H_{11}$)$_2$Co]$_2$ **(C4)** by recrystallization of the latter **C4** in acetonitrile solution, yellow needles suitable for X-ray diffraction were obtained corresponding to complex **C5.**

UV-vis (CH_3CN, 1.16x10^{-5} M): λ max nm (ε, M^{-1} cm^{-1}) 287 (59852), 308 (31314), 333(11997), 464 (5774).

III.2.3 Preparations of heterogeneous systems

The syntheses of Magnetic nanoparticles (MNP) were prepared according to literature procedures,[227] using the aqueous *co*-precipitation method. This core was then further encapsulated in a silica shell using the Stober process.[228] After having the MNPs coated with SiO_2, (MSNPs) they were further functionalized by amino groups.

-Synthesis of $\mathbf{Fe_3O_4}$ core

First, NaOH (15 g, 375.02 mmol) was dissolved into 25 mL of double-distilled water. Then, a mixture of $FeCl_2.4H_2O$ (2 g, 10.05 mmol), $FeCl_3.6H_2O$ (5.2 g, 19.23 mmol), 25 mL of double distilled water and 0.85 mL of HCl (12 M) was added dropwise with vigorous stirring to make a black solid product. The resultant mixture was heated using an oil bath for 4h at 80 ^{0}C. The black magnetite solid MNPs were isolated using an external magnet and washed three times with deionized water and finally one with ethanol, and then dried at 80 ^{0}C for 10 h.

-Synthesis of $\mathbf{Fe_3O_4}$ **@**$\mathbf{SiO_2}$ core-shells **(MSNP).**

Fe_3O_4 (0.5 g, 21 mmol) was dispersed in a mixture of ethanol (100 mL) and deionized water (25 mL) for 30-40 minutes using an ultrasound bath. Then, 2.5 mL of NH_3 (30 %, for analysis) was added followed by the dropwise addition of tetraethoxysilane (TEOS) (1.5 mL). This solution was stirred mechanically for 6 hours at room temperature. Then, the product $Fe_3O_4@SiO_2$ was separated using an external magnet and was washed three times with deionized water and finally with ethanol, and then dried at 80 ^{0}C for 10 hours. For this reaction our group designed a new Teflon covered system with a crystal mechanical stirring rod (**see Annex II**).

-Synthesis of **Small** and **Large particles.**

The smaller silica-coated particles are synthesized using the standard silica coating procedure reported above. In the case of larger particles, the magnetite core reaction is stirred for 6 h and the silica reaction is stirred for 12 or 18 hours depending on the size needed to be produced. The quantity of TEOS to be added can also be controlled on the necessity of thickness of the shell. The biggest advantage of this method lies in the fact that it helps to change the size of the particles by modifying the time and temperature of the reaction. The silica coating using Stober process can also be done at a mild temperature (40 ^{0}C) in need for thicker coatings over the magnetite core. This flexibility in the process makes it attractive but the disadvantage of this procedure lies in less control of the mono-dispersity of the particles.

-Synthesis of amine functionalized silica, **Fe_3O_4@SiO_2-NH_2 (MSNP-NH_2).**

A mixture of Fe_3O_4@SiO_2 (0.2 g) was dispersed in ethanol (45 mL). Then 5 mL of 3-(2-aminoethylamino)propylmethyldimethoxy silane (APMS) was dissolved in 20 mL of ethanol and added to the suspension of Fe_3O_4@SiO_2 in ethanol. The pH value of the reaction mixture was set to 11 using tetramethylammonium hydroxide (TMAH). The reaction mixture was then heated to 50 ^{0}C and stirred for 5 h. After ageing for a night, the suspension of functionalized nanoparticles was completely stable. It was then precipitated using NaCl solution. Then, the nanoparticles were thoroughly washed with distilled water using magnetic separation and finally dried at 80 ^{0}C in vacuo.

For this amine functionalization instead of APMS other reagents like (3-aminopropyl) triethoxy silane (APTES) of (3-aminopropyl) trimethoxy silane (APTMS) can also be used which give the same result.

-Synthesis of COSAN functionalized silica**, Fe_3O_4@SiO_2-NH_2-H[COSAN], (MSNP-NH_2@H[1]).**

Fe_3O_4@SiO_2-NH_2 (0.05 g) was suspended in 10 mL of water containing 5 mM of H [3,3'-Co (1,2-$C_2B_9H_{11}$)$_2$], **H[1].**[231] The mixture was sonicated in an ultrasound bath for 30 minutes and then washed 10 times with water using magnetic separation. Finally, the sample was dried under vacuum at 80 ^{0}C.

III.3. UV-visible studies from COSAN functionalized silica, Fe_3O_4 @SiO_2-NH_2-H [COSAN], (MSNP-NH_2@H[1])

The sample for this experiment was prepared by mixing 0.005 g of Fe_3O_4@SiO_2-NH_2 in a solution of 1mM of **H[1]** (0.0163 g, 0.0501 mmol) in 50 mL of water, sonicating for 15 minutes, and then collecting the MNPs with the help of a magnet for about 10 minutes; the MNPs are concentrated at the bottom of the flask and the clear liquid at the top is measured in the UV-Visible. This procedure was done for 0.005, 0.01, 0.015, 0.02, 0.025 and 0.03 g of $Fe_3O_4@SiO_2\text{-}NH_2$ keeping constant the amount of **H[1]**. The UV-visible absorbance decrease with the addition of magnetic nanoparticles and the difference between the two absorbance peaks permits to quantify the **H[1]** anchored to the surface of the nanoparticles.

III.4. Colloidal stability studies from Fe_3O_4 @SiO_2-NH_2

0.005 g of $Fe_3O_4@SiO_2\text{-}NH_2$ was suspended using ultrasound sonication in 10 mL of distilled water in 5 different vials. After 5 minutes of sonication the MNPs were well dispersed in water. Then 0.0025 g of five different surfactants were added in each vial and sonicated further for another 5 minutes. These samples were taken to be tested using ζ-potential to check the stability. After that, another 0.0025 g of the surfactants were added in their respective vials totaling the amount of surfactant to be 0.005 g in each vial and sonicated for another 5 minutes and tested for ζ- potential values. This was continued further by the addition of up to 0.03 g of surfactant in each of their respective vials, followed by sonication and then testing their stability by using ζ-potential.

III.5. Computational details from calculations.

All calculations were carried out with the Gaussian 09 program package[229] at the B3LYP/6-311+G** level of theory. For Ru the Def2TZVP basis set was used. Full geometry optimization calculations were performed and harmonic vibrational frequencies were calculated to establish the nature of the stationary points obtained, as characterized by no one negative eigenvalue of the Hessian for minima structures. The NTOs, electron and hole distributions, and charge-density difference maps were calculated with the Multiwfn program.[230] For the visualization the MOLDEN[231] and VMD programs[232] were used.

III.6. Crystallographic Data Collection and Structure

Measurement of the **C5** crystals were performed on a BRUKER SMART APEX CCD diffractometer using graphite-monochromated Mo Kα radiation (λ = 0.71073Å) from an X-Ray tube. Programs used: data collection, Smart Version 5.631 (BrukersAXS 1997-02); data reduction, Saint+ Version 6.36A (Bruker AXS 2001); absorption correction, SADABS version 2.10 (Bruker AXS 2001), structure solution SHELXTL (V 6.14, Bruker 2003) and structure refinement SHELXL-2018/3 (Sheldrick, 2018). The crystallographic data as well as details of the structure solution and refinement procedures are reported in **Annex S.I.III**. CCDC 2058809 for **C5** contains the supplementary crystallographic data for this compound, **C5**. These data can be obtained free of charge from The Cambridge Crystallographic Data Centre via www.ccdc.cam.ac.uk/products/csd/request/

Complex	**Color**	**Solvent of crystallization**	**T(K)**	**Θ range**	**Data collection**	**Number of reflections**	**Unique reflections [R(int)]**
C5	orange	acetonitrile	100	1.6-28.3^0	full-sphere, ω and φ scans	18893	11984[0.050]

III.7. Photocatalytic oxidation studies

III.7.1. Photocatalytic oxidation of alcohols

III.7.1.1. Homogeneous phase

Different metallacarboranes with the shape of the Greek letter Θ, such as [2.5·H_2O][3,3'-Co(1,2-$C_2B_9H_{11}$)$_2$] (**Na[1]**), dichloro derivative [2.5·H_2O][3,3'-Co(8-Cl-1,2-$C_2B_9H_{10}$)$_2$] (**Na[Cl$_2$-1]**) , hexachloro derivative [2.5•H_2O][3,3'-Co(8,9,12-Cl_3-1,2-$C_2B_9H_8$)$_2$] (**Na[Cl$_6$-1]**), [2.5·H_2O][3,3'-Fe(1,2-$C_2B_9H_{11}$)$_2$] (**Na[2]**), [Ru^{II}(trpy)(bpy)(H_2O)] (**C2'**) and cooperative catalysts with ruthenium aquo complexes as [Ru^{II}(trpy)(bpy)(H_2O)][(1,2-$C_2B_9H_{11}$)$_2$Co]$_2$ (**C4**), were tested ,as efficient photoredox catalysts in the oxidation of aromatic, aliphatic alcohols in water.

A quartz tube containing an aqueous solution (5 mL) at pH 7.2 (phosphate buffer) with the corresponding catalyst, alcohol as substrate, and $Na_2S_2O_8$ or an air stream as sacrificial acceptor was exposed to UV light (2.2 W, ʎ=253.7, 300 or 352 nm) for different times.

The complex: substrate: sacrificial oxidant ratios used (1:250:500, 1:1000:2000, 1:10000:20000, 1:10000:10000, 1:10000:5000, 1:10000:40000, 1:20000:40000 and 1:20000:20000) corresponding to concentrations of 0.08:20:40 mM, 0.02:20:40 mM, 0.002:20:40 mM, 0.002:20:20 mM, 0.002:20:10 mM, 0.002:20:80 mM, 0.001:20:40 mM and 0.001:20:20 mM, respectively), were varied according to the study. For each experiment, light illumination was supplied by a light reactor with twelve lamps that produce UVA light at room temperature. The resulting solutions were extracted with CH_2Cl_2 three times in the case of aromatic alcohols and with diethyl ether in the case of aliphatic alcohols. The solution was dried with anhydrous sodium sulfate and the solvent was evaporated under reduced pressure. To check the reproducibility of the reactions all the experiments were carried out three times. The reaction products were quantified and characterized by ^1H NMR spectroscopy using tetramethylsilane (TMS) as internal standard in the case of primary aromatic alcohols. In a second set of experiments, NEt_3 or K_2CO_3 was added to water as a base.

For comparison with NMR measurements, the oxidation products were also determined by gas chromatography. To each aliquot of the reaction, biphenyl or naphthalene as internal standards and analyzed in a Shimadzu GC-2010 gas chromatography apparatus equipped with an Astec CHIRALDEX G-TA column and a FID detector, and quantification was achieved from calibration curves.

III.7.1.2. Heterogeneous phase

Alcohol (0.1 mmol) and $Na_2S_2O_8$ (0.2 mmol) were dissolved in 5 mL of distilled water (K_2CO_3, pH=7) together with 5 mg of MSNP-NH_2@H[**1**] (0.1 µmol catalyst). The amount of heterogenized catalyst was calculated taking into account the functionalization of magnetic nanoparticles. In the case of addition of the surfactant cetyl trimethyl ammonium chloride (CTAC), the concentration used was 0.4 mM. The general photocatalytic oxidation experiments were all performed by exposing the reaction quartz vials to UV irradiation (ʎ= 300 nm), at room temperature and atmospheric pressure, for different times. The complex/substrate/sacrificial oxidant ratios used (1: 1000: 2000 and 1: 10000:20000 that correspond to the concentrations of 0.02: 20: 40 mM and 0.01: 100: 200 mM) were varied according to the study. For every experiment, light illumination was supplied by a light reactor with twelve lamps that produce UVA light at room temperature. A magnet was used for the separation of the catalytic material from the reaction medium. The reaction products were extracted with dichloromethane (3 x 10 mL). The combined organic phases were dried over sodium sulfate, and the solvent was evaporated under reduced pressure. To check the reproducibility of the reactions, all of the experiments were carried out three times. The reaction products were quantified using ^{1}H NMR spectroscopy and confirmed by gas chromatography-flame ionization detection (GC-FID) and gas chromatography-mass spectrometry (GC-MS) analysis or high-performance liquid chromatography-mass spectrometry (HPLC-MS).

Recycling experiments

After finishing each catalytic experiment, the heterogeneous catalyst was separated by a homemade structure based on magnets, used for catalyst separation material from the reaction medium. Upon the solution of interest to be extracted and analyzed was separated, the heterogeneous catalyst remaining in the catalytic quartz tube, thanks to the magnets, was washed four times with distilled water, and reused in subsequent runs.

III.7.2. Photocatalytic oxidation of alkenes

A quartz tube containing an aqueous solution (5 mL) at pH 7 (K_2CO3) with **Na[1]**, **Na[2]**, or **$[Ru(bpy)_3]Cl_2$** as catalysts, alkene as substrate, and $Na_2S_2O_8$ as sacrificial acceptor was exposed to UV light (2.2 W, ʎ= 300 nm) for different times. In the case of **Na[1]** or **Na[2]**, the complex: substrate: sacrificial oxidant ratios used (1:1000:2000, 1:1000:1300, 1:10000:20000 and 1:10000:13000 corresponding to concentrations of 0.02: 20: 40 mM, 0.02: 20: 26 mM, 0.002: 20: 40 mM and 0.002: 20: 26 mM, respectively. The concentrations were varied according to the study. For each experiment, a light reactor supplied light illumination with twelve lamps that produce UVA light at room temperature. The resulting solutions were extracted with CH_2Cl_2 six times. The solution was dried with anhydrous sodium sulfate and the solvent was reduced to a minimum volume under reduced pressure, then 100 µL of biphenyl 100 mM as internal standard was added to the resulting solution, 2 mM in the resulting 5 mL solution. To check the reproducibility of the reactions all the experiments were carried by triplicate and analyzed by Gas Chromatography. In the case of using methyl oleate as alkene substrate, a quartz tube containing an aqueous solution (5 mL) at pH 7 (K_2CO_3) with 3% of acetone and **Na[1]** was sonicated for 10 min. The complex: substrate: sacrificial oxidant ratios used were, 1:10000:13000 corresponding to concentrations of 0.002: 20: 26 mM, respectively. The samples were exposed to UVA light at room temperature during 60 min and the resulting solutions were extracted with CH_2Cl_2 six times. The solution was dried with anhydrous sodium sulfate and the solvent was reduced to 2 ml. The organic phase was analyzed by High Performance Liquid Chromatography.

III.8. Additional Instrumentation and measurements

FT-IR spectra were taken in a JASCO FTIR-4600 spectrometer.

UV/Vis spectroscopy was performed with a Cary 50 Scan (Varian) and a Cary-5000 Scan (Varian) UV/Vis spectrophotometer with 1 cm quartz cells or with an immersion probe of 5 mm path length.

Cyclic voltammetry (CV) and *differential pulse voltammetry* (DPV) were performed in an IJ-Cambria 660C potentiostat using a three electrode cell. Glassy carbon electrode (3 mm diameter) from BAS was used as working electrode, platinum wire as auxiliary and Ag as pseudo reference electrode or SCE, Ag/AgCl, as the reference electrode, and in some cases using ferrocene (Fc) as internal reference. All cyclic voltammograms presented in this work were recorded under nitrogen atmosphere. The complexes were dissolved in deoxygenated solvents containing the necessary [n-Bu_4N][PF]$_6$ (TBAH) from Alfa Aesar, Thermo Fisher Scientific to yield a 0.1 M ionic strength solution, or phosphate buffer at pH 7.02 from Panreac Applichem working as supporting electrolytes in organic or aqueous media, respectively. All $E_{1/2}$ values were estimated from cyclic voltammetry experiments as the average of the oxidative and reductive peak potentials (Ep_a+Ep_c)/2. Unless explicitly mentioned the concentration of the complexes was approximately 1mM.

Elemental analyses were performed using a CHNS-O Elemental Analyzer EA-1108 from Fisons. Mass spectra were recorded in negative-ion mode with a Bruker Biflex MALDITOF [N_2 laser; λ_{exc}=337 nm (0.5 ns pulses); voltage ion source 20000kV (Uis1) and 17 500 kV(Uis2)] without matrix. The intensity of the laser was fixed at 30%.

ESI-MS experiments were performed on a Navigator LC/MS chromatograph from Thermo Quest Finnigan, using acetonitrile as mobile phase.

Transmission electron microscopy (TEM) studies were carried out using JEOL JEM 1210 at 120 kV.

Scanning electron microscopy (SEM) and *energy-dispersive X-ray spectroscopy* (EDX) analyses were done using QUANTA FEI 200 FEG-ESEM device. The solid samples were analyzed for this.

High-resolution transmission electron microscopy (HRTEM) was done using JEM-2011 at 200 kV with 0.18 nm resolution.

High-resolution scanning electron microscopy (HRSEM) was done using a Zeiss Merlin instrument. ImageJ software was used for measuring the particles.

ζ-Potential studies were carried out using a Zetasizer Nano ZS (for DLS light source, a He-Ne laser was used, 633 nm, max 4 mW, backscattering angle used was 173^0, and for ζ-potential, electrophoretic light scattering principle was used for measurements). The magnetization hysteresis cycle was measured using a Quantum Design MPMS-XL system at 300 K with a maximum of 60 kOe.

Scanning transmission microscopy (STEM) and EELS measurements were done using an FEI Tecnai F20 S/TEM HRTEM device at 200 kV.

NMR spectra were recorded with a Bruker ARX 360 and 400 instruments. ^1H NMR spectra were recorded in $CDCl_3$, acetone-d_6 and D_2O. Chemical shifts were referenced to $SiMe_4$.

Gas chromatography studies were performed with a GC-2010 Gas Chromatograph from Shimadzu, equipped with an Astec CHIRALDEX G-TA column, 30m x 0.25 mm (i.d); FID detector, 250°C; injection: 250 °C; carrier gas: helium; rate: 1.57 mL/min; area normalization. For alcohols, substrates and products of catalysis were detected under the following conditions: column temperature: 80°C for 5 minutes, raising to 170°C in a rate of 10°C/min, holding at 170°C for 2 minutes. The product analyses in the catalytic experiments of 1-phenyletanol, benzyl alcohol and 4-methylbenzyl alcohol, were performed using biphenyl as internal standard. In the case of the product analysis in the catalytic experiment of 4-chlorobenzyl alcohol, was used naphthalene as internal standard.

For alkenes, substrates and products of catalysis were detected under the following conditions: styrene and derivatives: column temperature, 80°C for 5 minutes, raising to 170°C in a rate of 10°C/min, holding 170°C for 6 minutes. Trans-β-methyl-styrene, cis-β-methyl-styrene, cis-cyclooctene and derivatives: column temperature, 40°C for 5 minutes, raising to 170°C in a rate of 5°C/min, holding 170°C for 2 minutes. 4-vinyl-1-cyclohexene and derivatives: column temperature, 40°C for 5 minutes, raising to 170°C in a rate of 10°C/min, holding 170°C for 2 minutes. 1-octene and derivatives: column temperature, 30°C for 5 minutes, raising to 170°C in a rate of 10°C/min, holding 170°C for 3 minutes. Trans-stilbene and derivatives: column temperature, 50°C for 1 minutes, raising to 150°C in a rate of 15°C/min, holding 150°C for 2 minutes, then raising to 170°C in a rate of 4°C/min, holding 170°C for 12 minutes. The products analyses in the catalytic experiments were performed by GC with biphenyl as internal Standard.

Catalytic experiments analyses were performed as well, with an Agilent LC 1200 series HPLC system equipped with a UV-Vis detector was used to analyze samples. Separation of products was achieved on an Eclipse XDB-C18 column (150x4.6 nm,5μm) from Agilent Technologies. The column was thermostatically controlled at 25◦C. The flow rate was set to 1 mL/min, and the injection volume was 100 μL. The mobile phase consisted of two solvents: methanol (A, 100%) and Milli-Q water (B,100%). The system worked in isocratic mode and the volume ratios was as follows: 85% A, 15% B. The ultraviolet (UV) absorbance values of the peaks were collected at 242 nm. An Ion Trap mass spectrometer (Bruker Squire 6000 system from Agilent Technologies) equipped with an Orthogonal electrospray ionization (ESI) source was used to identify the derivatives. Positive mode was selected for data collection. The products were qualitatively identified according mass spectra peaks and matching with mass spectra with the software Bruker Compass DataAnalysis 4.0.

Chapter IV. Results and discussion

IV.1. Metallacarboranes as Photoredox Catalysts in Water

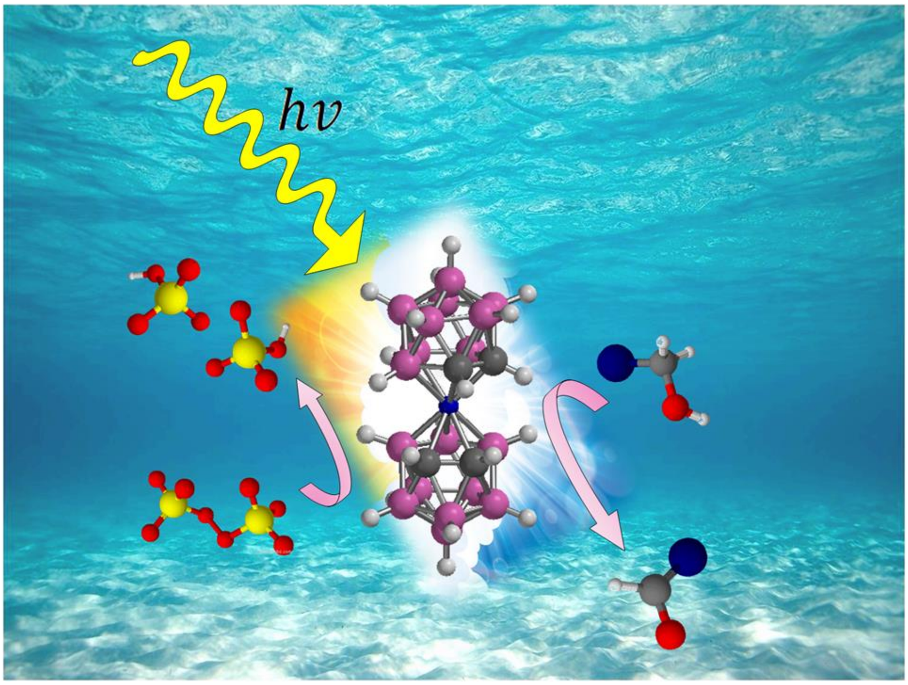

We describe here the photocatalytic behavior of the Cobaltabis(dicarbollide) [Na·2,5H_2O][3,3'-Co(1,2-$C_2B_9H_{11}$)$_2$], **Na[1]**, and its dichloro [Na·2,5H_2O][3,3'-Co(8-Cl-1,2-$C_2B_9H_{10}$)$_2$],**Na[Cl$_2$-1]**, and hexachloro derivatives [Na·2,5H_2O][3,3'-Co(8,9,12-Cl_3-1,2-$C_2B_9H_8$)$_2$]$^-$, **Na[Cl$_6$-1]** in the oxidation of alcohols in water. Remarkable, the metallabisdicarbollide performs two roles: photosensitizer and catalyst at once. We will use as oxidizing agents $Na_2S_2O_8$ or air showing that both are suitable to oxidize the alcohol. In addition we shall see how matching the lamp frequency and the maximum of the absorbance of the photoredox catalyst enhances the yield of the catalysis. The photoredox catalyst can be easily recovered after performing the catalysis.

IV.1.1. General strategy

Our main goal was to demonstrate that a metallacarborane like $[3,3\text{-Co}(1,2\text{-C}_2\text{B}_9\text{H}_{11})^{2-}$, with a nonconventional structure compared with existing photoredox catalysts can act as such, thanks to its own characteristics, as we have seen in the introduction chapter of this thesis. To carry out this, the first is to demonstrate that the reaction could be done under homogeneous conditions in water. Therefore, **Na[1]** was prepared from water-insoluble **Cs[1]** by using a cation-exchange resin[233] and its dichloro (**Na[Cl_2-1]**) and hexachloro (**Na[Cl_6-1]**) derivatives **(Figure IV.1.)** were prepared in a similar way.[234] All three Na^+ salts are soluble in water, as required by the catalysis conditions.

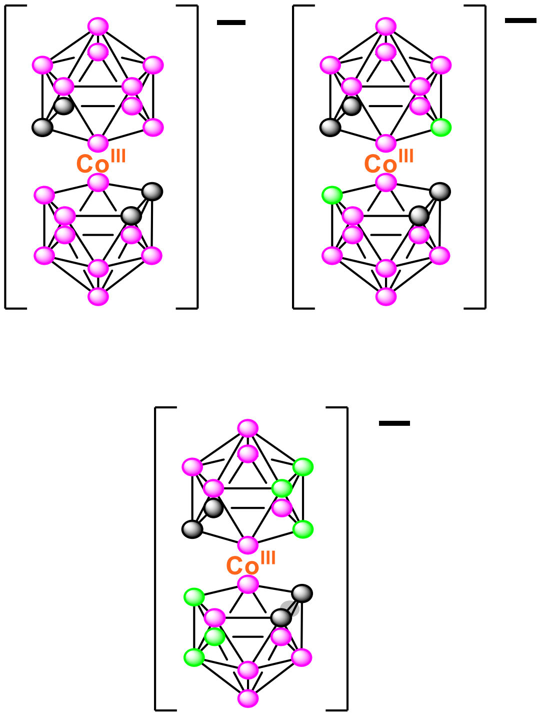

Figure IV.1. Metallacarboranes used in this work: $[3,3'\text{-Co}(1,2\text{-C}_2\text{B}_9\text{H}_{11})_2]^-$ (**[1]**$^-$, only the *trans* rotamer is shown) and its dichloro and hexachloro derivatives $[3,3'\text{-Co}(8\text{-Cl-}1,2\text{-C}_2\text{B}_9\text{H}_{10})_2]^-$ and $[3,3'\text{-Co}(8,9,12\text{-Cl}_3\text{-}1,2\text{-C}_2\text{B}_9\text{H}_8)_2]^-$, respectively. The green circles represent BCl units and the pink circles BH units.

Likewise, we wanted to show that the Cobaltabis(dicarbollide) anion could be adjusted for two reasons, on one hand, to alter the E^0 value of $[3,3'\text{-Co}(1,2\text{-C}_2\text{B}_9\text{H}_{11})_2]^{0/-1}$ to obtain a more oxidizing molecule, for example, $[3,3'\text{-Co}(1,2\text{-C}_2\text{B}_9\text{H}_{11})_2]^0$, and on the second hand, by shifting the absorption maximum to the visible region. By having two or six chloro substituents on the anion, we shifted the absorption maximum towards the visible range. By using lamps with the closest emission to the absorption maximum of the photoredox catalyst; we sought to improve the yield of the reaction in the less possible exposure time. The UV-Vis spectrum of **Na[1]** (**Figure IV.2.a**) shows one strong absorption band at 293 nm and two weaker ones at 345 and 445 nm, in accordance with the literature,[235] and the visible spectrum was interpreted on the basis of ligand-field theory.[236] The UV-Vis spectra of **Na[Cl$_2$-1]** and **Na[Cl$_6$-1]** show bands at 320 nm (ε=26000 M^{-1} cm^{-1}) and 384 nm (ε=3700 M^{-1} cm^{-1}) and at 327 nm (ε=29000 M^{-1} cm^{-1}) and 393 nm (ε=3500 M^{-1} cm^{-1}), respectively (**Figure IV.2.b**)

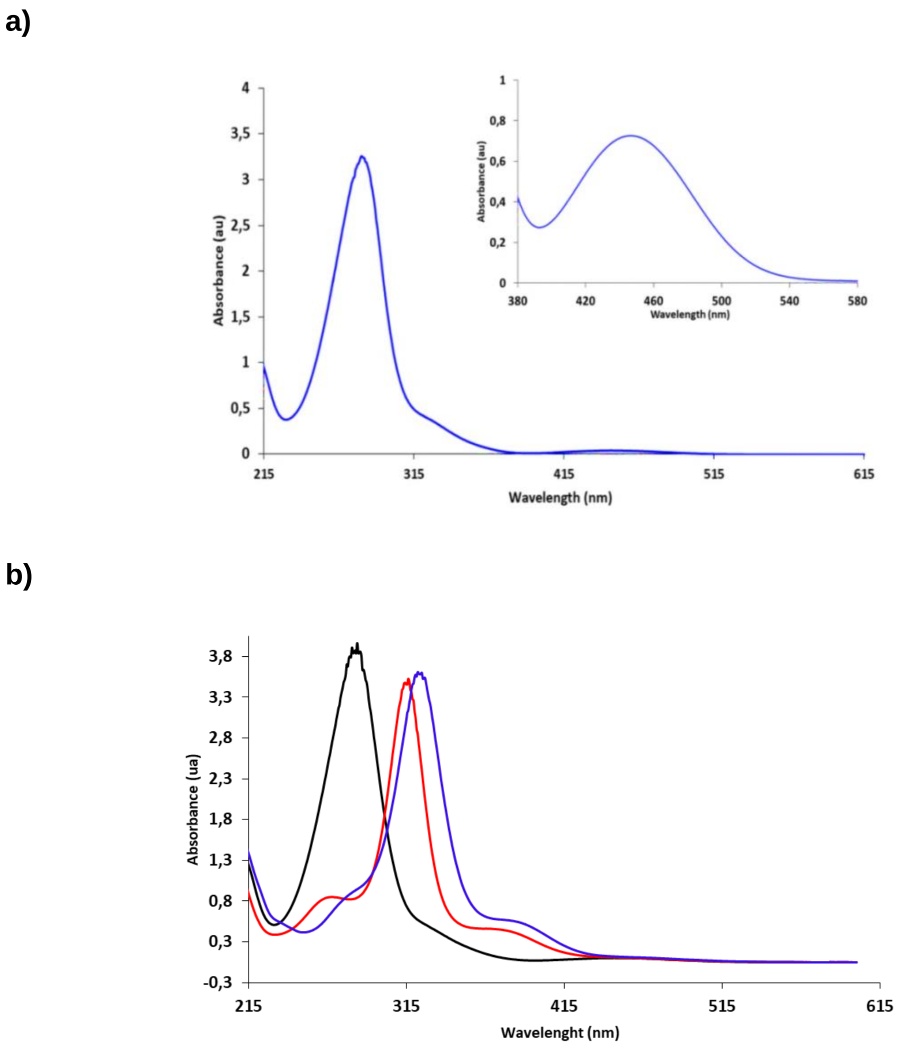

Figure IV.2. a) UV-Vis spectra of **Na[1]** in phosphate buffer solution, 1.3x10^{-4}M at pH 7.2. Inset: Magnification of the visible region of **Na[1]** in phosphate buffer solution, 2x10^{-3}M at pH 7.2. b) UV-visible spectra of carborane Na[3,3'-Co(1,2-$C_2B_9H_{11}$)$_2$] (black), Na[3,3'-Co(8-Cl-1,2-$C_2B_9H_{10}$)$_2$] (red) and Na[3,3'-Co(8,9,12-Cl_3-1,2-$C_2B_9H_8$)$_2$] (blue) in acetonitrile solution, 1.3 x10^{-4} M.

IV.1.2. Computational study

With the aim to get a detailed knowledge about the character of the electron transitions of $[3,3'\text{-Co}(1,2\text{-C}_2\text{B}_9\text{H}_{11})_2]^-$, TD-DFT calculations were performed at the B3LYP/6-311 + G** level of theory. The stabilities of the cisoid, gauche and transoid (**see, Figure IV.3**) are similar, but the stability depends on their interactions with the environment. Their relative stability depends on whether the environment is vacuum, water, or the solid state. [237] Thus, all three rotamers were computationally investigated in vacuum, and they exhibit practically identical electronic properties which were in good agreement with the previously published results.[238] During the investigation all the three rotamers were considered since the energy difference between them are small, thus under experimental conditions these rotamers may be populated as well. However, gas phase calculations showed that *gauche* and *cisoid* are less stable by 0.5 and 2.9 kcal/mol at B3LYP/6-311+G** level of theory, respectively. Our recent study demonstrates that the *cisoid* structure is more favoured in water do to the interactions with the solvent molecules.[239]

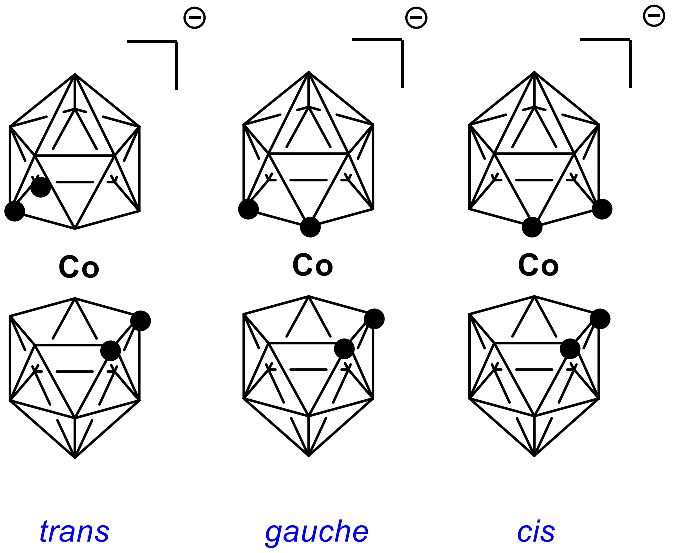

Figure IV.3. Different rotamers of $[3,3'\text{-Co}(1,2\text{-C}_2\text{B}_9\text{H}_{11})_2]^-$ (**[1]**$^-$).

We studied in more detail the excitation at 293 nm, which is the most intensive band in the spectrum. The calculated results reproduced well the position of the absorption peaks and they were in good agreement with the previously published results.[240] All of the three rotamers have transitions with large intensities (f>0.1) in the region of 257-290 nm (**Table IV.1**). While in case of the *transoid* isomer only one transition (S0→S11) exhibits large intensity, the other two rotamers have two significant transitions in this region (probably due to their lower symmetry).

Table IV.1. The main electronic transitions in the different rotamers of **[1]**$^{-}$.

Rotamer	Theoretical λ_{abs} (nm)	transition	Intensity	main contribution	Coefficient
trans	280	S0→S11	0.6625	HOMO-3 → LUMO+1	0.13
				HOMO-2 → LUMO	0.56
				HOMO-1 → LUMO+1	0.37
gauche	266	S0→S11	0.3252	HOMO-7 → LUMO	0.46
				HOMO-3 → LUMO+1	0.37
				HOMO-2 → LUMO	0.29
	257	S0→S13	0,4212	HOMO-7 → LUMO	0.49
				HOMO-3 → LUMO+1	0.32
				HOMO-9 → LUMO	0.21
				HOMO-2 →LUMO	0.21
cis	273	S0→S13	0.3498	HOMO-5 → LUMO	0.40
				HOMO-3 → LUMO	0.39
				HOMO-2 → LUMO+1	0.21
				HOMO-1 → LUMO+1	0.21
	268	S0→S15	0.2577	HOMO-4 → LUMO+1	0.34
				HOMO-3 → LUMO	0.26
				HOMO-5 → LUMO	0.26
				HOMO-8 → LUMO	0.25

Since there are no dominant MO transitions in these transitions especially in case of *gauche* and *cisoid* rotamers (3-4 pair of orbitals, see **Table IV.1**.), which make difficult to visualize the nature of the excitations, we generated and analysed the natural transition orbitals (NTOs) corresponding to the proper transitions (see **Annex I Table**

SIV 1.1). During the NTO calculations the ordinary orbitals are transformed to a more compact form in which each excited state is described as a single and sometimes a double pair of orbitals.[241] In our case two pairs of NTO orbitals are obtained for all investigated excitations and the common motif of them is that the excitation can be mainly regarded as a transition from the boron vertex on the skeleton towards the metal center. While the significant overlaps of the electron and hole distributions suggest rather local excitation modes with percentages of 34.9-49.3%, (**Table IV.2.**), the charge density difference maps generated (**Table IV.3** and **Annex I Figure SIV.1**) clearly show that the electron density shifted from the ligand toward the metal center (and a little bit towards the carbon atoms as well), as is showed more clearly in the charge-density difference map from **Figure IV.4,** during the excitation at 293 nm, and this indicates charge transfer from the ligand framework towards the metal center (LMCT) during the transition.

Table IV.2. The overlap of hole and electron distribution.

Rotamer	transition	overlap of hole and electron distribution
trans	S0→S11	41.92 %
gauche	S0→S11	36.78 %
	S0→S13	34.91 %
cis	S0→S13	37.21 %
	S0→S15	49.34 %

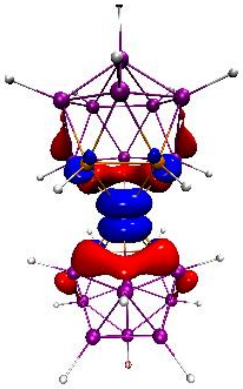

Figure IV.4. Charge-density difference map of the transition at 293 nm in case of the transoid structure. (The blue and red parts correspond to the regions in which electron density is increased and decreased after electron excitation, respectively). Isosurface value: 0.003.

This is in accordance with the double negative charge of the carborane ligands, which increases the energy level of these occupied orbitals ($\varepsilon_{HOMO}([3,3'\text{-Co}(1,2\text{-}C_2B_9H_{11})_2]^-)$ being -4.00 and -4.03 eV depending on the rotamer, whereas $\varepsilon_{HOMO}([\mathrm{Ru(bpy)}_3]^{2+})$ shows a value of -11.17 eV at the B3LYP/6-311+G** level of theory) and the ligands contribute significantly to HOMO-1 and HOMO-3. Hence, upon irradiation, electrons are promoted mainly from the orbitals with ligand-like character to the rather metal-based LUMO and LUMO+1. The last fact is contrary to the electron route in $[\mathrm{Ru(bpy)}_3]^{2+,}$ from the metal to the ligand, and is a first indication of a possible distinct behavior in electron transfer as a consequence of the difference in electronegativity among the elements participating in the bonding, the negative charge of the carboranyl ligands, and the overall negative charge of $[3,3'\text{-Co}(1,2\text{-}C_2B_9H_{11})_2]^-$.

Table IV.3. The charge density difference maps of the different transitions. (The blue and red parts correspond to the region where electron density is increased and decreased after electron excitation, respectively. Isosurface value: 0.003).

Rotamer (Transition)		
trans	***gauche***	
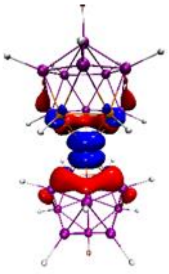 (S0→S11)	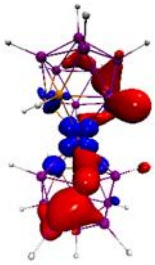 (S0→S11)	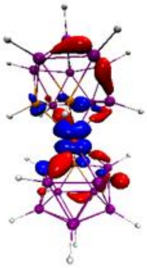 (S0→S13)
cis		
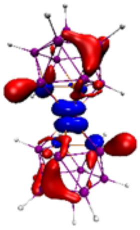 (S0→S13)	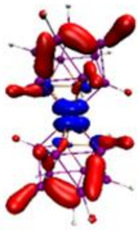 (S0→S15)	

IV.1.3. Photocatalytic oxidation of alcohols

IV.1.3.1. Photocatalytic oxidation of alcohols under common conditions (0.4 mol % catalyst versus substrate, 0.08 mM)

There are not much photoredox catalytic systems based on earth-abundant metals for organic transformations. Due to the importance of this fact, we elected the oxidation of alcohols to evaluate the photoredox properties of **Na[1]**. The first photocatalytic oxidation experiments, were all performed by exposing quartz reaction vials to UV irradiation (2.2 W, ʎ=253.7 nm) at room temperature and atmospheric pressure for different times. The samples were made from 5 mL of water (phosphate buffer, pH 7.2) and a mixture of **Na[1]** (0.08 mM), substrate (20 mM), and $Na_2S_2O_8$ (40 mM) as oxidizing agent. Following the irradiation for a determinate time (see **Table IV.5**), the reaction products were extracted with dichloromethane three times, dried with Na_2SO_4, quantified by ^{1}H NMR spectroscopy (see the following **Figure IV.5** and (**Annex I Figures SIV.2 - SIV.5**), and confirmed by GC-MS analysis (see **Annex I Figure SIV.6**)

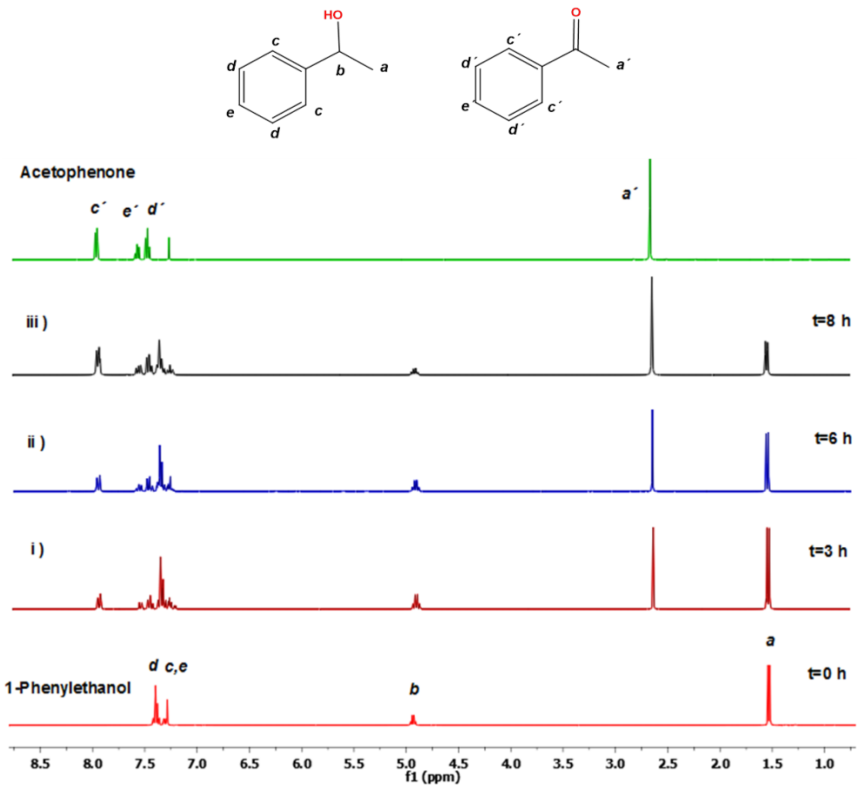

Figure IV.5. Representative ^{1}H NMR spectra of the reaction mixtures of the substrate (1-phenylethanol) and the corresponding oxidation product (acetophenone), dissolved in $CDCl_3$ at room temperature. i) 3h after irradiation, ii) 6h after irradiation, iii) 8h after irradiation after pH neutralization. The ^{1}H NMR spectra of 1-phenylethanol and acetophenone are included as control at the bottom and the top, respectively.

1-Phenylethanol was taken as the reference compound to find the optimal reaction conditions. Then, preliminary catalytic oxidation studies at different concentrations of **Na[1]** as photoredox catalyst were performed for 3h (see **Table IV.4.**) while maintaining constant concentrations of substrate (1-phenylethanol) and $Na_2S_2O_8$. The results showed that an increased amount of acetophenone is produced at higher catalyst loadings. However, as shown in **Table IV.4**, a six fold increase in catalyst concentration results only in a 1.7-fold increase in yield. Consequently, lower concentrations of catalyst seem to be more effective.

Table IV.4. Oxidation tests of 1-phenylethanol performed with cobaltabis(dicarbollide) complex Na[3,3'-Co(1,2-$C_2B_9H_{11})_2$]. Conditions: catalyst (0.08-0.48 mM), substrate (20 mM), $Na_2S_2O_8$ (40 mM), 5 ml 0.1M phosphate buffer solution at pH=7.2, light irradiation for 3h.

[Na[1]]	% Yield
0.08 mM	33
0.12 mM	38
0.16 mM	45
0.24 mM	52
0.48 mM	57

Thus, we took the lowest tested concentration of [3,3'-Co(1,2-$C_2B_9H_{11})_2]^-$ (0.08 mM) as optimal for extending the study to other alcohols. Also, different reaction times were tested with 1-phenylethanol as substrate (see in **Figure IV.6.**). We choose 8h as optimal time to perform the catalytic experiments, but we also studied the performance of the catalyst after 6h of reaction.

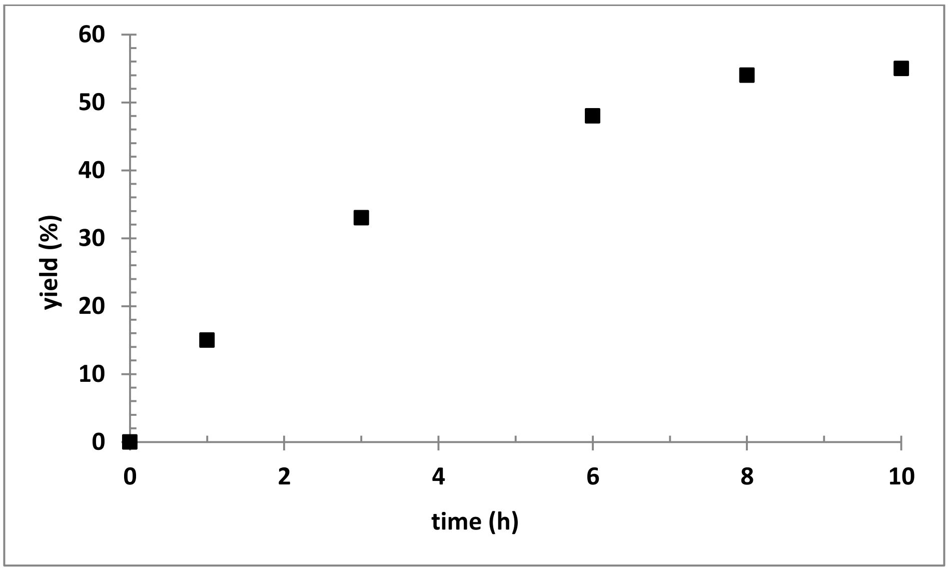

Figure IV.6. Plot of yield as a function of time for the photoredox catalysis of 1-phenylethanol. Conditions: Na[3,3'-Co(1,2-$C_2B_9H_{11})_2$] (0.08 mM), substrate (20 mM), $Na_2S_2O_8$ (40 mM), 5 ml 0.1M phosphate buffer solution at pH=7.2, light irradiation (2.2 W, λ ~253.7 nm).

Blank controls showed that after 8h of reaction in the dark with all reagents in the reaction pot, no significant oxidation of alcohol occurred (<2%). With all components and light, with no exception, aldehyde or ketone was detected as only product of the oxidation reaction, and the selectivity was greater than 99%. **Table IV.5** lists the results obtained in the catalytic oxidation of different alcohols with **Na[1]** in phosphate buffer solution at pH 7.2 after 6 and 8h of reaction. These results show moderate to high yields of aldehydes or ketones. Oxidation of the secondary alcohol 1-phenylethanol (**Table IV.5, entry 1)** gives the corresponding ketone with slightly lower conversion than in the case of benzyl alcohol (**Table IV.5, entry 2)**. Nevertheless, the oxidation of the secondary alcohol diphenylmethanol to benzophenone showed the highest yield (**Table IV.5, entry 5)**. The conversion is enhanced by the presence of electron-donating substituents on the aromatic ring of benzyl alcohol (**Table IV.5, entry 3)** but decreased by the presence of electron-withdrawing substituents such as chloro **(Table IV.5, entry 4).** The general trend was the decreasing of the initial neutral pH from 7.2 to 5 or 6 after 6h of irradiation. To investigate the role of the pH, the reaction mixture of 1-phenylethanol (**Table IV.5, entry 1c)** was recovered to neutral pH after 6h of reaction by the addition of dilute NaOH and further irradiation for 2h more. The yield of the oxidation product increased from 48 to 62 %. The results revealed that increasing acidity of the catalytic solution deactivates the system and prove that protons are released in the mechanism. This fact induced us to use NEt_3 to corroborate our hypothesis (see below).

Table IV.5. Oxidation tests performed with **Na[1].** Conditions: **Na[1]** (0.08 mM), substrate (20 mM), $Na_2S_2O_8$ (40 mM), 5 mL 0.1 M phosphate buffer solution at pH 7.2 light irradiation (2.2 W, ʎ=253.7 nm) for 6 and 8h. Yield values in the absence or in the presence of 40 mM NEt_3.

Entry	Substrate	Product	Yield(%) (no NEt_3)	Yield(%) (with NEt_3)
1	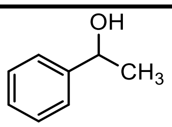	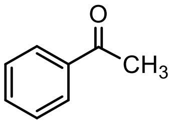	48 [a], 54 [b] 62 [c]	91 [b]
2	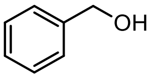	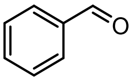	53 [a] 63 [b],	92 [b]
3	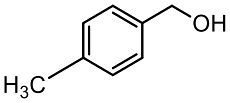	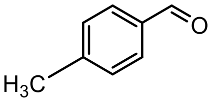	63 [a] 67 [b]	94 [b]
4	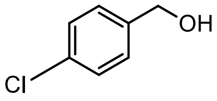	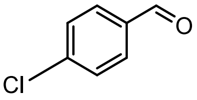	50 [a] 59 [b]	75 [b]
5	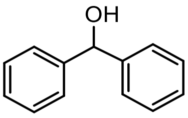	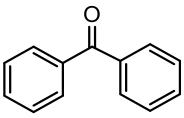	78 [a] 85 [b]	94 [b]

[a] After 6 h of reaction. [b] After 8 h of reaction. [c] After 8 h of reaction, with previous neutralization after 6 h.

The MALDI-TOF mass spectra of a solution of **Na[1]** were made before and after the catalytic experiments, showing that most of the catalyst remained unchanged after the catalysis, only 10 % was hydroxylated,[242] as is showed in **Figure IV.7**. According to the computational studies the hydroxylated derivative maintains the photoredox capacity, so its formation should not affect the conversion, as is showed in (**Annex I. Table SIV 1.2)**.

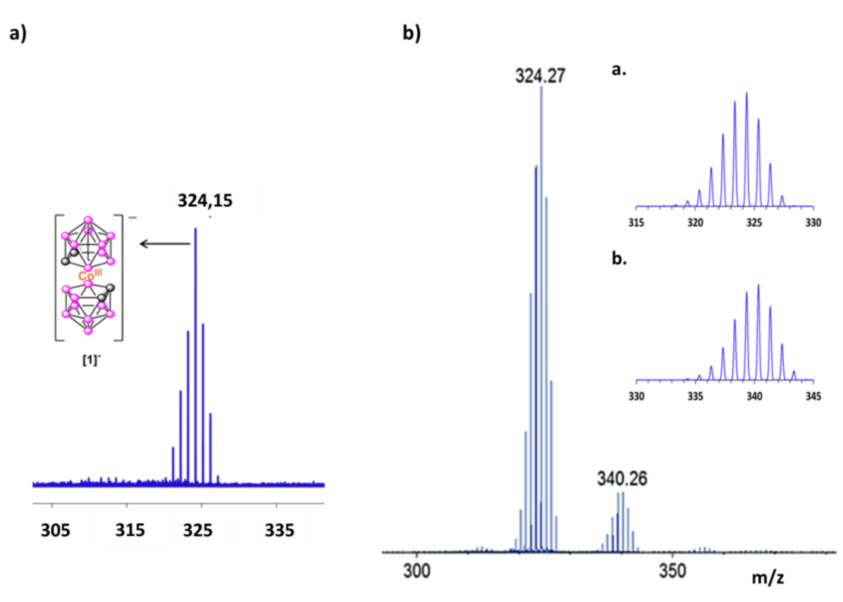

Figure IV.7. Experimental MALDI mass spectrum of **Na[1]** a) before and b) after the photocatalytic oxidation of 1-phenylethanol. In b) The peak at m/z 324 corresponds to $[3,3'\text{-}Co(1,2\text{-}C_2B_9H_{11})_2]^-$, and that on the right to $[3,3'\text{-}Co(1,2\text{-}C_2B_9H_{11})(1,2\text{-}C_2B_9H_{11}O)]^-$. Simulated spectra for a) $[3,3'\text{-}Co(1,2\text{-}C_2B_9H_{11})_2]^-$ = 324.28 (m/z) and b) $[3,3'Co(1,2\text{-}C_2B_9H_{11})(1,2\text{-}C_2B_9H_{11}O)]^-$ = 340.28 (m/z).

The LMCT mode suggested by the DFT calculations and the electrochemistry of **Na[1]** highlight that $[Co^{IV}]$ is a strong oxidizing agent which can be obtained by two ways, in an electrochemical or a photoinduced manner. The reaction pathway postulated showed in (**Figure IV.8**) accounts for the observed photoredox-catalyzed oxidation of alcohols by **Na[1]**. In the reaction pathway, incident photons are absorbed by photoredox catalyst $[3,3'\text{-}Co^{III}(1,2\text{-}C_2B_9H_{11})_2]^-$, which undergoes excitation to form $[3,3'\text{-}Co^{III}(1,2\text{-}C_2B_9H_{11})_2]^{*-}$, which experiences an oxidative quenching by $S_2O_8^{2-}$, the oxidizing agent, to generate two strong oxidizing agents: $[3,3'\text{-}Co^{IV}(1,2\text{-}C_2B_9H_{11})_2]$ and $SO_4^{\cdot -}$. The generation of $SO_4^{\cdot -}$ is well documented and is normal for the oxidation of other metals like Fe^{II} or Ag^{I} by $S_2O_8^{2-}$ to Fe^{III} or Ag^{II}, respectively.[243] The photogenerated strong oxidant Co^{IV} is able to oxidize the alcohol to the corresponding alcohol radical, which in the presence of the $SO_4^{\cdot -}$ leads to the corresponding aldehyde or ketone. With the proposed pathway, the exchange of two electrons and two protons takes place in the oxidation of alcohols, with associated increase of the acidity in the reaction medium, as we have also evidenced after the catalytic tests. The increased acidity could be responsible for the moderate yield observed in the absence of base, as we have seen at the results on (**Table IV.5)**.

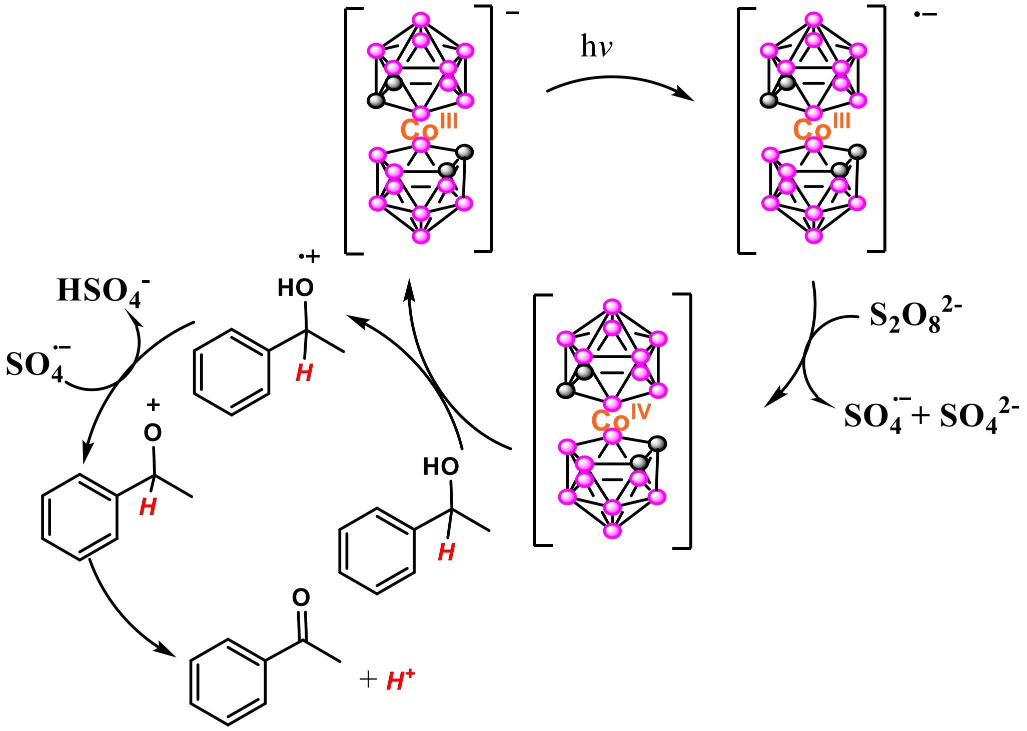

Figure IV.8. Suggested mechanism for the alcohol oxidation with **Na[1]** upon UV light irradiation.

To support the postulated pathway a weak base was added to the system. For convenience and availability, we added 0.2 mmol of NEt_3, twofold in concentration with respect the substrate added (0.1 mmol). For 1-phenylethanol as substrate, base addition resulted in a significant increase of the desired product (ketone), yielding to 91 % with turnover number (TON) of 227 after 8 h of irradiation (see **Table IV.5, entry 1**). We extended our study to other alcohols, to assess the catalytic activity in presence of NEt_3 (**Table IV.5**). In all experiments (see last column in **Table IV.5**) the degree of conversion improved remarkably, in most cases to greater than 90 %, while maintaining selectivity greater than 99%. This, along with the fact that the cobaltabis*ortho*dicarbollide remains practically unchanged after the catalytic oxidation reaction (only 10 % is hydroxylated) is consistent with the proposed pathway.

Just after irradiation and before extraction, on addition of $[Me_4N]Cl$ the salt $[Me_4N][3,3'\text{-}Co(1,2\text{-}C_2B_9H_{11})_2]$ precipitates. After filtration, solubilization with acetonitrile, and addition of water, the solution was passed to a cationic exchange resin loaded with Na^+ to regenerate **Na[1].** The resulting catalyst has been tested in a second catalytic reaction with 1-phenylethanol as substrate, in the presence of NEt_3, which produced 89 % of the corresponding ketone, which is similar to the yield observed in the first run. Notwithstanding, in the major part of studies, we skipped this step and proceeded directly after the irradiation to extraction with organic solvent (dichloromethane).

Cobaltabis*ortho*dicarbollide **[1]**$^-$ is a platform with many sites for the substitution of B-H by B-Cl, which results in the formation of chlorinated derivate **[Cl$_x$-1]$^-$,** successive substitutions of which, modulate the redox potentials,[244] as is showed in **Figure IV.9**, that shows the cyclic voltammetries from **Na[1]** and their dichloro **[Cl$_2$-1]** and hexachloro derivative **[Cl$_6$-1],** all vs $Fc^{+/0}$.

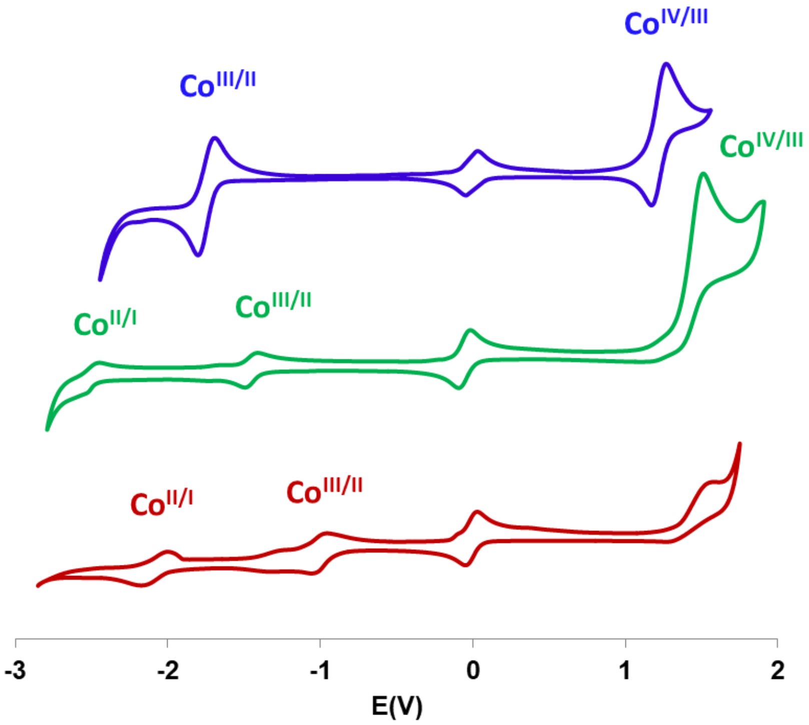

Figure IV.9. CV of **Na[1]** (blue), **Na[Cl$_2$-1]** (green) and **Na[Cl$_6$-1]** (brown) in CH_3CN+ 0.1M TBAH. All potentials *vs* Ferrocene.

[1]$^-$ shows three quasireversible waves in cyclic voltammetries at -2.70, -1.75 and +1.22 V *vs* ferrocene assigned to Co^{II}/Co^{I}, Co^{III}/Co^{II} and Co^{IV}/Co^{III}, respectively. The two latter redox couples are showed in (**Figure IV.9 blue line**).

It has been observed that a simple substitution produces a shift of the redox potential of approximately 0.12 V to more anodic voltages. Hence, examining the $E_{1/2}$ for the dichlorinated derivative, as is showed in (**Figure IV.9 green line**), the addition of two Cl would implies an estimated increase of 0.24 V to more positive values, and the real values are found at -2.50 V and 1.44 V, applied to the Co^{II}/Co^{I} and Co^{IV}/Co^{III} couples, respectively. The negative $E_{1/2}$ peaks indicate that introducing one and two electrons into Co^{III} system is energy intensive.[245] Thus, the real redox potential of the dichlorinated anion is -1.45 V for the couple Co^{III}/Co^{II}, about 0.3 V more positive than for **$[1]^-$,** corresponding to two steps of dehydrochlorination.

In the case of the hexachlorinated derivative (see **Figure IV.9 red line**), the addition of 6 Cl units to the structure allows to achieve the potentials -2 V, -1 V, approximately, corresponding to the Co^{II}/Co^{I}, Co^{III}/Co^{II}. Less data has been obtained for the Co^{IV}/Co^{III} couple due to the overall anodic shift upon higher chlorination that has taken the $E_{1/2}$ value for this couple to the almost anodic edge of the solvent.

As has been observed, the successive chlorine substitutions produce the shifting of the redox potentials to more anodic voltages. Consequently, this results in a decrease in the energy gap of the frontier orbitals, which leads to longer wavelengths with respect to unsubstituted **$[1]^-$.** This behavior allows the absorption maximum of the UV-Vis spectrum to be shifted towards the visible region. Among these chlorinated compounds, **$[Cl_2\text{-}1]^-$** and the **$[Cl_6\text{-}1]^-$** were selected to explore their behavior as catalysts in the oxidation of alcohols. The photocatalytic oxidation experiments were all carried out by exposing the quartz reaction vials to UV irradiation (λ=253.7 or 352 nm) for different reaction times under the same conditions as listed in the above **Table IV.5** exposed for **Na[1].** The results shown in (**Table IV.6)** indicate high yields, in some cases total conversion, after 6h of irradiation when using a wavelength of 352 nm of irradiation, closest to the maximum absorbance of the derivate catalysts (see above **Figure IV.2b**). As expected, the performance of the catalysts was lower when the irradiation of the samples was done with a lamp of wavelength 253.7 nm, far from their absorption maxima. In all cases, the selectivity for the corresponding aldehydes or ketones was greater than 99%. Under the studied conditions, **$Na[Cl_6\text{-}1]$** as catalyst, generally shows slightly higher activity than **$Na[Cl_2\text{-}1]$,** probably due to the enhanced oxidizing capacity of Co^{IV} in the former, as a consequence of the presence of more electron-withdrawing substituents on the metallacarborane platform.

With the purpose to decrease even more the requirements of these metallacarboranes, we tested the behavior of the three catalysts in the photoredox oxidation of one aromatic secondary alcohol like diphenylmethanol, using only water, no buffer, and NEt_3 or K_2CO_3 as base. For the use of **Na[1]** we employed lamps of irradiation of 300 nm, closer to the absorption maximum of this specie, observed in UV/Vis spectrum (293 nm). The results listed in (**Table IV.7**) unveil the high performance in water in absence of phosphate buffer for all the catalysts used and their activities are a little bit enhanced in all cases when we replaced the organic base by that inorganic like K_2CO_3. The results revealed by **[1]**$^-$ both using NEt_3 or K_2CO_3 after 6h of reaction with a 300 nm lamp are remarkable with yields of 96 % and >99%, respectively, which are slightly higher than those obtained in phosphate buffer media after 8h , being 94 % (see **Table IV.5, entry 5**).

Considering the good results exposed by the three catalysts shown above, we wanted to advance even more, by the replacement of $Na_2S_2O_8$ by air. In a preliminary study, we carried out the oxidation of a secondary aromatic alcohol like diphenylmethanol in a water/ K_2CO_3 solution using **[1]**$^-$ as a reference catalyst and an air stream during 6 h of irradiation at λ=300 nm. The results showed an almost total yield in benzophenone (98 %). This preliminary and promising result, suppose a step towards the development of practical processes with inorganic catalyst systems based on boron compounds and it is unprecedented in the literature. More studies are being performed in this regard.

To learn whether water was a key reaction medium, we tested the oxidation of diphenylmethanol as substrate in an organic solvent like acetonitrile using NEt_3 as base and an air stream as oxidant. After 6h of irradiation, practically no conversion was observed. Then the reaction medium was changed to acetonitrile/water in 9/1 and 8/2 ratio with K_2CO_3 and after 6h of irradiation we observed conversions of 26 and 34 %, respectively, with a total selectivity towards the desired product (benzophenone). This result may indicate that the acetonitrile in water/acetonitrile mixtures displaces the necessary water molecules for the catalysis to occur from the vicinity of $[3,3'\text{-}Co(1,2\text{-}C_2B_9H_{11})]^-$ (the catalyst) and thus prevents electron transfer, which is in accordance with experimental values reported earlier.[246] These results indicate that water is a key participant for these systems to work efficiently as catalysts in the photoredox oxidation processes. The fact that an all-inorganic catalyst system consisting of water as solvent, K_2CO_3 as base, a metallabisdicarbollide photoredox catalyst with fully inorganic ligands and an earth-abundant transition metal, and air as oxidizing agent can oxidize alcohols to aldehydes or ketones, indicates the feasibility of all-inorganic catalytic processes with earth-abundant transition metals.

Table IV.6. Oxidation tests performed with chlorinated cobaltabisdicarbollide complexes **Na[Cl$_2$-1]** and **Na[Cl$_6$-1]**. Conditions: catalyst (0.08 mM), substrate (20 mM), $Na_2S_2O_8$ (40 mM), NEt_3(40 mM), 5 mL 0.1 M phosphate buffer solution at pH 7.2, light irradiation for 4, 6, and 8h. Percentage yields.[a]

	8h λ= 253.7 nm		**4h λ= 352 nm**		**6h λ= 352 nm**	
Substrate	**[Cl$_6$-1]$^-$**	**[Cl$_2$-1]$^-$**	**[Cl$_6$-1]$^-$**	**[Cl$_2$-1]$^-$**	**[Cl$_6$-1]$^-$**	**[Cl$_2$-1]$^-$**
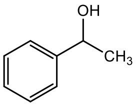	40	50	60	53	92	86
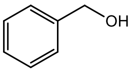	22	32	61	63	90	81
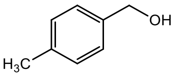	45	40	67	46	>99	85
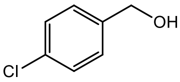	21	30	82	60	85	77
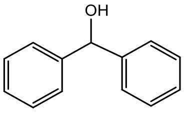	68	89	93	90	>99	93

[a] yields of products were determined by NMR spectroscopy.

Table IV.7. Oxidation tests on diphenylmethanol performed with **Na[1]**, **Na[Cl$_2$-1]**, and **Na[Cl$_6$-1]**. Conditions: catalyst (0.08 mM), substrate (20 mM), $Na_2S_2O_8$ (40 mM), 5 mL of an aqueous solution containing 40 mM of NEt_3 or K_2CO_3. Light irradiation for 6h.

Catalyst	**%Yield (Water/NEt$_3$)**	**%Yield (Water/K$_2$CO$_3$)**
Na[1], λ= 300 nm	96	>99
Na[Cl$_2$-1],λ= 352 nm	89	89
Na[Cl$_6$-1],λ= 352 nm	93	94

IV.1.3.2. Photocatalytic oxidation of alcohols under uncommon conditions (0.01-0.1 mol % of catalyst (0.002 mM - 0.02 mM)

As mentioned above, a six fold increase in catalyst concentration from 0.4 mol % (0.08 mM) to 2.5 mol% (0.5 mM) of **[1]**$^-$ results only in a 1.7-fold increase in conversion, whereas the UV-Vis absorption spectrum increases according to the increase in concentration. This seems to indicate that lower concentrations of catalyst are more effective. Thus, we maintain the concentrations of substrate and oxidizing agents constant, as in the earlier described experiments, but we reduced the catalyst loading to 0.1 mol% (0.02 mM) and 0.01 mol %(0.002 mM) as opposed to the original 0.4 mol% (0.08 mM), corresponding to catalyst: substrate: oxidizing agent ratios of 1:1000:2000 and 1:10000:20000, all in homogeneous phase. For these experiments, we used K_2CO_3 as base, a total irradiation time of 8h, and pH 7, with readjustment at t=4h. Control experiments revealed that no reaction occurred in the absence of photocatalyst **Na[1]** or light. **Table IV.8** lists the results corresponding to the photooxidation of different alcohols, including aliphatic alcohols. In general lines, primary and secondary aromatic alcohols with different substituents were found to be effective in the photooxidation process, and the primary aromatic alcohols were slightly less reactive than the secondary ones. The yields observed for 1-phenylethanol (**1**) and diphenylmethanol (**5**) were remarkable, greater than 99%, in both cases for 0.01 mol% catalyst loading (0.002 mM). To the best of our knowledge these are among the highest turnover numbers (TON=10000) achieved in alcohol photoredox oxidation under homogeneous conditions. With the same catalyst loading of 0.01 mol % (0.002 mM), **Na[1]** shows high efficiency towards primary and secondary aliphatic alcohols, with yields greater than 90 % and selectivities greater than 99 %. Cyclohexanol yielded in 93% into (**6**) product, 1-hexanol and 2-ethoxyethanol yielded acids in 90% of (**7**) and in 95% of (**8**), respectively. The observed quantitative conversion with 1-phenylethanol and diphenylmethanol is in support of the pathway exposed in (**Figure IV.8**)**.** If 1 mol of $S_2O_8^{2-}$ is needed for each mol of alcohol to perform the oxidation reaction, on reducing the fraction of oxidizing agent the conversion should be decreased if the ratio of oxidizing agent to substrate is smaller than 1:1. Under the same conditions as in (**Table IV. 8**), but with reduced amount of oxidizing agent in a ratio (1:10000:10000), the degree of conversion should be similar to 100 %, but it could be a bit lower due to the kinetics of the reaction; we found 91 %, and if the ratio is lowered to 1:10000:5000, the maximum yield would be of 50 %, being experimentally 43 %. This fact is in agreement with the pathway proposed in the (**Figure IV.8)**. Further studies on the application of these cobaltabis*ortho*dicarbollides as photoredox catalysts to other substrates are underway.

Table IV. 8. Product set obtained from photooxidation of alcohols by **Na[1]**.[a]

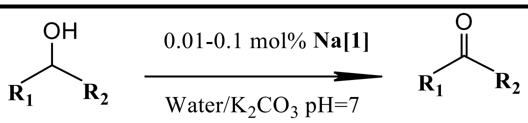

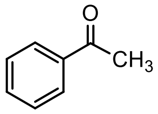

1

>99%, TON=1000 (0,1mol%)

>99%, TON=10000 (0,01mol%)

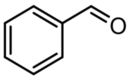

2

>96%, TON=960 (0,1mol%)

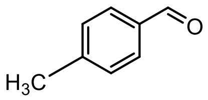

3

>97%, TON=970 (0,1mol%)

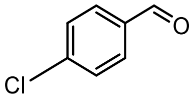

4

>94%, TON=9400 (0,01mol%)

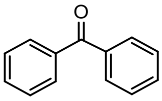

5

>99%, TON=1000 (0,1mol%)

>99%, TON=10000 (0,01mol%)

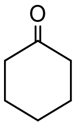

6

93%, TON= 9300 (0,01mol%)

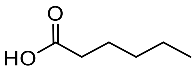

7

91%, TON=9100 (0,01mol%)

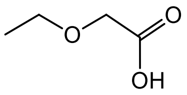

8

97%, TON=9700 (0,01mol%)

[a] Conditions: **Na[1]** (0.002 or 0.02 mM), substrate (20 mM), $Na_2S_2O_8$ (40 mM), 5 mL potassium carbonate solution at pH=7 ;light irradiation 8h using a lamp with λ =300 nm; yields and TONs values obtained are shown together with loading of **Na[1]** in parenthesis. Yields of products were determined by NMR spectroscopy (see **Annex I Figures SIV.7-14**).

In summary, we have shown that cobaltabis(dicarbollide), $[3,3'\text{-Co}(1,2\text{-}C_2B_9H_{11})_2]^-$, and its chloro derivatives represent efficient compounds, acting both as catalyst and photosensitizer, for the photooxidation of alcohols. In most of the studied examples, using a catalyst load of 0,4 mol %, high yields near 90-95% have been obtained, with selectivity values >99%. By reducing the catalyst load to 0,01 mol %, quantitative conversion of reactants into products have been achieved, in some cases over 99% yield, exhibiting the catalyst high efficiency to reach TON=10000, and proving that a higher yield is achieved with 45 times less concentrated catalyst. These compounds operate in a catalytic system in which the solvent is water, the metal in the catalyst is an earth-abundant transition metal, the ligand is inorganic, the base is an inorganic salt, the reagent is an inorganic salt or air and the excitation source is light. The only organic compound in the mixture is the substrate.

IV.2. Non-covalently Linked Metallacarboranes on Functionalized Magnetic Nanoparticles as Highly Efficient, Robust and Reusable Photocatalysts in Aqueous Medium

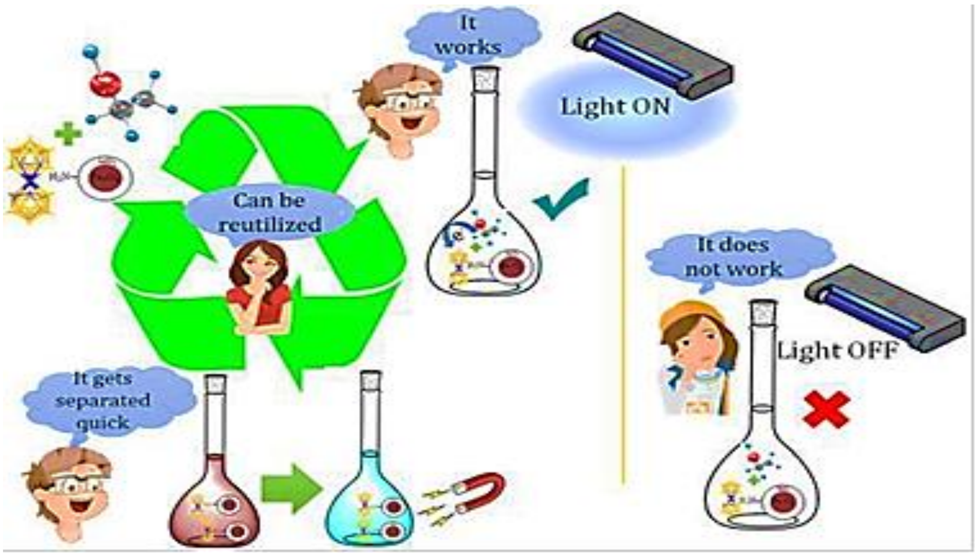

We have prepared heterogeneous catalysts in which the catalyst, that is molecular, is firmly bound to the magnetic support just by non-bonding interactions, and with a very efficient and fast process of binding. We shall see that the efficiency of the catalysis extends to many cycles without the loss of conversion.

With all this in mind, we describe the synthesis and characterization of magnetic nanoparticles (MNP) coated with an inorganic shell of silica (SiO_2), and their functionalization with amine groups ($-NH_2$), through which the cobaltabis(dicarbollide) complex is attached. The colloidal stability of the MNP in water has been studied using different surfactants, since this is a huge issue in catalysis. We also report the excellent performance of the cobaltabis(dicarbollide) as a heterogeneous catalyst for the photooxidation of aromatic and aliphatic alcohols in water, even using small loading of catalyst 0,01 mol % and short catalytic times, along with the re-utilization of the corresponding supported catalyst and its recovery by a magnet.

IV.2.1. Catalyst Preparation, Structural and Spectroscopic Characterization.

The synthetic strategy carried out for the immobilization of H[3,3'-Co(1,2-$C_2B_9H_{11})_2$], H**[1]**, on silica coated Fe_2O_3 magnetic nanoparticles (MSNPs) is shown in **Scheme IV.1**. The anchoring of **H[1]** to MSNP has never been explored before, and it has been done and studied by the groups for the first time. Cobaltabis*ortho*dicarbollide, **[1]**$^-$, is extremely stable in water and can form ion-pair complexes with protonated amino groups in the form ([cation-NH]$^+$ [COSAN]$^-$) through an ionic interaction.[247] Hence, the synthetic approach for the immobilization of H**[1]** is based on the formation of hybrid materials linked by ionic interactions between cobaltabis*ortho*dicarbollide and the functionalized magnetic nanoparticles with amine groups of the type ($-NH_2$), $Fe_3O_4@SiO_2-NH_2$ (MSNPs-NH_2). Then, these functionalized magnetic nanoparticles were used for the anchoring of the H**[1]** complex to them.

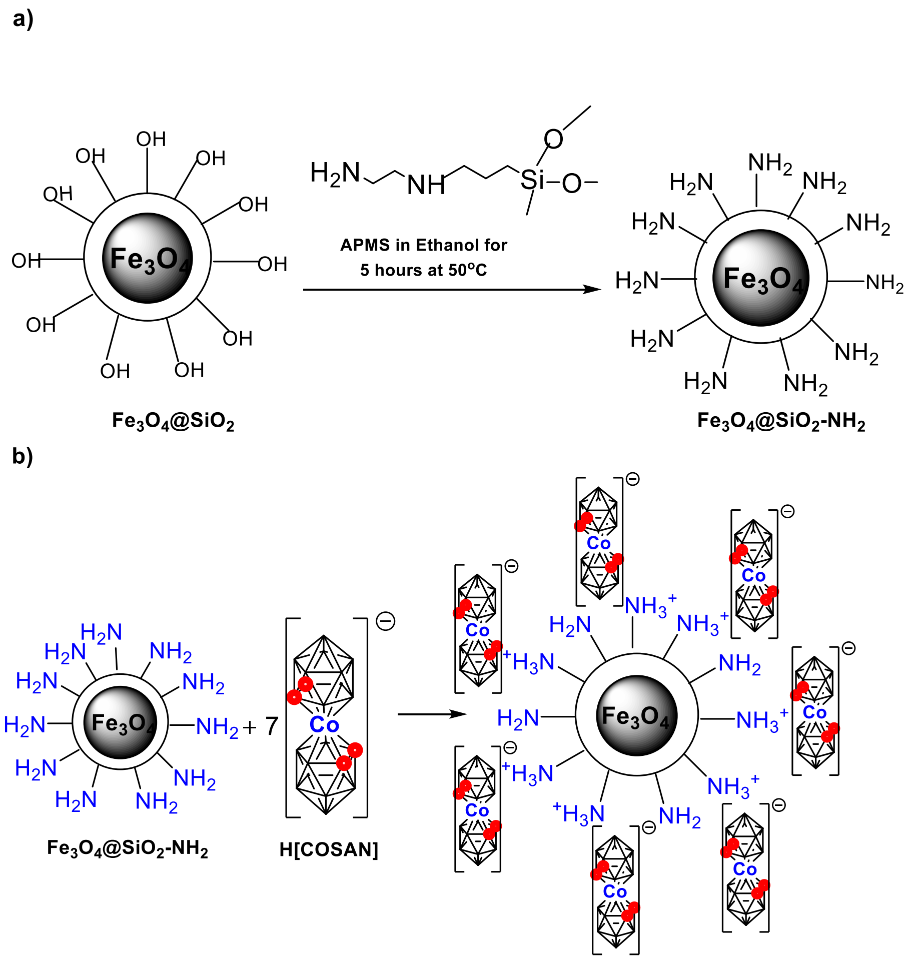

Scheme IV.1. The synthetic strategy used for a) the functionalization of MSNP with amine groups, MSNP-NH_2 and b) for the immobilization of H[COSAN], **H[1]**, MSNP-NH_2@**H[1].**

Previously, it was necessary to carry out the synthesis of Fe_3O_4 magnetic nanoparticles (MNPs) by means a coprecipitation method,[248] and this core of magnetite was then further encapsulated in a silica shell for the formation of silica-coated magnetic nanoparticles, $Fe_3O_4@SiO_2$ (MSNPs), see the procedures in (**Annex II Figure SIV.15)**.

These nanoparticles were functionalized with amine groups (**Scheme IV. 1a**) by mixing the MSNP with 3-(2-aminoethylamino)propylmethyldimethoxy silane (APMS) in ethanol at a temperature of 50^0C for 5h to reach the hydrolysis of the methyl groups.[249] The corresponding amine-coated nanoparticles ($MSNPs-NH_2$) were then mixed with cobaltabis*ortho*dicarbollide, **$[1]^-$,** in water and sonicated for 30 min to afford brown silica particles that were washed 10 times with water, separated by a magnet, and dried under vacuum at a temperature of 80 ^{0}C, giving the corresponding cobaltabis*ortho*dicarbollide anchored to the silica support $Fe_3O_4@SiO_2-NH_2-$H[COSAN] ($MSNPs-NH_2@$**H**[**1**]) in a noncovalently bonded manner (**Scheme IV. 1b**).

UV-visible spectra studies were carried out by our research group to quantify the anchoring of **H[1]** on the amine-functionalized silica, $Fe_3O_4@SiO_2-NH_2$, as is showed in **Figure IV.10** furthermore to confirm the presence of metallacarborane on the surface of the nanoparticles.

The UV-vis spectrum indicates that **H[1]** interacts with the nanoparticles $MSNPs-NH_2$ since the absorbance of the band at 446 nm decreases with increasing amount of nanoparticles. For every 5mg of $MSNPs-NH_2$, 0.14 ± 0.03 mM of **H**[**1**] is consumed to form the anchored complex MSNPs-NH2@H[**1**] (**Figure IV.10 a**). The saturation occurs when 30 mg of the nanoparticles has been added to the solution, bringing 0.028 mmol of total amount of metallacarborane anchored to $MSNPs-NH_2$ per 100 mg of nanoparticles (**Figure IV.10 b**).

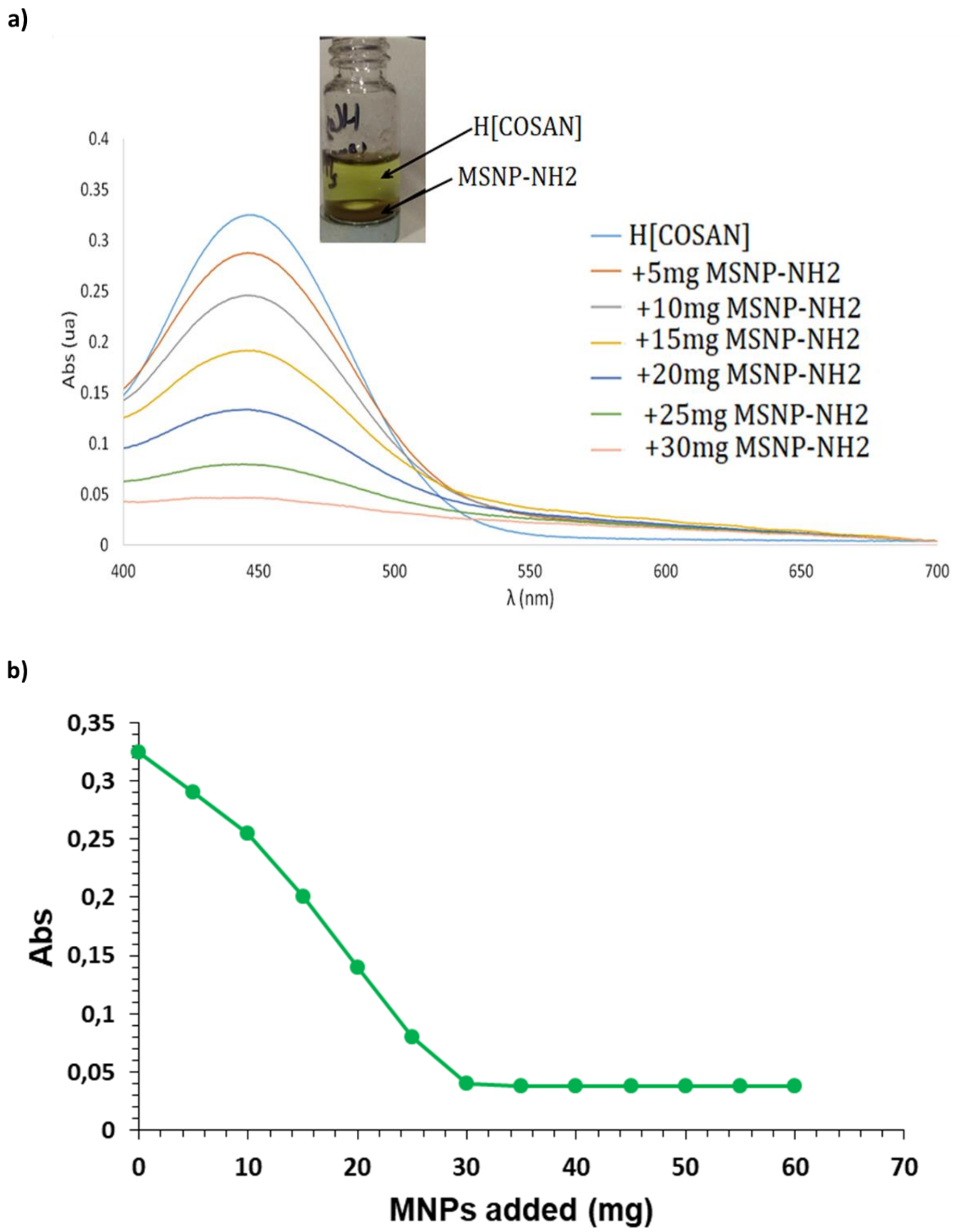

Figure IV.10. a) UV-vis spectra corresponding to the interaction of MSNP-NH_2 with 1 mM of **H[1]** in water. The inset photo shows the solution measured and the magnetic nanoparticles extracted using an external magnet at the bottom; b) Evolution of absorbance of a solution of 1 mM of **H[1]** in water with the addition of different amounts of MSNP-NH_2.

At the same time, another an UV-vis experiment was carried out to assess the time needed for the extraction of the magnetic nanoparticles with a magnet. The results showed that a time of 10 min was enough to attract all of the magnetic nanoparticles

(**Figure IV.11**).

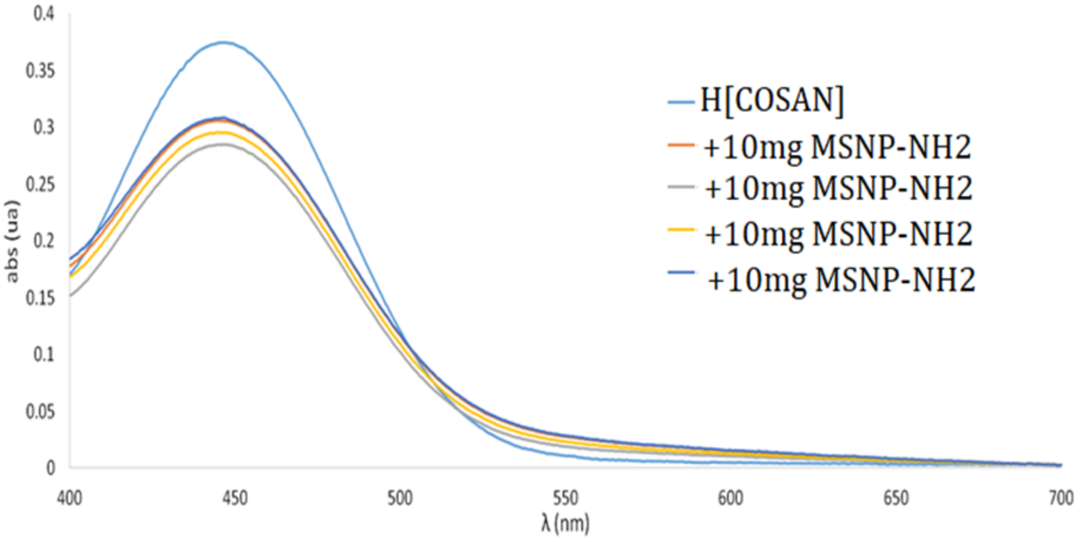

Figure IV.11. UV-vis spectra at different time of extraction of the MNP. It shows that 10 minutes is sufficient for the extraction of all the MNP by an external magnet.

The characterization of the nanoparticles synthesized has been done previously in our group.[249] Here we indicate a summary of this characterization.

The ζ-potential studies revealed that the positive value located in a range of 10-30 mV, indicated that the ammonium cations are located on the surface of nanoparticles,[250] and their tendency to aggregate. This value is transformed to a negative when **[1]**$^-$ is anchored on their surface.

The XRD pattern supported the presence of magnetite (Fe_3O_4)[251] or a mix with maghemite (γFe_2O_3)[248b] on the magnetic nanoparticles. Transmission electron microscopy (TEM), performed to observe the shape and size of the particles, and the Gaussian representation, showed the spherical shape of these nanoparticles with a mean size of 9.34 ± 1.6 nm, that increases to 11.22 ± 2.13 nm and 14.17 ± 1.03 nm, when the structures become MSNPs-NH_2 and MSNPs-NH_2@**H[1],** respectively, also evidencing that **[1]**$^-$ is located between MSNPs-NH_2 and tends to aggregate the complex. All these trends are showed in (**Annex II Figure SIV.16**).

IR spectra of MSNPs-NH_2 and MSNPs-NH_2@**H[1]** show the bands near 546 cm^{-1} for the case of MSNPs-NH_2 and 542 cm^{-1} in the nanoparticles functionalized with **[1]$^-$,** MSNPs-NH_2@**H[1],** which can be assigned to $\upsilon_{Fe\text{-}O}$ stretching modes, while the $\upsilon_{Si\text{-}O}$

stretching mode is located to 1074 and 1071 cm^{-1}, respectively. The IR spectrum of the latter shows a band corresponding to the υ_{B-H} stretching mode at around 2560 cm^{-1}, typical in metallacarborane compounds. These absorptions indicate the fact of the anchoring of the complex **H[1]** to the support (**Figure IV.12**).

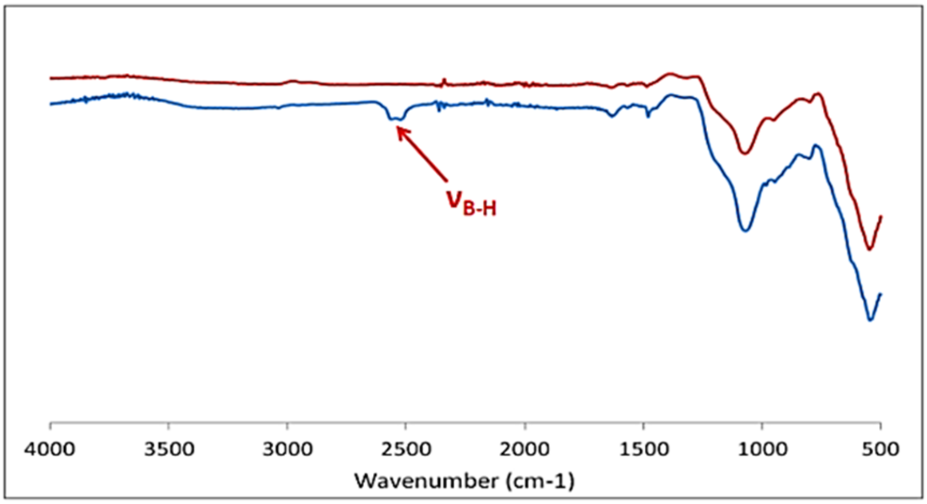

Figure IV.12. IR spectra of MSNP-NH_2 (red) and MSNP-NH_2@**H[1]** (blue).

Magnetic Hysteresis studies were carried out and revealed that the anchoring of the photocatalyst onto the magnetic nanoparticles does not vary the magnetic behaviour of the nanoparticles, since a saturation magnetization (Ms) value of 29.1 emu/g has been observed in both cases (**Annex II Figure SIV.17**).

Colloidal Stability

The colloidal stability is an important issue in the study of nanoparticles. The more these magnetic nanoparticles are stable in a colloidal state, the more difficult is to separate them by a magnet. Large MNPs evidence higher magnetization values although with less stability in the colloidal state, and they tend to form aggregates. To improve the stability of the MNPs synthesized in this work, the sonication was used as an effective way for the disaggregation to maintain the dispersion of them in the colloidal state.

The MSNPs-NH_2@**H[1]** composite is maintained in a suspended state just for a few hours; however, it is enough for the applications sought and large enough to allow magnetic separation in a few minutes of time. Then, to improve the stability for catalytic applications which need longer times, the surface of the nanoparticles was coated with different surfactants with the goal to increase the viscosity of the media, which furthermore for preventing the aggregation.

In this sense, five different surfactants were tested, the results are showed in (**Annex II Table SIV 2.3**), where are showed the ζ-potential values of each surfactant. The stability was tested for amine-functionalized MSNPs-NH_2, and in the case of surfactants tested, dimethyl di-octadecyl ammonium chloride provided long-term stability, due to that it increased the viscosity of the medium and hence stopped MSNPs-NH_2 from aggregating. The increase of the viscosity of the medium, results in the dramatically reduction of the diffusion rate for the nanoparticles and therefore prevented the aggregation of particles into larger dimensions.

Notwithstanding, a major drawback was that these MNPs were difficult to extract using an external magnet. Then, different concentrations of dimethyl di-n-octadecyl ammonium chloride were studied (see **Annex II Figure SIV.18**). The tendency was the same; the more stable are they became, the more difficult to extract them. Up to 15 mg of the surfactant, the dispersion was stable, and with lots of time, a small amount of MNPs could be extracted by the magnet. Nevertheless, the obtention of total dryness in MNPs, free from surfactant is difficult due to the highly viscosity of the suspension. As was said before, a compromise between colloidal stability and ease of MSNPs recovery was made, and for our case we observed that cetyl trimethyl ammonium chloride (CTAC), with the lowest ζ-potential, but still higher than 20 mV (negative), was the most suitable.

IV.2.2. Photocatalytic Alcohol Oxidation.

The heterogeneous photocatalytic activity of MSNPs-NH_2@**H[1]** was tested in the oxidation of different alcohols in water (pH=7, K_2CO_3), using $Na_2S_2O_8$ as the oxidizing agent. All the substrates were tested under analogous conditions using a loading of 0.1 or 0.01 mol % of the catalyst based on the amount of complex anchored on the nanoparticles, by exposing the reaction quartz vials to UV irradiation at ʎ=300 nm, at room temperature and atmospheric pressure. Initially, an optimization of the reaction time was carried out for the photooxidation process using 1-phenylethanol as the substrate and the yield values obtained at different times are showed in the following (**Figure IV.13)**. We have observed a certain degree of aggregation in the nanoparticles after 4h, which could be responsible for the 76 % of yield found after 8h of catalytic reaction (**Table IV.9, entry 4**). Then, we sonicated the mixture for 3 min after 4h of the reaction and continued the catalysis until 8h. In this way, we optimized the reaction times shown in (**Figure IV.13**), where almost a total conversion was attained after 8h of reaction. This time should be chosen as the optimal time to carry out the catalytic assays. In all cases, acetophenone was detected as an only product and the selectivity achieved were higher than 99%.

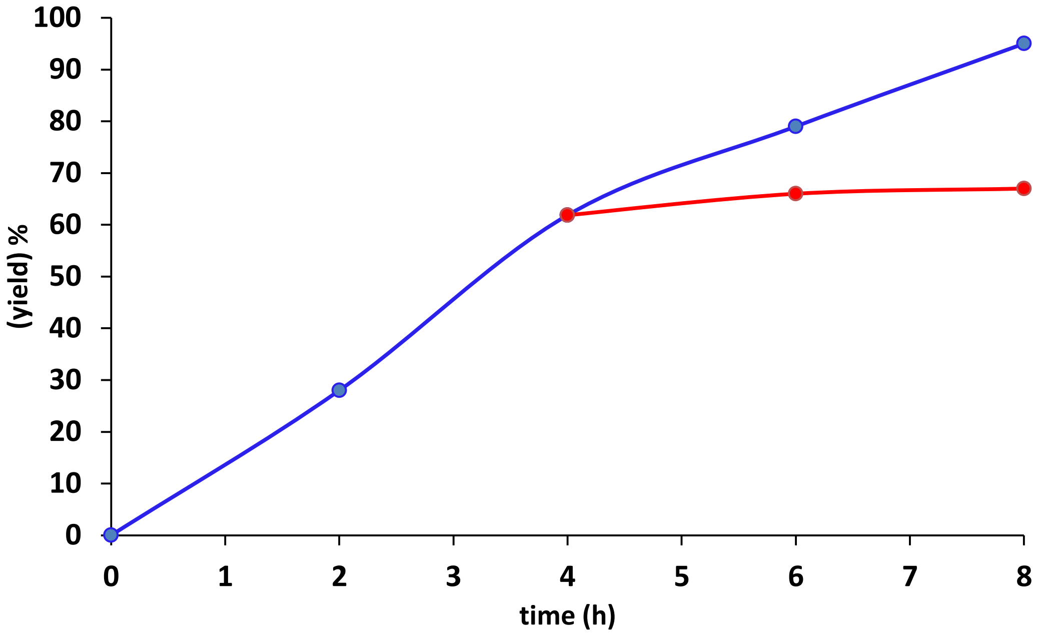

Figure IV.13. Plot of yield as a function of time for the photoredox catalysis of 1-phenylethanol using MSNP-NH_2@**H**[**1**] as catalyst. The blue curve shows the dependence of substract yield with the reaction time in presence of MSNP-NH_2@**H[1]** catalyst. The red curve shows the dependence of substracte yield with the reaction time after the catalyst was removed at 4h. Conditions: MSNP-NH_2@**H**[**1**] (0,1µmol), substrate (0,1 mmol), $Na_2S_2O_8$ (0,2 mmol), 5 mL potassium carbonate solution at pH=7 ;light irradiation using a lamp with λ =300 nm. Sonication after 4 hours**.**

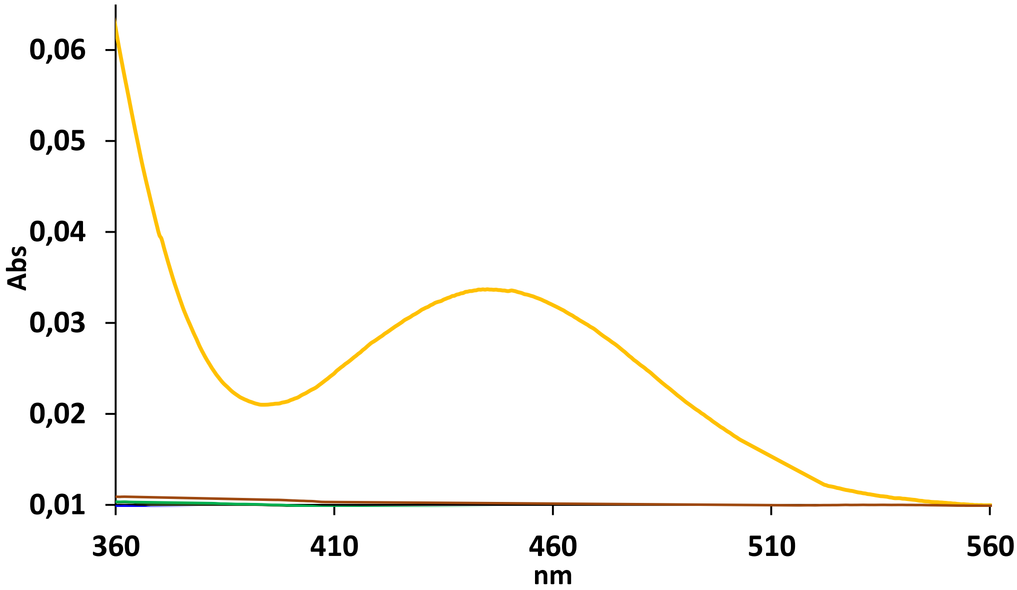

Figure IV.14. UV-vis spectra corresponding to a solution of 0.02 mM of [**1**]$^-$ in 5 ml of water (yellow line). UV-visible spectra of the solutions after the oxidation of 1-phenylethanol by MSNP-NH_2@**H[1]** catalyst, throughout the different reuses.

The results showed in (**Table IV.9**) highlights the extraordinarily effectivity of the heterogeneous catalyst in the photooxidation of aromatic and aliphatic alcohols. Blank experiments using nude MSNPs-NH_2 (**Table IV.9, entry 1**) or performed in the absence of light (**Table IV.9, entry 3)** with yield less than 6 % of acetophenone, revealing that the metallacarborane-free material is ineffective in the photooxidation process and that light is also needed.

The yields observed in the photooxidation of 1-phenylethanol by the homogeneous complex **Na[1]** (**Table IV.9, entry 2**) and by the supported MSNPs-NH_2@**H[1]** (**Table IV.9, entry 5**) are >99% in both cases, which seems to indicate that the support does not modify the catalytic properties of the metallacarborane under the same reaction conditions. In general, primary and secondary alcohols were found to be effective in the photooxidation process, the secondary aromatic alcohols were slightly more reactive than the primary ones. The quantitative conversion was obtained with 1-phenylethanol (**Table IV.9, entry 5**) .For the primary aromatic benzyl alcohol, the photooxidation to benzaldehyde showed high yield, 90 % (**Table IV.9, entry 6**)**.** The yield values enhanced by the presence of electron-donating substituents on the aromatic ring of the benzyl alcohol (**Table IV.9, entry 7**) but decreased by the presence of electron-withdrawing substituents, such as chloro (**Table IV.9, entry 8**). In the case of the aliphatic alcohols 1-butanol, 1-pentanol, 1-hexanol, and 2-ethoxyethanol, all were oxidized to the corresponding acids with high yields of 97 %, 98 %, 92 % and 96 % (**Table IV.9, entries 10, 11, 12 and 14**), respectively. The lower yield was exhibited by the isobutanol substrate (**entry 13**), being the latter 87 %. Using the secondary aliphatic alcohol, cyclohexanol a conversion of 98 % was achieved. Furthermore, we extended the study to interesting diols at an industrial level, diethylene glycol and 1,6-hexanediol. In both cases, the diacid has been obtained with good yields of 75 % and 92 % (**Table IV.9, entries 16 and 17**) respectively**.** Using the same conditions expressed in (**Table IV.9**)**,** although increasing the amount of oxidizing agent due to the presence of two alcohol groups , being the final ratio used (1:1000:4000), the degree of conversion increased to 99 % and 95 %, respectively. Important to remark is that blank controls have shown that after 8h of reaction, under the latter conditions and in the absence of MSNPs-NH_2@**H[1]** in the reaction medium, no significant oxidation of alcohol occurred (<10%).

A fact observed was the decreasing of the initial neutral pH of the system, ranged from 5 to 6. In the latter cases, it was necessary the readjustment of the pH after 4h of reaction, but obtaining high selectivity values >99%.

Furthermore, we verified that the catalytic activity proceeds from the heterogeneous catalyst and not from the release of the active catalytic species from the support during the catalysis, which indicates the presence of a homogeneous (leached) catalyst. Therefore, two experiments have been done. On one hand, the experiment consisted of stopping the photooxidation reaction of the substrate (1-phenylethanol) at 4h, removing the nanoparticles by a magnet, and continuing the reaction with the rest of solution until 8h. We have not observed further reaction in the absence of the MNPs; then, we can argue a lack of metal leaching in our photocatalytic experiment as was exposed in the above **Figure IV.13**. On the other hand, we experimented on the evaluation, through UV-visible spectroscopy, of the amount of metallacarborane complex in the reaction solvent after the oxidation of 1-phenylethanol. The results are showed in the above (**Figure IV.14**), where the absorption band corresponding of the complex is not observed, which reconfirms that the leaching of metallacarborane is negligible for the heterogeneous system.

As we have commented previously, after 4h of reaction, we have observed a certain degree of aggregation that has led to a decrease in the activity of the heterogeneous catalyst. With respect this fact, we have studied the effect of the presence of the surfactant, cetyl trimethyl ammonium chloride (CTAC) in a concentration that represents 2% (0.4. mM) with respect the concentration of the substrate, on the oxidation of 1-phenylethanol by the heterogeneous system, MSNPs-NH_2@**H[1].** The concentration of surfactant was selected in base of a compromise between the stability of the nanoparticles in solution and their recovery employing a magnet.

The **(Figure IV.15)** displays the yields after 1, 2 or 4 h of catalytic procedure. We can observe that total conversion of 1-phenylethanol after 4 h, indeed after 2h, the yield was of 95 %; with high selectivity values >99 %. These results confirm the positive effect of the surfactant on the catalytic performance of the nanoparticles since, on one hand, (i) the presence of surfactant does not detract the activity of the catalyst, which indicates that the surfactant does not block the active sites of the supported catalyst, while, on the other, (ii) the surfactant decreases the aggregation of these nanoparticles during the catalysis. For at least 4h, the nanoparticles remain highly dispersed. This behavior improves the performance of the heterogeneous catalyst, probably due to a greater number of active centers exposed to the substrate, which could facilitate their interaction.

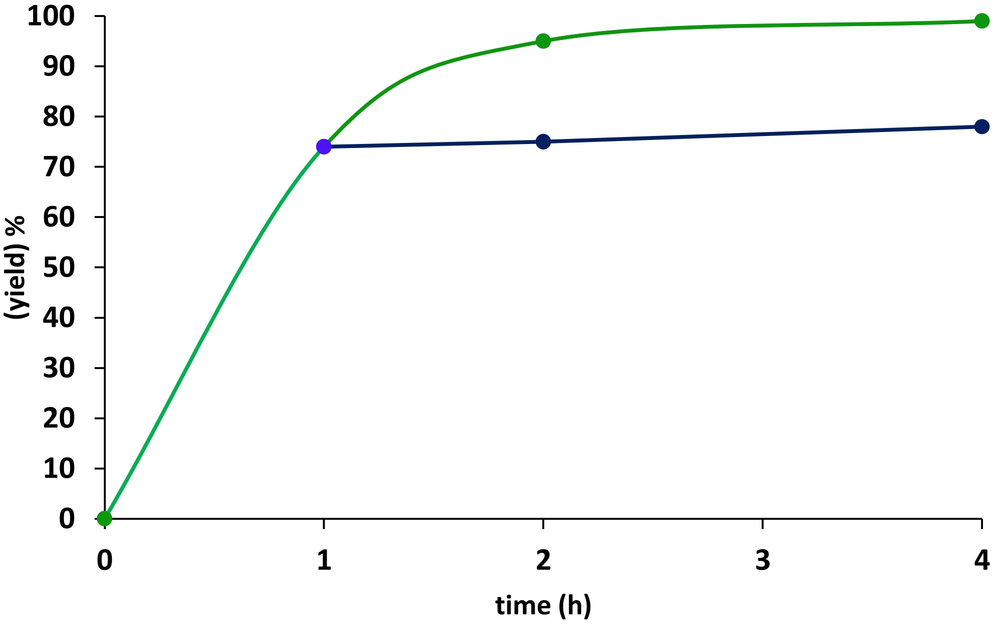

Figure IV.15. Plot of yield as a function of time for the photoredox catalysis of 1-phenylethanol using MNSP-NH_2@**H[1]** as the catalyst in the presence of 0,4 mM of cetyl trimethyl ammonium chloride (CTAC) as a surfactant. The blue curve shows the dependence of substrate yield on the reaction time after the catalyst was removed at 4h. Conditions: MNSP-NH_2@**H[1]** (0,1μmol), substrate (0,1 mmol), $Na_2S_2O_8$ (0,2 mmol), CTAC (2 μmol), potassium carbonate solution (5 mL) at pH=7; light irradiation using a lamp with λ =300 nm.

Table IV.9. Photocatalytic oxidation of alcohols.[a]

Entry	catalyst	Substrate	Yield(%)(TON)
1	MSNP-NH_2	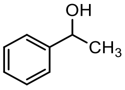	6
2	**Na[1]**	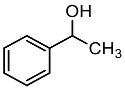	>99 (1000)
3	MSNP-NH_2@**H[1]**	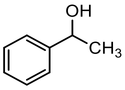	4[b]
4	MSNP-NH_2@**H[1]**	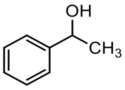	76 (760)[c]
5	MSNP-NH_2@**H[1]**	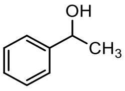	>99 (1000)
6	MSNP-NH_2@**H[1]**	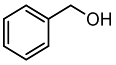	90 (900)
7	MSNP-NH_2@**H[1]**	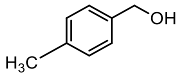	97 (970)
8	MSNP-NH_2@**H[1]**	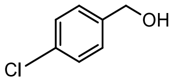	86 (860)
9	MSNP-NH_2@**H[1]**	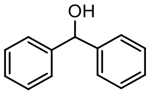	95 (950)
10	MSNP-NH_2@**H[1]**	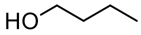	97 (970)
11	MSNP-NH_2@**H[1]**	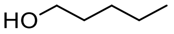	98 (980)
12	MSNP-NH_2@**H[1]**	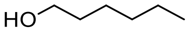	92 (920)
13	MSNP-NH_2@**H[1]**	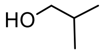	87 (870)
14	MSNP-NH_2@**H[1]**	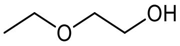	96 (960)
15	MSNP-NH_2@**H[1]**	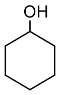	98 (980)
16	MSNP-NH_2@**H[1]**	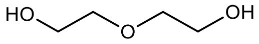	75 (750)** 98[d] (980)**
17	MSNP-NH_2@**H[1]**	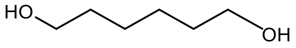	90 (900)** 95[d] (950)**

[a] Conditions: MNSP-NH_2@**H[1]** or **Na[1]** (0,1μmol), substrate (0,1 mmol), $Na_2S_2O_8$ (0,2 mmol), 5 ml of potassium carbonate solution at pH=7 ;light irradiation (8h) using a lamp with λ =300 nm; sonication after 4 hours. [b] absence of light [c] without sonication. Yield values obtained are shown together with TON that is shown in parenthesis. Yields of products were determined by NMR spectroscopy and gas chromatography (GC). [d] MNSP-NH_2@H[**1**] or Na[**1**] (0,1μmol), substrate (0,1 mmol), $Na_2S_2O_8$ (0,4 mmol), 5 mL of potassium carbonate solution at pH=7 ;light irradiation (8h) using a lamp with λ =300 nm; sonication after 4 hours. ** Analysis was done on the neat reaction. No attempt to separate was done. (see **Annex II Figures SIV.20-23**).

Based on the above results, we have studied the photooxidation of alcohols in the presence of surfactant, using the same conditions displayed in the above **Figure IV.15** and considering 2 and 4 h as the optimal times to perform the catalytic assays. The yields obtained are showed in the **Table IV.10.** In all cases, selectivity values were greater than 99%. The results show that MSNPs-NH_2@**H[1]** is also an efficient catalyst for the photooxidation of alcohols in times as short as 2h and 4h, which confirm the positive effect of the surfactant on the catalytic behavior. We have reduced the catalyst loading to 0.01 mol % vs the used 0.1 mol %, corresponding to ratios of 1:10000:20000 of the catalyst/substrate/oxidizing agent, in the oxidation of 1-phenylethanol (1b), and we have obtained a yield greater than 99% corresponding to TON=10000. The latter value is similar to that previously obtained in homogeneous conditions after 8h; but in this case, we have used short reaction times, 4h.

We have also verified the performance of the heterogeneous catalyst by removing the nanoparticles after 1h of operation by magnetic separation, followed by reaction with the rest of the solution until 4h (**Figure IV.15**, blue curve). No increasing of the product yield was observed after removal of the catalyst, proving that either no leaching or negligible leaching occurred.

The lifetime of the catalyst and its level of reusability are very important factors for practical applications. In this way and based on the results shown above, we have investigated the recyclability of the heterogeneous MSNPs-NH_2@**H[1]** catalytic system in water on two different substrates, 1-phenylethanol and diphenylmethanol (**Figure IV.16 a**), and on the cyclohexanol (**Figure IV.16 b**). In all cases, after 4h of reaction, the heterogeneous catalyst was recovered from the catalysis medium by magnet separation. Afterward, the particles were washed with water, dried, and exposed to a new loading of substrate under the same experimental conditions.

Table IV.10. The substrate scope of photooxidation of alcohols by MSNP-NH$_2$@**H[1]**.[a]

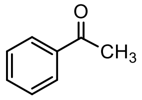 **1** 95%, TON=950 (2h) >99%, TON=1000 (4h) >99%, TON=10000 (4h)^{b}	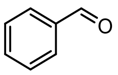 **2** 80%, TON=900 (2h) 95%, TON=950 (4h)	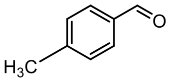 **3** 94%, TON=940 (2h) 96%, TON=960 (4h)
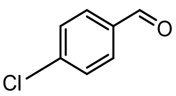 **4** 72%, TON=720 (2h) 83%, TON=830 (4h)	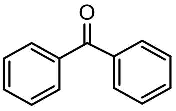 **5** 83%, TON=830 (2h) 90%, TON=900 (4h)	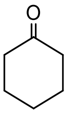 **6** 85%, TON=850 (2h) 98%, TON=980 (4h)
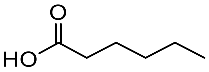 **7** 90%, TON=900 (2h) >99%, TON=1000 (4h)	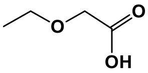 **8** 92%, TON=920 (2h) 95%, TON=950 (4h)	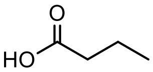 **9** 96%, TON=960 (2h) 98%, TON=980 (4h)
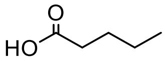 **10** 91%, TON=910 (2h) 94%, TON=940 (4h)	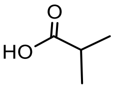 **11** 79%, TON=790 (2h) 84%, TON=840 (4h)	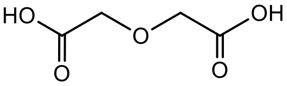 **12** 55%,** TON=550 (2h)^{c} 81%,** TON=810(4h)^{c}
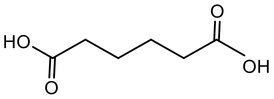 **13** 62%,**TON=620 (2h)^{c} 90%,**TON=900 (4h)^{c}		

[a] Conditions: MNSP-NH$_2$@**H[1]** (0,1µmol), substrate (0,1 mmol), Na$_2$S$_2$O$_8$ (0,2 mmol), CTAC (2 µmol), 5 mL potassium carbonate solution at pH=7 ;light irradiation using a lamp with λ =300 nm. yields and TON values obtained are shown together with the time of the catalyst that is shown in parenthesis. ^{b} MNSP-NH$_2$@**H[1]** (0,05 µmol), substrate (0,5 mmol), Na$_2$S$_2$O$_8$ (1 mmol), CTAC (2 µmol), 5 mL potassium carbonate solution at pH=7. ^{c} MNSP-NH$_2$@**H[1]** (0,1 µmol), substrate (0,1 mmol), Na$_2$S$_2$O$_8$ (0,4 mmol), CTAC (2 µmol), 5 mL potassium carbonate solution at pH=7. Yields of products were determined by NMR spectroscopy and GC. **Analysis was done on the neat reaction. No attempt to separate was done.

a)

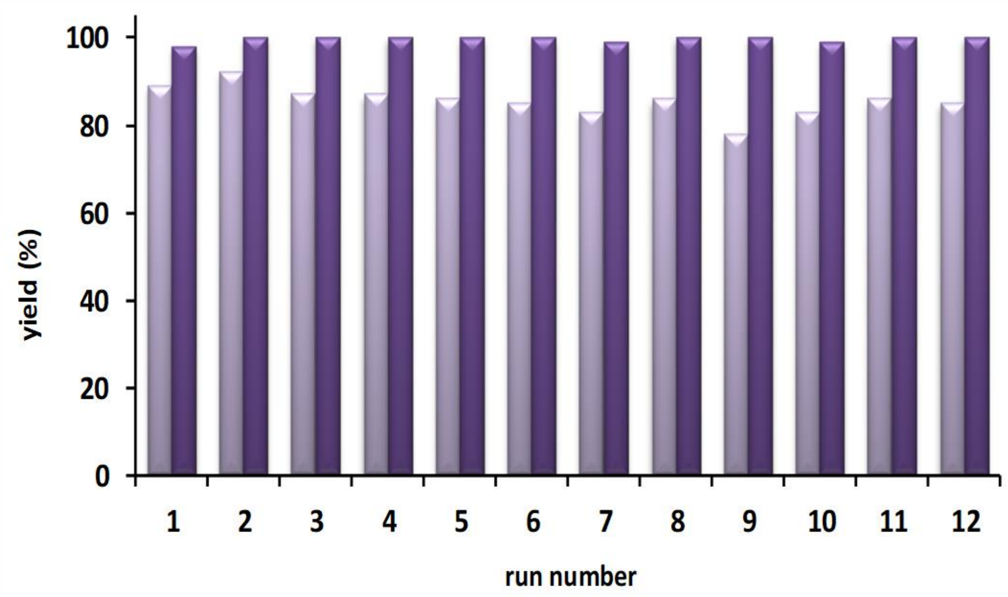

b)

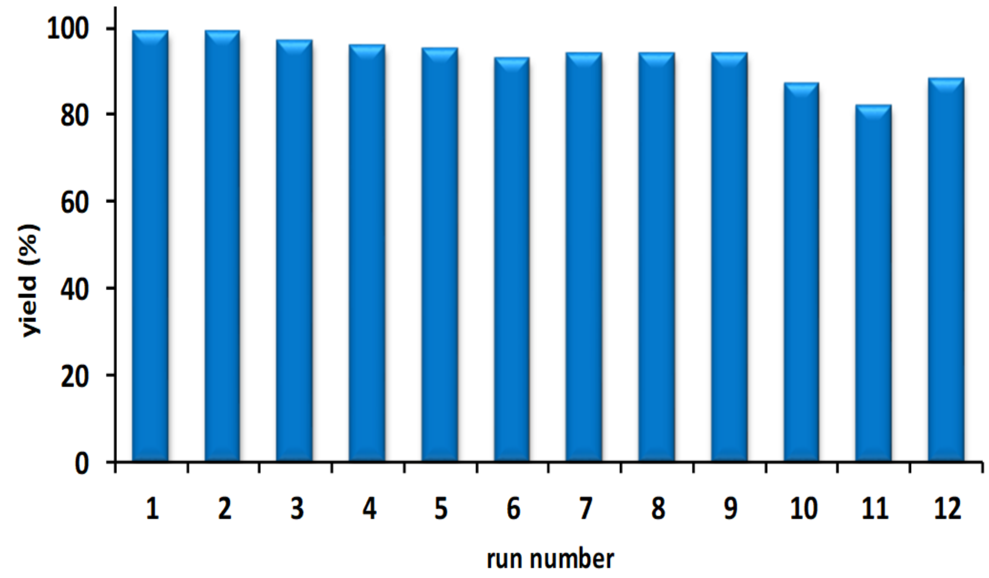

Figure IV.16. Yield values obtained throughout a number of successive reuses of catalyst MSNP-NH_2@**H[1]** in the photooxidation of (a) diphenylmethanol (light purple) and 1-phenylethanol (dark purple); (b) cyclohexanol. Conditions: MNSP-NH_2@**H[1]** (0,1μmol), substrate (0,1 mmol), $Na_2S_2O_8$ (0,2 mmol), CTAC (2 μmol), potassium carbonate solution (5mL) at pH=7; light irradiation using a lamp with λ =300 nm, 4 h per run.

These results evidence that the heterogeneous catalyst maintains a good performance throughout the twelve runs, with good yields values for 1-phenylethanol, diphenylmethanol, and cyclohexanol as substrates, maintaining the selectivity values greater than 99%. The overall turnover numbers (TONs) are 11960 for 1-phenylethanol, 9490 for diphenylmethanol, and 11180 for cyclohexanol. To the best of our knowledge, these values are among the highest turnover numbers achieved in alcohol photoredox oxidation in heterogeneous conditions. Furthermore, we have observed that the activity of the catalysts does not decrease through the repeated uses. The high stability shown by the catalyst seems to be due to the favorable nonbonding interactions mostly B-H…H-N between cobalbis*ortho*dicarbollide, **[1]$^-$,** and NH_3^+ groups from the nanoparticles which lead to the formation of a hybrid material with enhanced stability. UV-visible spectroscopy was performed to the solutions after the consecutive recycling experiments indicating that no noticeable loss of catalyst takes place as was showed in the above (**Figure IV.14**). The morphology of the recovered catalyst was analyzed, after 12 runs, in the photooxidation of 1-phenylethanol. The SEM image obtained was compared with that of the catalyst before the catalysis (**Annex II Figure SIV.19**). The results show that the morphology is maintained.

In summary, we have shown that proton cobaltabisdicarbollide, H[3,3'-Co(1,2-$C_2B_9H_{11})_2$] has been heterogenized on magnetic nanoparticles (MNPs) coated with a silica layer, maintaining the homogeneous catalytic properties. The heterogeneous catalyst synthesized showed an easy magnetic separation and recyclability. In the structure of the heterogeneous catalyst, magnetic silica nanoparticles amine terminated was anchored in a non-covalently manner to H[3,3'-Co(1,2-$C_2B_9H_{11})_2$] (**H[1]**) to achieve a highly stable photoredox catalyst in water, MSNP-NH2@**H[1]** which was analysed in depth to understand their morphology, characterization and colloidal stability. The heterogeneous catalyst was tested in the photooxidation of different aromatic and aliphatic alcohols as substrates, using catalyst loads of 0.1 mol %, and 0.01 mol %. Cetyl trimethyl ammonium chloride was chosen as surfactant to prevent the nanoparticles aggregation and maintain the stability at the same time allow a fast magnetic separation. The recyclability of the catalytic system was demonstrated over the course of 12 runs, with the maintenance of the high yields and selectivity. Hence, the metallacarborane catalyst supported on silica-coated magnetic nanoparticles has proven to be a robust, efficient, reusable and green photoredox oxidation heterogeneous catalyst in water.

IV.3. Aqueous Persistent Noncovalent Ion-Pair Cooperative Coupling in a Ruthenium Cobaltabis*ortho*dicarbollide System as a Highly Efficient Photoredox Oxidation Catalyst

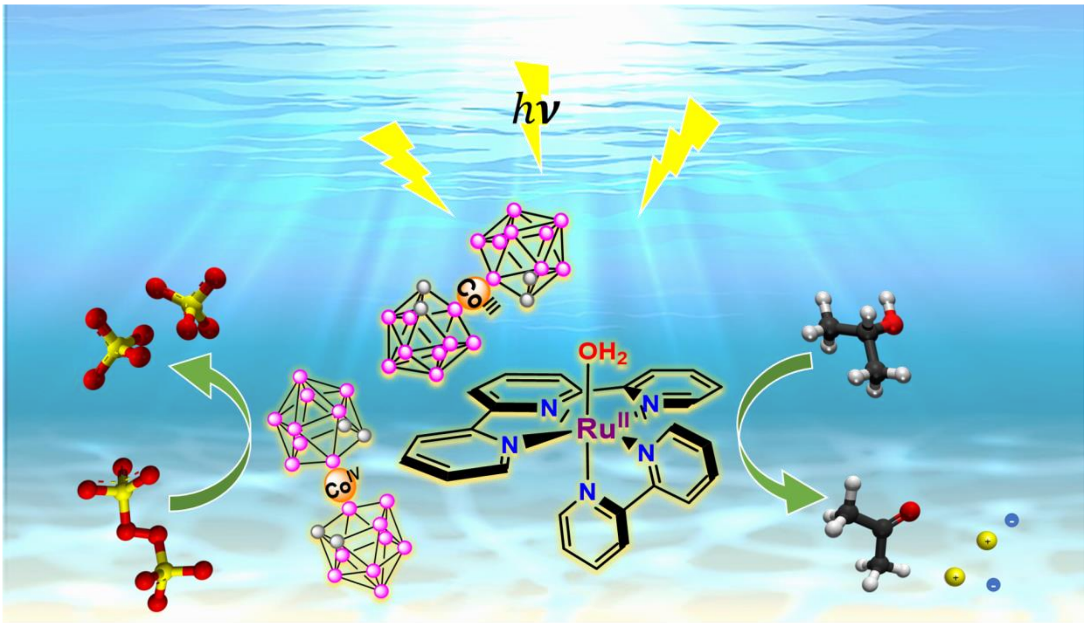

Here, we describe the synthesis of a new air-stable ruthenium-cobaltabis(dicarbollide) compound, [Ru^{II}(trpy)(bpy)(H_2O)][(3,3´-Co(1,2-$C_2B_9H_{11}$)$_2$]$_2$, **C4,** where the [Ru-OH_2] cation belongs to the family of redox oxidation catalysts, together with their complete spectroscopic and electrochemical characterization. The recrystallization of **C4** in acetonitrile, leads to the formation of [Ru^{II}(trpy)(bpy)(CH_3CN)][(3,3´-Co (1,2-$C_2B_9H_{11}$)$_2$]$_2$, **C5** complex, that has been structurally characterized. **C4** has been tested as a cooperative photoredox catalyst in the oxidation of aromatic and aliphatic alcohols in water showing high performance, using very low catalyst loads.

IV.3.1. Synthetic Strategy, Structure, and Redox Characterization.

The synthetic procedure used for preparation of the compounds is showed in **Scheme IV.2**. The aqua complex **C4** is obtained by dissolving the chloride ruthenium (II) complex [Ru^{II}(trpy)(bpy)(Cl)]Cl (**C2**), obtained following the method described in the literature,[252] in a mixture of water/acetone (1:1) in the presence of **Ag[1], C3**, under reflux. The latter compound was synthesized by a cationic exchange resin from **Cs[1],** as was described in the literature.[253] After filtration of AgCl, the complex was isolated. The recrystallization of **C4** in acetonitrile led to the substitution of water by acetonitrile ligand, and then the formation of complex **C5** took place. It is important to note, that, this is the first example of a molecular aqua ruthenium (II) complex containing two cobaltabis*ortho*dicarbollide anions as counterions.

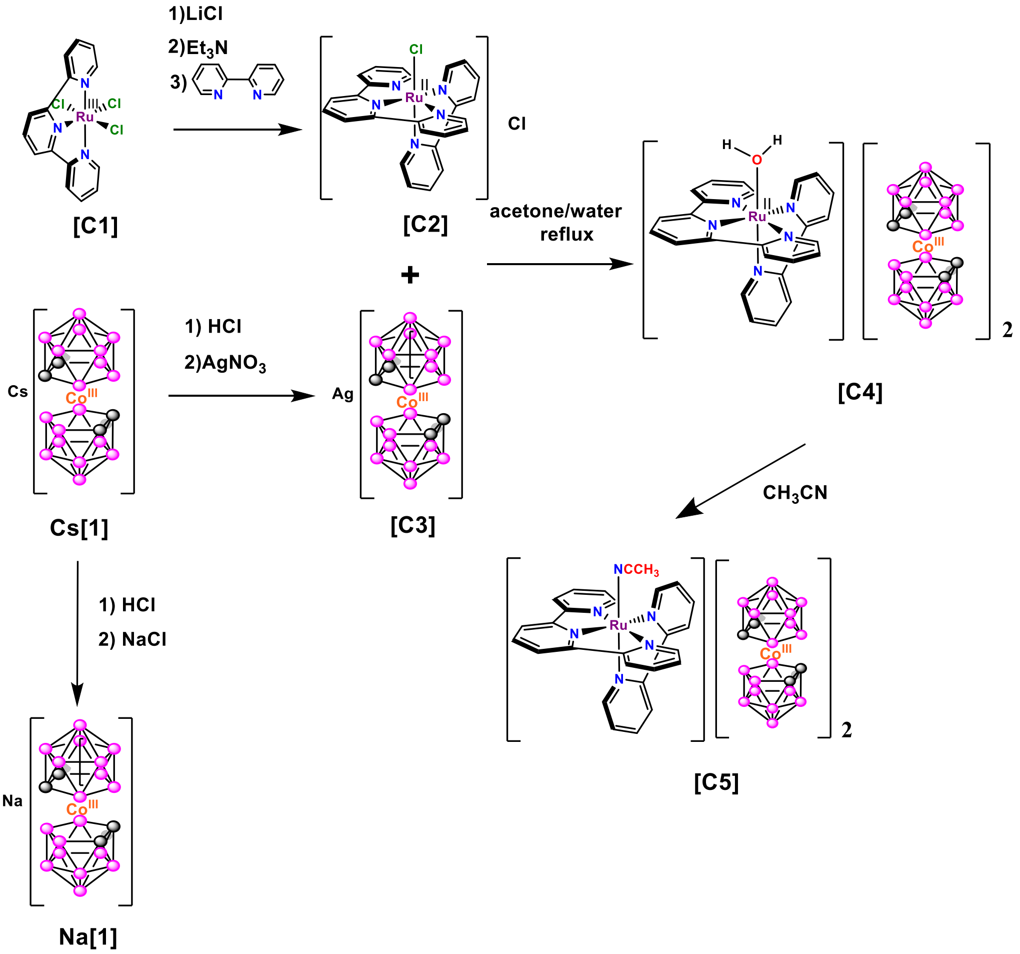
1)LiCl
2)Et3N
3)
[C1]
[C2]
Cl
acetone/water
reflux
+
[C4]
2
Cs
1) HCl
2)AgNO3
Ag
Co III
Cs[1]
[C3]
CH3CN
NCCH3
1) HCl
2) NaCl
Na
[C5]
Na[1]

Scheme IV.2. Synthetic Strategy for the Preparation of Complexes **C4** and **C5**.

Single crystals of **C5** were grown by recrystallization of **C4** in acetonitrile. Although all attempts to obtain crystals of **C4** in water or noncoordinating solvents were unsuccessful.

X-ray diffraction analysis was used to solve the crystal structure of complex **C5**, as is showed in the following (**Figure IV.17)**.

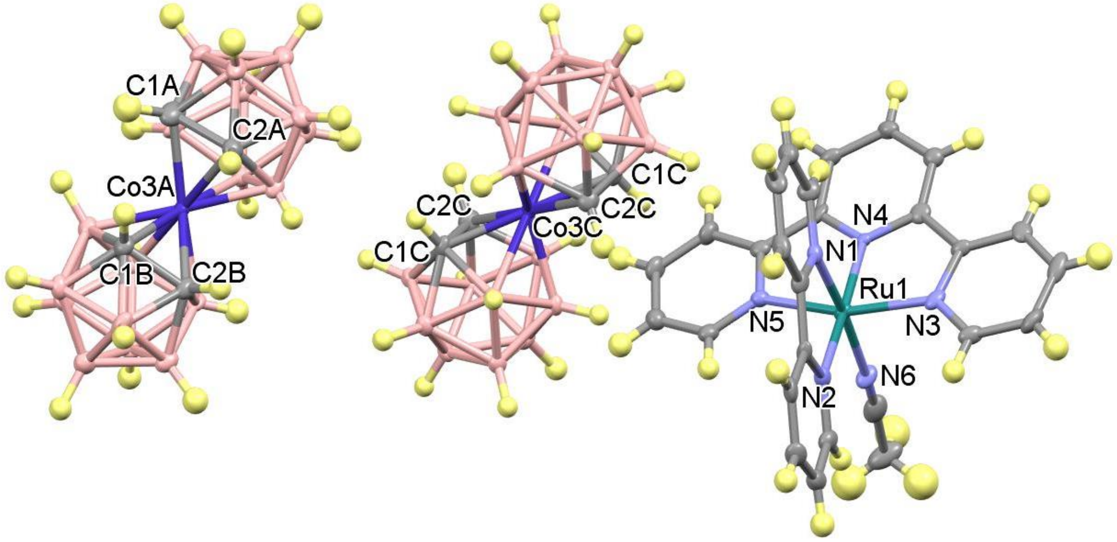

Figure IV.17. Crystal structure of complex **C5**.

The main crystallographic data, together with selected bond distances and angles, are showed in (**Annex III Tables SIV 3.4 and SIV 3.5**). The cationic moiety of compound **C5** is formed by a ruthenium (II) complex, where the Ru center displays an octahedral distorted type of coordination, in which the trpy ligand is bonded to the Ru^{II} cation in a meridional manner and the bpy ligand is coordinated in a bidentate fashion. The sixth coordination site is occupied by the monodentate acetonitrile ligand. All bond distances and angles are within the expected values for these types of complexes.[254] For instance, it is interesting to note that the Ru-N2 bond length in the bpy ligand, where the N2 atom is placed trans to the pyridyl N4 atom of trpy, is longer (2.069 Å) than the analogous distance Ru-N1 (2.033 Å), where the N1 atom is trans to the N6 atom of the acetonitrile ligand. This evidence highlights the stronger trans influence of the pyridine ring with respect to the acetonitrile ligand. The N3-Ru-N4 and N4-Ru-N5 angles are 79.88^0 and 79.13^0, respectively, less than the 90^0 expected for an ideal octahedral geometry. This may be due to the geometry of the trpy ligand, which defines the equatorial plane of the structure; as a consequence, the other two equatorial angles, N3-Ru-N2 and N2-Ru-N5, are larger than 90^0. The anionic moiety is formed by two anionic metallabis*ortho*dicarbollide units, which display different rotamers: one cisoid and the other transoid. The C1A-C2A (1.661 Å) and C1B-C2B (1.642 Å) bond lengths are different in the cisoid anion, while the C1C-C2C bond lengths are similar (1.649 Å) in the transoid rotamer anion. The packing showed in the following (**Figure IV.18**) displays the arrangement adopted between the metallacarborane anions and cationic moieties.

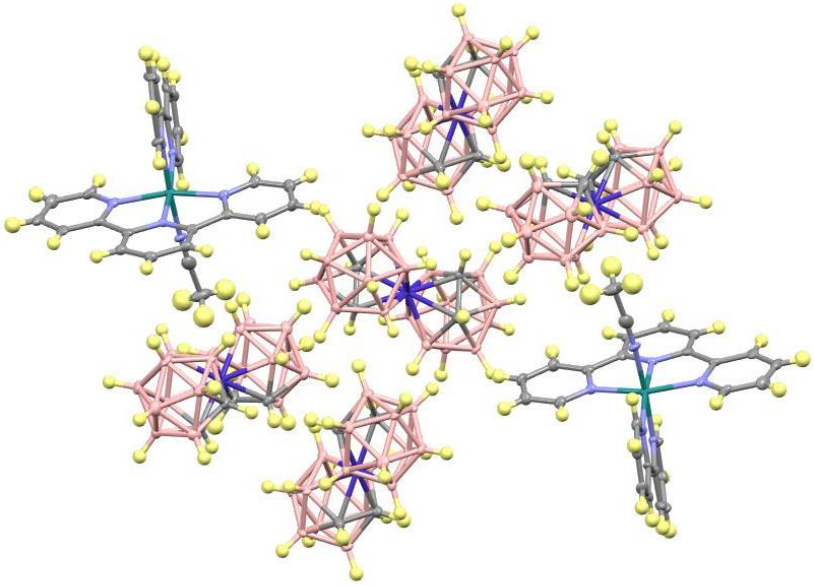

Figure IV. 18. Packing displayed by **C5.**

The IR spectrum of complex **C4** shows vibrations around 2900 cm^{-1} that can be assigned to the $\upsilon_{C\text{-}H}$ stretching modes for the aromatic rings, while the bands around 3030 cm^{-1} correspond to the $\upsilon_{C\text{-}H}$ stretching of the C_c-H bonds in the different rotamers. A band over 3500 cm^{-1} can be seen that corresponds to the $\upsilon_{O\text{-}H}$ stretching of the aqua ligand. We have also observed a significant vibration around 2530 cm^{-1} that corresponds to the $\upsilon_{B\text{-}H}$ stretching mode for the B-H bond, as is showed in the following (**Figure IV.19**).

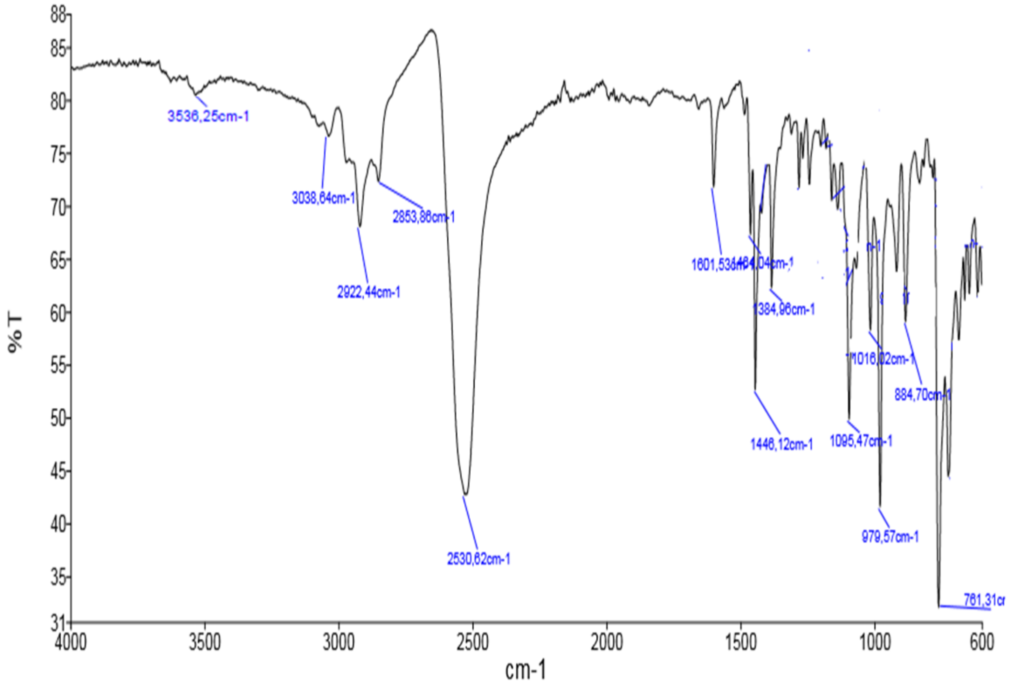

Figure IV.19. IR spectrum of **C4.**

The 1D and 2D ^{1}H NMR spectra of complexes **C3** and **C4** were recorded in acetone-d_6 and are displayed in (**Annex III Figure SIV.25** and **Figure IV.20 a**), respectively, and COSY NMR spectrum is displayed in (**Annex III Figure SIV.26**). The ^{1}H NMR spectrum of **C4** shows two set of signals as is showed in (**Figure IV.20 a**): one in the aromatic region corresponding to the protons of the bipyridine and terpyridine ligands of the $[Ru\text{-}OH_2]^{2+}$ cation and the second set in the aliphatic region that can be assigned to the C_c-H of the cobaltacarborane anions, with resonances of near δ = 3.98 ppm. The ^{1}H {^{11}B} NMR spectrum exhibits the resonances of H atoms bonded to B atoms over a wide range of chemical-shift in the region from δ =1.50 to 3.5 ppm. These resonances appear as broad bands, as is showed in (**Figure IV.20 b**). The ^{11}B {^{1}H} NMR resonances represented the typical pattern of the pristine cobaltabisorthodicarbollide cluster in the range from δ =15 to -22 ppm, as is showed in the following (**Figure IV.20 c**).[255]

a)

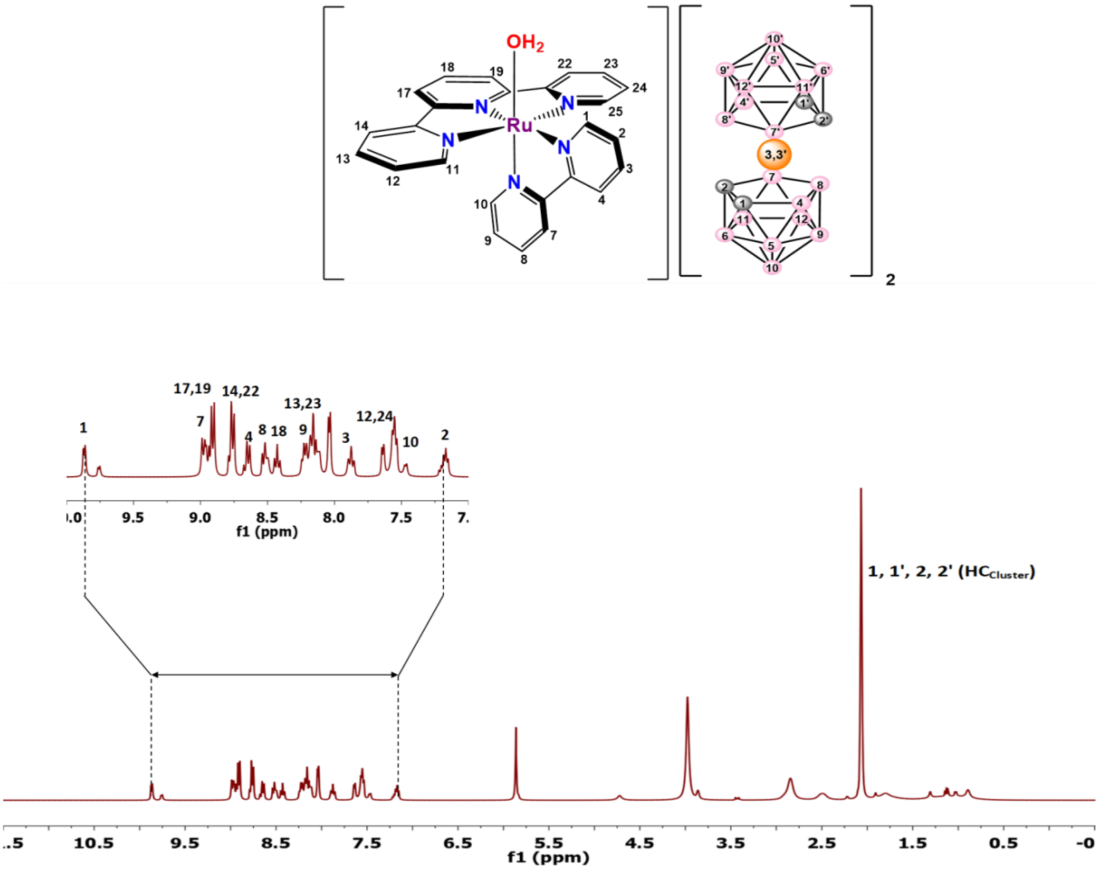
OH2
Ru
N
1, 1', 2, 2' (HCCluster)
17,19
14,22
13,23
12,24
f1 (ppm)

b)

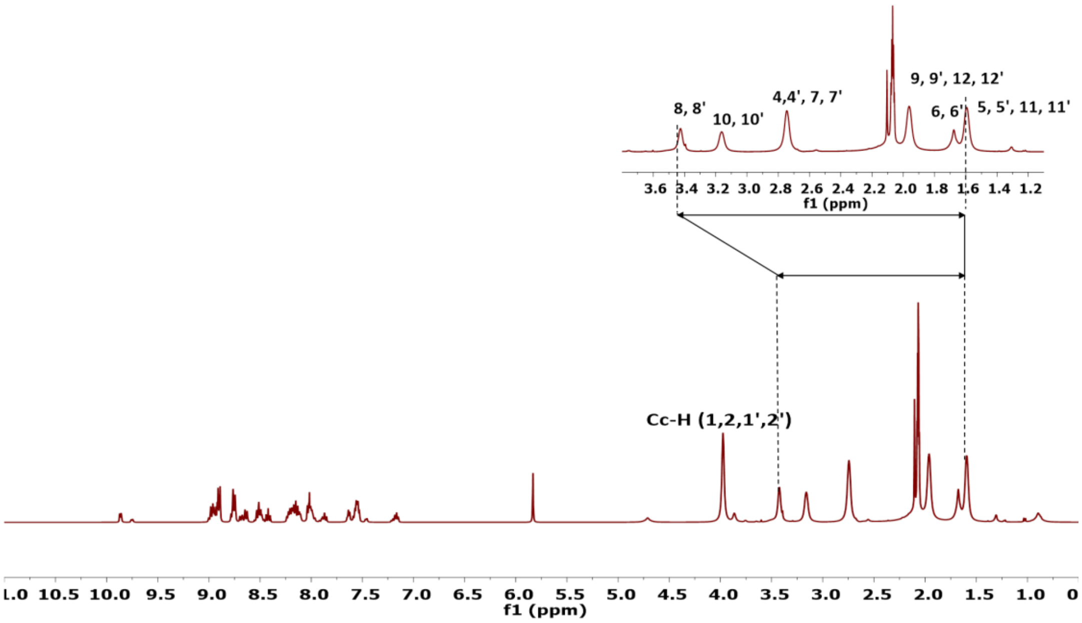
8, 8'
10, 10'
4,4', 7, 7'
9, 9', 12, 12'
6, 6'
5, 5', 11, 11'
Cc-H (1,2,1',2')
f1 (ppm)

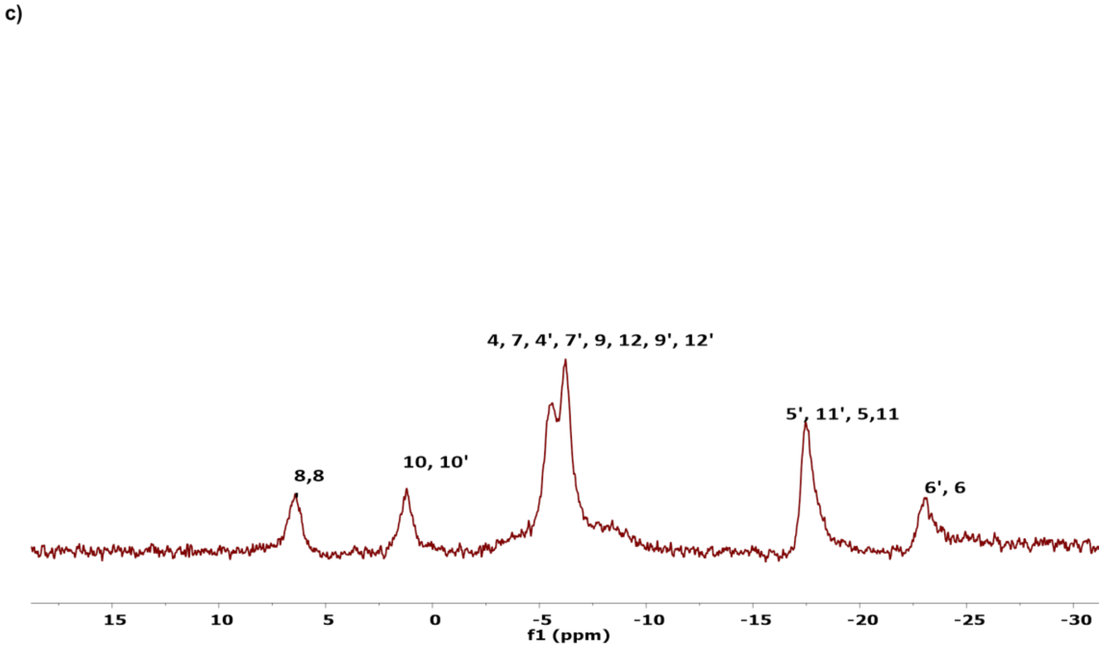

Figure IV.20. a) ^{1}H-NMR; b) ^{1}H{^{11}B}-NMR; c) ^{11}B{^{1}H}-NMR spectra of cobaltabis(dicarbollide) **C4** compound in acetone-d_6.

The UV-vis spectra of **Ag[1]**, **C3**, is showed in the (**Annex III Figure SIV.27**), **C2’** and **C4**, are showed in the following (**Figure IV.21**). The UV-vis spectrum of **Ag[1]**, **C3** in **Figure SIV.27**, shows one strong absorption band at 286 nm and others with less intensity at 210, 333, and 450 nm, in accordance with the literature.[256] The spectrum of the aqua complex **C2’** showed in (**Figure IV.21 a**) (black line) shows ligand-based π-π^* bands and dπ(Ru)- π^*(L) metal-to-ligand charge-transfer (MLCT) transitions, as is usual for these complexes.[257] The UV-visible spectrum corresponding to complex **C4** is showed as well in (**Figure IV.21 a**) (dash dotted line) and (**Figure IV.21 b)**, where is exhibited the ligand-based π-π^* bands of the cationic part below 350 nm that are partially eclipsed by strong absorptions corresponding to the cobaltabis*ortho*dicarbollide anionic moiety. Above 350 nm, the spectra show less intense bands that correspond to dπ(Ru)- π^*(L) MLCT transitions. In (**Figure IV.21 b)** are showed the UV-spectra of **C4** in CH_2Cl_2, phosphate buffer, and CH_3CN. It is worth mentioning that the shift to higher energy absorptions observed for **C4** in acetonitrile with regard to the same complex in the other solvents mentioned. This is expected because of substitution of the aqua ligand by acetonitrile; this ligand shows a higher π-acceptor capacity with respect to the aqua ligand, which provokes stabilization of the dπ (Ru) donor orbitals.

a)

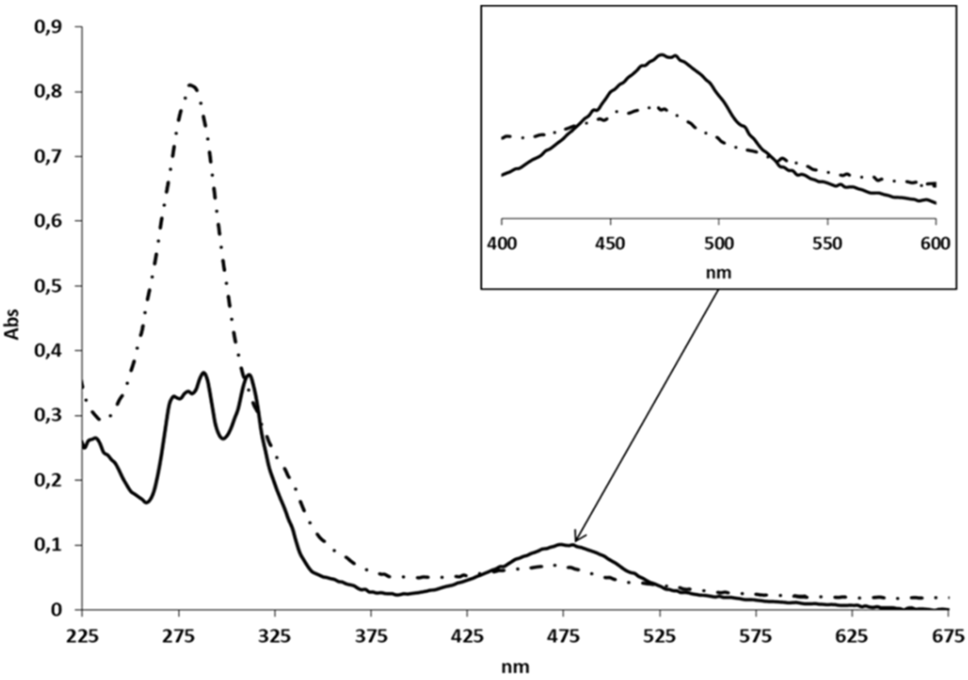

b)

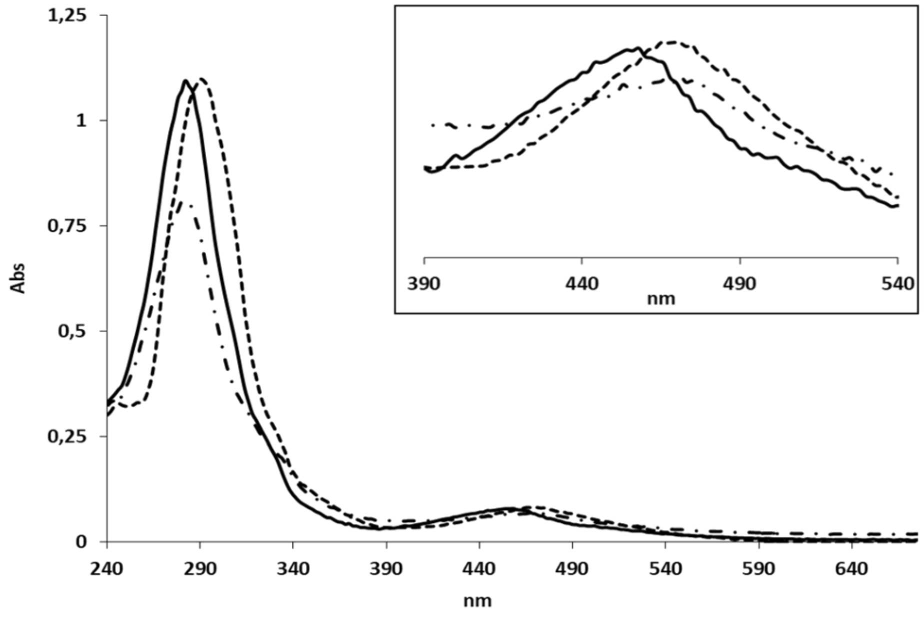

Figure IV.21. a) UV-vis spectra of complex **C2'** (black line) and **C4** (dash dotted line) in phosphate buffer at 7.02 pH. b) UV-vis spectra of complex **C4** in CH_2Cl_2 (dotted line), phosphate buffer at 7.02 pH (dash-dotted line), and CH_3CN (solid line).

The electrochemical behavior of complexes **C3**, **Na[1],** and **C4** have been studied by means of cyclic voltammetry (CV) and differential pulse voltammetry (DPV). The CV curve of **C3** in acetonitrile shows two reversible one-electron-redox processes at $E_{1/2}$=-1.69 and 1.27 V versus Ag/AgCl as reference electrode, which can be assigned to Co^{III}/Co^{II} and Co^{IV}/Co^{III}, respectively and it is showed in (**Annex III Figure SIV. 28**).

The CV curve of the aqua complex **C4** in dichloromethane exhibits different redox processes because of the Ru and Co ions. Two are almost reversible monoelectronic $Co^{III}Ru^{III}/Co^{III}Ru^{II}$ and $Co^{III}Ru^{IV}/Co^{III}Ru^{III}$ redox waves at $E_{1/2}$ around 0.68 and 0.96 V versus Ag and two monoelectronic $Co^{III}Ru^{II}/Co^{II}Ru^{II}$ and $Co^{IV}Ru^{IV}/Co^{III}Ru^{IV}$ redox waves at $E_{1/2}$=-1.57 and 1.38 V Versus Ag/AgCl, respectively and it is showed in (**Figure IV.22**).

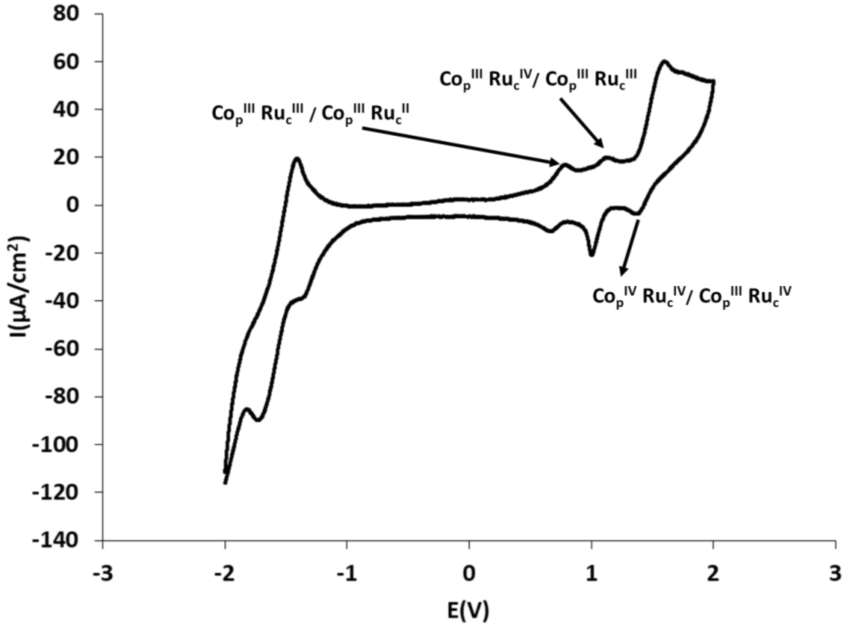

Figure IV.22. CV of **C4** in CH_2Cl_2 + 0.1 M TBAH *vs* Ag/AgCl.

The electrochemical behaviour of **C4** is showed and was also studied in aqueous solution and it is showed in (**Figure IV. 23** and **Figure IV.24**). The CV curve of **C4** is showed in (**Figure IV.23,** red line) and DPV curve in (**Figure IV.24 a**) exhibit two successive one-electron-oxidation waves at 0.55 and 0.67 V (vs Ag/AgCl), which correspond to $Co^{III}Ru^{III}/Co^{III}Ru^{II}$ and $Co^{III}Ru^{IV}/Co^{III}Ru^{III}$ redox couples, respectively, and are assigned to two proton-coupled electron-transfer (PCET) processes (**equations 1 and 2**). These values have been assigned to the Ru^{III}/Ru^{II} and Ru^{IV}/Ru^{III} couples of the catalytic unit, based in the values presented by the mononuclear

$[Ru^{II}(trpy)(bpy)(H_2O)]^{2+}$ compound.[258]

The CV curve in (**Figure IV.24 b**) shows that the above mentioned waves corresponding to Ru, are followed by another two-electron oxidation wave at 1.19 V (vs Ag/AgCl), which was attributed to the $Co^{IV}Ru^{IV}/Co^{III}Ru^{IV}$ redox couple. In this case, this value is assigned to the Co^{IV}/Co^{III} couple of the photoactive unit given the similarity with the potential value of **Na[1],** whose CV curve presents a Co^{IV}/Co^{III} redox wave at $E_{1/2}$ = 1.36 V, as is showed in (**Figure IV. 23**, blue line) and in (**Annex III Figure SIV.29**).

$$Co_p^{III}\,Ru_c^{III}-OH \; + \; 1\,e^- + 1\,H^+ \rightleftharpoons Co_p^{III}\,Ru_c^{II}-OH_2 \qquad E_{1/2} = 0.55\ V \qquad (1)$$

$$Co_p^{III}\,Ru_c^{IV}=O \; + \; 1\,e^- + 1\,H^+ \rightleftharpoons Co_p^{III}\,Ru_c^{III}-OH \qquad E_{1/2} = 0.67\ V \qquad (2)$$

$$Co_p^{IV}\,Ru_c^{IV}=O \; + \; 1\,e^- \rightleftharpoons Co_p^{III}\,Ru_c^{IV}=O \qquad E_{1/2} = 1.19\ V \qquad (3)$$

$$Co^{IV} \; + \; 1\,e^- \rightleftharpoons Co^{III} \qquad E = 1.36\ V \qquad (4)$$

Equations 1-4. The electrochemical transition reaction corresponding to each redox couple processes at pH=7.12. Ref Ag/AgCl.

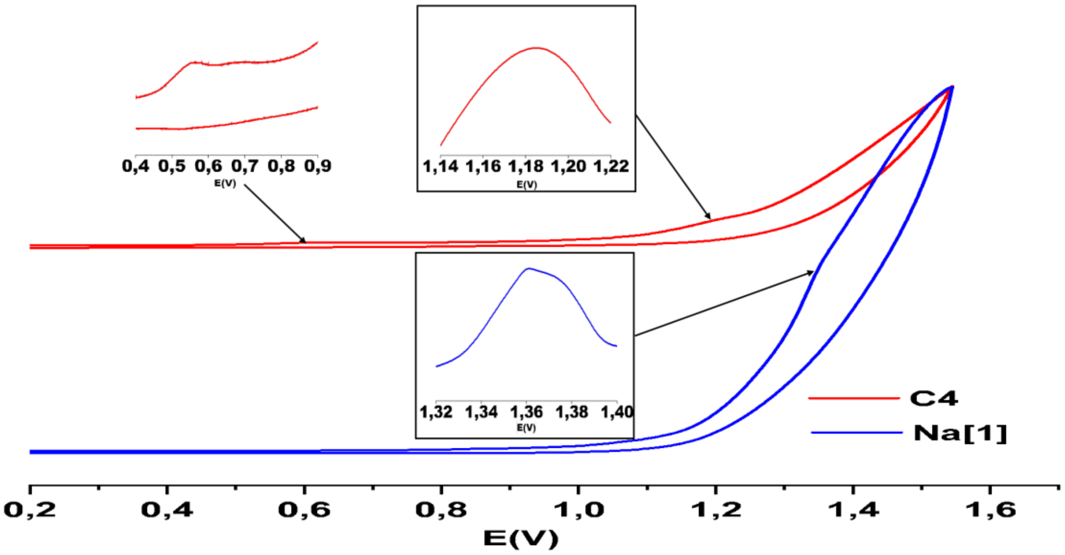

Figure IV.23. CV for complexes **C4** (red line) and **Na[1]** (blue line) registered in a phosphate buffer (pH= 7.12) *vs* Ag/AgCl. The right red and blue inserts show dI/dE to better appreciate the position of the couple Co^{IV}/Co^{III}. Further proof of this will be shown later when dealing with the **C4** precedents that we will henceforth call the **C4** history**.**

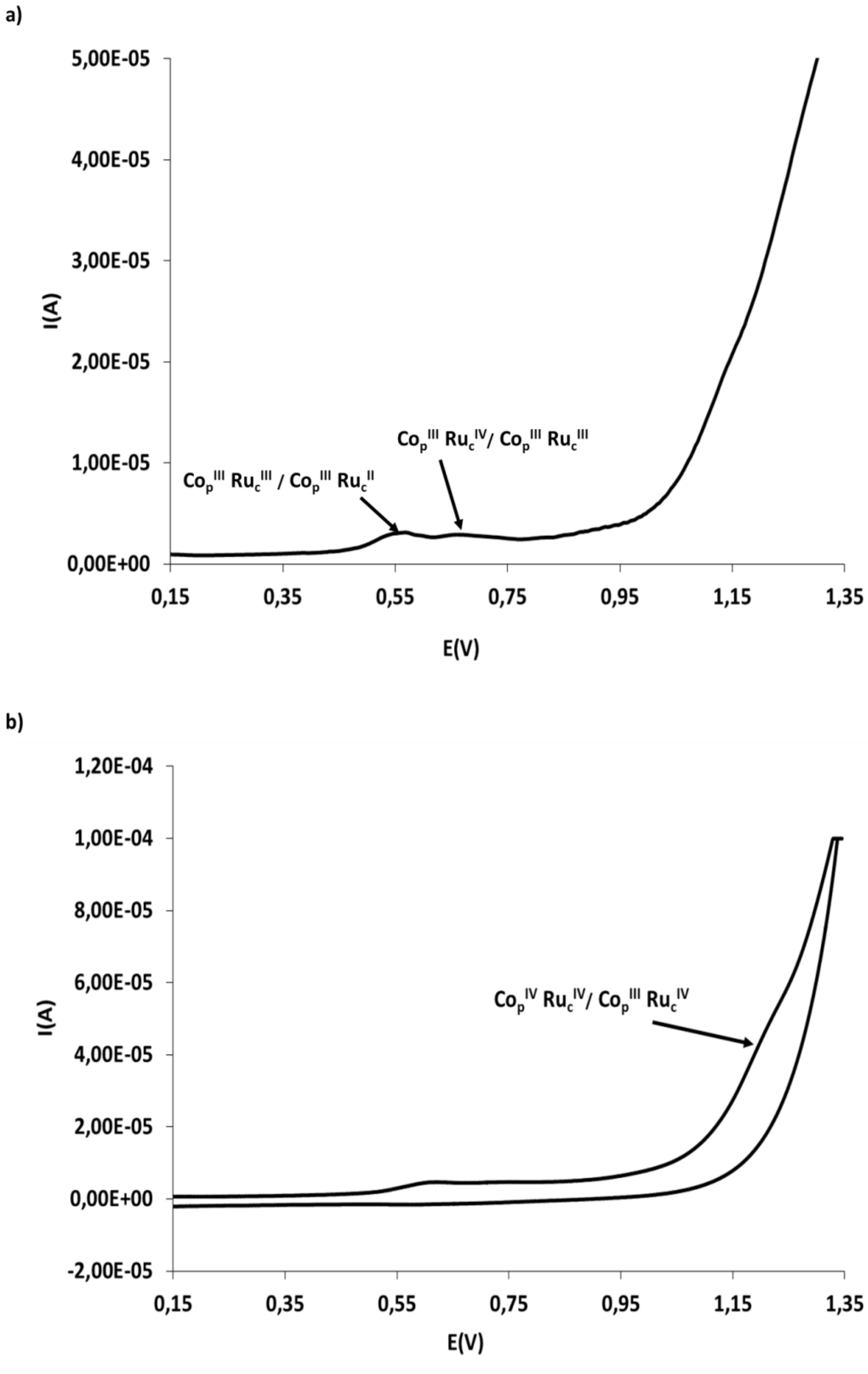

Figure IV.24. a) DPV for complex **C4** registered in a phosphate buffer (pH= 7.12) *vs* Ag/AgCl. b) CV for complex **C4** registered in a phosphate buffer (pH= 7.12) *vs* Ag/AgCl.

For **C4**, the Co^{IV}/Co^{III} redox potential value is 170 mV more cathodic with respect to the potential of **Na[1],** which indicates a certain and significant electronic coupling between the two units. To check this out, we have measured the redox potentials of

Na[1] after adding different concentrations of two divalent salts, $CaCl_2$ and $ZnCl_2$ as is showed in (**Table IV.11 and Annex III Figure SIV.30**), where is reproduced the dipositive charge of the ruthenium complex, and no substantial change in the redox potential of **Na[1]** has been observed. This is consistent with a coupling between the cation and anion in **C4**. (**Equations 1-4)** contain the electrochemical transition reactions corresponding to each redox couple processes at pH=7.12 with reference electrode Ag/AgCl.

Table IV.11. Potential values of complex **Na[1]**, corresponding to the couple Co^{IV}/Co^{III} after the addition of different concentrations of a) $CaCl_2$ and b) $ZnCl_2$.

a)

Entry	[Na[1]](M)	$E^{CoIV/III}$(Na[1]) (V)[a]	$[CaCl_2]_{added}$(M)	$E^{CoIV/III}$(Na[1]+$CaCl_2$)[a](V)
1	$1x10^{-3}$	1.36	$2.5x10^{-4}$	1.354
2	$1x10^{-3}$	1.36	$5x10^{-4}$	1.346
3	$1x10^{-3}$	1.36	$1x10^{-3}$	1.352

b)

Entry	[Na[1]](M)	$E^{CoIV/III}$(Na[1]) (V)[a]	$[ZnCl_2]_{added}$(M)	$E^{CoIV/III}$ (Na[1]+$ZnCl_2$)[a](V)
1	$1x10^{-3}$	1.36	$2.5x10^{-4}$	1.348
2	$1x10^{-3}$	1.36	$5x10^{-4}$	1.368
3	$1x10^{-3}$	1.36	$1x10^{-3}$	1.338

a. potentials registered in a phosphate buffer (pH=7.12) vs Ag/AgCl.

Therefore, the observed oxidation potentials indicate that the photogenerated Co^{IV} is able to easily oxidize $[Ru^{III}\text{-}OH]^{2+}$ to $[Ru^{IV}{=}O]^{2+}$, with a driving force of 520 mV, since the potential for Co^{IV}/Co^{III} is high enough, compared to the Ru^{IV}/Ru^{III} couple. This would be thermodynamically possible in water via PCET processes.[259] Therefore, on the basis of these studies, it is expected that, for photocatalytic oxidation of organic substrates, **[1]**$^-$ could act as a good photosensitizer.

In (**Figure IV.23**) is showed that there is an ion-pair contact effect, which causes the Co^{IV}/Co^{III} redox couple potential to vary near 170 mV under the influence of the ruthenium complex.

IV.3.2. Photocatalytic Oxidation.

C4 is $[Ru][Co]_2$ ion-pair complex in which the photocatalytic system is based on cobalt, an abundant transition metal, whereas the redox part is the ruthenium complex. The photocatalytic oxidation experiments were all carried out by exposing the reaction quartz vials to UV irradiation (2.2 W, ʎ ~ 300 nm), for different times, at atmospheric pressure and room temperature. The samples were 5mL of water, a K_2CO_3 solution at pH=7, and a mixture of **C4** as a substrate, $Na_2S_2O_8$ as a sacrificial oxidant (air could also do the work, as we have seen in the above section IV.1), and 0.005 mol % catalyst. The blank experiments were performed in the absence of catalyst, sacrificial oxidant, or light for 8 h. The results evidenced that a negligible amount of oxidation product was formed, less than 8% in all cases. After irradiation for a specified time, the reaction products were extracted with dichloromethane three times, quantified by means of ^1H NMR spectroscopy, and confirmed by gas chromatography with flame ionization detection (GC-FID) analysis. The results are showed in (**Table IV.12**), which displays the catalytic results obtained in the photooxidation of aromatic and aliphatic alcohols, after different times of reaction. In general, high yields of conversion and selectivity have been obtained, even when short reaction times have been used. After 8h of irradiation and timely neutralization at 4h, the yields observed in the photooxidation of 1-phenylethanol (**entry 1**) and diphenylmethanol (**entry 5**), both secondary aromatic alcohols, were remarkably >99%, with selectivity values of >99% and turnover numbers equal to TON = 20000 in both cases. However, the yield values observed for benzyl alcohol are slightly less than the secondary ones. It is worth mentioning that, after 4h of irradiation, the achieved high selectivity values were to obtain only the corresponding aldehydes. The conversion values enhanced by the presence of electron-donating substituents, such as methyl, on the aromatic ring of the benzyl alcohol (**entry 3d**) and decreased with the presence of chloro, an electron-withdrawing substituent (**entry 4d**). In the case of both benzyl alcohol and the substituted substrates, the selectivity decreases after 8h of irradiation, and it is observed an alcohol overoxidation toward the formation of the corresponding acids. **C4** displays high efficiency by primary and secondary aliphatic alcohols, with yields larger than 76% after 4h of irradiation and selectivity values of >99%.

1-Hexanol (**entry 6**), 1-butanol (**entry 7**), isobutyl alcohol (**entry 8**) and 2-ethoxyethanol (**entry 9**) were converted to the corresponding acids with yields of 82 % (4h) and 92 % (8h) (**entry 6**), 89% (4h) and 98 % (8h) (**entry 7**), 83 % (4h) and 92 %

(8h) (**entry 8**), and 76 % (4h) and 93 % (8h) (**entry 9**), respectively. Conversely, cyclohexanol converted to cyclohexanone in 79 % yield after 4h and 95 % (8h) (**entry 10**). When the amount of oxidizing agent was lowered (ratio applied 1:20000:20000), we observed that the degree of conversion for 1-phenylethanol and benzyl alcohol after 4h, is on the same order as the values obtained using a ratio 1:20000:40000 (**entries 1e and 2e**), respectively. It should be noticed that the conversion was a little bit less because of the kinetics of the reaction. These results are consistent because 1 mol of $S_2O_8^{2-}$ is needed for each 1 mol of alcohol to achieve the oxidizing reaction. We have no evidence that the catalyst has undergone any transformation following catalysis, as has been evidenced in other cases with ruthenium complexes containing trpy.[260] We performed matrix-assisted laser desorption ionization time-of-flight mass spectrometry (MALDI-TOF MS) of **C4** after the catalytic experiments, and it can be seen that the catalyst remains unchanged after catalysis, as is showed in (**Annex III Figure SIV.31**).

Relevance of the History of C4.

As mentioned in the introduction Chapter I of this thesis, **Na[1]** tends to self-aggregate in water, producing micelles and/or vesicles.[261] Upon the process of dissolving **C4**, the constituent ions would become free; for the vast majority of salts, this is completely independent. However, this apparently would not be the case here; see also the electrochemical section in which the $[Ru\text{-}OH_2]^{2+}$ affects the redox couple of **[1]$^-$**. Persistence even in the water ion-pair coupling between the cation and anion would be possible, which would prevent full dissociation and therefore maintain cooperation. Indeed, no noticeable changes have been observed at the UV-vis spectra in catalytic conditions near 10^{-6} M upon a 10-fold increase in concentration, as is showed in (**Annex III Figure SIV.32**).

To evidence the noncovalent bonding relevance between the photosensitizer **[1]$^-$** and the redox catalyst, we took advantage of the photooxidation process and studied the yields with the same concentrations of cations and anions but whose origins were different. Thus, we have studied the behavior of a mixture of two separate compounds, $[Ru^{II}(trpy)(bpy)(H_2O)](ClO_4)_2$ (**C2'**) and $Na[3,3'\text{-}Co(1,2\text{-}C_2B_9H_{11})_2]$ (**Na[1]**), after 4h of catalysis and using the Co/Ru ratios 1:1 and 2:1, maintaining the same ruthenium concentrations as that for the **C4** photocatalyst. (**Table IV.13**) displays the results obtained for two substrates, 1-phenylethanol and 4-methylbenzyl alcohol. The results show that the noncovalent ion pair **C4** displays a better catalytic performance than the equal 1:2 mixture of **C2’** and **Na[1]**, evidencing the advantage of the coupling history between the two compounds, where nonbonding interactions between $[Ru^{II}(trpy)(bpy)(H_2O)]^{2+}$ and $[1]^-$ could facilitate or stimulate ET and, consequently, the efficiency of the cooperative system in the alcohol oxidation. For comparison purposes, the ratio 1:1 ratio of **C2’** and **Na[1]** as well as **C2’** and **Na[1]** alone was also studied. All of these are reported in **Table IV.13,** showing a distinct and lower yield than **C4**.

Dynamic light scattering (DLS) measurements of catalytic mixtures were done, and the results are displayed in (**Annex III Figure SIV.33**). The hydrodynamic radius value of **C4** in the catalytic mixture is D = 140.9 nm, which is of the same order as that presented by **Na[1],**[262] which indicates the absence of larger aggregates in the medium, despite the presence of the $[Ru\text{-}OH]^{2+}$. On the other hand, the value of D = 128.4 nm, in the case of using a mixture of a 1:2 ratio of **C2’** and **Na[1]** as catalysts, is less than that for **C4**, indicating to what extent the history of the catalytic medium influences the generated aggregates and hence, although limited, the results.

Table IV.13. Photooxidation tests performed with **C4** and **C2’** + **Na[1]**[a].

Entry	Photocatalyst	Substrate	Product	TON (Yield, select. %)
1	C4	1-phenylethanol	acetophenone	16200 (81, ≥ 99)
2	C2’	1-phenylethanol	acetophenone	4400 (22, ≥ 99)
3	Na[1]	1-phenylethanol	acetophenone	6200 (62, ≥ 99)
4	C2’ + Na[1] (1:1)	1-phenylethanol	acetophenone	12800 (64, ≥ 99)
5	C2’ + Na[1] (1:2)	1-phenylethanol	acetophenone	15200(76, ≥ 99)
6	C4	4-methylbenzylalcohol	4-methylbenzaldehyde	19600 (98, ≥ 99)
7	C2’	4-methylbenzylalcohol	4-methylbenzaldehyde	5200 (25, ≥ 96)
8	C2’ + Na[1] (1:1)	4-methylbenzylalcohol	4-methylbenzaldehyde	17200 (70, 82)
9	C2’ + Na[1] (1:2)	4-methylbenzylalcohol	4-methylbenzaldehyde	18000 (86, 96)

[a]Conditions: **C4** (0.001 mM); **C2’** and **Na [1]** (0.001 mM) for ratio 1:1 (**C2’**/**Na[1]**); **C2’** (0.001 mM) and **Na[1]** (0.002 mM) for ratio 1:2 (**C2’/Na[1]**), substrate (20 mM), $Na_2S_2O_8$ (40 mM), 5 mL potassium carbonate solution at pH=7. Light irradiation during 4h.

This study represents the first work, to the best of our knowledge, in which a photoredox catalyst based on an abundant first transition metal (Co^{3+}) is noncovalently bonded to an active oxidation catalyst ($[Ru^{II}(trpy)(bpy)(H_2O)]^{2+}$), producing a persistent ion-pair interaction even in water and showing high selectivity in the photooxidation of alcohols.

The observed values of conversion obtained using **C4**, together with the previous electrochemical study, are consistent and support the proposed mechanism shown in the **Figure IV.25.**

Under irradiation, photons are absorbed by the photosensitizer Co_p^{III} that experiences excitation to form Co_p^{III*}, which undergoes oxidative quenching by the oxidizing agent $S_2O_8^{2-}$, generating Co_p^{IV}. This photogenerated strong oxidizing Co^{IV} is able to oxidize Ru_c^{II}-OH_2 to Ru_c^{III}-OH. Then the $SO_4^{\bullet -}$ radical oxidizes a new Co_p^{III} to Co_p^{IV}, which oxidizes Ru_c^{III}-OH to Ru_c^{IV}=O species. The Ru_c^{IV}=O specie reacts with the corresponding alcohols to afford the oxidized products with regeneration of the corresponding catalyst Ru_c^{II}-OH_2. With the proposed mechanism, the exchange of two electrons and two protons takes place in the photooxidation of alcohols.

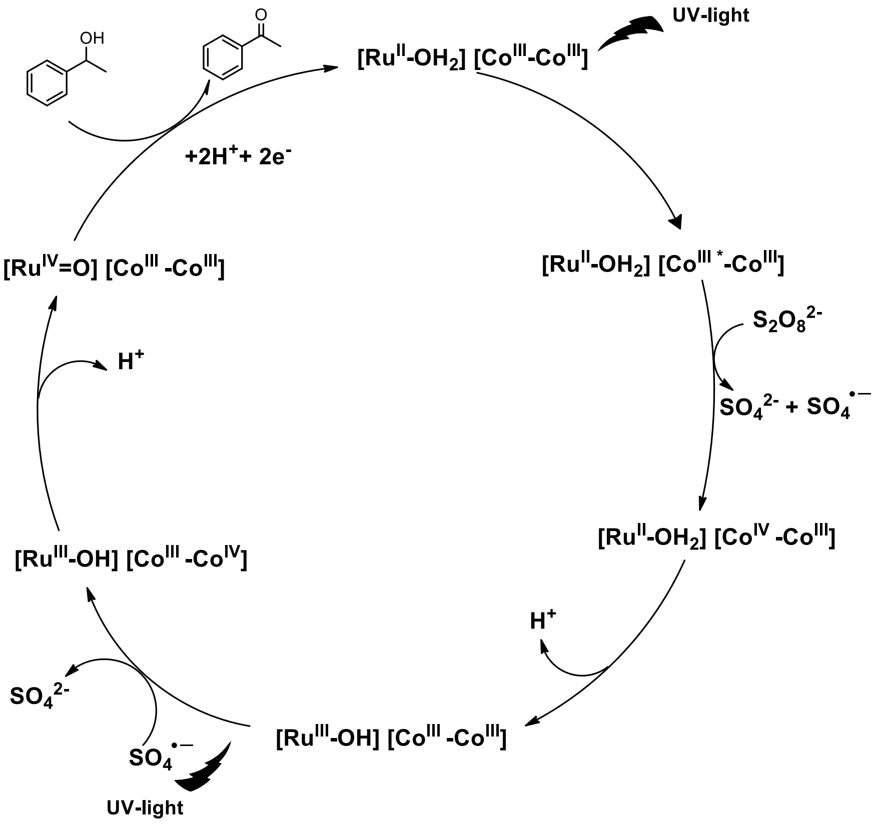
OH
O
UV-light
$[Ru^{II}-OH_2]\ [Co^{III}-Co^{III}]$
$+2H^+ + 2e^-$
$[Ru^{IV}=O]\ [Co^{III}-Co^{III}]$
$[Ru^{II}-OH_2]\ [Co^{III*}-Co^{III}]$
$S_2O_8^{2-}$
H^+
$SO_4^{2-} + SO_4^{\bullet -}$
$[Ru^{II}-OH_2]\ [Co^{IV}-Co^{III}]$
$[Ru^{III}-OH]\ [Co^{III}-Co^{IV}]$
H^+
SO_4^{2-}
$SO_4^{\bullet -}$
$[Ru^{III}-OH]\ [Co^{III}-Co^{III}]$
UV-light

Figure IV.25. Proposed mechanism for alcohol photooxidation using **C4**.

Table IV.12. Photooxidation tests performed with ruthenium cobaltabis(dicarbollide) complex **C4**.[a]

Entry	**Substrate**	**Product**	**t(h)**	**TON(Yield, select. %)**
1	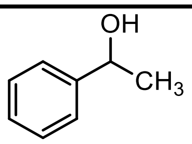	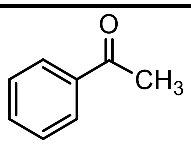	8[b] 6[c] 4 [d] 4 [e]	20000 (≥99, ≥99) 19200 (96, ≥99) 16200 (81, ≥99) 14600 (73, ≥99)
2	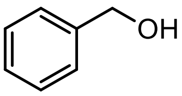	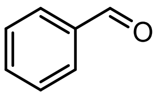	8[b] 4 [d] 4 [e]	18000 (75, 84) 16800 (84, 98) 16200 (77, 95)
3	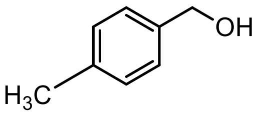	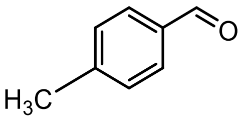	8[b] 4 [d]	19800 (93, 94) 19600 (98, ≥99)
4	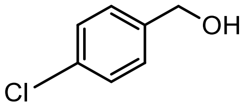	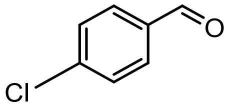	8[b] 4 [d]	19000 (90, 95) 15000 (75 , ≥99)
5	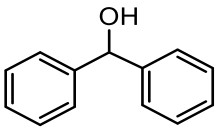	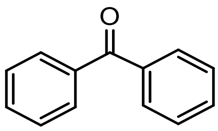	8[b] 4 [d]	20000(≥99,≥99) 15800(79, ≥99)
6	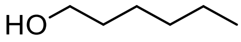	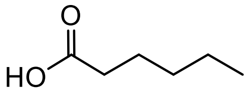	8[b] 4 [d]	18400 (92, ≥99) 16400 (82, ≥99)
7	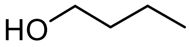	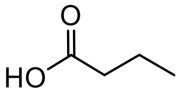	8[b] 4 [d]	19600 (98, ≥99) 17800 (89, ≥99)
8	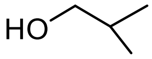	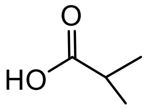	8[b] 4 [d]	18400(92, ≥99) 16600 (83, ≥99)
9	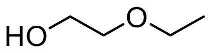	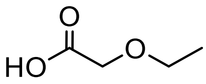	8[b] 4 [d]	19400 (93, ≥99) 18600 (76 , ≥99)
10	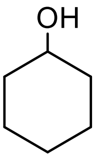	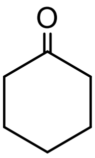	8[b] 4 [d]	19000 (95, ≥99) 15800 (79, ≥99)

[a]Conditions: **C4** (0.001 mM), substrate (20 mM), $Na_2S_2O_8$ (40 mM), 5 mL potassium carbonate solution at pH=7. Ratio 1:20000:40000: [b] 8h of reaction, with previous neutralization after 4 h.[c] 4h of reaction, with previous neutralization after 3 h. [d] 4 h of reaction, without neutralization. [e] Ratio 1:20000:20000; after 4 h of reaction.

In summary we have synthetized a cooperative ion-pair photoredox system, $[Ru^{II}(trpy)(bpy)(H_2O)][(3,3'-Co(1,2-C_2B_9H_{11})_2]_2$, **C4**, where the metallacarborane, as photoredox catalyst and the ruthenium aquo complex, as oxidation catalyst are linked by non-covalent interactions which persist even after water dissolution. The recrystallization of **C4** in acetonitrile, leads to the substitution of the water by the acetonitrile ligand and the formation of $[Ru^{II}(trpy)(bpy)(CH_3CN)][(3,3'-Co(1,2-C_2B_9H_{11})_2]_2$, **C5** complex.

The electrochemical studies in water revealed a significant coupling between $[Ru^{II}(trpy)(bpy)(H_2O)]^{2+}$, **C2’** and $[(3,3'-Co(1,2-C_2B_9H_{11})_2]^-$, **[1]**$^-$. This cooperative system was an efficient photoredox catalyst for the oxidation of alcohols in aqueous media, through a Proton Coupled Electron Transfer process (PCET), operating at room temperature under UV irradiation, using 0.005 mol% of catalyst and high turnover number (TON=20000) was obtained.

The photocatalytic studies showed that **C4** complex displayed better catalytic performance than separated mixtures of **C2’** and **Na[1]**, with the same concentrations and ratios of Ru/Co. Cooperative catalytic systems with this kind of interactions have not been described before, and represent an advance in the cooperativity avoiding the expensive covalent bonds. A possible mechanism for this photoredox catalytic mechanism has been proposed.

IV.4. A Stand-Alone Cobaltabis(dicarbollide) Photoredox Catalyst Epoxidates Alkenes in Water at Extremely Low Catalyst Load

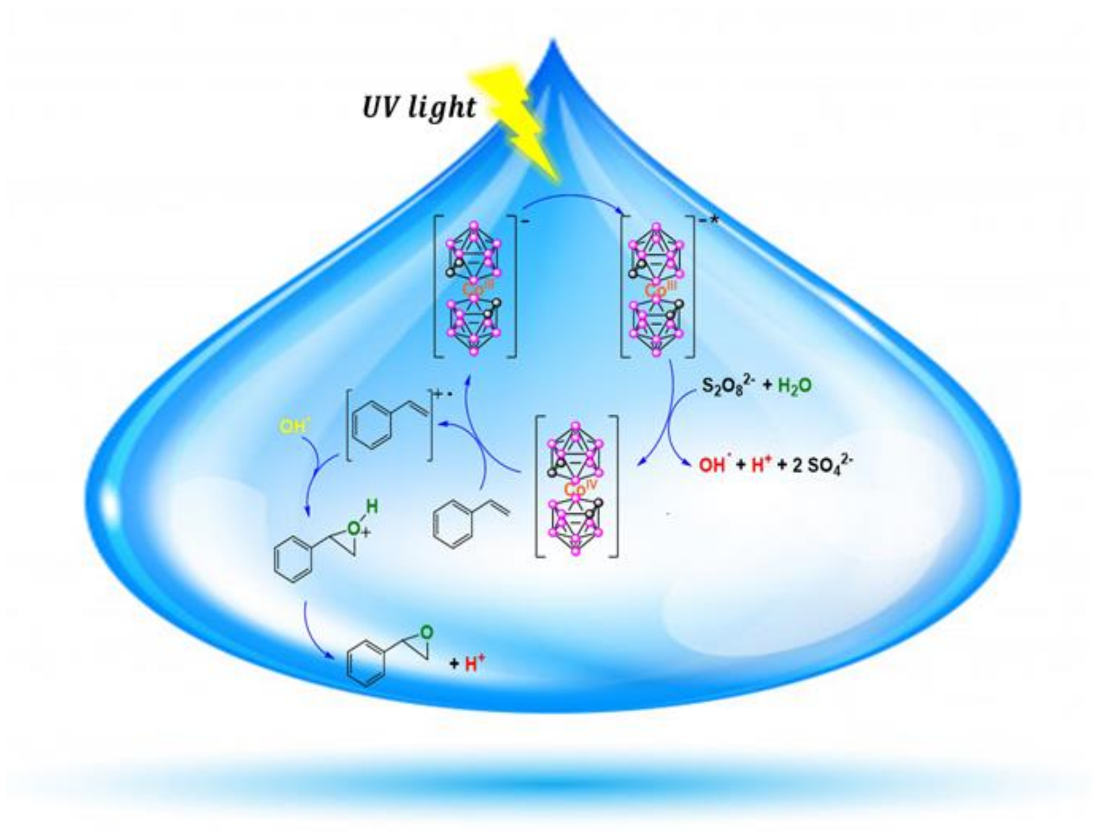

We describe the photoredox oxidation of alkenes by the sodium salt of anionic cobaltabis(dicarbollide), Na[Co($C_2B_9H_{11}$)$_2$], in water and we establish a comparison with the photocatalytic behavior of the conventional photoredox, Ru(bpy)$_3^{2+}$ widely studied in the literature. The comparison shows that the performance of [Ru(bpy)$_3$]$^{2+}$ in the photo oxidation of alkenes in water is very low or null efficiency. We shall see that low concentrations of **Na[1]** enhance the selectivity for the corresponding epoxide with high TON values in short reaction times. We have verified that Na[3,3'-Co(1,2-$C_2B_9H_{11}$)$_2$], acts as a photocatalyst in both processes, in the epoxidation of alkenes and in their hydroxylation in aqueous medium with a higher rate for epoxidation than for hydroxylation. Preliminary photooxidation tests using methyl oleate as substrate, led to the selective epoxidation of the double bond.

IV.4.1. Photocatalytic alkene oxidations

As we mentioned above **Na[1]** was prepared by cationic exchange resin from the water insoluble **Cs[1]** as is described in the literature.[263]

The first photocatalytic alkene oxidation experiments using **Na[1]** as catalyst were all performed by exposing reaction quartz vials to UV irradiation (2.2 W, ʎ ~ 300 nm, 12 lamps in the walls of a box), at room temperature and atmospheric pressure, and using styrene as substrate; this was the reference compound used to find the reaction optimal conditions. The samples were made of 5 mL of water (0.4 µM in K_2CO_3 pH=7) with a mixture of **Na[1]** (0.02 mM), styrene (20 mM) and $Na_2S_2O_8$ (26 mM) as oxidizing agent, ratios 1:1000:1300. Then, different reaction times were tested in order to know the conversion and the yields obtained along the time. Following irradiation for a specified time, as we can see in the (**Figure IV.26**), the reaction products were extracted with dichloromethane six times, dried with Na_2SO_4 and quantified by means of GC-FID and GC-MS analysis. As can be observed in **Figure IV.26**, after 30 minutes of reaction all the styrene was converted, and different products of oxidation were obtained as function of the reaction time.

The evolution of yields with the reaction time and the evolution of the molar fractions of the styrene together with those of the oxidation products have been displayed in (**Figure IV .27**). (**Figure IV.27 a**) shows that after 5 minutes of reaction the amount of epoxide obtained is greater (37%) with respect to the other generated products (diol, benzaldehyde and benzoic acid); however, after 15 minutes it is observed that the amount of diol increases (35 % diol *vs* 27 % epoxide) and finally after 30 minutes the amount of epoxide is maintained whereas the diol increases (50 % vs 25 % epoxide). Along this time, benzaldehyde and benzoic acid have been formed but in less ratio. Moreover, as is shown in **Figure IV.27** an increase of time results in a decrease in yield and selectivity values for the epoxide formation. Therefore, we have chosen 15 minutes as the time to perform the catalytic experiments, though in some cases, we have also studied the performance of the catalyst after 30 minutes of reaction.

Blank experiments after 30 minutes of reaction, in the absence of catalyst, light or oxidizing agent, have shown that no significant conversion of styrene occurred.

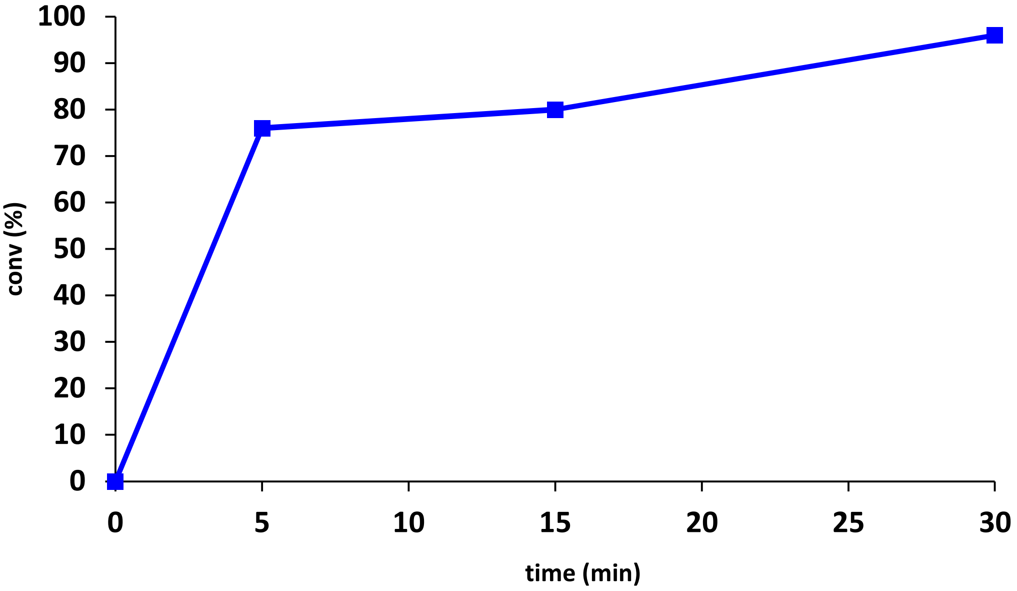

Figure IV.26. Plot of conversion as a function of time for the photoredox catalysis of styrene. Conditions: Na[3,3'-Co(1,2-$C_2B_9H_{11}$)$_2$] (0.02 mM), styrene (20 mM), $Na_2S_2O_8$ (26 mM), 5 ml K_2CO_3 solution at pH=7, light irradiation (2.2 W, λ ~300 nm).

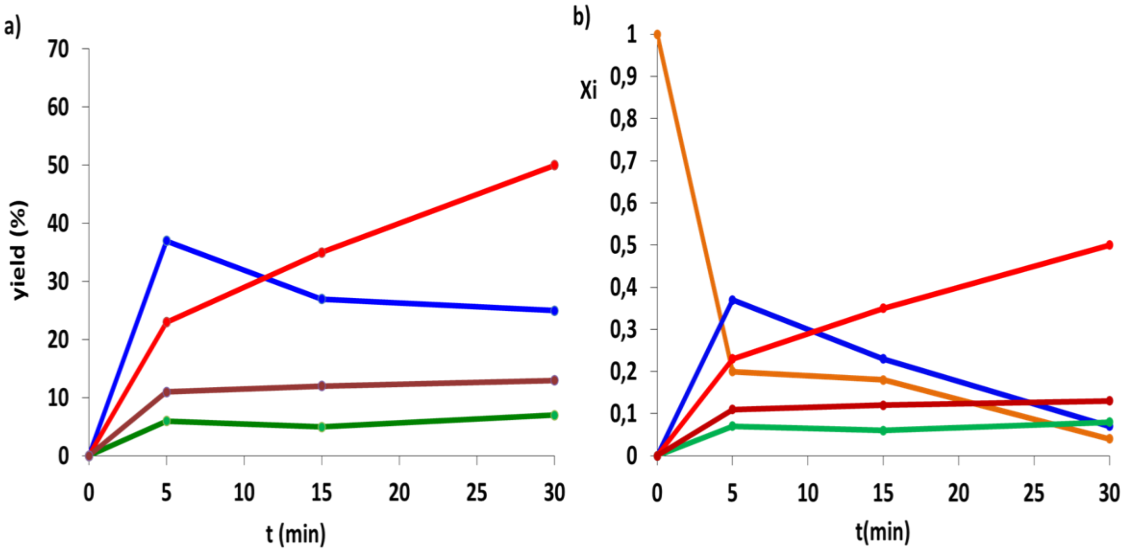

Figure IV.27. a) Plot of yield as a function of time and b) plot of the molar fractions (X_M) *versus* a time for the photoredox catalysis of styrene. Blue: styrene oxide; red: 1-phenyl-1,2-ethanediol; green: benzaldehyde; brown: benzoic acid; orange: styrene. Conditions: Na[3,3'-Co(1,2-$C_2B_9H_{11}$)$_2$] (0.02 mM), styrene (20 mM), $Na_2S_2O_8$ (26 mM), 5 ml K_2CO_3 solution at pH=7, light irradiation (2.2 W, λ ~300 nm).

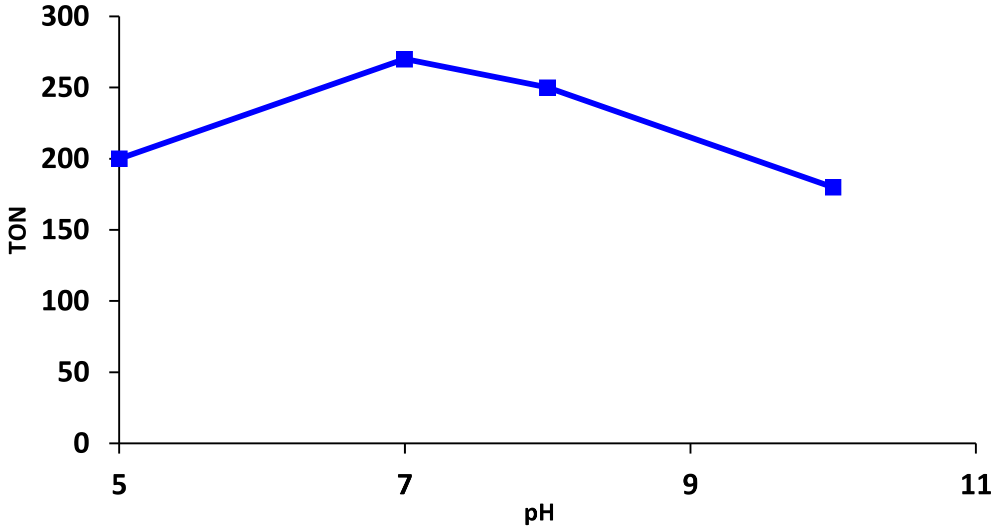

Figure IV.28. Plot of TON of styrene oxide as a function of pH. Conditions: Na[3,3'-Co(1,2-$C_2B_9H_{11})_2$] (0.02 mM), styrene (20 mM), $Na_2S_2O_8$ (26 mM), 5 ml of water, light irradiation (2.2 W, λ ~300 nm). TON = (mol of product)/(mol of catalyst).

The effect of the pH on the photocatalytic oxidation of styrene has been also examined. As is showed in the above (**Figure IV.28**), the optimal TON value for the epoxidation of styrene to styrene oxide after 15 minutes of reaction is obtained to pH=7 (TON=270) since this value decreases at lower (pH=5, TON=200) and higher (pH=8, TON=250) and (pH=10, TON=180) values of pH. The lower value observed at pH=5, probably is due to the easy epoxy ring opening in acidic medium.[264]

Table IV.14. Photooxidation tests performed with **Na[1]** complex.

Entry	substrate	Conv. %	product	TON	Selectivity %
1	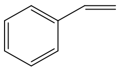	78[a] 80[b] 96[c]	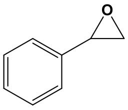	370[a] 270[b] 250[c]	47 34 26
2	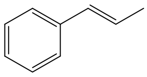	85[b] 91[c]	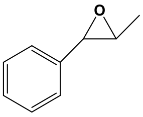	440[b] 200[c]	52 22
3	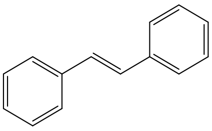	66[b] 95[c]	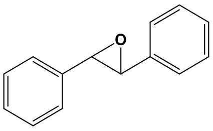	390[b] 290[c]	44 41
4	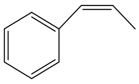	92[b] ≥99[c]	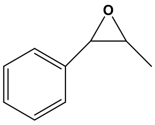	750(97%,cis)[b] 330(48%,cis)[c]	82 33
5	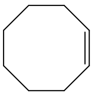	91[b] ≥99[c]	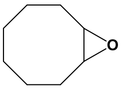	470[b] 380[c]	47 42
6	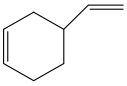	97[b] ≥99[c]	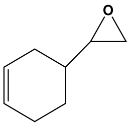	700[b] 370[c]	72 37
7	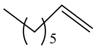	81[b] ≥99[c]	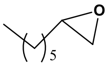	580[b] 160[c]	72 16

Conditions: **Na[1]** (0.02 mM), substrate (20 mM), $Na_2S_2O_8$ (26 mM), 5 mL potassium carbonate solution at pH=7. Ratio 1:1000:1300: [a] 5 min of reaction [b] 15 min of reaction. [c] 30 min of reaction.

IV.4.2. Photocatalytic oxidations using catalyst load of 0.1 mol %

Once the catalytic conditions have been optimized, we have also studied the photocatalytic oxidation of other alkenes using **Na[1]** as photoredox catalyst. **Table IV.14** and in (**Annex IV Table SIV 4.6**) displays the performance of the photocatalyst after 5, 15 and 30 minutes of reaction. In general it can be observed that high conversion values were achieved after 15 minutes of reaction, being in many cases, total conversion after 30 minutes. However the moderate selectivity for the epoxide decreases with the reaction time, along to the TON values. This happens simultaneously with an increase in the amount of the corresponding diol for most of the substrates studied, as is showed in **Table SIV 4.6**.

As is showed in **Table IV.14,** the photoepoxidation of *trans*-β-methylstyrene (**entry 2**), trans-stilbene (**entry 3**) and *cis*-β-methylstyrene (**entry 4**), led to the formation of the corresponding isomer without isomerization in the first 15 minutes; however in the case of *cis*-β-methylstyrene, the stereoselectivity towards the formation of the *cis*-epoxide isomer decreases greatly, up to half, after 30 minutes of reaction. This could be due to the formation of more long-lived free radical from the substrate that lead to the rotation of the C-C bond during the oxygen-transfer process, and consequently to the isomerization of *cis* to *trans* isomer.[265]

For the aromatic alkenes, the conversion values are enhanced by the presence of electron-donating substituents on the double bond (**entry 2** and **4**) but it is decreased by the presence of electron withdrawing substituents (**entry 3**).

Oxidation of the aliphatic alkenes have been also tested, being the linear 1-octene (**entry 7**) slightly less efficient that cyclooctene (**entry 5**) and 4-vinyl-1-cyclohexene (**entry 6**). The photooxidation of this last substrate, occurs on the external double bond, which indicates that this reaction is regiospecific.

On the other hand, the highly studied octahedral tris (2,2'-bipyridine)ruthenium(II) ($[Ru(bpy)_3]^{2+}$),[181] participates in electron transfer through an outer sphere mechanism, that implies that no major structural modification occurs upon ET. To the best our knowledge this compound has never been studied as photocatalyst for the epoxidation of alkenes in water medium. Then for the purpose of comparison, we also studied the performance of this compound in the photoredox oxidation of *trans*-stilbene, *cis*-β-methylstyrene, cyclooctene and 1-octene, under the conditions described in **Table IV.14** and after 30 minutes of reaction (**Table IV.15**). As can be observed in **Table**

IV.15, only in the case of the activated *trans*-stilbene and *cis*-β-methylstyrene, 10 % and 3 % respectively, of the corresponding epoxides were obtained after 30 minutes. In the case of aliphatic alkenes, cyclooctene and 1-octene, the conversion to the oxidized products was inexistent after this time. Based on these results, we can conclude that, unlike the photosensitizer $[Ru(bpy)_3]^{2+}$, the cobalt based **Na[1],** acts both as an efficient photosensitizer and a redox catalyst for the epoxidation of alkenes in water.

Table IV.15. Comparative results of Photooxidation tests performed with **Na[1]** *vs* $[Ru(bpy)_3]^{2+}$complex.

Entry	substrate	Conv.%		product
		Na[1]	$[Ru(bpy)_3]^{2+}$	
1	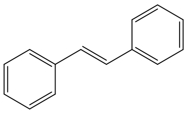	$95^{[c]}$	$10^{[c]}$	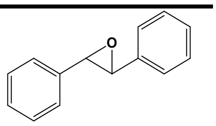
2	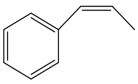	$\geq 99^{[c]}$	$3^{[c]}$	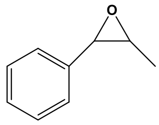
3	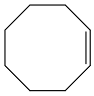	$\geq 99^{[c]}$	$0^{[c]}$	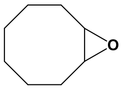
4	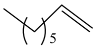	$\geq 99^{[c]}$	$0^{[c]}$	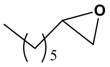

Conditions: **Na[1]** (0.02 mM), substrate (20 mM), $Na_2S_2O_8$ (26 mM), 5 mL potassium carbonate solution at pH=7. Ratio 1:1000:1300: [c] 30 min of reaction.

It is important to remark that **Na[1]**, just after irradiation and before extraction, upon addition of $[Me_4N]Cl$ yields the $[Me_4N][Co(C_2B_9H_{11})_2]$ salt that precipitates. This salt was filtered. The material produced from various catalytic processes was solubilized in acetonitrile and upon addition of water, the solution is passed to a cationic exchange resin loaded with Na^+ to generate again the **Na[1]**, which purity was proven either by ^1H- and ^{11}B-NMR spectra and by MALDI-TOF-MS. Once confirmed the stability of the catalyst after its recovery we confirmed that its catalytic activity remained. This recovered catalyst was tested for a second catalytic reaction using *trans*-β-methylstyrene, producing 80 % of the epoxide, similar value to the observed in the first catalytic run.

Based in the results above exposed, we have proposed a mechanism, displayed in the **Figure IV.29**, for the photoepoxidation of alkenes carried out by **Na[1]**. In the mechanism, the absorption of light by the photoredox catalyst $[Co^{III}(C_2B_9H_{11})_2]^-$ in the presence of water and $S_2O_8^{2-}$ (the oxidizing agent) generates the oxidized $[Co^{IV}(C_2B_9H_{11})_2]^-$ compound together with radical hydroxyl ($OH^\bullet$), protons (H^+) and sulphate anion (SO_4^{2-}). The posterior oxidation of the alkene by $[Co^{IV}(C_2B_9H_{11})_2]^-$ and the addition of radical hydroxyl ($OH^\bullet$) to the double bond, lead to the formation of the corresponding epoxide.

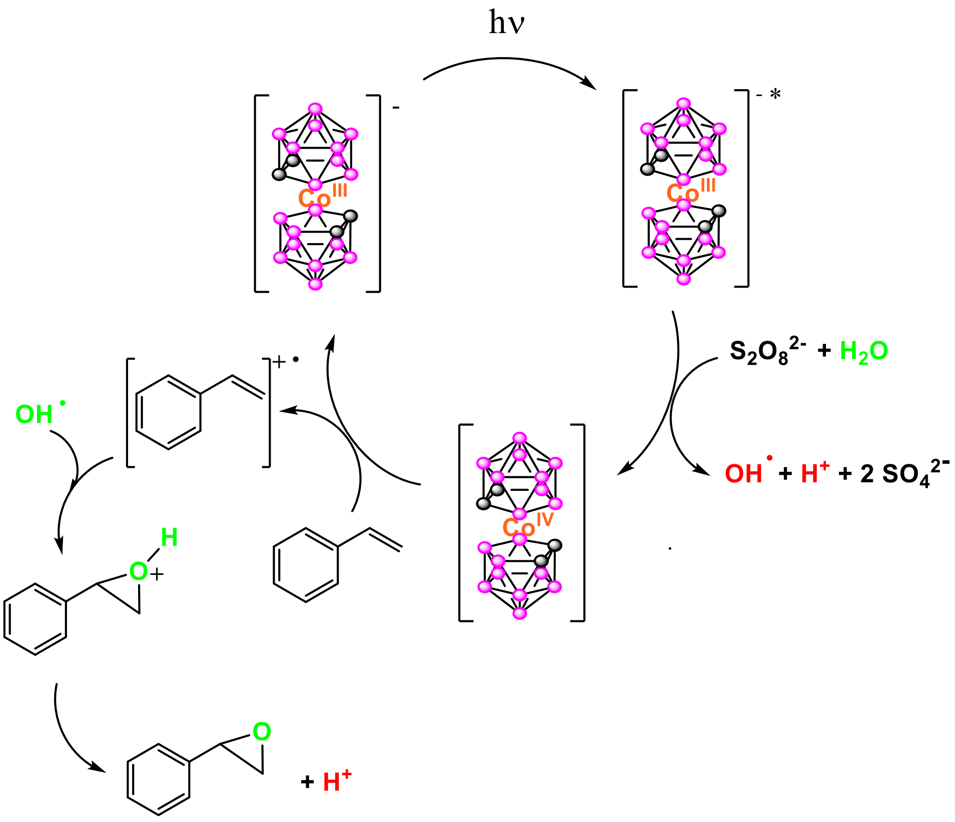

Overall reaction

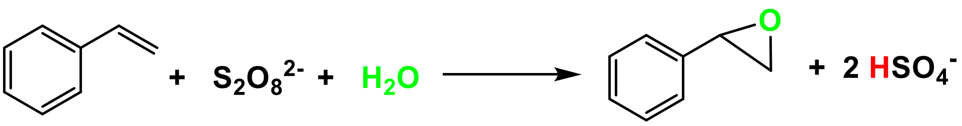

Figure IV.29. Proposed mechanism for the alkene epoxidation in water, with **Na[1]** as photoredox catalyst upon UV light irradiation.

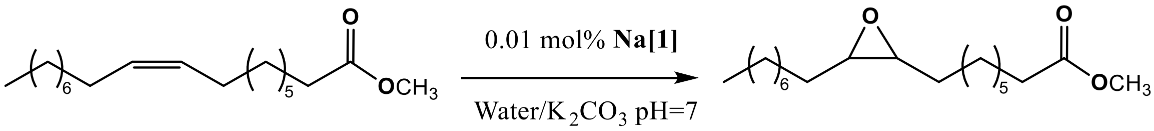

Scheme IV.3. Oxidation of methyl oleate by **Na[1]**

Earlier we indicated that the selectivity towards the epoxide decreased with reaction time. The study graphs shown in **Figure IV.27** reflects that when the epoxide decreases, the diol increases, which proves that this is a consequence of the evolution of the epoxide in aqueous media. It should also be noted that ring opening of epoxides is a promising process to produce 1,2-diols, an important functional group to produce surfactants, pharmaceuticals or their intermediates.[264,266]

It is known that in an aqueous medium an opening of the epoxide ring occurs, but in our case, we wanted to know if this opening was due solely to water or if **Na[1]** catalyzed the process. Then different experiments were performed by exposing the sealed reaction quartz vials to UV irradiation (2.2 W, ʎ ~ 300 nm, 12 lamps), at room temperature and atmospheric pressure, for 15 and 30 minutes, using three different epoxides, 1,2-epoxyoctane, styrene oxide and *trans*-stilbene oxide.

The samples were made of 5 mL of water (K_2CO_3 pH=7) with a mixture of **Na[1]** (0.02 mM), epoxide (20 mM) and $Na_2S_2O_8$ (26 mM) as oxidizing agent, following irradiation for a specified time, the results are showed in (**Table IV.16**). Previously, a set of different blank experiments were performed for 15 and 30 minutes.

These results show that the formation of the corresponding diols in water take place if the photocatalyst is present, since their absence in the reaction medium led to lower or nonexistent yield of diols in the short times of reaction that we have studied. Therefore, we can conclude that **Na[1]** acts as a photocatalyst in both processes, in the epoxidation of alkenes and in their hydroxylation in aqueous medium.

IV.4.3. Photocatalytic oxidations under lower catalyst load.

As have been described in previous works, $[3,3'\text{-Co}(1,2\text{-}C_2B_9H_{11})_2]^-$ despite does not have the typical surfactant structure performs as a surfactant and at concentrations of $[3,3'\text{-Co}(1,2\text{-}C_2B_9H_{11})_2]^-$ between 10^{-3} – 10^{-2} M, vesicles, free molecules, and micelles coexist, but at lower concentrations the ratio of molecules is higher.[267] Based on the non-parallel conversion of substrate *vs* the amount of catalyst given in previous works, described above in the first section of this chapter, we assumed that free molecules were more efficient, in terms of catalytic activity, than vesicles or micelles and we wanted to know if this also occurred in the photooxidation reaction of alkenes. Then we kept the concentrations of substrate and oxidizing agents constant as we have presented in **Table IV.14** and we have reduced the catalyst load to 0.01 mol % *vs* the original 0.1 mol %, corresponding to ratios of 1:10000:13000 of catalyst: substrate: oxidizing agent. The corresponding results are displayed in the following **Table IV.17**. We can observe that the conversion values were remarkable, higher than 90 % in most cases, after 30 minutes of reaction, with high TON in the photoepoxidation of alkenes, that to the best of our knowledge corresponds to the one of the highest turnover number achieved in alkene photoredox oxidation in homogeneous conditions. It is worth noting that in most of the substrates studied with the exception of styrene, the selectivity for the corresponding epoxide is greater than 99 % after 15 minutes of reaction, being higher than that obtained when working with higher loads of catalyst. At this point we can assert that our catalyst in low loads increase the selectivity towards the epoxidation of alkenes in relatively short times of reaction.

Under these conditions of reaction, we have done a preliminary photooxidation test using methyl oleate, the ester of oleic acid, as substrate (**Scheme IV.3**). Natural fats and oils are known to be a valuable source of hydrocarbons for the chemical industry. In many cases, their successful application as renewable raw materials depends on the efficiency of oxidative transformation of their alkyl chain. It was found that after 60 minutes of reaction and after the organic phase was analyzed by HPLC/ESI-MS, the oxidation took place selectively on the double bond C=C, detecting the presence of epoxide, as we can see in (**Annex III Figure SIV.31**). These preliminary studies show the high potential of this compound as photocatalyst to produce high added value products from animal fats.

Table IV.16. Photooxidation of epoxides performed with **Na[1]** complex. Conditions: **Na[1]** (0.02 mM), epoxide (20 mM), $Na_2S_2O_8$ (26 mM), 5 mL potassium carbonate solution at pH=7.

Entry	substrate	Conv.	Product	Yield(select.)%
1	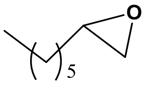	85[a] ≥99[b]	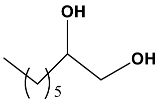	70(82)[a] 60(60)[b]
2	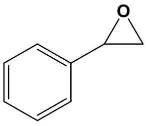	90[a] ≥99[b]	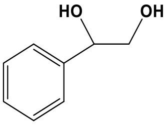	67(74)[b] 80(80)[c]
3	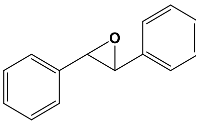	70[b] ≥99[c]	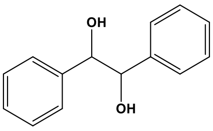	70(≥99)[b] ≥99(≥99)[c]

Ratio 1:1000:1300: [a]15 min of reaction [b]30 min of reaction. Yield and selectivity with respect the overall diol produced.

Table IV.17. Photooxidation tests performed with **Na[1]** complex.

Entry	substrate	Conv.%	product	TON	Selectivity%
1	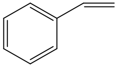	68[a] 98[b]	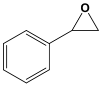	3600 [a] 2000 [b]	53 20
2	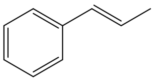	85[a] 93[b]	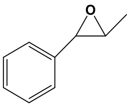	8500[a] 9300[b]	≥99 ≥99
3	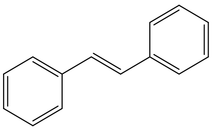	75[a] 95[b]	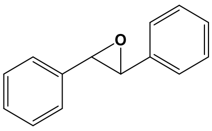	7500[a] 6400[b]	≥99 75
4	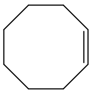	76[b]	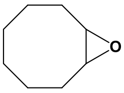	7600 [b]	≥99
5	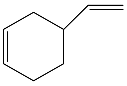	78[a] 90[b]	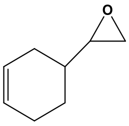	7800[a] 3900[b]	≥99 43
6	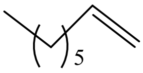	85[a] ≥99[b]	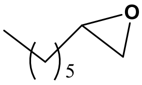	8500[a] 5000[b]	≥99 50

Conditions: **Na[1]** (0.002 mM), substrate (20 mM), $Na_2S_2O_8$ (26 mM), 5 mL potassium carbonate solution at pH=7. Ratio 1:10000:13000: [a] 15 min of reaction. [b] 30 min of reaction.

In summary, we have tested the cobaltabis(dicarbollide), Na[3,3'-Co(1,2-$C_2B_9H_{11})_2$], **Na[1]** as photoredox catalyst in the oxidation of different aromatic and aliphatic alkenes in aqueous media exhibiting excellent efficiency. The comparative catalytic studies of both **Na[1]** and ($[Ru(bpy)_3]^{2+}$), catalysts under the same catalytic conditions, for the photo oxidation of different alkenes showed in the case of $[Ru(bpy)_3]^{2+}$ a low or non-existent efficiency. **Na[1]** displayed moderate to high conversion and moderate selectivity values for the corresponding epoxide at a catalyst load of 0.1 mol % in short reaction times. The moderate selectivity values were due to the formation of diols as main by-products, but the selectivity for the epoxide increased to be >99% with the reduction of the catalyst concentration to 0.01 mol %. High TON values were obtained (TON=8500) for the epoxidation of alkenes in aqueous media. The studies carried out ensured that the metallacarborane acts as a photoredox catalyst in the epoxidation and hydroxylation of the alkenes studies, being the latter process lower in ratio versus the first. Preliminary photo oxidation catalytic studies using methyl oleate as substrate, led to the selective epoxidation of the substrate. The results obtained represent a hopeful starting point for the development of practical processes for the treatment of unsaturated fatty acids, such as the valorization of animal fat waste by using this sustainable photoredox catalyst.

IV.5. Ferrabis(dicarbollide), an Abundant Metal Photoredox Oxidation Catalyst in water

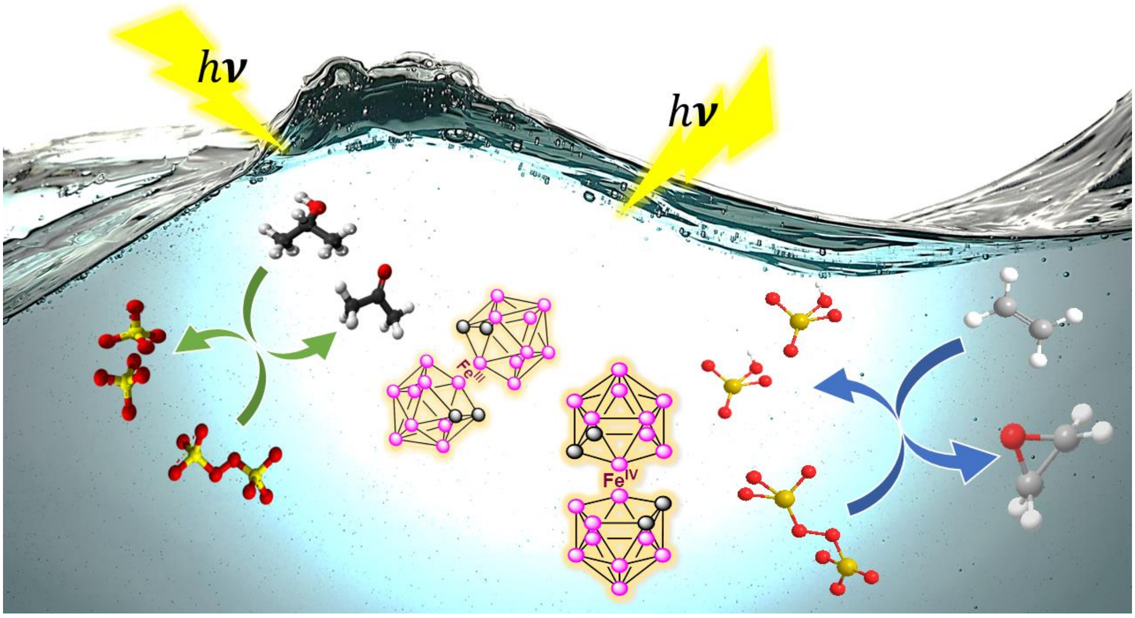

We describe here the photocatalytic behavior of the ferrabis(dicarbollide) [Na·2,5H_2O][3,3’-Fe(1,2-$C_2B_9H_{11}$)$_2$] **Na[2]** in the oxidation of alcohols and alkenes in water. In the same manner as cobaltabis(dicarbollide) **Na[1],** there is a duality in their performing in the catalytic aqueous media, photosensitizer and catalyst at the same time. In the experiments we will use the $Na_2S_2O_8$ as sacrificial oxidant in a K_2CO_3 neutral media, using lamps of frequency near to the maximum absorbance of the photoredox catalyst (ʎ=300 nm). Due to the excellent results we have found in the photooxidation of these substrates with the well-known **Na[1]** at a low load of catalyst, we decided to use **Na[2]** as photoredox catalyst to stablish a comparison with the **Na[1]**. As **Na[1], Na[2]** is highly soluble in aqueous media, showing the same molecular compact shape, but with different properties mostly due to the redox potential of the Fe$^{4+/3+}$ couple.

IV.5.1. Ferrabisorthodicarbollide: general properties.

Once it has been demonstrated the high performance of **Na[1]** as a photoredox catalyst, which act both as catalyst and photosensitizer, being highly efficient in the photooxidation of alcohols and alkenes in water, through single electron transfer processes (SET), we wanted to study if another very similar metallacarborane like ferrabis(dicarbollide) $[3,3\text{-Fe}(1,2\text{-C}_2B_9H_{11})]^{2-}$ **Na[2]**, could perform as photoredox catalyst, as well as it does **Na[1]**, given their similar characteristics as, the absence of fluorescence, surfactant behavior and water solubility. So we wanted to demonstrate that the catalysis could also be carried out under homogeneous conditions in aqueous media. Hence, **Na[2]** was prepared from the ortho-*nido*-carborane compound, following the methods described in the literature (**Figure IV.30**).[47]

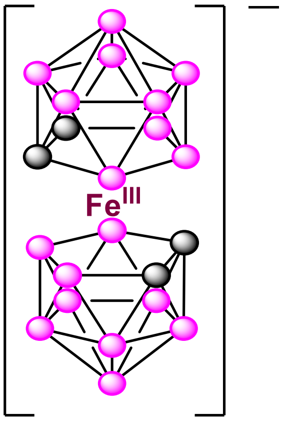

Figure IV.30. Metallacarborane used in this work: $[3,3'\text{-Fe}(1,2\text{-C}_2B_9H_{11})_2]^-$ ($[2]^-$, only the *trans* rotamer is shown). The grey circles represent Cc-H units and the pink circles B-H units.

Although both are soluble in water, they display different electrochemistry, as we have seen in the introduction chapter of this thesis. **Na[1]** or COSAN has three accessible redox reversible processes, formally $Co^{II/I}$, $Co^{III/II}$ and $Co^{IV/III}$ at -2.64, -1.75 and +1.22 V *vs* Fc, respectively. In the case of **Na[2]** or FESAN, presents a redox potential reversible at -0.78 V vs Fc corresponding to the couple $Fe^{III/II}$ and a second one at 0.76 V corresponding to $Fe^{IV/III}$ (**Figure IV.31**). Comparing these redox potentials with those for **Na[1]**, the difference between the $M^{IV/III}$ and $M^{III/II}$ couples is less in **Na[2]** and also comparing the $M^{IV/III}$ redox couples, the one for Fe is 460 mV less anodic than that corresponding to Co**.** Comparing the redox potentials of the metallacarboranes mentioned above with these found corresponding to $[Ru(bpy)_3]Cl_2$, a well-known photosensitizer, at -1.76 V ($Ru^{II/I}$) and +0.85 V ($Ru^{III/II}$),[268] the latter value is similar to the potential of **Na[2]** corresponding to the couple $Fe^{IV/III}$ (+0.76 V), although both values are less anodic than the potential value for $Co^{IV/III}$(1.22 V) in **Na[1]**. With all this in mind, we can hypothesize that **Na[2]** based on a cheap abundant metal can act as photoredox oxidation catalyst, but probably with less oxidizing power than **Na[1]**, based on these electrochemical results.

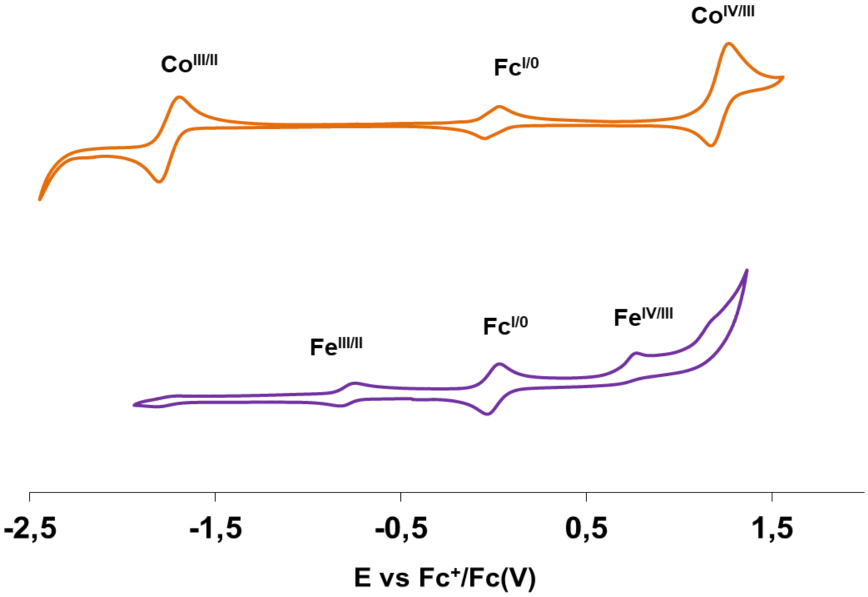

Figure IV. 31. Cyclic voltammetries of **Na[1]** (orange) and **Na[2]** (purple) in CH_3CN+ 0.1M TBAH. All potentials *vs* Ferrocene.

Despite the differences in the electrochemical behaviour, both metallacarboranes display similar differences in electronegativity between the atoms, (e.g., X_{Fe}-X_B= -0.21 in $[Fe(C_2B_9H_{11})_2]^-$ and X_{Co}-X_B= -0.16 in $[Co(C_2B_9H_{11})_2]^-$) , compared to organometallic complexes like $[Ru(bpy)_3]^{2+}$ or $Fe[(C_5H_5)_2]$. Lower negative values can translate into better overlap of orbitals of the metal and ligands, and the orbitals in the frontial orbital region for both metallacarboranes are less metal-based. Also, the metallacarboranes present negative charge and double negative charge for the ligands. This fact results in occupied high energy molecular orbitals and with ligand-like character. These features are responsible for the ability to self-assemble and for the presence of differences in the hydrogen atoms which influence the existence of hydrogen bonding to construct supramolecular structures.[269] The interactions in a supramolecular approach seem to be significant in the processes of electron transfer and in the effectivity of the photocatalytic systems.[270]

With respect to the UV- visible spectrum, **Na[2]** shows bands at 278 nm (ε=14213 M^{-1} cm^{-1}) , 303 (ε=12465 M^{-1} cm^{-1}) and two weaker at weaker one at 452 nm (ε=633 M^{-1} cm^{-1}) and other at 560 nm (ε=236 M^{-1} cm^{-1}) (**Figure IV.32 a**), slightly similar to **Na[1]** which shows bands at 293 nm (ε =27172 M^{-1} cm^{-1}) and two weaker ones at 345 nm (ε =1928 M^{-1} cm^{-1})and 452 nm (ε =300 M^{-1} cm^{-1}), in acetonitrile as solvent, as is shown in (**Figure IV.32 b**). Thus, we decided to perform the catalytic studies operating under UVA light in the same conditions used with **Na[1],** using a UVA lamp that irradiates at ʎ ~300 nm because this frequency is near to the maximum absorbance of the catalyst.

IV.5.2. Photocatalytic oxidation of alcohols

As Iron is the fourth most abundant element in the earth's crust and the most abundant element as a transition metal it was highly attractive to be tested as a photocatalyst. Then we could replace Co by the very abundant Fe metal, and therefore, to have a major sustainable and green photocatalyst. This motivated us to use **Na[2]** to test the oxidation of different aromatic and aliphatic alcohols to evaluate their photoredox properties as catalyst.

As stated earlier, when using **Na[1]** as photocatalyst, preliminary studies revealed that lower concentrations of **Na[1]** resulted to be more effective in conversion. Hence, initial photocatalytic alcohol oxidation experiments using 0.01 mol % of **Na[2]** as photocatalyst were all performed by exposing the reaction quartz vials to UV irradiation (2.2 W, ʎ ~300 nm, 12 lamps in the walls of a box), at room temperature and atmospheric pressure, and using 1-phenylethanol as substrate, in order to test the optimal time to perform the catalytic studies. The samples were made of 5 mL of water (K_2CO_3 pH=7) with a mixture of **Na[2]** (0.002 mM), 1-phenylethanol (20 mM) and $Na_2S_2O_8$ (40 mM) as oxidizing agent, ratios 1:10000:20000. After 4 h of irradiation, the reaction products were extracted with dichloromethane three times, dried with Na_2SO_4, and quantified by ^{1}H NMR spectroscopy and GC chromatography. We found that 4 h was the optimal time to convert 1-phenylethanol into acetophenone, as it can see in **Table IV.18**. However we have extended the time of reaction to 8h for other alcohols. Control experiments revealed that no reaction occurred in the absence of photocatalyst, light or oxidizing agent, after 8h of reaction.

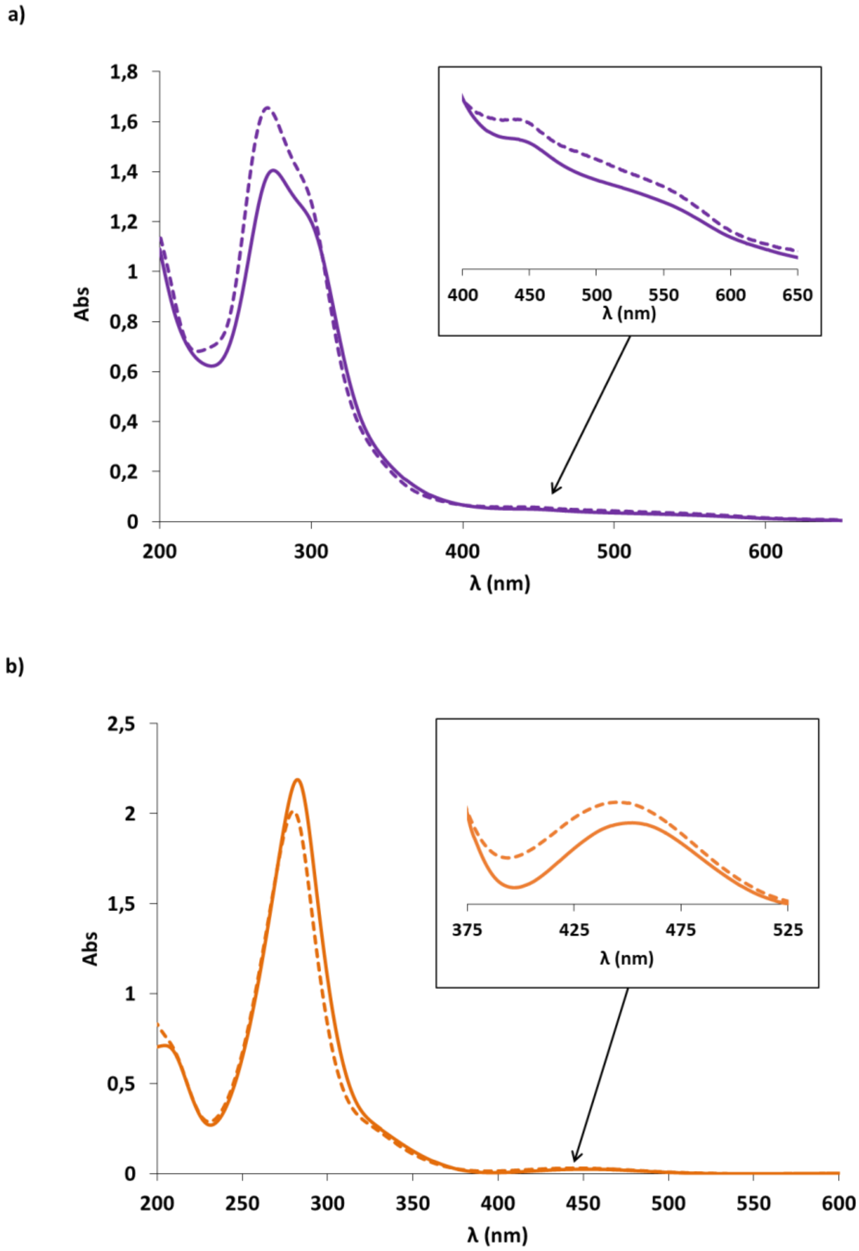

Figure IV.32. a) UV-Vis spectrum of Na[3,3'-Fe(1,2-$C_2B_9H_{11})_2$] **Na[2]** in acetonitrile (purple line) and in water (dashed line), 8.0x10^{-5} M. b) UV-visible spectra of Na[3,3'-Co(1,2-$C_2B_9H_{11})_2$] **Na[1]** in acetonitrile (orange line) and in water (dashed line), 8.0 x10^{-5} M.

As we can see in **Table IV.18**, in general, high yields have been achieved for all the substrates tested. For the secondary aromatic alcohols 1-phenylethanol and diphenylmethanol, we have observed an almost total conversion towards the corresponding ketones, after 4h of reaction (**entry 1b and 5b**), even when the amount of sacrificial oxidant was reduced to half for the photooxidation of 1-phenylethanol (**entry 1c**). For the primary aromatic benzyl alcohol (**entry 2**), the photooxidation process led to the formation of 90 % of benzaldehyde at 8h. The reduction of the reaction time to 4 h allowed the enhancing of the selectivity towards the aldehyde accompanied by a reduction in yield 80 % (**entry 2**). The yield values were enhanced by the presence of electron-donating substituents on the aromatic ring of the benzyl alcohol (**entry 3**), whereas the presence of electron withdrawing substituents, decreased the yield (**entry 4**), at 4 and 8h. In the case of aliphatic alcohols 1-hexanol (**entry 6**), and 2-ethoxyethanol (**entry 7**), high yields towards the corresponding acids were observed after 4h. For the secondary cyclohexanol (**entry 8**), 95 % of cyclohexanone was obtained. In general, the selectivity values are remarkable, >99% with the exception of benzyl alcohol, as we have commented above.

MALDI-TOF mass spectrum of **Na[2]** (**Figure IV.33**) was made after a catalytic experiment using 1-phenylethanol as substrate. The results show the increase in the hydroxylated derivative to 24 %, after 4h of irradiation; with the formation of the corresponding mono- (10%), di- (3%), tetra- (2%), hexa- (2%), hepta- (5%) and octa (2%) hydroxylated forms of **Na[2]**. After the corresponding sample treatment, the catalyst was tested in a second catalytic experiment, showing a yield in acetophenone of 93 %, evidencing that the formation of hydroxylated catalyst maintain the photoredox capacity.

To gain more insights to the behavior of our photoredox catalyst, we studied the photooxidation of diols interesting at an industrial level, like diethylene glycol and 1,6-hexanediol and other alcohols like 1-butanol, 1-pentanol and isobutanol as substrates, as we can see in (**Table IV.19**). In the case of 1-butanol, 1-pentanol and isobutanol (**entries 1, 2 and 3**) moderate yields in the corresponding acids, have been observed (76%, 72% and 71% respectively) after 4h. The photooxidation of diethylene glycol and 1,6-hexanediol (**entries 4 and 5**) displayed lower yields (57 % and 42 % respectively). In any case, high selectivity (>99%) and TON values have been achieved with these substrates.

Table IV.18. Oxidation tests performed with ferrabis(bisdicarbollide) complex **Na[2]**. Conditions: **Na[2]** (0.002 mM), substrate (20 mM), $Na_2S_2O_8$ (40 mM), 5 mL potassium carbonate solution at pH=7 .light irradiation 4h.

Entry	Substrate	Product	Yield (select.) %
1	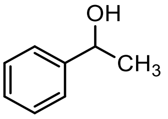	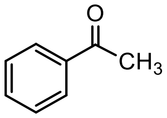	99 (≥ 99) [b] 95 (≥ 99) [c]
2	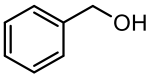	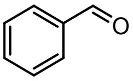	90 (91)[a] 80 (95)[b] 75 (95)[c]
3	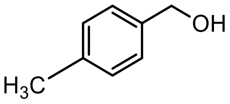	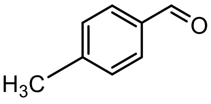	92 (≥ 99) [a] 83 (≥ 99) [b]
4	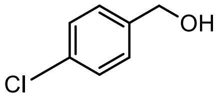	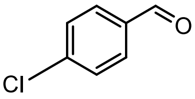	85 (≥ 99)[a] 65 (≥ 99)[b]
5	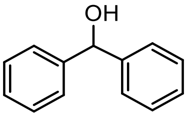	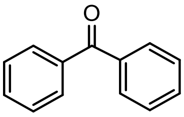	99 (≥ 99)[a] 92 (≥ 99)[b]
6	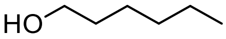	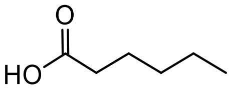	79 (≥ 99)[b]
7	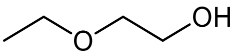	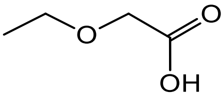	93 (≥99)[b]
8	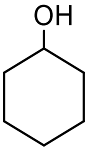	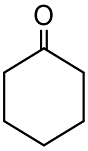	95(≥99)[b]

[a] After 8 h of reaction. [b] After 4 h of reaction. [c] After 4h of reaction with ratio 1:10000:10000.

Table IV. 19. Products obtained from photooxidation of alcohols by **Na[2]**

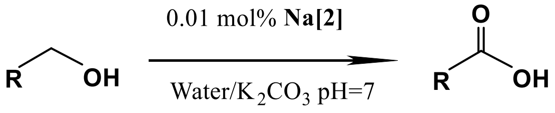

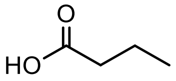	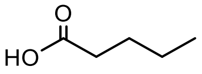	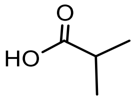
1	**2**	**3**
76% [a], TON=7600	72% [a], TON=7200	71% [a], TON=7100
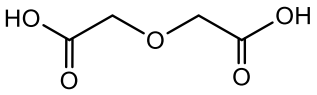	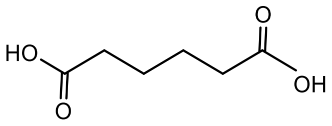	
4	**5**	
57% [a] ,** TON=5700	42% [a] ,** TON=4200	

[a] Conditions: **Na[2]** (0.002 mM), substrate (20 mM), $Na_2S_2O_8$ (40 mM), 5 mL potassium carbonate solution at pH=7 ;light irradiation 4h using a lamp with λ =300 nm· Yields and TONs values obtained are shown. Yields of products were determined by NMR spectroscopy. **Analysis was done on the neat reaction.

These results show that the ferrabis(dicarbollide) acts as an efficient catalyst in the photooxidation of alcohols with results comparable to those obtained with cobaltabis(dicarbollide). Furthermore, **[2]**$^-$ displays total conversion values even after 4h of reaction and high TON values, for most of the substrates studied evidencing the high performance of this photoredox catalyst.

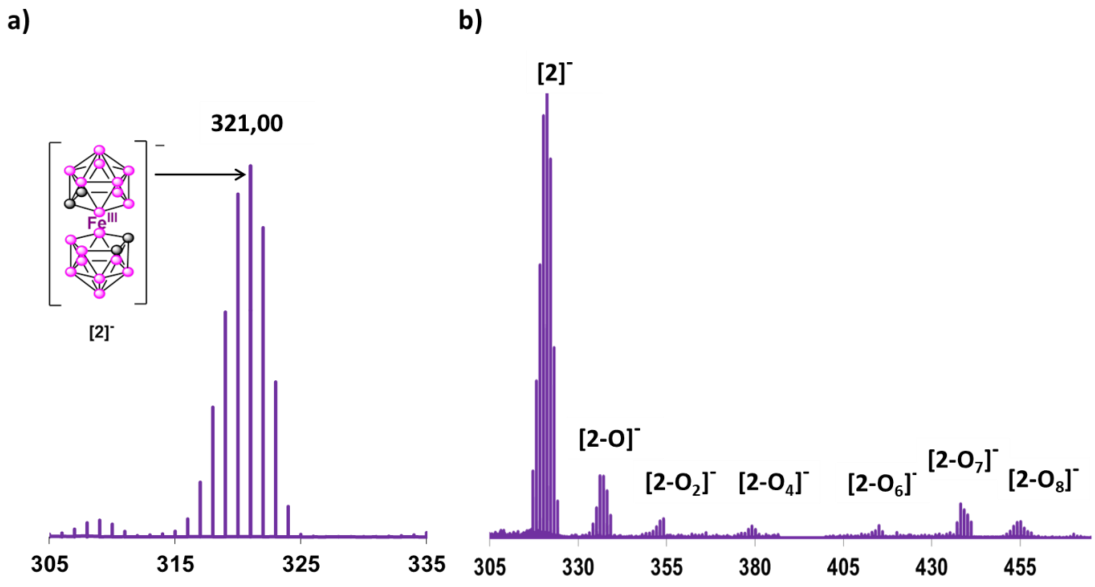

Figure IV.33. Experimental MALDI mass spectrum of **Na[2],** a) before of photocatalytic oxidation of 1-phenylethanol The peak at m/z 321 corresponds to [3,3'-Fe(1,2-$C_2B_9H_{11})_2]^-$. b) Experimental MALDI mass spectrum after of photocatalytic oxidation of 1-phenylethanol. The peaks correspond to [3,3'-Fe(1,2-$C_2B_9H_{11})_2]^-$ $[1]^-$ and that on the to [3,3'-Fe(1,2-$C_2B_9H_{11}$)(1,2-$C_2B_9H_{11}O)]^-$ $[2\text{-}O]^-$ = 336 (m/z), to [3,3'-Fe(1,2-$C_2B_9H_{11}$)(1,2-$C_2B_9H_{11}O_2)]^-$ $[2\text{-}O_2]^-$=353 (m/z), [3,3'-Fe(1,2-$C_2B_9H_{11}$)(1,2-$C_2B_9H_{11}O_4)]^-$ $[2\text{-}O_4]^-$=383 (m/z), [3,3'-Fe(1,2-$C_2B_9H_{11}$)(1,2-$C_2B_9H_{11}O_6)]^-$ $[2\text{-}O_6]^-$=417 (m/z), [3,3'-Fe(1,2-$C_2B_9H_{11}$)(1,2-$C_2B_9H_{11}O_7)]^-$ $[2\text{-}O_7]^-$=438 (m/z), [3,3'-Fe(1,2-$C_2B_9H_{11}$)(1,2-$C_2B_9H_{11}O_8)]^-$ $[2\text{-}O_8]^-$=454 (m/z).

IV.5.3. Comparative overview of Na[2] *vs* Na[1] as photoredox catalysts in the oxidation of alcohols.

Table IV.20 displays a comparison of the results corresponding to the photooxidation of different alcohols, using **Na[1]** or **Na[2]** as catalysts. In general we can observe excellent yields, with selectivity values >99 % for both photocatalysts. In the case of secondary aliphatic and aromatic alcohols, almost total conversion have been observed after 4 h using the Na[2] as catalyst. However, for the photooxidation of primary aromatic and aliphatic alcohols the yields obtained using **Na[1]** as photocatalyst are slightly higher than the obtained using **Na[2]**. This fact could be explained due to the higher oxidizing power of Na[1] vs. Na[2].

These results show that the ferrabis(dicarbollide) acts as an efficient catalyst in the photooxidation of alcohols with results comparable to those obtained with cobaltabis(dicarbollide); therefore, this iron photoredox catalyst based on the most abundant metal in nature is even postulated as a *greener* photocatalyst from a sustainable point of view.

Table IV. 20. Comparison product set obtained from photooxidation of alcohols by **Na[2]** vs **Na[1]** [a]

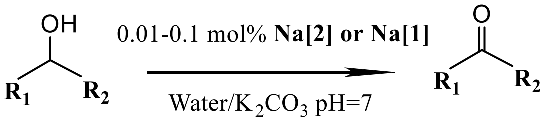

	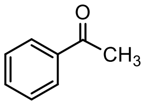	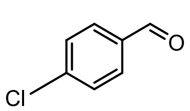	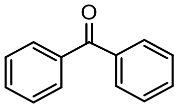
	1	**2**	**3**
Na[2]	>99%, TON=10000 >99%[b], TON=10000	85%, TON=8500 65%[b], TON=6500	>99%, TON=10000 92%[b], TON=9200
Na[1]	>99%, TON=10000	>94%, TON=9400	>99%, TON=10000
	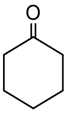	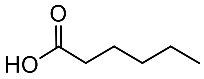	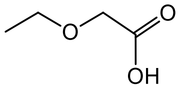
	4	**5**	**6**
Na[2]	95%[b], TON= 9500	79% , TON=7900	93% TON=9300
Na[1]	93% , TON= 9300	91% , TON=9100	97% , TON=9700

[a] Conditions: **Na[1]** or **Na[2]** (0.002 mM), substrate (20 mM), $Na_2S_2O_8$ (40 mM), 5 mL potassium carbonate solution at pH=7 ;light irradiation 8h using a lamp with λ =300 nm; [b] light irradiation 4h. Yields and TONs values obtained are shown. Yields of products were determined by NMR spectroscopy (see **Annex V**).

IV.5.4. Photocatalytic alkene oxidation

Photocatalytic oxidation of alkenes has also been investigated. The first photocatalytic experiments were all performed by exposing reaction quartz vials to UV irradiation (2.2 W, ʎ ~ 300 nm). The samples were made of 5 mL of water (K_2CO_3 pH=7) with a mixture of 0.1 mol % of **Na[2]** (0.02 mM), alkene (20 mM) and $Na_2S_2O_8$ (26 mM) as oxidizing agent, in ratios 1:1000:1300. Using styrene as substrate, as substrate, different reaction times were tested (**Figure IV.34**) observing that after 30 minutes of reaction 86 % of styrene was converted. In addition, blank experiments at this time have shown that no significant conversion of styrene occurred.

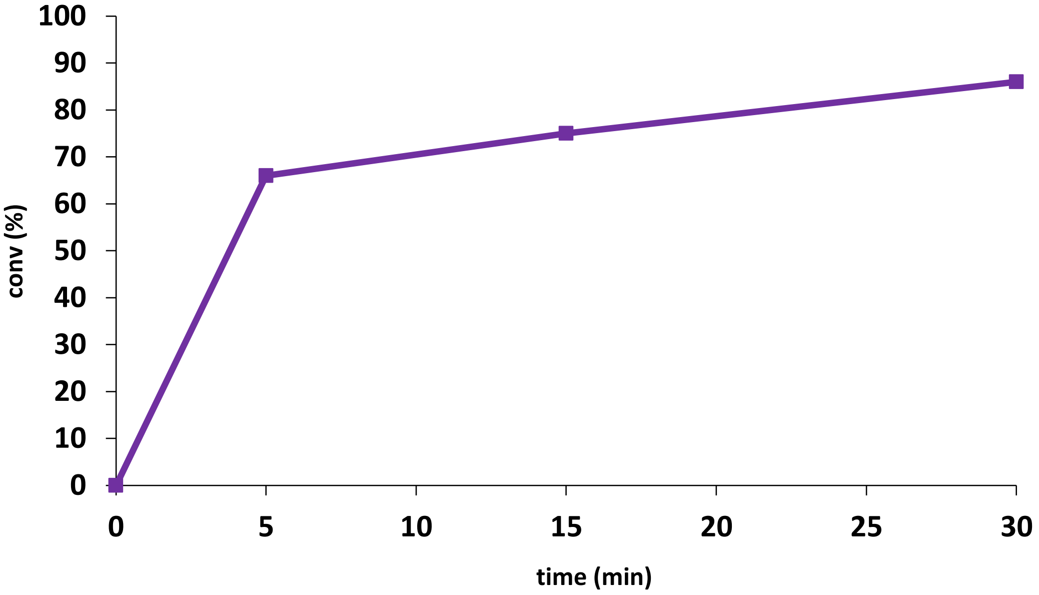

Figure IV.34. Plot of conversion as a function of time for the photoredox catalysis of styrene. Conditions: Na[3,3'-Fe(1,2-$C_2B_9H_{11})_2$] (0.02 mM), styrene (20 mM), $Na_2S_2O_8$ (26 mM), 5 ml K_2CO_3 solution at pH=7, light irradiation (2.2 W, λ ~300 nm).

The oxidation products formed over this time and the evolution of the molar fractions of styrene together with the oxidation products (**Figure IV.35**) show that after 5 and 15 minutes of reaction the amount of epoxide obtained is greater (43% and 36% respectively) with respect to other generated products (diol, benzaldehyde and benzoic acid); however, after 15 minutes it is observed that yields of benzaldehyde and benzoic acid progressive increase, and after 30 minutes these values are 21% and 50 % respectively, being the amount of epoxide of 14%. It is important to highlight that after 15 minutes of reaction the formation of 1-phenyl-1,2-ethanediol is practically negligible (1 %).

The performance of **[2]**$^-$ in the epoxidation of other alkenes have been studied after 15 and 30 min (**Table IV.21**). In general, it can be observed high conversion values achieved after 15 minutes of reaction, with high selectivity values for the epoxide, in some cases (entries 3, 4, 7). However, the selectivity and TON values decrease with the reaction time for styrene (**entry 1**), cis-cyclooctene (**entry 5**) and 1-octene (**entry**

7). This happens simultaneously with an increase in the amount of the corresponding overoxidation products (see **Table SIV 5.1** in **Annex V**) mainly the corresponding acid or aldehyde in the case of styrene, diol in *cis*-cyclooctene and aldehyde and acid in 1-octene. In the case of cis-β-methylstyrene (**entry 4**), the selectivity for the *cis*-epoxide is maintained, after 15 minutes (92% cis). Epoxidation of the linear 1-octene (**entry 7**) was less efficient that the epoxidation of *cis*-cyclooctene (**entry 5**) and 4-vinyl-1-cyclohexene (**entry 6**), being this last substrate epoxidated on the external double bond, indicating that the reaction is regiospecific. After the epoxidation of trans-β-methylstyrene, **Na[2]** was precipitated as [Me_4N][$Fe(C_2B_9H_{11})_2$], and recovered as sodium salt through a cationic exchange. The catalyst was tested in a second run, using the same substrate and the same yield in epoxide was obtained.

Table IV.21. Photoepoxidation tests performed with **Na[2]** complex.

Entry	substrate	Conv.%	product	TON	Select. %
1	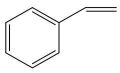	66[a] 75[b] 86[c]	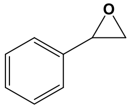	430[a] 360[b] 140[c]	65 48 16
2	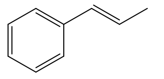	≥99[b] ≥99[c]	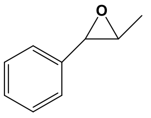	570[b] 440[c]	57 44
3	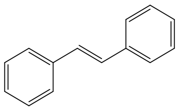	≥99[b] ≥99[c]	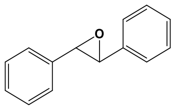	950[b] 900[c]	95 90
4	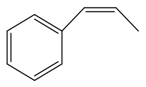	≥99[b] ≥99[c]	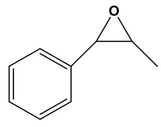	960 (92%,cis)[b] 940 (69%,cis)[c]	96 94
5	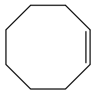	95[b] ≥99[c]	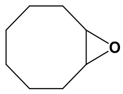	560[b] 90[c]	59 9
6	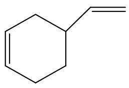	≥99[b] ≥99[c]	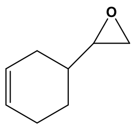	440[b] 310[c]	44 31
7	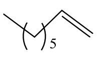	86[b] 95[c]	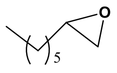	830[b] 20[c]	97 2

Conditions **Na[2]** (0.02 mM), substrate (20 mM), $Na_2S_2O_8$ (26 mM), 5 mL potassium carbonate solution at pH=7. Ratio 1:1000:1300: [a] 5 min of reaction [b] 15 min of reaction. [c] 30 min of reaction.

A comparison of the catalytic performance of **Na[2]** with (2,2’-bipyridine)ruthenium(II) ($[Ru(bpy)_3]^{2+}$) for alkene photooxidation is fully in favor of our compound, as $[Ru(bpy)_3]^{2+}$ shows very low or null efficiency, under the same conditions (**Table IV.22**).

Table IV.22. Comparative results of Photooxidation tests performed with **Na[2] or Na[1]** *vs* $[Ru(bpy)_3]^{2+}$complex.

Entry	**substrate**	**Conv.%**		**product**
		Na[2]	**$[Ru(bpy)_3]^{2+}$**	
1	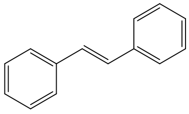	≥99[c]	10[c]	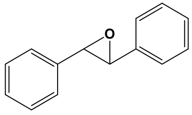
2	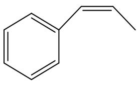	≥99[c]	3[c]	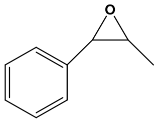
3	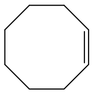	≥99[c]	0[c]	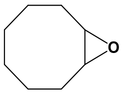
4	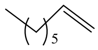	95[c]	0[c]	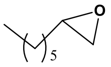

Conditions: **Na[2]** (0.02 mM), substrate (20 mM), $Na_2S_2O_8$ (26 mM), 5 mL potassium carbonate solution at pH=7. Ratio 1:1000:1300: [c] 30 min of reaction.

On the other hand, as we have observed earlier, the selectivity towards the formation of the epoxide in styrene, decreased after 15 min and benzaldehyde and benzoic acid increase, the same fact was observed for other substrates studied. As we discussed in the previous section, the opening of the epoxide ring occurs in aqueous medium. After a set of experiments, including blank experiments, we can assert that **[2]**$^-$ acts as photocatalyst also in the overoxidation of epoxides to diols, aldehydes or acids, in the reaction times that we have studied, because in the absence of catalyst the opening of the epoxide ring takes place a very small extent (**Table IV.23**).

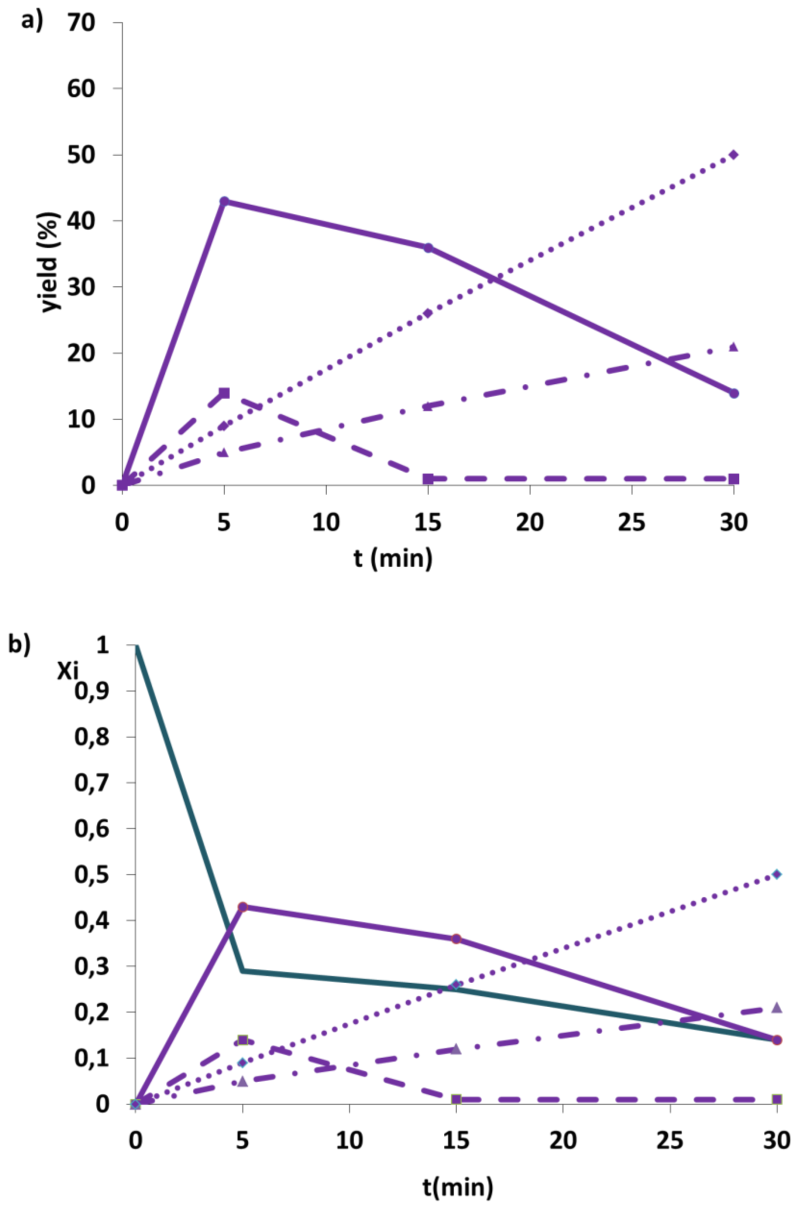

Figure IV.35. Plot of a) yield and b) molar fractions (Xi) *vs* time for the photoredox catalysis of styrene. Dark green line: styrene, line: styrene oxide, dashed line: 1-phenyl-1,2-ethanediol. Dash dotted line: benzaldehyde. Dotted line: benzoic acid. Conditions: Na[3,3'-Fe(1,2-$C_2B_9H_{11})_2$] (0.02 mM), styrene (20 mM), $Na_2S_2O_8$ (26 mM), 5 ml K_2CO_3 solution at pH=7, light irradiation (2.2 W, λ ~300 nm).

The use of 1,2-epoxyoctane (**entry 1**), as substrate allowed the obtention of octane-1,2-diol up to 15 minutes of reaction with selectivity >80 %, and after 30 minutes total conversion were obtained with the formation of octanal and octanoic acid. In the case of using styrene oxide (**entry 2**) as substrate, the obtention of 1-phenyl-1,2-ethanediol up to 15 minutes of reaction shows low selectivity (47 %), that decreases even more towards the production of benzaldehyde and benzoic acid, after 30 minutes of reaction. Finally, the photooxidation of *trans*-stilbene oxide (**entry 3**) led to the only formation of *meso*-hydrobenzoin compound.

Table IV.23. Photooxidation of epoxides performed with **Na[2]** complex. Conditions: **Na[2]** (0.02 mM), epoxide (20 mM), $Na_2S_2O_8$ (26 mM), 5 mL potassium carbonate solution at pH=7.

Entry	**substrate**	**Conv.%**	**Yield(select.)%**	**Conv.% Blank experiments*** **	
		Na[2]		**Experiment A**	**Experiment B**
1	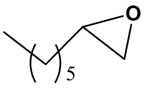	$90^{[a]}$ $\geq 99^{[b]}$	$75(83)^{[a]1}$ $\geq 99(\geq 99)^{[b]2}$	$0^{[a]}$ $0^{[b]}$	$5^{[a]}$ $11^{[b]}$
2	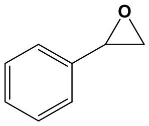	$85^{[a]}$ $\geq 99^{[b]}$	$40(47)^{[a]3}$ $75(75)^{[b]4}$	$4^{[a]}$ $13^{[b]}$	$7^{[a]}$ $10^{[b]}$
3	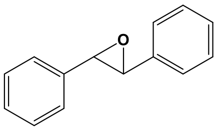	$\geq 99^{[a]}$ $\geq 99^{[b]}$	$\geq 99(\geq 99)^{[a]5}$ $\geq 99(\geq 99)^{[b]5}$	$0^{[a]}$ $0^{[b]}$	$0^{[a]}$ $0^{[b]}$

Ratio 1:1000:1300: [a]15 min of reaction [b]30 min of reaction. Yield and selectivity with respect the overall diol produced. [1] yield in octane-1,2-diol. [2] yield in octanal and octanoic acid, (30 and 70 % respectively). [3] yield in 1-phenylethane-1,2-diol. [4] yield in benzaldehyde and benzoic acid, (20 and 55 % respectively). [5] yield in *meso*-hydrobenzoin. *** Experiments: A: catalytic experiment with oxidant, without light irradiation and catalyst. B: catalytic experiment with oxidant and light irradiation and without catalyst.

IV.5.4.1. Photocatalytic oxidations reducing catalyst loads.

We have described in previous chapters that metallacarboranes as **[1]**$^-$ performs as a surfactant and at lower concentrations (10^{-3}-10^{-2} M) we assumed that free molecules were more efficient, in terms of catalytic activity, than vesicles or micelles. Hence, we wanted to know if this also occurred in the photooxidation of alkenes by **[2]**$^-$**.** Therefore, we reduced the photocatalytic load to 0.01 mol % vs the initial 0.1 mol % and we kept the concentrations of substrate and oxidizing agents constant (ratios of 1:10000:13000 of catalyst: substrate: oxidizing agent). **Table IV.24** displays the corresponding results, where we can observe total conversion values in most cases, after 15 min, with high TON values (TON=10000) for the photooxidation of *trans*-stylbene (**entry 3**) and cis-β-methylstyrene (**entry 4**), that to the best of our knowledge corresponds to one of the highest turnover numbers achieved in alkene photoredox oxidation in homogeneous conditions in short reaction times. Also, the selectivity for the corresponding epoxide is higher that the values observed with greater amount of catalyst. It is worth noting that in the case of cis- cis-β-methylstyrene the selectivity for the *cis*-epoxide is maintained, after 15 minutes (99% cis), it is even higher than that observed with larger amounts of catalyst.

IV.5.5. Comparative overview of photocatalytic oxidation of alkenes .Na[2] *vs* Na[1]

We wanted to establish a comparison of the behavior of ferrabis(dicarbollide) photocatalyst **Na[2]** *vs* the previously studied cobaltabis(dicarbollide) **Na[1]** in the photooxidation of alkenes. **Figures IV.36** and **Figure IV.37** display the evolution of the yields of styrene in their oxidation products and their molar fractions in function of time, for both photocatalysts. The reaction conditions were, catalyst (0.02 mM), alkene (20 mM) and $Na_2S_2O_8$ (26 mM) as oxidizing agent, in ratios 1:1000:1300. These figures show that after 5 minutes of reaction the amount of epoxide formed by both catalysts is higher that the formation of diol, benzaldehyde or acid, observing in **[2]**$^-$ greater amount of epoxide with respect to other over-oxidation products (43 % *vs* 14 % diol), however in **[1]**$^-$, although greater quantity of epoxide is obtained, an appreciable quantity of diol is also observed (37 % vs 23 % diol). After 15 min the main oxidation product formed by **[2]**$^-$ is the epoxide (36 %), but when **[1]**$^-$ is the photocatalyst the main product is the diol (35 %). This behavior is maintaining for the rest of substrates studied in **Table**

IV.25. In general, we can see that the photooxidation of substrates by **[2]**$^-$, display good selectivity values for the corresponding epoxides after 15 minutes of catalysis, being these values lower for **[1]**$^-$. The selectivity values decrease after 30 minutes since both compounds photocatalyze the opening epoxide ring and then others over-oxidation products are obtained.

Table IV.24. Photooxidation tests performed with **Na[2]** complex.

Entry	substrate	Conv. %	product	TON	Select .%
		Na[2]		Na[2]	Na[2]
1	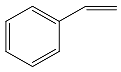	60[a] 75[b]	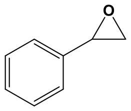	4200 [a] 2025 [b]	70 27
2	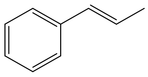	80[a] 88[b]	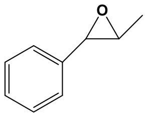	6000[a] 4100[b]	75 47
3	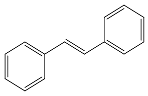	≥99[a] ≥99[b]	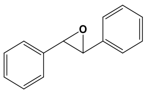	10000[a] 8200[b]	≥99 82
4	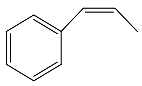	≥99[a] ≥99[b]	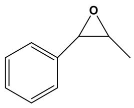	10000 (>99%,cis)[b] 10000 (88%,cis)[c]	≥99 ≥99
5	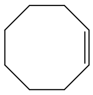	70[a] 85[b]	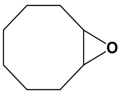	7000 [a] 8500 [b]	≥99 ≥99
6	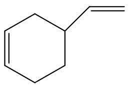	86[a] ≥99[b]	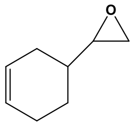	6700[a] 7700[b]	78 77
7	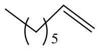	≥99[a] ≥99[b]	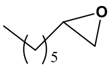	7100[a] 4600[b]	71 46

Conditions: **Na[2]** (0.002 mM), substrate (20 mM), $Na_2S_2O_8$ (26 mM), 5 mL potassium carbonate solution at pH=7. Ratio 1:10000:13000: [a] 15 min of reaction. [b] 30 min of reaction.

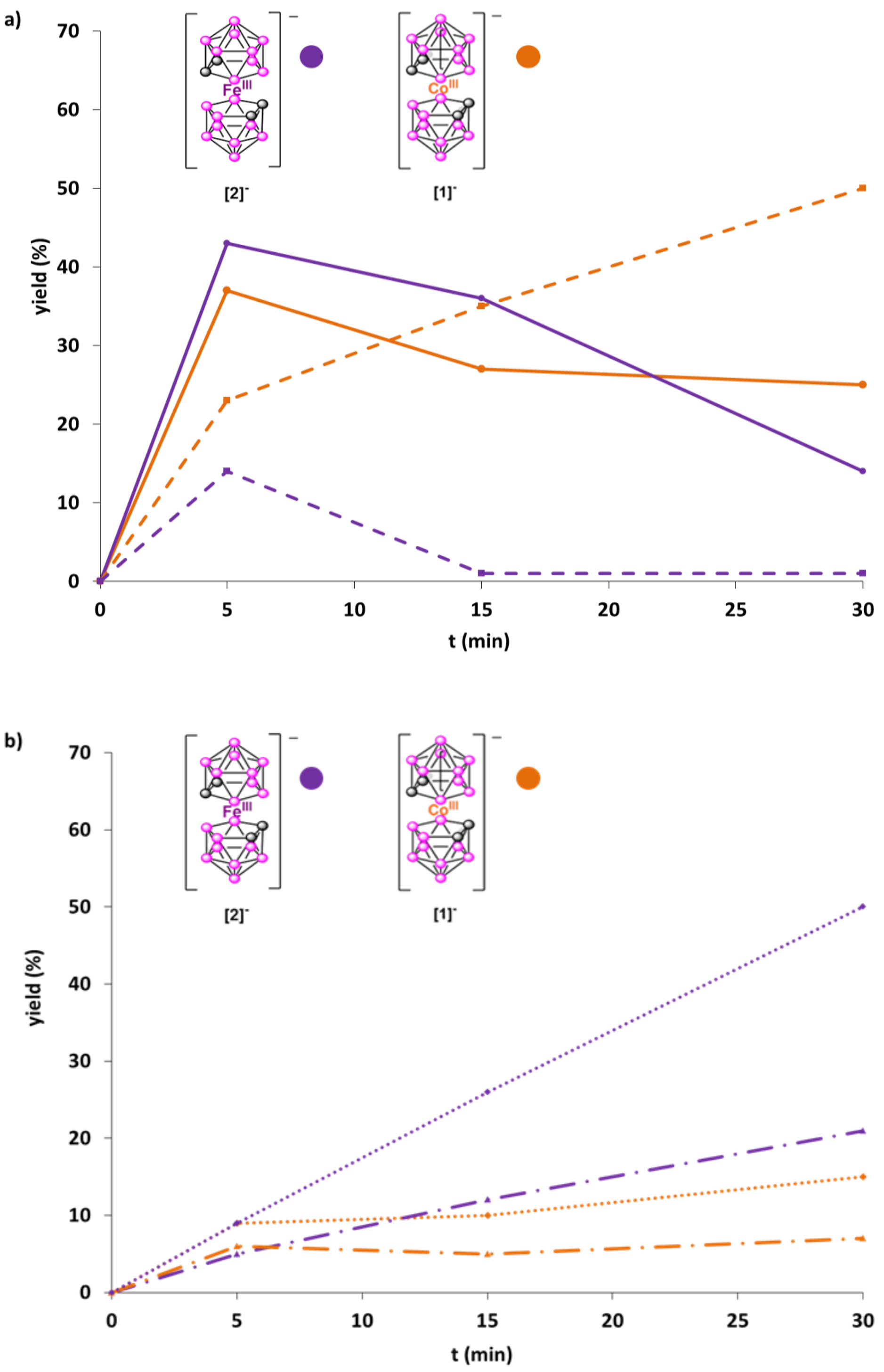

Figure IV.36. a) Plot of yield in styrene oxide and 1-phenylethanediol as a function of time for the photoredox catalysis of styrene. Line: styrene oxide, dashed line: 1-phenyl-1,2-ethanediol. b) Plot of yield in benzaldehyde and benzoic acid as a function of time for the photoredox catalysis of styrene. Dash dotted line: benzaldehyde; dotted line: benzoic acid. Conditions: Na[3,3'-Fe(1,2-$C_2B_9H_{11}$)$_2$] (purple) or Na[3,3'-Co(1,2-$C_2B_9H_{11}$)$_2$] (orange)(0.02 mM), styrene (20 mM), $Na_2S_2O_8$ (26 mM), 5 ml K_2CO_3 solution at pH=7, light irradiation (2.2 W, λ ~ 300 nm).

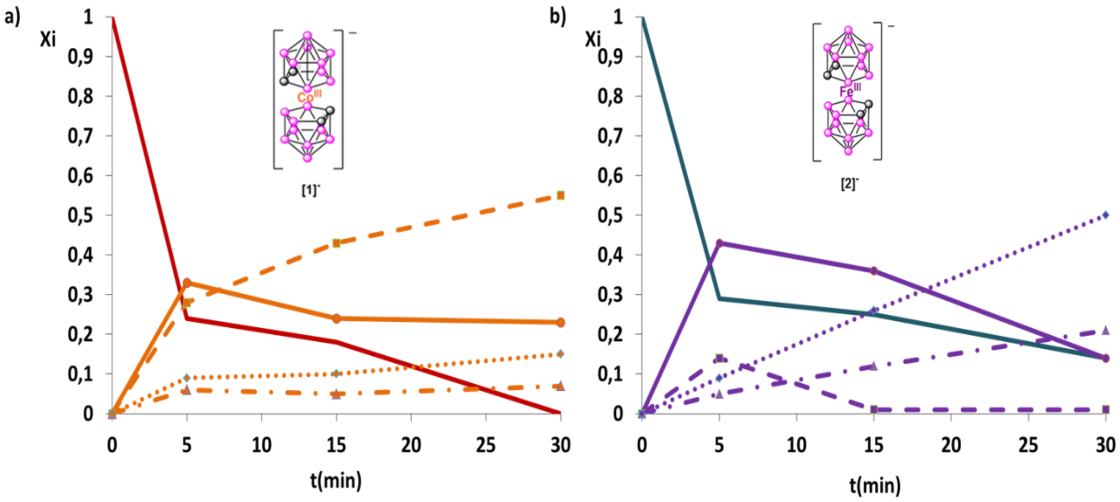

Figure IV.37. Plot of the molar fraction (Xi) versus time for the photoredox catalysis of styrene. a) Using **Na[1]** as catalyst. Vermilion line: styrene, orange line: styrene oxide, dashed line: 1-phenyl-1,2-ethanediol, dash dotted line: benzaldehyde, dotted line: benzoic acid. b) Using **Na[2]** as catalyst. dark green line: styrene, purple line: styrene oxide, dashed line: 1-phenyl-1,2-ethanediol, dash dotted line: benzaldehyde, dotted line: benzoic acid Conditions: Na[3,3'-Fe(1,2-$C_2B_9H_{11})_2$] (purple) or Na[3,3'-Co(1,2-$C_2B_9H_{11})_2$] (orange)(0.02 mM), styrene (20 mM), $Na_2S_2O_8$ (26 mM), 5 ml K_2CO_3 solution at pH=7, light irradiation (2.2 W, λ ~ 300 nm).

These results highlight the excellent performance displayed by ferrabis(dicarbollide) compound, obtaining high yields and selectivity values for the corresponding epoxides in relatively short reaction times.

Table IV.25. Comparative overview about photooxidation tests performed with **Na[1]** *vs* **Na[2]** complexes.

Entry	substrate	Conv.%		product	TON		Select. %	
		Na[1]	**Na[2]**		**Na[1]**	**Na[2]**	**Na[1]**	**Na[2]**
1	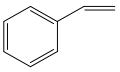	78[a] 80[b] 96[c]	66[a] 75[b] 86[c]	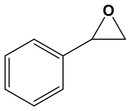	370[a] 270[b] 250[c]	430[a] 360[b] 140[c]	47 34 26	65 48 16
2	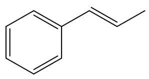	85[b] 91[c]	≥99[b] ≥99[c]	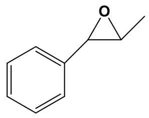	440[b] 200[c]	570[b] 440[c]	52 22	57 44
3	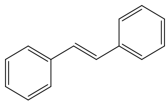	66[b] 95[c]	≥99[b] ≥99[c]	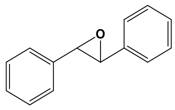	390[b] 290[c]	950[b] 900[c]	44 41	95 90
4	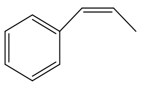	92[b] ≥99[c]	≥99[b] ≥99[c]	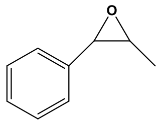	750 (97%,cis)[b] 330 (48%,cis)[c]	960 (92%,cis)[b] 780 (69%,cis)[c]	82 33	96 78
5	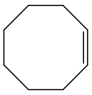	91[b] ≥99[c]	95[b] ≥99[c]	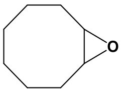	470[b] 380[c]	560[b] 90[c]	47 42	59 9
6	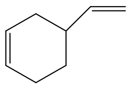	97[b] ≥99[c]	≥99[b] ≥99[c]	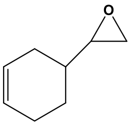	700[b] 370[c]	440[b] 310[c]	72 37	44 31
7	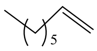	81[b] ≥99[c]	86[b] 95[c]	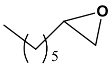	580[b] 160[c]	830[b] 20[c]	72 16	97 2

Conditions: **Na[1] or Na[2]** (0.02 mM), substrate (20 mM), $Na_2S_2O_8$ (26 mM), 5 mL potassium carbonate solution at pH=7. Ratio 1:1000:1300: [a] 5 min of reaction [b] 15 min of reaction. [c] 30 min of reaction.

In summary, we have studied the ferrabis(dicarbollide) compound, [3,3'-Fe(1,2-$C_2B_9H_{11})_2]^-$ **[2]**$^-$ as photocatalyst for the photooxidation of alcohols in water. As cobaltabis(dicarbollide) [3,3'-Co(1,2-$C_2B_9H_{11})_2]^-$ **[1]**$^-$, it acts as catalyst and photosensitizer through SET processes. The electrochemical behaviour indicates that Fe metallacarborane have less oxidizing power related to the couple $Fe^{4+/3+}$ compared with the $Co^{4+/3+}$ in **[1]**$^-$ (0.76 V and 1.22 V vs Fc, respectively).

We have highlighted the capacity of **[2]**$^-$ to perform as excellent photoredox catalyst in the oxidation of alcohols in water, achieving high yields, TON an selectivity values for most of the substrates studied, even when short reaction times of irradiation have been used (4h). These results show that the ferrabis(dicarbollide) acts as an efficient catalyst in the photooxidation of alcohols with results comparable to those obtained with cobaltabis*ortho*dicarbollide, in some cases greater for the former.

Furthermore, it has been also demonstrated that **Na[2]**, is an efficient photoredox catalyst for the epoxidation of alkenes in water, achieving high conversion and selectivity values for the corresponding epoxide after 15 minutes of reaction, even using low catalyst loads of 0.01 mol %. High TON have been obtained (TON=10000) for the photooxidation of *trans*-stilbene and cis-*β*-methylstyrene.

It is concluded that this behaviour is possible thanks to the properties of **Na[2]**, as their high solubility in water, its molecular compactness, their lack of photoluminescence, probably their surfactant behaviour in aqueous media and the high oxidizing power for the couple $Fe^{4+/3+}$ high enough to oxidize substrates, and at the same time to be able to obtain high selectivity values for the corresponding aldehydes, ketones or epoxides.This last characteristic make the difference with cobaltabis(dicarbollide) **Na[1]**, which displays lower selectivity values for the corresponding epoxides after 15 minutes of catalysis in comparison with the ferrabis(dicarbollide). We have also proven that **Na[2]**, acts as a photocatalyst/catalyst in both processes, in the epoxidation of alkenes and in the formation of over oxidation products, in aqueous medium.

Our results demonstrated that **Na[2]** is an efficient photocatalyst based in a green, cheap and abundant metal that operates in water in relatively short reaction times, moreover, we can assert that **Na[2]** could be a useful platform for the construction of highly efficient derivative systems for photoredox oxidation catalysis.

Chapter V. Conclusions

The most important conclusions arising from the present work are summarized below:

Regarding cobaltabisorthodicarbollide and derivatives

It has been demonstrated for the first time that cobaltabisdicarbollide, $[3,3'\text{-Co}(1,2\text{-}C_2B_9H_{11})_2]^-$, and its chloro derivatives, dichloro $[3,3'\text{-Co}(8\text{-Cl-}1,2\text{-}C_2B_9H_{10})_2]^-$ and hexachloro $[3,3'\text{-Co}(8,9,12\text{-}Cl_3\text{-}1,2\text{-}C_2B_9H_8)_2]^-$, are efficient tunable photoredox catalysts for the oxidation of alcohols in water, including aliphatic alcohols, through Single Electron Transfer processes. This behaviour has been possible thanks to the properties of metallacarboranes as their high solubility in water, their lack of photoluminescence, the easy modification of HOMO-LUMO gap, their high oxidizing power for the couple $Co^{4+/3+}$ and their colloidal behaviour in aqueous media.

Computational studies show that ligand-to-metal charge transfer (LMCT) takes place during the excitation at 293 nm, probably due to the difference in electronegativity among Co and B (-0.16) and evidence that a strong Co^{IV} oxidizing agent can be obtained by a photoinduced manner, which seems to be responsible of the good performance of the catalysts.

$[3,3'\text{-Co}(1,2\text{-}C_2B_9H_{11})_2]^-$ and derivatives showed high conversions and selectivity values in the photooxidation of alcohols, with yields near 90-95%, using catalysts load of 0.4 mol % (0.08 mM), in neutral media. Further the catalyst can be recovered easily by precipitation upon the addition of $[NMe_4]Cl$. A preliminary and promising result represents the high conversion value (98%) obtained in the photooxidation of diphenylmethanol by **[1]**$^-$ using an air stream as oxidizing agent. This fact can represent an input towards the development of practical processes with inorganic systems based in boron compounds.

The more striking fact was, that reducing the catalyst load to 0.01 mol % (0.002 mM), the high performance of **Na[1]** in the oxidation of alcohols is maintained, including aliphatic alcohols. High yields in the corresponding aldehyde or ketone have been achieved, > 99% in the case of 1-Phenylethanol, and diphenylmethanol, reaching TON= 10000. To the best of our knowledge this value is among the highest turnover number achieved in the alcohol photoredox oxidation performed in homogeneous conditions. These results highlight the interplay between water and catalyst due to the surfactant behaviour of the catalysts. Cobaltabisdicarbollide, and its chloro derivatives, in the form of free molecules are more efficient, in terms of photocatalytic activity, than vesicles or micelles.

These Metallacarboranes in the concentration range between 10^{-3} to 10^{-2} M coexist as molecules, micelles and vesicles; however at lower concentrations of metallacarborane the ratio of molecules is higher. A possible mechanism is also proposed.

We synthetized successfully a heterogeneous catalyst based in the anchored proton cobaltabis(dicarbollide), $H[3,3'\text{-}Co(1,2\text{-}C_2B_9H_{11})_2]$ onto magnetic nanoparticles (MNPs) coated with a silica layer, through no chemicals bindings. The non-bonding linkage between the “homogeneous catalyst” and the MNP was based on the well-established interaction between the θ shape metallabis(dicarbollide) $[\mathbf{1}]^-$ and ammine or ammonium functionalities. Thus the magnetite MNPs were first coated with SiO_2 to provide a certain degree of stability to the MNP and importantly enough silanol groups to be tethered to ammine carrying units. These were the MSNP-NH_2 on which was easily anchored, in water, the photoredox catalyst $H[3,3'\text{-}Co(1,2\text{-}C_2B_9H_{11})_2]$, H[**1**], to generate MSNP-NH_2@H[**1**]. Dedicated techniques have been utilized to study the morphology, characterization and colloidal stability of the MNPs produced. To optimize the MNP, the model was the homogeneous catalysis performance of H[**1**], on the oxidation of alcohols that did require about 8 h of reaction to achieve near 100% conversion. Thus the stability of the MNP was focused on this period of time. As the reaction does produce H^+, and pH tuning was advisable to reach high conversion the reaction was stopped at 4 h for pH adjusting, so the MNP were aimed at being in a stable colloidal form for a minimum of 4 h. Then, by sonication they were set back into a colloidal stable phase for an additional reaction period of 4 h. This was successful and catalyst loads of 0,1mol %, and 0,01 mol% were studied. The substrates studied did contain either aromatic or aliphatic groups. To the best of our knowledge, the ratios catalyst: substrate indicated are among the highest ever reported. We had the feeling, however, that the reaction could even take less time and that there still was the opportunity to lessen it if we prevented somehow aggregation. For this purpose several surfactant agents were studied in combination with the MNPs and their zeta-potentials were studied. Even though some did provide excellent colloid stability, they were in turn difficult to separate magnetically. We decided to use the cetyl trimethyl ammonium chloride (CTAC) that provided an adequate zeta-potential, thus adequate stability, without hampering a quick magnetic separation. The results with a 1:20 ratio of catalyst to surfactant proved our hypothesis and demonstrated that the reaction could be speeded up if aggregation was prevented. Again, however, one must balance if the reaction shortening in time compensates a more difficult working up.

It has been demonstrated that the water soluble cobaltabis(dicarbollide), **Na[1]**, is an efficient photoredox catalyst for the epoxidation of aromatic and aliphatic alkenes in water, requiring short reaction times (15-30 min), operating through single electron transfer processes (SET). This compound acts both as a catalyst and a photosensitizer. It is concluded that this behaviour is possible thanks to the properties of $Na[3,3'-Co(1,2-C_2B_9H_{11})_2]$, as their high solubility in water, its molecular compactness, the donor ability of the boron unit ligand, their lack of photoluminescence, the high oxidizing power for the couple $Co^{4+/3+}$ and their surfactant behaviour in aqueous media. These characteristics make the difference with the well-known and widely used photosensitizer tris (2,2′-bipyridine) ruthenium(II) ($[Ru(bpy)_3]^{2+}$), which also participates in electron transfer through an outer sphere mechanism. We have compared the $[Ru(bpy)_3]^{2+}$performance in the photo oxidation of alkenes in water following the procedures described earlier for $Na[3,3'-Co(1,2-C_2B_9H_{11})_2]$, and the comparative epoxidation tests have been strongly supportive of $Na[3,3'-Co(1,2-C_2B_9H_{11})_2]$, showing for $[Ru(bpy)_3]^{2+}$ a very low or null efficiency. The catalyst can be recovered easily by precipitation upon the addition of $[NMe_4]Cl$, and re-utilized. In general, under catalyst loads of 0,1 mol % high conversion values can be found with only 15 minutes of reaction, being in most of the cases the conversion total after 30 minutes. The major product after 15 minutes is the epoxide that gradually upon reaction with water converts into the dihydroxide. This reaction prevents a high throughput of the epoxide. This is in agreement with the increase in the amount of the corresponding diol for most of the substrates studied. We have also proven that $Na[3,3'-Co(1,2-C_2B_9H_{11})_2]$, acts as a photocatalyst/catalyst in both processes, in the epoxidation of alkenes and in their hydroxylation in aqueous medium. The question was whether the catalyst was faster for epoxidation than for hydroxylation. If this was the case it would enable the epoxide ratio to be improved in a short time reaction operation. And indeed it was so.

When $Na[3,3'-Co(1,2-C_2B_9H_{11})_2]$ was added in a very low ratio 0,01%, it was observed an extremely good performance for the epoxidation of alkenes in short times of reaction, with less ratio of the diol, proving our hypothesis.

Following these conditions, preliminary photooxidation tests using methyl oleate as substrate, have shown the selective epoxidation on the double bond C=C. This can represent a milestone towards the development of practical processes as the valorization of animal fat waste using $Na[3,3'-Co(1,2-C_2B_9H_{11})_2]$, as to promote circular economy.

Regarding Ruthenium- Cobaltabisorthodicarbollide Systems

A cooperative ion-photoredox system $[Ru^{II}(trpy)(bpy)(H_2O)][(3,3'-Co(1,2-C_2B_9H_{11})_2]_2$, **C4,** formed by cobaltabis(dicarbollide), $[(3,3'-Co(1,2-C_2B_9H_{11})_2]^-$ **$[1]^-$**, as photosensitizer, and the aqua ruthenium complex, $[Ru^{II}(trpy)(bpy)(H_2O)]^{2+}$ **C2'**, as oxidation catalyst, has been synthesized. Both are linked by non-covalent interactions that in large degree persist even after water dissolution. This represents a step forward in cooperative catalysis, avoiding expensive covalent bonds. **C4** has been easily synthesized by the reaction of the chloride Ru(II) complex, with **Ag[1]** in water/acetone (1:1) under reflux and the recrystallization of **C4** in acetonitrile yield $[Ru^{II}(trpy)(bpy)(CH_3CN)][(3,3'-Co(1,2-C_2B_9H_{11})_2]_2$, **C5** complex, in which the aqua ligand was substituted by CH_3CN, as shown in the X-ray diffraction.

The electrochemical studies evidence a significant electronic coupling between the two units in the non-covalent ion pair ruthenium-cobaltabis(dicarbollide) compound. The photogenerated Co^{IV} can easily oxidize $[Ru^{III}-OH]^{2+}$ to $[Ru^{IV}=O]^{2+}$ in water via Proto Coupled Electron Transfer (PCET) processes. This cooperative system performed as excellent cooperative photoredox catalyst in the oxidation of alcohols in water, under UV irradiation, using catalyst load of 0.005 mol% achieving high yields even when short reaction times of irradiation have been used. In some cases, a high turnover number (TON= 20000) has been observed.

The $Co^{IV/III}$ redox couple of **$[1]^-$** in water, differed by 170 mV when **$[1]^-$** had Na^+ as cation *versus* when the Ru complex was the cation. The catalytic results revealed that **C4** displays better performance that the mixtures based on **C2'** and **Na[1]**, proving that the non-covalent bonding existing in **C4** allows the electron-transfer between the photosensitizer and the catalyst and hence the efficiency of the cooperative system in the photo oxidation process. Cooperative catalytic systems with this kind of interactions have not been described before, and represent an advance in the cooperativity avoiding the expensive covalent bonds.

Regarding Ferrabis(dicarbollide)

The ferrabis(dicarbollide) compound, $[3,3'-Fe(1,2-C_2B_9H_{11})_2]^-$ **$[2]^-$,** has been studied as photocatalyst for the oxidation of alcohols and alkenes in water. This compound acts as catalyst and photosensitizer through SET processes. The electrochemical behaviour of the compound indicates less oxidizing power related to the couple $Fe^{4+/3+}$ compared with the couple $Co^{4+/3+}$ in **[1]**$^-$ (0.76 V and 1.22 V vs Fc, respectively).

We have highlighted the capacity of **[2]**$^-$ to perform as excellent photoredox catalyst in the oxidation of alcohols in water, achieving high yields, TON an selectivity values for most of the substrates studied, even when short reaction times of irradiation have been used (4h). These results show that the ferrabis(dicarbollide) acts as an efficient catalyst in the photooxidation of alcohols with results comparable to those obtained with cobaltabis*ortho*dicarbollide.

Furthermore, it has been also demonstrated that **Na[2]**, is an efficient photoredox catalyst for the epoxidation of alkenes in water, achieving high conversion and selectivity values for the corresponding epoxide after 15 minutes of reaction, even using low catalyst loads of 0.01 mol %. High TON have been obtained (TON=10000) for the photooxidation of *trans*-stilbene and cis-*β*-methylstyrene.

It is concluded that this behaviour is possible thanks to the properties of **Na[2]**, as their high solubility in water, its molecular compactness, their lack of photoluminescence, probably their surfactant behaviour in aqueous media and the high oxidizing power for the couple $Fe^{4+/3+}$ high enough to oxidize substrates, and at the same time to be able to obtain high selectivity values for the corresponding aldehydes, ketones or epoxides.This last characteristic make the difference with cobaltabis(dicarbollide) **Na[1]**, which displays lower selectivity values for the corresponding epoxides after 15 minutes of catalysis in comparison with the ferrabis(dicarbollide). We have also proven that **Na[2]**, acts as a photocatalyst/catalyst in both processes, in the epoxidation of alkenes and in the formation of over oxidation products, in aqueous medium.

Our results demonstrated that **Na[2]** is an efficient photocatalyst based in a green, cheap and abundant metal that operates in water in relatively short reaction times, moreover, we can assert that **Na[2]** could be a useful platform for the construction of highly efficient derivative systems for photoredox oxidation catalysis.

Chapter V

Chapter VI .References

---

[1] A. Stock, C. Massanez. *Chem. Ber.* **1912**, *45*, 3539.

[2] W. C. Price. *J. Chem. Phys.* **1947**, *15*, 614.

[3] H. C. Longuet-Higgin, R. P Bell. *J. Chem. Soc.* **1943**, 250.

[4] S. Hermanek. *Chem. Rev.* **1992**, *92*, 175-175.

[5] W. N. Lipscomb, *Science*, **1977**, *196*, 1047-1055.

[6] http://www.nobelprize.org/nobel_prizes/chemistry/laureates/1976/

[7] H. Brown. *Inc, New York*. **1975**.

[8] N. W. Lipscomb, Boron Hydrides, Benjamin, New York, **1963**.

[9] R. Hoffmann, W. N. Lipscomb. *J. Chem. Phys.* **1962**, *36*, 3489.

[10] Z. F. Chen, R. B. King. *Chem. Rev.* **2005**, *105*, 3613.

[11] a) J. Poater, M. Solà, C. Viñas, F. Teixidor. *Chem. Eur. J.* **2013**, 19, 4169-4175. b) J. Poater, M. Solà, C. Viñas and F. Teixidor. *Angew. Chemie. Int. Ed.* **2014**, *53*, 12191-12195.

[12] a) J. Poater, M. Solà, C. Viñas and F. Teixidor. *Chem. Eur. J.* **2016**, *22*, 7437-7443. b) J. Poater, C. Viñas, I. Bennour, S. Escayola, M. Solà and F. Teixidor. *J. Am. Chem. Soc*. *2020*, *142*(20), 9396-9407.

[13] H. C. Longuet-Higgins. *J. Chim. Phys.* **1949**, *46*, 268-275.

[14] N. Greenwood and A. Earnshaw. *Chemistry of the Elements 2nd Edition*, Butterworth-Heinemann, **1997**.

[15] W. N. Lipscomb. *Boron hydrides*, Courier Corporation, **2012**.

[16] J. Aihara. *J. Am. Chem. Soc*. **1978**, *100*, 3339-3342.

[17] V. Volkov and V. Ikorskii. *J. Struct. Chem*. **2004**, *45*, 694-705.

[18] R. King. *Russ. Chem. Bull.* **1993**, *42*, 1283-1291.

[19] R. B. King. *Chem. Rev*. **2001**, *101*, 1119-1152.

[20] R. N. Grimes. *Carboranes (Second Edition);* Academic Press: Oxford, **2011**.

[21] D. M. Schubert, D. M. *Boron Hydrides, Heteroboranes, and their Metalla Derivates*; John Wiley & Sons, Inc., **2002**.

[22] a) R. W. Rudolph. *Acc. Chem. Res*. **1976**, *9*, 446-452. b) K. Wade, *Advances in Inorganic Chemistry and Radiochemistry*, eds. H. J. Emeléus and A. G. Sharpe, Academic Press. **1976**, vol. 18, pp. 1-66. c) R. E. Williams. *Advances in Inorganic Chemistry and Radiochemistry*, **1976**, *18*, 67-142.

[23] a) D. Mingos. *Nature*. **1972**, *236*, 99-102. b) R. Rudolph and W. Pretzer. *Inorg. Chem*. **1972**, *11*, 1974-1978. c) R. E. Williams. *Inorg. Chem*. **1971**, *10*, 210-214.

[24] a) R. N. Grimes. *Ann. N. Y. Acad. Sci.* **1974**, *239*, 180; b) R. W. Rudolph. *Acc. Chem. Res.* **1976**, *9*, 446. c) R. E. Williams. *Inorg. Chem.* **1971**, *10*, 210-214. d) K. Wade. *Adv. Inorg. Radiochem.* **1976**, *18*, 1. e) D. M. P. Mingos, *Nature, Phy. Sci.* **1972**, *236*, 99. f) R. W. Rudolph, W. R. Pretzer. *Inorg. Chem.* **1972**, *11*, 1974. g) K. Wade. *Chem. Commun.* **1971**, 792.

[25] a) R. N. Grimes. *Angew. Chem*. Int. Ed. **1993**, *32*, 1289. b) J. Plesek. *Chem. Rev.* **1992**, *92*, 269. c) W. H. Eberhardt, J. Crawford, W. N. Lipscomb. *Chem. Phys.* **1954**, *22*, 98.

[26] a) F. Teixidor, G. Barberà, A. Vaca, R. Kivekäs, R. Sillanpää, J. Oliva, C. Viñas, *J. Am. Chem.Soc*. **2005**, *127*, 10158. b) R. B. King. *Chem. Rev.* **2001**, *101*, 1119.

[27] M. M. Fein, J. Bobinski, N. Mayes, N. Schwartz and M. S. Cohen. *Inorg. Chem*. **1963**, *2*, 1111-1115.

[28] T. Heying, J. Ager Jr, S. Clark, D. Mangold, H. Goldstein, M. Hillman, R. Polak and J. Szymanski. *Inorg. Chem.* **1963**, *2*, 1089-1092.

[29] a) H. Kimura, K. Okita, M. Ichitani, T. Sugimoto, S. Kuroki, I. Ando. *Chem. Mater.* **2003**, *15*, 355. b) M. K. Kolel-Veetil, T. M. Keller. *J. Polym. Sci. A*. **2006**, *44*, 147. c) A. González-Campo, B. Boury, F. Teixidor, R. Núñez. *Chem. Mater.* **2006**, *18*, 4344. d) E. Hao, B. Fabre, F. R. Fronczek, M. G. H. Vicente. *Chem. Mater.* **2007**, *19*, 6195. e) O. K. Farha, A. M. Spokoyny, K. L. Mulfort, M. F. Hawthorne, C. A. Mirkin, J. T. J. Hupp. *J. Am. Chem. Soc.* **2007**, *129*, 12680.

[30] R. N. Grimes. *Carboranes*, Academic Press, New York, **1970**, 54.

[31] M. F. Hawthorne. *Advances in Boron Chemistry*. The Royal Society of Chemistry, Cornwall, U.K, **1997**.

[32] D. Gtafstein, J. Bobisnski, J. Dvorak, H. Smith, N. Schwartz, M. S. Cohen, M.M. Fein. *Inorg. Chem*. **1963**, *2*, 1120.

[33] V. I. Bregadze. *Chem. Rev.* **1922**, *92*, 209.

[34] F. Teixidor, R. Núñez, C. Viñas, R. Sillanpää, R. Kivekäs. *Angew. Chem*. **2000**, *112*, 4460.

[35] R. Núñez, P. Farràs, F. Teixidor, C. Viñas, R. Sillanpää, R. Kivekäs. *Angew. Chem. Int. Ed*. **2006**, *45*, 1270.

[36] a) H. Schroeder, T. L. Heying, J. L. Reiner. *Inorg. Chem.* **1963**, *2*, 1092. b) J. F. Sieckhaus, N. S. Semenuk, T. A. Knowles, H. Schroeder. *Inorg. Chem.* **1969**, *8*, 2452.

[37] a) C. Viñas, G. Barberà, J. Oliva, F. Teixidor, A. J. Welch, G. M. Rosair. *Inorg. Chem.* **2001**, *40*, 26 . b) C. Viñas, G. Barberà, F. Teixidor. *J. Organom. Chem.* **2002**, *642*, 16. c) G. Barberà, C. Viñas, F. Teixidor, G. M. Rosair, A. J. Welch. *J. Chem. Soc. Dalton Trans.* **2002**, 3647.

[38] R. N. Grimes. *Coord. Chem. Rev.* **2000**, *200*, 773-811.

[39] N. Hosmane and J. Maguire. *Comprehensive Organometallic Chemistry III*. **2007**, *3*, 175-264.

[40] M. F. Hawthorne, D. C. Young and P. A. Wegner. *J. Am. Chem. Soc*. **1965**, *87*, 1818-1819.

[41] I. Bennour, A. M. Cioran, F. Teixidor and C. Viñas. *Green Chemistry*. **2019**, *21*, 1925.

[42] M. F. Hawthorne and T. D. Andrews. *Chem. Commun.* **1965**, 443-444.

[43] a) R. N. Grimes. *Carboranes*, 3rd ed., Elsevier, **2016**. b) C. Masalles, S. Borrós, C. Viñas, F. Teixidor. *Adv. Mater*. **2002**, *14*, 826–829.

.

[44] C. Masalles, S. Borrós, C. Viñas and F. Teixidor. *Adv. Mater.* **2000**, *12*, 1199-1202.

[45] C. Masalles, J. Llop, C. Vinas and F. Teixidor. *Adv. Mater.* **2002**, *14*, 826.

[46] J. Buchanan, E. J. M. Hamilton, D. Reed, A. J. Welch. *Dalton Trans*. **1990**, 677.

[47] M. F. Hawthorne, D. C. Young, T. D. Andrews, D. V. Howe, R. L. Pilling, A. D. Pitts, M. Reintjes, L. F. Warren Jr and P. A. Wegner. *J. Am. Chem. Soc*. **1968**, *90*, 879-896.

[48] D. Olid, R. Núñez, C. Viñas and F. Teixidor. *Chem. Soc. Rev.* **2013**, *42*, 3318-3336.

[49] P. Farràs, E. J. Juárez-Pérez, M. Lepsik, F. Luque, R. Núñez, F. Teixidor. *Chem*. *Soc*. *Rev*. **2012**, *41*, 3445.

[50] J. Rak, B. Dejlová, H. Lampová, R. Kaplánek, P. Matějíček, P. Cígler and V. Král. *Mol. Pharm.* **2013**, *10*, 1751-1759.

[51] P. Matějíček, P. Cígler, K. Procházka and V. Král. *Langmuir*. **2006**, *22*, 575-581.

[52] I. B. Sivaev and V. V. Bregadze. *Eur. J. Inorg. Chem.* **2009**, 1433-1450.

[53] D. Olid, R. Núñez, C. Viñas, F. Teixidor. *Chem. Soc. Rev*. **2013**, *42*, 3318 –3336.

[54] H. Li, F. Li, B. Zhang, X. Zhou, F. Yu, L. Sun. *J. Am. Chem. Soc*. **2015**, *137*, 4332–4335.

[55] R. Núñez, M. Tarrés, A. Ferrer-Ugalde, F. Fabrizi de Biani, F. Teixidor. *Chem. Rev*. **2016**, *116*, 14307–14378.

[56] J. G. Planas, F. Teixidor, C. Viñas, M. E. Light and M. B. Hursthouse. *Chem. Eur. J.* **2007**, *13*, 2493-2502.

---

[57] C. Masalles, S. Borrós, C. Viñas, F. Teixidor. *Adv. Mater*. **2002**, *14*, 826–829.

[58] a) M. J. Hardie, C. L. Raston. *Chem. Commun*. **2001**, *26*, 905–906. b) M. A. Fox, A. K. Huges. *Coord. Chem. Rev.* **2004**, *248*, 457–476. c) D. Brusselle, P. Bauduin, L. Girard, A. Zaulet, C. Viñas, F. Teixidor, I. Ly, O. Diat. *Angew. Chem. Int. Ed*. **2013**, *52*, 12114–12118; *Angew. Chem.* **2013**, *125*, 12336–12340.

[59] M. Tarrés, C. Viñas, P. Gonzalez-Cardoso, M. M. Hänninen, R. Sillanpää, V. Dordovic, M. Uchman, F. Teixidor, P. Matejicek. *Chem. Eur. J.* **2014**, *20*, 6786–6794.

[60] a) P. Bauduin, S. Prevost, P. Farras, F. Teixidor, O. Diat, T. Zemb. *Angew. Chem. Int. Ed.* **2011**, *50*, 5298–5300; *Angew. Chem*. **2011**, *123*, 5410 – 5412. b) C. Viñas, M. Tarres, P. Gonzalez-Cardoso, P. Farras, P. Bauduin, F. Teixidor. *Dalton Trans*. **2014**, *43*, 5062–5068. c) V. Dordovic, Z. Tosner, M. Uchman, A. Zhigunov, M. Reza, J. Ruokolainen, G. Pramanik, P. Cígler, K. Kalíková, M. Gradzielski, P. Matejicek. *Langmuir* **2016**, *32*, 6713–6722. d) M. Uchman, V. Dordovic, Z. Tosner, P. Matejicek. *Angew. Chem. Int. Ed*. **2015**, *54*, 14113–14117; *Angew. Chem*. **2015**, **127**, 14319–14323.

[61] D. Olid, R. Núñez, C. Viñas, F. Teixidor. *Chem. Soc. Rev*. **2013**, *42*, 3318 –3336.

[62] I. B. Sivaev, V. I. Bregadze, *Collect*. *Czech*. *Chem*. *Commun*. **1999**, *64*, 783.

[63] D. Olid, R. Núñez, C. Viñas, F. Teixidor, *Chem*. *Soc*. *Rev*. **2013**, *42*, 3318.

[64] Ozin, G. Arsenault. A. *Nanochemistry – A Chemical Approach to Nanomaterials*; The Royal Society of Chemistry: Cambridge, **2005**.

[65] M. Uchman, V. Ďorďovič, Z. Tošner, P. Matějíček. *Angew. Chem. Int. Ed.* **2015**, *54*, 14113–14117.

[66] M. Corsini, F. Fabrizi de Biani, P. Zanello. *Coord*. *Chem*. *Rev*. **2006**, *250*, 1351.

[67] F. Teixidor, C. Viñas. *Pure Appl*. *Chem*. **2012**, *84*, 2457.

[68] a) P. Farràs, C. Viñas and F. Teixidor. *J. Organomet. Chem.* **2013**, *747*, 119-125. b) A. N. Gashti, J. C. Huffman, A. Edwards, G. Szekeley, A. R. Siedle, J. A. Karty, J. P. Reilly and L. J. Todd. *J. Organomet. Chem*. **2000**, *614*, 120-124. c) P. K. Hurlburt, R. L. Miller, K. D. Abney, T. M. Foreman, R. J. Butcher and S. A. Kinkhead*.* *Inorg. Chem*. **1995**, *34*, 5215-5219.

[69] P. Farràs, C. Viñas and F. Teixidor. *J. Organomet. Chem.* **2013**, *747*, 119-125.

[70] R. Núñez, M. Tarrés, A. Ferrer-Ugalde, F. F. de Biani and F. Teixidor. *Chem. Rev.* **2016**, *116*, 14307-14378.

---

[71] a) L. I. Zakharkin, V. A. Olshevskaya, E. V. Balagurova, P. V. Petrovskii. *Russ*. *J*. *Gen*. *Chem*., **2000**, *70*, 550. b) O. N. Kazheva, G. G. Aleksandrov, A. V. Kravchenko, V. A. Starodub, G. G. Zhigareva, I. B. Sivaev, V. I. Bregadze, L. I. Buravov, L. V. Titov, O. A. Dyachenko. *Russ*. *Chem*. *Bull*. **2010**, *59*, 1137. c) P. Hurlburt, R. Miller, K. Abney, T. Foreman, R. Butcher, S. Kinkead. *Inorg*. *Chem*. **1995**, *34*, 5215. d) L. Mátel, F. Macášek, P. Rajec, S. Heřmánek, J. Plešek. *Polyhedron*, **1982**, *1*, 511. e) P. Selucký, H. Baše, J. Plešek, S. Heřmánek, J. Rais, J. Czech. Patent 215 282, *Chem*. *Abstr*. **1986**, *104*, 186637g. f) J. Rais, P. Selucký, M. Kyrs. *J*. *Inorg*. *Nucl*. *Chem*. **1976**, *38*, 1376. g) O. N. Kazheva, G. G. Alexandrov, A. V. Kravchenko, V. A. Starodub, I. A. Lobanova, I. B. Sivaev, V. I. Bregadze, L. V. Titov, L. I. Buravov, O. A. Dyachenko. *J*. *Organomet*. *Chem*. **2009**, *694*, 2336.

[72] A. Pepiol, F. Teixidor, R. Sillanpää, M. Lupu, C. Viñas. *Angew*. *Chem*. *Int*. *Ed*. **2011**, *50*(52), 12491.

[73] a) P. E. Behnken, D. C. Busby, M. S. Delaney, R. E. King III, C. W. Kreimendahl, T. B. Marder, J. J. Wilczynski, M. F. Hawthorne. *J. Am. Chem. Soc*. **1984**, *106*, 7444–7450 and references therein. b) H. Shen, Z. Xie, Boron Science New Technologies and Applications, chapter 21 (Ed.: N. S. Hosmane), CRC, Boca Raton, **2012**, pp. 517–528. c) S. Bauer, E. Hey-Hawkins, Boron Science New Technologies and Applications, chapter 22 (Ed.: N. S. Hosmane), CRC, Boca Raton, 2012, pp. 529–579. d) Handbook of Boron Chemistry in Organometallics Catalysis, Materials and Medicine, Vol. 2, Boron in Catalysis (Eds.: N. S. Hosmane, R. Eagling), World Science Publishers, New Jersey **2018**. e) Z. W. Xie. *Coord. Chem. Rev.* **2006**, *250*, 259–272. f) H. Ying-Feng, J. Guo-Xin. *Acc. Chem. Res.* **2014**, *47*, 3571–3579. g) S. P. Fisher, A. W. Tomich, S. O. Lovera, J. F. Kleinsasser, J. Guo, M. J. Asay, H. M. Nelson, V. Lavallo. *Chem. Rev.* **2019**, *119*, 8262–8290. h) F. Teixidor, M. A. Flores, C. Viñas, R. Kivekäs, R. Sillanpää. *J. Am. Chem. Soc.* **2000**, *122*, 1963–1973. i) A. R. Popescu, F. Teixidor, C. Viñas. *Coord. Chem. Rev*. **2014**, *269*, 54–84.

[74] P. Qu, D. W. Thompson, G. J. Meyer. *Langmuir.* **2000**, *16*, 4662.

[75] a) T. J. Meyer, M. H. V. Huynh. *Inorg. Chem*. **2003**, *42*, 8140. b) W. K. Seok, T. J. Meyer. *Inorg. Chem*. **2005**, *44*, 3931. c) J. C. Goeltz, C. J. Hanson, C. P. Kubiak. *Inorg. Chem*. **2009**, *48*, 4763.

[76] S. V. Ley, J. Norman, W. P. Griffith, S. P. Marsden. *Synthesis.* **1994**, *7*, 639.

[77] a) F. Ding, Y.-G. Sun, F. Verpoort, V. Dragutan, I. Dragutan. *J. Mol. Cat. A-Chem.* **2014**, *386*, 86. b) K.-H. Chan, X. Guan, V. K.-Y. Lo, C.-M. Che. *Angew. Chem. Int. Ed.* **2014**, *53*, 2982.

[78] a) R. Hemelaere, F. Caijo, M. Mauduit, F. Carreaux, B. Carboni. *Eur. J. Org. Chem.* **2014**, 3328. b) E. Ascic, R. G. Ohm, R. Petersen, M. R. Hansen, C. L. Hansen, D. Madsen, D. Tanner, T. E. Nielsen. *Chem. Eur. J.* **2014**, *20*, 3297.

[79] A. D. Bokare, W. Choi. *J. Haz. Mat.* **2014**, *275*, 121.

[80] a) M. Pagliaro, S. Campestrini, R. Ciriminna. *Chem. Soc. Rev.* **2005**, *34*, 837. b) B. Bagh, A. M. McKinty, A. J. Lough, D. W. Stephan. *Dalton Trans.* **2014**, *43*, 12842. c) J. Aguiló, L. Francàs, H. J. Hiu, R. Bofill, J. Garcia-Anton, J. Benet-Buchholz, A. Llobet, L. Escriche, X. Sala. *Cat. Sci. Tech.* **2014**, *4*, 190.

[81] M. A. Fernandez-Zumel, G. Kiefer, K. Thommes, R. Scopelliti, K. Severin, K. *Eur. J. Inorg. Chem.* **2010**, 3596.

[82] a) N. Siffert, M. Bühl, M. *J. Am. Chem. Soc.* **2010**, *132*, 8056. b) S. Duman, S. Özkar. S. *Int. J. Hyd. Ener.* **2013**, *38*, 180.

[83] a) M. Aydemir, A. Baysal, A. *J. Organomet. Chem.* **2010**, *695*, 2506. b) P. Anitha, R. Manikandan, A. Endo, T. Hashimoto, P. Viswanathamurthi. *Spect. Acta Part A: Mol. Biomol. Spect.* **2012**, *99*, 174. c) L. Zeng, F. Wu, Y.-Y. Li, Z.-R. Dong, J.-X. Gao *J. Organomet. Chem.* **2014,** *762*, 34. d) F. Ok, M. Aydemir, F. Durap, A. Baysal. *Appl. Organomet. Chem.* **2014**, *28*, 38.

[84] a) S. Mandal, S. Samanta, T. K. Mondal, S. Goswami. *Organometallics.* **2012**, *31*, 5282. b) M. C. Reddy, M. Jeganmohan . *Org. Lett.* **2014**, *16*, 4866.

[85] a) S. L. Mangold, D. J. O'Leary, R. H. Grubbs. *J. Am. Chem. Soc.* **2014**, *136*, 12469. b) J. Hartung, P. K. Dornan, R. H. Grubbs. *J. Am. Chem. Soc.* **2014**, *136*, 13029. c) A. Antonucci, M. Bassetti, C. Bruneau, P. H. Dixneuf, C. Pasquini. *Organometallics.* **2010**, *29*, 4524.

[86] a) J. G. Vos, J. M. Kelly. *Dalton Trans*. **2006**, *41*, 4869. b) S. Zhang, Y. Ding, H. Wei. *Molecules.* **2014**, *19*, 11933.

[87] a) P. H. Xie, Y.-J. Hou, T.-X. Wei, B.-W. Zang, Y. Cao, C. H. Huang. *Inorg. Chim. Acta.* **2000**, *308*, 73. b) C. Chen, N. Pootrakulchote,S. Wu, M. Wang, J. Li, J. Tsai, C. Wu, S. M. Zakeeruddin, M. Grätzel. *J. Phys. Chem. C*. **2009**, *113*, 20752. c) P. Sirimanne, B. Winther-Jensen, H. Weerasinghe, Y. Cheng. *Thin Solid Films.* **2010**, *518*, 2871. d) J.-F. Yin, M. Velayudham, D. Bhattacharya, H.-C. Lin, K.-L. Lu. *Coord. Chem. Rev*. **2012**, *256*, 3008. e) S. A. Kurzeev, A. V. Medved'ko, V. A. Grinberg, S. A. Kozyukhin, V. V. Emets, A. A. Sadovnikav, A. E. Baranchikov, V. K. Ivanov, V. N. Andreev, E. A. Nizhnikovskii. *J. Rus. Inorg. Chem*. **2014**, *59*, 658.

[88] a) F. Barigelletti, L. Flamigni. *Chem. Soc. Rev*. **2000**, *29*, 1. b) P. Belser, L. De Cola, F. Hartl, V. Adamo, B. Bozic, Y. Chriqui, V. M. Iyer, R. T. F. Jukes, J. Kühni, M. Querol, S. Roma, N. Salluce. *Adv. Funct. Mater*. **2006**, *16*, 195. c) L. Mishra, A. K. Yadaw, G. Govil. *Indian J. Chem. Sect. A: Inorg. Bioinorg. Phys. Theor. Anal. Chem*. **2003**, *42A*, 1797. d) G. R. Newkome, T. J.

Cho, C. N. Moorefield, P. P. Mohapatra, L. A. Godínez. *Chem. Eur. J.* **2004**, *10*, 1493.

[89] C. Costentin, M. Robert, J.-M. Saveant. *Chem. Rev.* **2010**, *110*, PR1-PR40.

[90] D. S. Eggleston, K. A. Goldsby, D. J. Hodgson, T. J. Meyer. *Inorg. Chem.* **1985**, *24*, 4573.

[91] a) B. A. Moyer, T. J. Meyer. *J. Am. Chem. Soc.* **1978**, *100*, 3601. b) B. A. Moyer, T. J. Meyer. *Inorg. Chem.* **1981**, *20*, 436. c) R. A. Binstead, B. A. Moyer, G. J. Samuels, T. J. Meyer. *J. Am. Chem. Soc.* **1981**, *103*, 2897.

[92] a) K. J. Takeuchi, M. S. Thompson, D. W. Pipes, T. J. Meyer. *Inorg. Chem.* **1984**, *23*, 1845. b) L. Roecker, W. Kutner, J. A. Gilbert, M. Simmons, R. W. Murray, T. Meyer. *Inorg. Chem.* **1985**, *24*, 3784. c) H. F. Suen, S. W. Wilson, M. Pomerantz, J. K. Walsh. *Inorg. Chem.* **1989**, *28*, 786. d) A. Llobet. *Inorg. Chim. Acta.* **1994**, *221*, 125.

[93] A. Dovletoglou, S. A. Adeyemi, T. J. Meyer. *Inorg. Chem*. **1996**, *35*, 4120.

[94] T. J. Meyer. *J. Electrochem. Soc.* **1984**, *131*, 221C.

[95] F. R. Keene. *Coord. Chem. Rev.* **1999**, *187*, 121.

[96] R. A. Binstead, M. E. McGuire, A. Dovletoglou, W. K. Seok, L. E. Roecker, T. J. Meyer. *J. Am. Chem. Soc.* **1992**, *114*, 173.

[97] M. K. Tse, M. Klawonn, S. Bhor, C. Döbler, G. Anilkumar, H. Hugo, H. Mägerlein, M. Beller. Org. Lett. **2005**, *7*, 987.

[98] I. Ferrer. (2015). *Development of new reusable materials based on Ru complexes with catalytic activity for olefin epoxidation and nitrile hydration.* [Doctoral thesis. Universitat de Girona]. http://hdl.handle.net/10803/322785.

[99] a) J. Gladysz. *Chem. Rev.* **2002**, *102*(10), 3215-3216. b) A. T. Bell. *Science.* **2003**, *299*(5613), 1688-1691. c) R. Schlögl, S. B. Abd Hamid. *Angew. Chem. Int. Ed.* **2004**, *116*(13), 1656-1667. d) J. M. Thomas, W. J. Thomas. *Principles and practice of heterogeneous catalysis* (2n ed.). Wiley-VCH: Weinheim (Germany), **2015**.

[100] a) F. Cozzi. *Adv. Synth. Catal*. **2006**, *348*(12-13), 1367-1390. b) B. M. L. Dioos, I. F. J. Vankelecom, P. A. Jacobs. *Adv. Synth. Catal.* **2006**, *348*(12-13), 1413-1446. c) J. Lu, P. H. Toy. *Chem. Rev.* **2009**, *109*(2), 815-838.

[101] a) R. A. Sheldon, H. van Bekkum. *Fine Chemicals through Heterogeneous Catalysis.* Wiley-VCH: Weinheim (Germany), **2001**. b) R. A. Sheldon. *Chem. Commun.* **2008**, *29*, 3352-3365.

[102] V. Meille. *Appl. Catal. A-Gen.* **2006**, *315*, 1-17. b) M. Campanati, G. Fornasari, A. Vaccari. *Catal. Today.* **2003**, *77*(4), 299-314.

[103] a) P. McMorn, G. Hutchings. *J. Chem. Soc. Rev.* **2004**, *33*(2), 108-122. b) J. M. Thomas, R. Raja, D. W. Lewis. *Angew. Chem. Int. Ed.* **2005**, *44*(40), 6456-6482. c) V. Dal Santo, F. Liguori, C. Pirovano, M. Guidotti. *Molecules.* **2010**, *15*(6), 3829-3856.

[104] a) R. K. Sharma, S. Dutta, S. Sharma, R. Zboril, R. S. Varma, M. B. Gawande, M. B. *Green. Chem*. **2016**, *18*, 3184−3209. b) D. Wang, D. Astruc. *Chem. Rev.* **2014**, *114*, 6949−6985. c) Q. Zhang, X. Yang, J. Guan.. *ACS Appl. Nano Mater*. **2019**, *2*, 4681−4697. d) M. B. Gawande, P. S. Branco, R. S. Varma. *Chem. Soc. Rev.* **2013**, *42*, 3371−3393.

[105] C. C. Gheorghiu, C. Salinas-Martínez de Lecea, C. M. Román-Martínez. *Ap. Cat. A: Gen.* **2014**, *478*, 194-203.

[106] P. Barbaro, F. Liguori. *Chem. Rev*. **2009**, *109*(2), 515-529. b) K. H. Shaughnessy. *Chem. Rev.***2009**, *109*(2), 643-710.

[107] a) R. F. Parton, I. F. J. Vankelecom, M. J. A. Casselman, C. P. Bezaukhanova, J. B. Uytterhoeven, P. A. Jacobs. *Nature.* **1994**, *370*, 541-544. b) P.-P. Knops-Gerrits, D. de Vos, F. Thibault-Starzyk, P. A. Jacobs. *Nature.* **1994**, *369*, 543-546. c) K. Mori, K. Kagohara, H. Yamashite. *J. Phys. Chem*. *C.* **2008**, *112*(7), 2593-2600. d) C. –H. Le, H. –C. Lin, S. –H. Cheng, T. –S. Lin, C. –Y. Mou. *J. Phys. Chem. C.* **2009**, *113*(36), 16058-16069.

[108] J. Dupont, R. F. de Souza, P. A. Suarez. *Chem. Rev.* **2002**, 102(*10*), 3667-3692. b) M. Freemantle. *Chem. Eng. News.* **2001**, *79*(1), 21-25.

[109] a) P. H. Mutin, G. Guerrero, A. Vioux. *J. Mater. Chem.* **2005**, *15*(35-36), 3761-3768. b) S. M. Ribeiro, A. C. Serra, A. G. Rocha.. *Tetrahedron.* **2007**, *63*(33), 7885-7981. c) R. Sayah, E. Framery, V. Dufaud. *Green Chem*. **2009**, 11(10), 1694-1702. d) A. Stamatis, D. Giasafaki, K. C. Christoforidis, Y. Deligiannakis, M. Louloudi. *J. Mol. Catal. A: Chem*. **2010**, *319*(1-2), 58-65.

[110] J. Kreuter, *Int. J. Pharm.* **2007,** *331*, 1.

[111] a) Z. Wang, P. Xiao, N. Shen, B. He. *Colloids Surf. A Physicochem. Eng. Asp.* **2006**, *276*(1-3), 116-121. b) A. Shätz, M. Hager, O. Reiser. *Adv. Funct. Mater*. **2009**, *19*(13), 2109-2115. c) G. Schmid. *Nanoparticles: From Theory to Application*. Wiley-VCH: Weihem (Germany), **2010**. d) C. W. Lim, I. S. Lee. *Nano Today.* **2010**, *5*(5), 412-434. e) V. PolshettiwarR. S. Varma. R*Green Chem*. **2010**, *12*(5), 743-754. f) F. Zhang, J. Jin, X. Zhong, S. Li, J. Niu, R. Li, J. Ma. *Green Chem.* **2011**, *13*(5), 1238-1242. g) V. Polshettiwa, R. Luque, A. Fihri, H. Zhu, M. Bouhrara, J. M. Basset. *Chem. Rev.* **2011**, *111*(5), 3036-3075. h) J. Deng, L. P. Mo, F. Y. Zhao, L. L. Hou, L. Yang, Z. H. Zhang. *Green Chem*. **2011**,*13*(9), 2576-2584. i) J. Mondai, T. Sen, A. Bhaumik. *Dalton Trans*. **2012**, *41*(20), 6173-6181. j) Y. H. Liu, J. Deng, J. W. Gao, Z. H. Zhang. *Adv. Synth. Catal.* **2012**, *354*(2-3), 441-447;. k) P. H. Li, B. L. Li, Z. M. An, L. P. Mo, Z. S. Cui, Z.

H. Zhang. *Adv. Synth, Catal*. **2013**, *355*(14-15), 2952-2959. l) F. P. Ma, P. H. Li, B. L. Li, L. P. Mo, N. Liu, H. J. Kang, Y. N. Liu, Z. H. Zhang. *Appl. Catal. A Gen.* **2013**, *457*, 34-41. m) J. Lu, X. T. Li, E. Q. Ma, L. P. Mo, Z. H. Zhang. *Chem.Cat.Chem.* **2014**, *6*(10), 2854-2859.

[112] United Nations; Questions About Nanotechnology, 2012.

[113] a) S. Shylesh, V. Schünemann, W. R. Thiel. *Angew. Chem. Int. Ed.* **2010**, *49*(20), 3428-3459. b) L. Vaquer, P. Riente, X. Sala, S. Janast, J. Benet-Buchholz, A. Llobet, M. A. Pericàs. *Catal. Sci. Technol.* **2013**, *3*(3), 706-714.

[114] D. Faivre, M. Bennet. *Nature*. **2016**, *535:235*, 6.

[115] a) Q. A. Pankhurst, N. T. K. Thanh, S. K. Jones, J. Dobson. *Appl. Phys*. **2009**, *42*(22), 224001-16. b) N. Lee, D. Yoo, D. Ling, M. H. Cho, T. Hyeon, J. Cheon. *Chem. Rev.* **2015**, *115*, 10637-10689.

[116] a) S. Shylesh, V. Schünemann, W. R. Thiel. *Angew. Chem. Int. Ed.* **2010**, *49*(20), 3428-3459. b) N. Zoreh, S. H. Hosseini, A. Pourjavadi, C. Bennet. *RSC Adv.* **2014**, *4*(91), 50047-50055. c) J. Safari, L. Javadian. *RSC Adv.* **2014**, *4*(90), 48973-48979. d) H. Keypour, M. Balali, M. M. Haghdoost, M. Bagherzadeh. *RSC Adv.* **2015**, *5*(66), 53349-53356.

[117] a) S. E. García-Garrido, J. Francos, V. Cadierno, J.-M. Basset, V. Polshettiwar. *Chem. Sus. Chem.* **2011**, *4*(1), 104-111. b) R. B. N. Baig, R. S. Varma. *Chem. Commun.* **2012**, *48*(50), 6220-6222.

[118] a) S. Santra, R. Tapec, N. Theodoropoulou, J. Dobson, A. Hebard, W. Tan. *Langmuir*. **2001**, *17*, 2900−2906. b) H. Yang, S. Q. Zhang, X. L. Chen, Z. H. Zhuang, J. G. Xu, X. R. Wang. *Anal. Chem.* **2004**, *76*, 1316−1321.

[119] a) E. Ertem, N. Murillo-Cremaes, R. P. Carney, A. Laromaine, E.-R. Janeček, A. Roig, F. Stellacci. Chem. Commun. **2016**, *52*, 5573−5576. b) S. Shylesh, V. Schünemann, W. Thiel. *Angew. Chem. Int. Ed.* **2010**, *49*, 3428−3459. c) K. S. M. Salih, P. Mamone, G. Dörr, T. O. Bauer, A. Brodyanski, C. Wagner, M. Kopnarski, R. N. Klupp-Taylor, S. Demeshko, F. Meyer, V. Schünemann, S. Ernst, L. J. Gooßen, W. R. Thiel. *Chem. Mater*. **2013**, *25*, 1430−1435.

[120] C. L. Zhu, M. L. Zhang, Y. L. Qiao, G. Xiao, F. Zhang, Y. J. Chen. *J. Phys. Chem. C***.** **2010**, *114*(39), 16229-16235.

[121] a) R. A. Sheldon, J. K. Kochi. Metal Catalyzed Oxidation of Organic Compounds. Academic Press; New York, **1981**. b) B. Meunier. Ed. Biomimetic Oxidations Catalyzed by Transition Metal Complexes, Imperial College Press, **2000**. c) J. E. Bäckvall. Modern Oxidation Methods, Wiley-VCH: Weinheim, **2004**. d) P. C. A. Bruijnincx, G. van Koten, R. J. M. K. Gebbink. *Chem. Soc. Rev.* **2008**, *37,* 2716. e) R. H. Crabtree. Oxidation Catalysis by Transition Metal Complexes,

---

Encyclopedia of Inorganic and Bioinorganic Chemistry, John Wiley & Sons: New York, **2011**.

[122] a) G. De Faveri, G. Ilyashenko, M. Watkinson. *Chem. Soc. Rev.* **2011**, *40*, 1722−1760. b) E. Manrique, X. Fontrodona, A. Poater, M. Sola, M. Rodríguez, I. Romero. *Dalton Trans*. **2015**, *44*, 17529−17543. b) E. Manrique, X. Fontrodona, M. Rodríguez, I. Romero. *Eur. J. Inorg. Chem*. **2019**, *15*, 2124−2133. c) M. Fontanet, M. Rodríguez, C. Viñas, F. Teixidor, I. Romero. *Eur. J. Inorg. Chem.* **2017**, 4425−4429.

[123] S. J. Lippard, J. M. Berg. Principles of Bioinorganic Chemistry, University Science Books: Mill Valley, California, **1994**.

[124] a) S. M. S. Chauhan, P. C. Ray. *Bioinorg. Med. Chem. Let.* **1991**, *1,* 601. b) J. H. Han, S. K. Yoo, J. S. Seo, S. J. Hong, S. K. Kim, C. Kim., 402. c) L. B. Bolzon, H. R. Airoldi, F. B. Zanardi, J. G. Granado, Y. Iamamoto. *Microp. and mesop. Mat.* **2013**, *168,* 37.

[125] a) P. Mathur, M. Crowder, G. C. *Dismukes. J. Am. Chem. Soc.* **1987***, 109,* 5227*. b) G. C. Dismukes. Chem. Rev.* ***1996****, 96,* 2909. c) C. Palopoli, N. Bruzzo, C. Hureau, S. Ladeira, D. Murgida, S. Signorella. *Inorg. Chem.* **2011**, *50*, 8973.

[126] a) S. I. Murahashi, N. Komiya. *Cat. Today*. **1998**, *41*, 339. b) G. Csjernyik, A. H. Ell, L. Fadini, B. Pugin, J. –E. Bäckvall. *J. Org. Chem.* **2002**, *67*, 1657. c) B. P. Babu, Y. Endo, J. –E. Bäckvall. *Chem. Eur. J.* **2012**, *18*, 11524. d) Y. Endo, J. –E. Bäckvall. *Chem. Eur. J.* **2012**, *18,* 13609. e) F. Papfotiou, K. Karidi, A. Garoufis, M. Louloudi. *Polyhedron*. **2013**, *52*, 634.

[127] M. Hudlicky. Oxidations in Organic Chemistry; *American Chemical Society*: Washington, DC, **1990**.

[128] a) J. M. Hoover, S. S. Stahl. *J. Am. Chem. Soc.* **2011**, *133*, 16901−16910. b) D. R. Jensen, M. J. Schultz, J. A. Mueller, M. S. A. Sigman. *Angew. Chem. Int. Ed.* **2003**, *42,* 3810−3813. c) X. Jiang, J. Zhang, S. Ma. *J. Am. Chem. Soc.* **2016**, *138*, 8344−8347.

[129] A. J. Esswein, D. G. Nocera. *Chem. Rev.* **2007**, *107*, 4022−4047.

[130] R. A. Sheldon, I. W. C. E. Arends, G. J. Brink and A. Dijksman. *Acc. Chem. Res*., **2002**, *35*, 774–781.

[131] R. L. Olivera, P. K. Kiyohara, L. M. Rossi. *Green Chem*. **2010**, *12*, 144-149.

[132] R. K. Sharma, M. Yadav, Y. Monga, R. Gaur, A. Adholeya, R. Zboril, R. S. Varma, R. K. Sharma. *Acs Sustainable Chem. Eng*. **2016**, *4*, 1123-1130.

[133] T. Karimpour, E. Safaei, B. Karimi, Y.-III. Lee. *ChemCatChem*. **2018**, *10*, 1889-1899.

[134] S. D. H. F. Gagnon, *Encyclopedia of Polymer Science and Engineering*, 2nd ed., Eds. H. F.

Mark, N. M. Bikales, C. G. Overberger, G. Menges, J. I. Kroschwitz, John Wiley & Sons: New York, **1985**, Vol. **6**, pp 273-307.

[135] G. de Faveri, G. Ilyashenko and M. Watkinson, *Chem. Soc. Rev.* **2011**, *40*, 1722-1760.

[136] J. G. Smith. *Synthesis.* **1984**, 629-656.

[137] E. N. Jacobsen. *Acc. Chem. Res*. **2000**, *33*, 421-431.

[138] E. J. de Vries and D. B. Janssen. *Curr. Opin. Biotechnol*. **2003**, *14*, 414-420.

[139] J. Muzart. *Eur. J. Org. Chem*. **2011**, 4717-4741.

[140] E. N. Jacobsen, W. Zhang, A. R. Muci, J. R. Ecker, and L. Deng. *J. Am. Chem. Soc.* **1991**, *113*, 7063-7064.

[141] O. Cussó, I. Garcia-Bosch, X. Ribas, J. Lloret-Fillol, and M. Costas. *J. Am. Chem. Soc.* **2013**, *135*, 14871-14878.

[142] N. K. Jana, and J. G. Verkade. *Org. Lett.* **2003**, *5*, 3787-3790.

[143] H. Hussain, A. Al-Harrasi, I. R. Green, I. Ahmed, G. Abbasa and N. Ur Rehmana, *RSC Adv.* **2014**, *4*, 12882-12917.

[144] S.-J. Jeon, H. Li, and P. J. Walsh. *J. Am. Chem. Soc*. **2005**, *127*, 16416-16425.

[145] S. K. Sartori, I. L. Miranda, M. A. N. Diaz and G. Diaz-Munoz. *Mini Rev. Org. Chem.* **2021**, *18*, 606-620.

[146] Z.-X. Wang, Y. Tu, M. Frohn, J.-R. Zhang, and Y. Shi. *J. Am. Chem. Soc.* **1997**, *119*, 11224-11235.

[147] H. Tian, X. She, L. Shu, H. Yu and Y. Shi. *J. Am. Chem. Soc.* **2000**, *122*, 11551-11552.

[148] I. Serrano, M. I. López, I. Ferrer, A. Poater, T. Parella, X. Fontrodona, M. Solà, A. Llobet, M. Rodríguez and I. Romero. *Inorg. Chem*. **2011**, *50*, 6044-6054.

[149] E. Manrique, X. Fontrodona, A. Poater, M. Sola, M. Rodríguez and I. Romero. *Dalton Trans*. **2015**, *44*, 17529-17543.

[150] I. Ferrer, X. Fontrodona, A. Roig, M. Rodríguez and I. Romero. *Chem. Eur. J.* **2017**, *23*, 4096-4107.

[151] M. Fontanet, M. Rodríguez, C. Viñas, F. Teixidor and I. Romero. *Eur. J. Inorg. Chem*. **2017**, 4425-4429.

---

[152] F. Glasser, and O. S. Wenger. *Coord. Chem. Rev.* **2020**, *405*, 213-129.

[153] W. Chen, F. N. Rein and R. C. Rocha. *Angew. Chem. Int. Ed.* **2009**, *48*, 9672-9675.

[154] W. Chen, F. N. Rein, B. L. Scott and R. C. Rocha. *Chem. Eur. J.* **2011**, *17*, 5595-5604.

[155] A. J. J. Lennox, S. Fischer, M. Jurrat, S. P. Luo, N. Rockstroh, H. Junge, R. Ludwig and M. Beller. *Chem. Eur. J.* **2016**, *22*, 1233-1238.

[156] P. Farràs, S. Maji, J. Benet-Buchholz and A. Llobet. *Chem. Eur. J.* **2013**, *19*, 7162-7172.

[157] X. Lang, J. Zhao and X. Chen. *Chem. Soc. Rev.* **2016**, *45*, 3026-3038.

[158] B. M. Hockin, C. Li, N. Robertson and E. Zysman-Colman. *Catal. Sci. Technol*. **2019**, *9*, 889-915.

[159] S. Fukuzumi, T. Kishi, H. Kotani, Y. M. Lee and W. Nam. *Nat. Chem*. **2011**, *3*, 38-41.

[160] G. Chen, L. Chen, L. Ma, H.-K. Kwonga and T.-C. Lau. *Chem. Commun.* **2016**, *52*, 9271-9274.

[161] a) P. T. Anastas, J. C. Warner. *Green Chemistry: Theory and Practice*; Oxford University Press: Oxford, U.K., **1998**. b) M. Lancaster. *Handbook of Green Chemistry and Technology*; J. H. Clark, D. J. Macquarrie. Eds.; Blackwell Publishing: Abingdon, U.K. **2002**. c) M. Poliakoff, J. M. Fitzpatrick, T. R. Farren, P. T. Anastas. *Science,* **2002**, *297*, 807. d) R. A. Sheldon. *Green Chem*. **2005**, *7*, 267. e) R. A. Sheldon, I. Arends, U. Hanefeld. Green Chemistry and Catalysis; Wiley-VCH: Weinheim, Germany, **2007**.

[162] a) C. Capello, U. Fischer, K. Hungerbühler. *Green Chem*. **2007**, *9*(9), 927-934. b) H. García-Marín, J. C. Van der Toorn, J. A. Mayoral, J. I. García, I. W. C. E. Arends. *Green Chem.* **2009**, *11*(10), 1605-1609.

[163] a) H. I. Schlesinger, H. C. Brown. *J.Am.Chem.Soc*. **1953**, *75*, 186. b) H. I. Schlesinger, A. B. Bur. *Chem. Rev.* **1942**, *31*, 1.

[164] a) R. H. Crabtree. Energy Production and Storage−Inorganic Chemical Strategies for a Warming World. In Encyclopedia of Inorganic Chemistry, 2nd ed.; John Wiley & Sons, Inc., **2010**; pp 73−87. b) G. Renger. Energy Transfer and Trapping in Photosystem II. In The Photosystems: Structure, Function, and Molecular Biology, 1st ed.; Barber, J., Ed.; Elsevier Science Publishers: Amsterdam, The Netherlands, **1992**; pp 45−99.

[165] a) Y. Xia, K. Xiao, B. Cheng, J. Yu, L. Jiang, M. Antonietti, S. Cao. *ChemSusChem*. **2020**, *13*, 1730−1734. b) A. Savateev, M. Antonietti. *ChemCatChem*. **2019**, *11*, 6166−6176. c) A.

Avateev, I. Ghosh, B. König, M. Antonietti. *Angew. Chem. Int. Ed*. **2018**, *57*, 15936−15947.

[166] J. Kiwi, K. Kalyanasundaram and M. Grätzel. Solar Energy Materials, Springer Berlin Heidelberg, Berlin, Heidelberg, **1982**, pp.37-125.

[167] G. E. M. Crisenza, P. Melchiorre. *Nat. Commum*. **2020**, *11*, 803.

[168] a) M. H. Shaw, J. Twilton, D. W. C. MacMillan. *J. Org. Chem.* **2016**, *81*, 6898-6926.

[169] a) Crabtree, R. H. *Energy Production and Storage – Inorganic Chemical Strategies for a Warming World*. *Encyclopedia of Inorganic Chemistry*, ed., John Wiley & Sons, Inc., 2ⁿᵈed, **2010**, 73–87. b) Renger, G. *Energy Transfer and Trapping in Photosystem II, in The Photosystems: Structure, Function and Molecular Biology*. 1ˢᵗed. J. Barber, Elsevier Science Publishers, Amsterdam, The Netherlands, **1992**, 45-99.

[170] L. Capaldo, D. Ravelli. Eur. *J. Org. Chem.* **2020**. 2783-2806.

[171] D. A. DiRocco, K. Dykstra, S. Krska, P. Vachal, D. V. Conway, M. Tudge. *Angew. Chem. Int. Ed.* **2014**, *53*, 4802 –4806.

[172] H. Anhua, G. Jing-Jing, H. Pan, Z. Zhiwei. *Science*. **2018**, *361*(6403), 668-672.

[173] K. L. Skubi, T. R. Blum, T. P. Yoon. *Chem. Rev*. **2016**, *116*, 10035-10074.

[174] C. K. Prier, D. A. Rankic and D. W. C. MacMillan. *Chem. Rev*. **2013**, *113*, 5322–5363.

[175] D. M. Arias-Rotondo, J. K. McCusker. *Chem. Soc. Rev*. **2016**, *45*, 5803.

[176] T. P. Yoon, M. A. Ischay, J. Du. *Nat. Chem*. **2010**, *2*, 527−532.

[177] S. Lin, M. A. Ischay, C. G. Fry, T. P. J. Yoon. *J. Am. Chem. Soc.* **2011**, *133*, 19350−19353.

[178] H. Huo, X. Shen, C. Wang, L. Zhang, P. Röse, L. A. Chen, K. Harms, M. Marsch, G. Hilt, E. Meggers. *Nature.* **2014**, *515*, 100−103.

[179] S. Campagna, F. Puntoriero, F. Nastasi, G. Bergamini, V. Balzani. *To. Curr. Chem.* **2007**, *280*, 117-214.

[180] S. Hohloch, D. Schweinfurth, M. G. Sommer, F. Weisser, N. Deibel, F. Ehret, B. Sarkar. *Dalton Trans.,* **2014**, *43*, 4437-4450.

[181] C. K. Prier, D. A. Rankic, D. W. C. MacMillan. *Chem. Rev.* **2013**, *113*, 5322-5363.

[182] Kalyanasundaram. *Coord. Chem. Rev*. **1982**, *46*, 159.

[183] F. E. Lytle and D. M. Hercules. *J. Am. Chem. Soc*. **1969**, *91*, 253–257.

---

[184] N. Sutin and C. Creutz. *Adv. Chem. Ser.* **1978**, *168*, 1–27.

[185] A. Juris, V. Balzani, F. Barigelletti, S. Campagna, P. Belser and A. von Zelewsky. Coord. Chem. Rev. **1988**, *84*, 85–277.

[186] H. Cano-Yelo, A. Deronzier. *Tetrahedron Lett.* **1984**, *25*, 5517-5520.

[187] F. R. Rocha, W. Chen, B. L. Scott, R. C. Rocha. *J. Braz. Chem. Soc*. **2020**, 31, *11*, 2421-2429.

[188] B. Tambosco, k. Seguram C. Seyrig, D. Cabrera, M. port, C. Ferroud, Z. Amara. *ACS Catal*. **2018**, *8*, 4383-4389.

[189] a) M. T. Pope. *Springer:* Berlin, **1983**. b) C. L. Hill, C. M. Prosser-McCartha. *Coord. Chem. Rev.* **1995**, *143*, 407-455. c) I. V. Kozhenikov. *Chem. Rev.* **1998**, *98*, 199-218. d) N. Mizuno, M. Misono. *Chem. Rev*. **1998**, *98*, 199-218. e) M. Sadakane, E. Steckhan. *Chem. Rev*. **1998**, *98*, 219-238. f) D. E. Katsoulis. *Chem. Rev*. **1998**, *98*, 359-388. g) C. L. Hill. In Comprehensive Coordination; Chemistry, I, McCleverty, J. A. Meyer, T. J.,Eds.; Elsevier Pergamon: Amsterdan, **2004**; Vol. 4, p 679. h) D.-L. Long, E. Burkholder, L. Cronin. *Chem. Soc. Rev*. **2007**, *36*, 105-121. i) D.-L. Long, R. Tsunashima, R. Cronin. *Angew. Chem. Int. Ed*. **2010**, *49*, 1736-1758. j) Y.-F. Song, R. Tsunashima. *Chem. Soc. Rev*. **2012**, *41*, 7384-7402. k) H. Ly, Y. V. Geletii, C. Zhao, J. W. Vickers, G. Zhu, Z. Luo, J. Song, T. Lian, D. G. Musaev, C. L. Hill. *Chem. Soc. Rev*. **2012**, *41*, 7572-7589. l) S.-S. Wang, G.-Y. Yang. *Chem. Rev.* **2015**, *115*, 4893-4962. m) L. Vila-Nadal, L. Cronin. *Nat. Rev.* **2017**, *2*, 17054. n) N. I. Gumerova, A. Rompel. *Nat. Rev. Rev*. **2018**, *2*, 112.

[190] K. Suzuki, N. Mizuno, K. Yamaguchi. *ACS Catal.* **2018**, *8*, 10809-10825.

[191] J. M. Kern, J. P. Sauvage. *J. Chem. Soc., Chem. Commun*. **1987**, 546–548.

[192] a) M. Gulias and J. L. Mascarenas. *Angew. Chem., Int. Ed*. **2016**, *55*, 11000–11019. b) W. H. Rao and B. F. Shi. *Org. Chem. Front*. **2016**, *3*, 1028–1047. c) K. S. Singh. *Catalysts*. **2019**, *9*, 173. d) A. E. Wendlands, A. M. Suess and S. S. Stahl. *Angew. Chem*. Int. Ed. **2011**, *50*, 11062–11087. e) X. X. Guo, D. W. Gu, W. Wu and W. Zhang. *Chem. Rev*. **2015**, *115*, 1622–1651. f) N. S. Upadhyay, V. H. Thorat, R. Sato, P. Annamalai, S. C. Chuang and C. H. Cheng. *Green Chem*. **2017**, *19*, 3219–3224.

[193] V. P. Charpe, A. Ragupathi, A. Sagadevan, K. C. Hwang. *Green Chem*. **2021**, *23*, 5024.

[194] J. Zhou, X. Huang-Fu, Y-Y. Huang, C-N. Cao, J. Han, X-L. Zhao, X-D. Chen. *Inorg. Chem*. **2020**, *59*, 254-263.

[195] S. Gazi, M. Dokic, K. F. Chin, P.R. Ng, H. S. Soo. *Adv. Sci*. **2019**, *6*, 1902020.

---

[196] W-J. Zhou, X-D. Wu, M. Miao, Z-H. Wang, L. Chen, S-Y. Shan, G-M. Cao, D-G. Yu. *Chem. Eur. J.* **2020**, *26*, 15052-15064.

[197] B. Mehldorf, R. Wolf. *Angew. Chem. Int. Ed.* **2016**, *55*, 427–430; *Angew. Chem*. **2016**, *128*, 437–441.

[198] a) D. H. R. Barton, D. Dolle. *Acc. Chem. Res.* **1992**, *25*, 504–512. b) C. Limberg, *Angew. Chem. Int. Ed.* **2003**, *42*, 5932–5954; *Angew. Chem*. **2003**, *115*, 6112–6136.

[199] S. L. Li, B. Zhu, R. Lee, B. K. Qiao, Z. Y. Jiang. *Org. Chem. Front*. **2018**, *5*, 380–385.

[200] J. Chen, S. Stepanovic, A. Draksharapu, M. Gruden, W. R. Browne. *Angew. Chem. Int. Ed.* **2018**, *57*, 3207–3211*; Angew. Chem*. **2018**, *130*, 3261–3265.

[201] a) J. Chen, A. Draksharapu, E. Harvey, W. Rasheed, L. Que, W. R. Browne. *Chem. Commun*. **2017**, *53*, 12357 –12360. b) C. Cordes, M. Morganti, I. Klawitter, C. Schremmer, S. Dechert, F. Meyer. *Angew. Chem. Int. Ed.* **2019**, *58*, 10855–10858; *Angew. Chem*. **2019**, *131*, 10971–10974.

[202] J-J. Guo, A. Hu, Z. Zuo. *Tetrahedron Lett.* **2018**, *59*, 2103-2011.

[203] J-J. Guo, A. Hu, Y. Chen, J. Sun, H. Tang, Z. Zuo. *Angew. Chem. Int. Ed*. **2016**, *55*, 15319-15322.

[204] X. Lang, J. Zhao, X. Chen. *Chem. Soc. Rev.* **2016**, *45*, 3026−3038.

[205] S. Fukuzumi, T. Kishi, H. Kotani, Y. M. Lee and W. Nam. *Nat. Chem*. **2011**, *3*, 38–41.

[206] A. Company, G. Sabenya, M. González-Béjar, L. Gómez, M. Clémancey, G. Blondin, A. J. Jasniewski, M. Puri, W. R. Browne, J.-M. Latour, L. Que, M. Costas, J. Pérez- Prieto and J. Lloret-Fillol. *J. Am. Chem. Soc*. **2014**, *136*, 4624–4633.

[207] W. M. Singh, D. Pegram, H. F. Duan, D. Kalita, P. Simone, G. L. Emmert and X. Zhao. *Angew. Chem. Int. Ed*. **2012**, *51*, 1653–1656.

[208] G. Chen, L. Chen, L. Ma, H-K. Kwong, T-C, L. *Chem. commum*, **2016**, *52*, 9271.

[209] M. D. Kärkäs, I. Bosque, B. S. Matsuura and C. R. J. Stephenson. *Org. Lett.* **2016**, *18*, 5166.

[210] W. Z. Chen, F. N. Rein and R. C. Rocha. *Angew. Chem. Int. Ed*. **2009**, *48*, 9672–9675.

[211] D. B. Chao and W. F. Fu, *Chem. Commun.* 2013, *49*, 3872–3874.

[212] X. Lang, J. Zhao, X. Chen. *Angew. Chem. Int. Ed*. **2016**, *55*, 4697–4700; *Angew. Chem.* **2016**, *128*, 4775–4778.

---

[213] X. Lang, J. Zhao, X. Chen. Angew. *Chem. Int. Ed.* **2016**, *55*, 4697–4700; Angew. Chem. **2016**, *128*, 4775–4778.

[214] X. Gu, X. Li, Y. Chai, Q. Yang, P. Li, Y. Yao. *Green Chem*. **2013**, *15*, 357 – 361.

[215] W. Iali, P.-H. Lanoe, S. Torelli, D. Jouvenot, F. Loiseau, C. Lebrun, O. Hamelin and S.Ménage. *Angew. Chem. Int. Ed.* **2015**, *54*, 8415–8419.

[216] a) S. Phungsripheng, K. Kozawa, M. Akita, A. Inagaki. *Inorg. Chem*. **2016**, *55*, 3750–3758. b) P. Guillo, O. Hamelin, P. Batat, G. Jonusauskas, N. D. McClenaghan, S. Ménage. *Inorg. Chem*. **2012**, *51*, 2222–2230. c) T.-T. Li, F.-M. Li, W.-L. Zhao, Y.-H. Tian, Y. Chen, R. Cai, W.-F. Fu. *Inorg. Chem*. **2015**, *54*, 183–191. d) K. Senthil Murugan, T. Rajendran, G. Balakrishnan, M. Ganesan, V. K. Sivasubramanian, J. Sankar, A. Ilangovan, P. Ramamurthy, S. Rajagopal. *J. Phys. Chem. A*. **2014**, *118*, 4451–4463.

[217] W. Li, Z. Xie, X. Jing. *Catal. Commun*. **2011**, *16*, 94–97.

[218] D. Chao, M. Zhao. *Chem. Sus. Chem.* **2017**, *10*, 3358-3362.

[219] P. Guillo, O. Hamelin, P. Batat, G. Jonusauskas, N. D. McClenaghan, S. Ménage. *Inorg. Chem.* **2012**, *51*, 2222–2230.

[220] I. Fuentes, A. Andrio, F. Teixidor, C. Viñas, V. Compañ, *Phys. Chem. Chem. Phys.* **2017**, *19*, 15177–15186.

[221] L. Mátel, F. Macášek, P. Rajec, S. Heřmánek and J. Plešek. *Polyhedron*. **1982**, *1*, 511-519.

[222] I. Fuentes, J. Pujols, C. Viñas, S. Ventura and F. Teixidor. *Chem. Eur. J.* **2019**, *25*, 12820.

[223] a) M. J. Hardie, C. L. Raston. C. L. *Chem. Commun*. **2001**, *26*, 905−906. b) M. Tarrés, C. Viñas, P. Gonzalez-Cardoso, M. M. Hänninen, R. Sillanpää, V. Dordovic, M. Uchman, F. Teixidor, P. Matějíček. *Chem. Eur. J.* **2014**, *20*, 6786−6794. c) J. Plešek, K. Base, F. Mares, F. Hanousek, B. Stibr, S. Hermanek. S. *Collect. Czech. Chem. Commun*. **1984**, *49*, 2776-2789.

[224] Z. Xie, T. Jelinek, R. Bau, C. A. Reed. *J. Am. Chem. Soc.* **1994**, *116*, 1907-1913.

[225] B. P. Sullivan, J. M. Calvert, T. J. Meyer. *Inorg. Chem.* **1980**, *19*, 1404-1407.

[226] a) B. A. Moyer, M. S. Thompson, T. J. Meyer. *J. Am. Chem. Soc.* **1980**, *102*, 2310-2312. b) K. J. Takkeuchi, M. S. Thompson, D. W. Pipes, T. J. Meyer. *Inorg. Chem*. **1984**, *23*, 1851-1858. c) J. D. Wasylenko, C. Ganesamoorthy, B. D. Koivisto, M. A. Henderson, and C. P. Berlinguette. *Inorg. Chem. Vol.49*, No. 5, **2010**, 2202-2209.

[227] H. Hassani, B. Zakerinasab, M. A. Nasseri, M. Shavakandi. RSC Adv. **2016**, *6*, 17560-17566.

[228] X-D. Wang, Z-X. Shen, T. Sang, X-B. Cheng, M. F. Li, L. Y. Chen, Z-S. Wang. *J. Colloid Interface Sci.* **2010**, *341,* 23–29.

[229] Gaussian 09, Revision B.01, M. J. Frisch et al., Gaussian Inc., Wallingford CT, **2010**.

[230] T. Lu, F. Chen. *J. Comput. Chem*. **2012,** *33*, 580–592.

[231] G. Schaftenaar, J. H. Noordik. *Comput. Aided Mol. Design*. **2000**, *14*, 123 –134.

[232] W. Humphrey, A. Dalke, K. J. Schulten. *J. Mol. Graphics*.**1996**, *14*, 33–38.

[233] I. Fuentes, A. Andrio, F. Teixidor, C. Viñas, V. Compañ. *Phys. Chem. Chem. Phys.* **2017**, *19*, 15177–15186.

[234] a) L. Mátel, F. Macášek, P. Rajec, S. Heřmánek and J. Plešek, *Polyhedron*. **1982**, *1*, 511-519. b) . Fuentes, J. Pujols, C. Viñas, S. Ventura and F. Teixidor. *Chem. Eur. J.* **2019**, *25*, 12820.

[235] I. Rojo, F. Teixidor, C. Viñas, R. Kivekäs, R. Sillanpää. *Chem. Eur. J.* **2003**, *9,* 4311–4323.

[236] V. Cerný, J. Pavlík, E. Kustková-Maxová. *Collect. Czech. Chem. Commun.* **1976**, *41*, 3232–3244.

[237] a) D. C. Malaspina, C. Viñas, F. Teixidor, J. Faraudo. *Angew. Chem. Int. Ed.* **2020**, *59*, 3088–3092; *Angew. Chem.* **2020**, *132*, 3112–3116. b) E. Juarez-Pérez, R. Núñez, C. Viñas, R. Sillanpää, F. Teixidor. *Eur. J. Inorg. Chem*. **2003**, 4311–4323.

[238] M. Behl, D. Hnyk, J. Machacek. *Chem. Eur. J.* **2005**, *11*, 4109–4120.

[239] D. C. Malaspina, C. Viñas, F. Teixidor, J. Faraudo. *Angew. Chem. Int. Ed*. **2020**, *59*, 3088-3092.

[240] V. Cerný, J. Pavlík, E. Kustková-Maxová. *Collect. Czech. Chem. Commun.* **1976**, *41*, 3232–3244.

[241] R. Martin, Natural Transition Orbitals. *J. Chem. Phys*. **2003**,*118*, 4775.

[242] J. Plesek, B. Grener, J. Báca, J. Fusek, I. Císarová. *J. Organomet. Chem.* **2002**, *649*, 181–190.

[243] a) D. A. House. *Chem. Rev*. **1962**, *62*, 185–203. b) Q. Jiang, J. Jia, B. Xu, A. Zhao, C.-C. Guo. *J. Org. Chem.* **2015**, *80*, 3586–3596. c) L. Cui, H. Chen, C. Liu, C. Li. *Org. Lett.* **2016**, *18*, 2188–2191. d) C. Liu, X. Wang, Z. Li, L. Cui, C. Li. *J. Am. Chem. Soc.* **2015**, *137*, 9820–9823.

[244] P. González-Cardoso, A-J Stoica, P. Farràs, A. Pepiol, C. Viñas, F. Teixidor. *Chem. Eur. J.*

2010, *16*, 6660–6665.

[245] D. A. Rudakov, V. L. Shirokii, V. A. Knizhnikov, A. V. Bazhanov, E. I. Vecher, N. A. Maier, V. I. Potkin, A. N. Ryabtsev, P. V. Petrovskii, I. B. Sivaev, V. I. Bregadze, I. L. Eremenko. *Russ. Chem. Bull., Int. Ed.* **2004**, *53*, 2554.

[246] R. Fernández-Alvarez, V. Dordovic, M. Uchman, P. Matejícek. *Langmuir,* **2018**, *34*, 14448–14457.

[247] A. Stoica, C. Viñas, F. Teixidor. *Chem. Commun.* **2009**, *33*, 4988−4990.

[248] a) R. Massart. *IEEE Trans. Magn*. **1981**, *17*, 1247−1248. b) E. Oleshkevich, F. Teixidor, A. Rosell, C. Viñas. *Inorg. Chem*. **2018**, *57*, 462−470.

[249] Saha, A. (**2019**). *Tuning the Properties of Quantum Nanocrystals and Magnetic Nanoparticles using Spherical Ligands : Carboranes and Metallacarboranes*. http://hdl.handle.net/10803/667956

[250] J. D. Clogston, A. K. Patri. *McNeil, S., Ed.; Humana Press*, **2011**; Vol. 697.

[251] a) M. M. Can, M. Coşkun, T. Firat. *J. Alloys Compd*. **2012**, *542*, 241−247. b) M. B. Gawande, A. K. Rathi, J. Tucek, K. Safarova, N. Bundaleski, O. M. N. D. Teodoro, L. Kvitek, R. S. Varma, R. Zboril. *Green Chem*. **2014**, *16*, 4137−4143. c) A. K. Rathi, M. B. Gawande, J. Pechousek, J. Tucek, C. Aparicio, M. Petr, O. Tomanec, R. Krikavova, Z. Travnicek, R. S. Varma, R. Zboril. *Green Chem*. **2016**, *18*, 2363−2373.

[252] K. J. Takeuchi, M. S. Thompson, D. V. Pipes, T. J. Meyer. *Inorg. Chem.* **1984**, *23.*

[253] Xie, Z.; Jelinek, T.; Bau, R.; Reed, C. A. New Weakly Coordinating Anions. III. Useful Silver and Trityl Salt Reagents of Carborane Anions. *J. Am. Chem. Soc.* **1994**, *116*, 1907−1913.

[254] a) M. Dakkach, M. I. López, I. Romero, M. Rodríguez, A. Atlamsani, T. Parella, X. Fontrodona, A. Llobet. *Inorg. Chem*. **2010**, *49*, 7072−7079. b) I. Ferrer, X. Fontrodona, A. Roig, M. Rodríguez, I. Romero. *Chem. Eur. J.* **2017**, *23*, 4096−4107. c) E. Manrique, X. Fontrodona, M. Rodríguez, I. Romero. *Eur. J. Inorg. Chem*. **2019**, *2019*, 2124−2133.

[255] L. J. Todd, A. R. Siedle. *Prog. Nucl. Magn. Reson. Spectrosc*. **1979**, *13*, 87−176.

[256] a) I. Rojo, F. Teixidor, C.Viñas, R. Kivekäs, R. Sillanpää. R. *Chem. Eur. J.* **2003**, *9,* 4311−4323. b) V. Cerný, J. Pavlík, E. Kustková-Maxová. *Collect. Czech. Chem. Commun*. **1976**, *41*, 3232−3244.

[257] V. Balzani, M. Juris, M. Venturi, S. Campagna, S. Serroni. *Chem. Rev*. **1996**, *96*, 759−834.

---

[258] a) B. A. Moyer, M. S. Thompson, T. J. Meyer. *J. Am. Chem. Soc*. **1980**, *102*, 2310-2312. b) K. J. Takkeuchi, M. S. Thompson, D. W. Pipes, T. J. Meyer. *Inorg. Chem*. **1984**, *23*, 1851-1858.

[259] D. Chao, W-F. Fu. *Chem.Commun*. **2013**, *49*, 3872-3874.

[260] A. K. Ravari, G. Zhu, R. Ezhov, Y. Pineda-Galvan, A. Page, W. Weinschenk, L. Yan, Y. Pushkar, Y. *J. Am. Chem. Soc*. **2020**, *142*, 884−893.

[261] a) D. Brusselle, P. Bauduin, L. Girard, A. Zaulet, C. Viñas, F. Teixidor, I. Ly, O. Diat. *Angew. Chem. Int. Ed.* **2013**, *52* (46), 12194−12194. b) P. Matejicek, P. Cigler, K. Prochazka, V. Kral. *Langmuir.* **2006**, *22*, 575−581.

[262] P. Matejicek, P. Cigler, K. Prochazka, V. Kral. *Langmuir*. **2006**, *22*, 575−581.

[263] I. Fuentes, A. Andrio, F. Teixidor, C. Viñas and V. Compañ. *Phys. Chem. Chem. Phys*. **2017**, *19*, 15177-15186.

[264] S. M. Danov, O. A. Kazantsev, A. L. Esipovich, A. S. Belousov, A. E. Rogozhin and E. A. Kanakov. *Catal. Sci. Technol*. **2017**, *7*, 3659-3675.

[265] M. Palucki, M. S. Finney, P. J. Pospisil, M. L. Güler, T. Ishida and E. N. Jacobsen. *J. Am. Chem. Soc*. **1998**, *120*, 948-954.

[266] A. Behr, Chem. Eng. Technol., 2008, 31, 700-714.

[267] a) D. Brusselle, P. Bauduin, L. Girard, A. Zaulet, C. Viñas, F.; Teixidor, I. Ly and O. Diat. *Angew. Chem. Int. Ed.* **2013**, *52* (46) 12194-12194. b) P. Matejicek, P. Cigler, K. Prochazka and V. Kral. *Langmuir* **2006**, *22*, 575-581.

[268] S. Hohloch, D. Schweinfurth, M. G. Sommer, F. Weisser, N. Deibel, F. Ehret, B. Sarkar. *Dalton Trans.* **2014**, *43*, 4437–4450.

[269] a) M. J. Hardie, C. L. Raston. *Chem. Commun*. **2001**, *26*, 905-906. b) M. A. Fox, A. K. Huges. *Coord. Chem. Rev.* **2004**, *248(5-6)*, 457-476. c) D. Brusselle, P. Bauduin, L. Girard, A. Zaulet, C. Viñas, F. Teixidor, I. Ly and O. Dia. *Angew. Chem. Int. Ed.* **2013**, *52* (46), 12114-12118.

[270] H. Li, F. Li, B. Zhang, X. Zhou, F. Yu and L. Sun. *J. Am. Chem. Soc.* **2015**, *137*, 4332−4335.

ANNEX. Supporting Information

ANNEX I. Supporting Information

Chapter IV.1

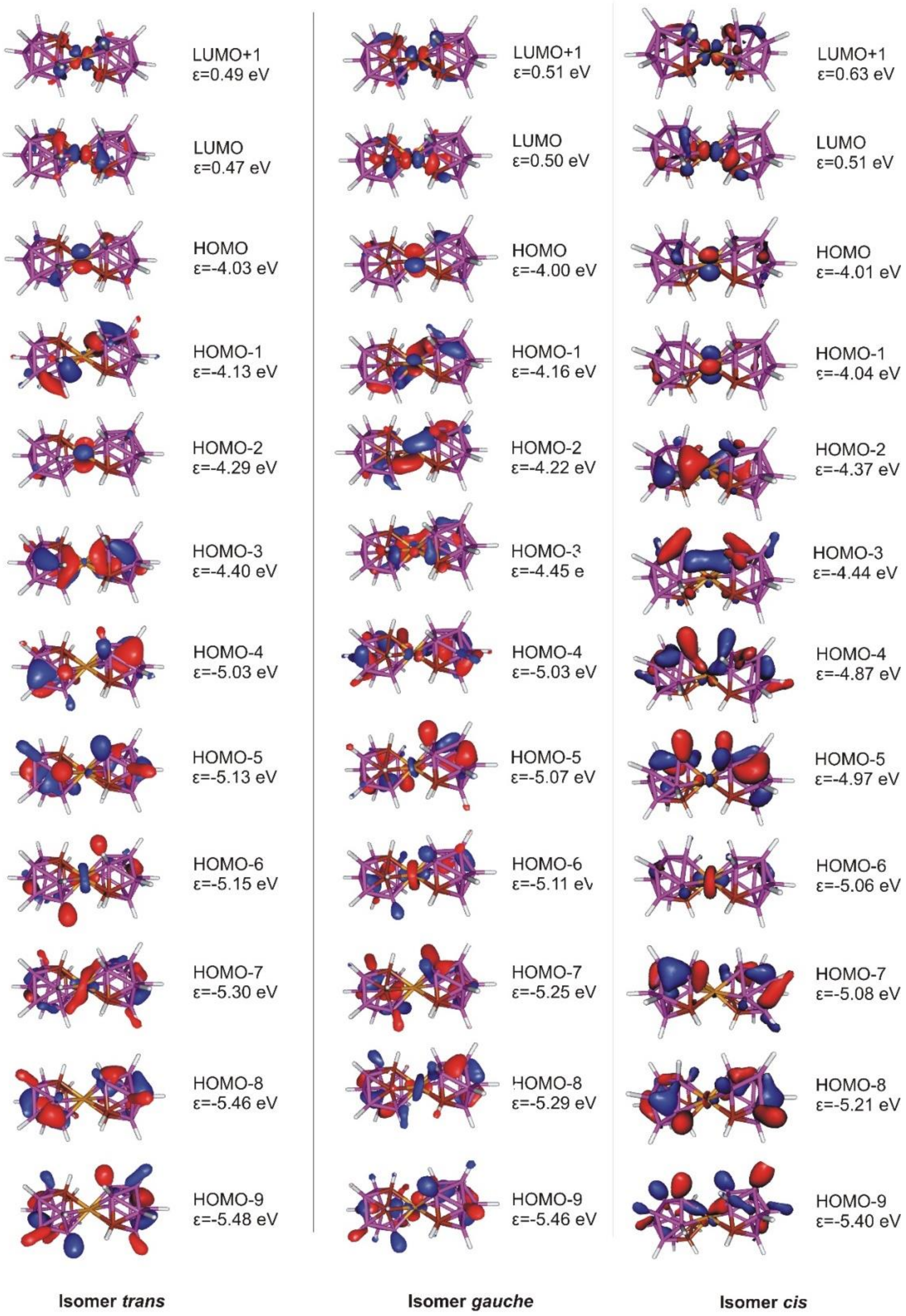
LUMO+1
ε=0.49 eV
LUMO
ε=0.47 eV
HOMO
ε=-4.03 eV
HOMO-1
ε=-4.13 eV
HOMO-2
ε=-4.29 eV
HOMO-3
ε=-4.40 eV
HOMO-4
ε=-5.03 eV
HOMO-5
ε=-5.13 eV
HOMO-6
ε=-5.15 eV
HOMO-7
ε=-5.30 eV
HOMO-8
ε=-5.46 eV
HOMO-9
ε=-5.48 eV
LUMO+1
ε=0.51 eV
LUMO
ε=0.50 eV
HOMO
ε=-4.00 eV
HOMO-1
ε=-4.16 eV
HOMO-2
ε=-4.22 eV
HOMO-3
ε=-4.45 e
HOMO-4
ε=-5.03 eV
HOMO-5
ε=-5.07 eV
HOMO-6
ε=-5.11 eV
HOMO-7
ε=-5.25 eV
HOMO-8
ε=-5.29 eV
HOMO-9
ε=-5.46 eV
LUMO+1
ε=0.63 eV
LUMO
ε=0.51 eV
HOMO
ε=-4.01 eV
HOMO-1
ε=-4.04 eV
HOMO-2
ε=-4.37 eV
HOMO-3
ε=-4.44 eV
HOMO-4
ε=-4.87 eV
HOMO-5
ε=-4.97 eV
HOMO-6
ε=-5.06 eV
HOMO-7
ε=-5.08 eV
HOMO-8
ε=-5.21 eV
HOMO-9
ε=-5.40 eV
Isomer *trans*
Isomer *gauche*
Isomer *cis*

Figure SIV.1. Selected Kohn-Sahm orbitals of the different rotamers of **1**$^-$ anion.

Table SIV 1.1. Natural Transition Orbitals (NTOs) of the different rotamers.

Rotamer	Transition	eigen-value	
trans	S0→S11	0.64	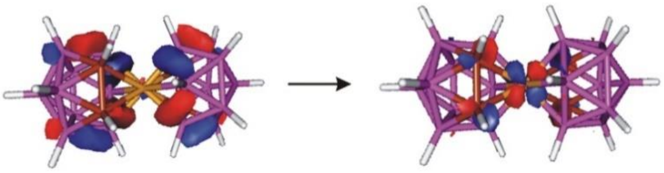
		0.34	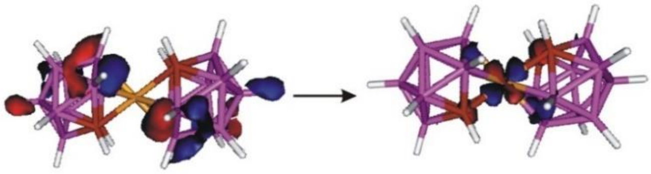
gauche	S0→S11	0.84	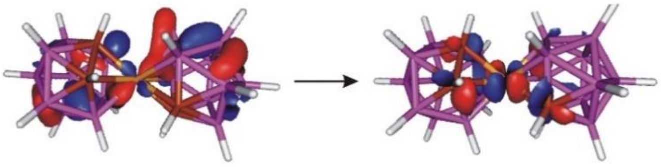
		0.15	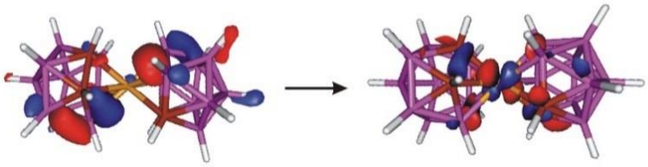
	S0→S13	0.63	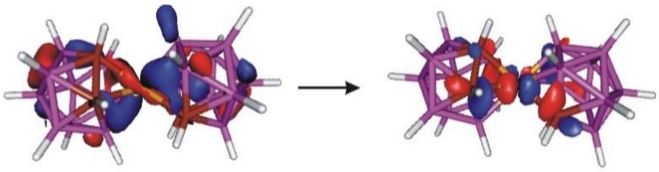

		0.35	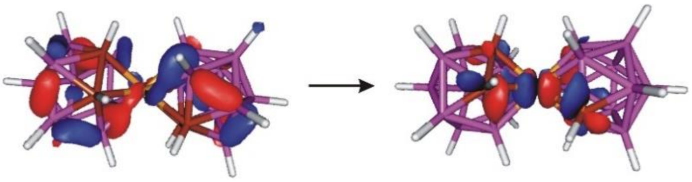
cis	S0→S13	0.65	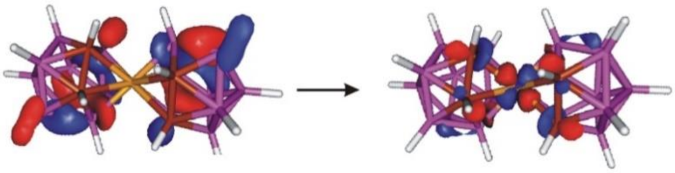
		0.34	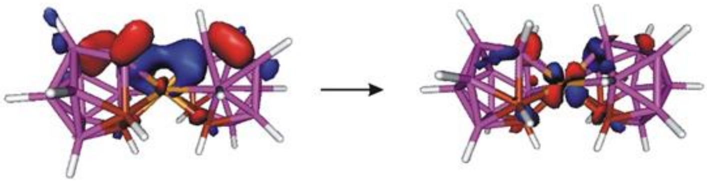
	S0→S15	0.75	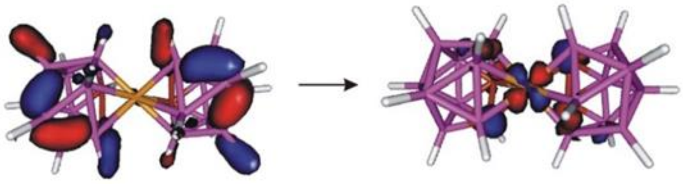
		0.24	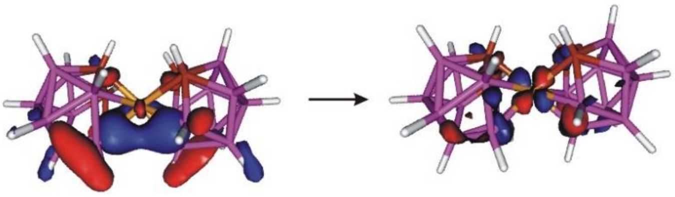

XYZ matrix and total energies (in atomic unit) of the optimized structures

isomer cis

E(B3LYP/6-311+G**)= -1996.261847

B	-0.035903	-0.183755	-0.091513
B	0.026157	-0.071157	1.704528
B	1.727128	0.006439	2.209533
B	0.745468	1.470529	2.164354
B	2.398265	1.513265	1.552525
B	2.728975	-0.022847	0.730738
B	1.246332	-1.013537	0.823931
B	1.655012	-0.174472	-0.708156
B	2.351886	1.411975	-0.238281
C	1.130511	2.185894	0.647158
C	-0.205420	1.293810	0.732576
Co	0.463878	1.540323	-1.202825
C	0.930251	3.140682	-2.417673
B	0.901225	3.154072	-4.108835
B	-0.820512	3.216790	-4.539406
B	-1.600835	1.765899	-3.848543
B	0.046738	1.655243	-4.528028
B	1.206258	1.643954	-3.176403
B	-0.353203	0.758553	-3.026415
B	-1.447550	1.825287	-2.084184
B	-1.734072	3.328429	-3.021078
B	-0.203172	4.183994	-3.200473
C	-0.553782	3.239084	-1.805196
H	1.014574	3.261560	0.683345
H	-1.149788	1.813053	0.816507
H	3.177878	2.060378	-0.788799
H	-0.987310	-0.753365	-0.497369
H	2.033841	-0.828540	-1.618687
H	1.269360	-2.198035	0.903092
H	3.819243	-0.493302	0.736900

H	-0.885430	-0.480953	2.339594
H	3.172174	2.242249	2.075352
H	0.335324	2.168985	3.025899
H	2.085035	-0.435334	3.251020
H	-0.458226	-0.418458	-3.090213
H	-2.327089	1.532065	-1.345118
H	2.305473	1.229157	-3.295007
H	-0.693397	3.867127	-0.934651
H	1.713037	3.701659	-1.926728
H	-0.072706	5.351874	-3.068853
H	1.798100	3.662839	-4.691092
H	-2.712491	3.964705	-2.817145
H	0.286953	1.084727	-5.541257
H	-2.546679	1.270938	-4.368583
H	-1.191760	3.749390	-5.532639

isomer gauche

E(B3LYP/6-311+G**)= -1996.2657531

C	0.000000	0.000000	0.000000
Co	0.000000	0.000000	2.064117
C	1.415153	0.000000	3.541631
B	1.209975	-0.575743	5.123361
B	2.363057	-1.355952	4.037988
C	1.609138	-1.216240	2.502415
B	0.186188	-2.109007	2.311147
B	-0.999215	-1.357097	3.415754
B	-0.092961	-2.827414	3.909055
B	1.558550	-2.728557	3.276130
B	1.248907	-2.346240	4.983143
B	-0.314801	-1.485109	5.061830
B	-0.171951	0.051611	4.163118
B	-1.287945	0.542963	-0.996135
B	0.290022	1.331216	-1.015944
B	0.994519	1.216614	0.623877

B	-0.034530	2.138003	1.756475
B	-1.627433	1.307735	1.782890
C	-1.475109	0.044969	0.647167
B	-2.325883	1.418386	0.132024
B	-1.399601	2.780042	0.798005
B	0.231189	2.722517	0.078922
B	-1.193165	2.303453	-0.911725
H	0.393533	2.775724	2.662437
H	2.172301	1.057930	0.661985
H	-2.439523	1.250656	2.638062
H	0.368113	-0.964886	-0.317285
H	-2.021509	-0.883799	0.716435
H	-1.685418	-0.176351	-1.845458
H	-3.499348	1.341039	-0.004799
H	0.981885	1.179293	-1.965553
H	-1.943861	3.794983	1.087667
H	0.875032	3.696195	-0.141432
H	-1.576588	2.958849	-1.823509
H	-0.019868	-2.684486	1.291264
H	2.335199	-1.078090	1.714422
H	-2.175132	-1.429611	3.265240
H	2.027572	0.878907	3.405890
H	-0.620163	1.060794	4.581120
H	1.629636	0.071071	6.021828
H	-1.008298	-1.564869	6.022520
H	3.535427	-1.222282	4.104522
H	-0.636011	-3.877291	4.027353
H	2.229508	-3.606469	2.848816
H	1.665038	-3.026526	5.861751

isomer trans

E(B3LYP/6-311+G**)= -1996.2665465

C	0.000000	0.000000	0.000000
B	0.000000	0.000000	1.721270

B	1.705935	0.000000	2.168209
B	2.663199	0.073389	0.662389
B	2.443556	-1.483082	1.500682
B	0.788124	-1.522979	2.140041
C	-0.199718	-1.415344	0.762288
B	1.186742	-2.393399	0.629905
B	2.362687	-1.414199	-0.285423
B	1.539698	0.107585	-0.717124
B	1.140881	0.976769	0.793680
Co	0.389685	-1.617854	-1.180477
C	0.779351	-3.235713	-2.360918
B	-0.361513	-4.212484	-3.154608
B	-0.926511	-3.235725	-4.529141
B	-1.664140	-1.752617	-3.861661
B	-1.883809	-3.309073	-3.023348
B	-0.760285	-3.343281	-1.643830
B	-1.583276	-1.821497	-2.075529
B	-0.407336	-0.842298	-2.990862
B	-0.008724	-1.712719	-4.501008
B	0.779364	-3.235719	-4.082211
C	0.979107	-1.820381	-3.123251
H	3.241456	-1.888778	-0.936308
H	1.713770	0.794558	-1.664802
H	1.097541	-3.572003	0.687024
H	-0.881567	0.482020	-0.394868
H	-1.204147	-1.804017	0.836331
H	-0.945635	0.434852	2.280855
H	0.386355	-2.123146	3.078562
H	0.989520	2.151176	0.776404
H	3.323821	-2.045905	2.065920
H	3.703549	0.644974	0.616637
H	2.046639	0.501330	3.188244
H	-2.462062	-1.346922	-1.424663
H	-0.318105	0.336303	-3.047983

H	-0.934342	-4.030250	-0.696147
H	1.983541	-1.431723	-3.197308
H	1.660904	-3.717733	-1.966018
H	1.725008	-3.670568	-4.641786
H	-0.210150	-5.386891	-3.137321
H	0.393079	-1.112584	-5.439535
H	-2.924174	-3.880635	-2.977607
H	-2.544388	-1.189791	-4.426921
H	-1.267193	-3.737050	-5.549187

$[Ru(bpy)_3]^{2+}$

E(B3LYP/6-311+G**)= -1541.7828268

C	-0.228327	2.923471	-0.064736
N	0.286025	1.901460	-0.805147
C	1.010867	2.186830	-1.907335
C	1.268571	3.488248	-2.321502
C	0.756293	4.542977	-1.567441
C	0.001442	4.253639	-0.434455
Ru	-0.091495	-0.094883	-0.150338
N	-1.846978	-0.404147	-1.266926
C	-2.522080	-1.552376	-0.984983
C	-3.659992	-1.911846	-1.711899
C	-4.108648	-1.089600	-2.743218
C	-3.404756	0.078309	-3.027249
C	-2.279013	0.381382	-2.266431
C	-1.964730	-2.367612	0.113156
N	-0.815468	-1.898131	0.676343
C	-0.234490	-2.586461	1.677582
C	-0.765717	-3.769882	2.177242
C	-1.943542	-4.260443	1.613442
C	-2.544921	-3.552583	0.575334
C	-1.036039	2.539347	1.114156
N	-1.173078	1.204520	1.323486
C	-1.903140	0.780799	2.369631

C	-2.528896	1.650314	3.257991
C	-2.391315	3.022379	3.052494
C	-1.637589	3.469345	1.970135
N	0.890755	-0.973104	-1.504879
C	2.208789	-1.163456	-1.233799
C	3.084329	-1.804202	-2.130191
C	4.441704	-1.974647	-1.798470
C	4.943321	-1.503671	-0.594243
C	4.101900	-0.839363	0.349231
C	2.736626	-0.688561	0.015497
N	1.831335	-0.077954	0.832633
C	2.263282	0.408128	1.998916
C	3.604726	0.303527	2.414630
C	4.528996	-0.321063	1.596189
H	1.522738	0.894116	2.626219
H	3.894608	0.716126	3.374814
H	5.568123	-0.413094	1.899554
H	5.994877	-1.637486	-0.355295
H	5.104775	-2.476524	-2.495569
H	2.688119	-2.164774	-3.074686
H	1.378592	1.334818	-2.466565
H	1.855763	3.661101	-3.216844
H	0.935203	5.573641	-1.856716
H	-0.409445	5.063755	0.154927
H	-1.983447	-0.293643	2.492865
H	-3.108635	1.255998	4.085543
H	-2.863328	3.735436	3.720873
H	-1.526184	4.533130	1.800075
H	-1.698095	1.274977	-2.457354
H	-3.711933	0.746370	-3.824404
H	-4.989292	-1.362369	-3.315729
H	-4.191211	-2.828708	-1.487134
H	0.681303	-2.166046	2.075136
H	-0.262310	-4.290748	2.984276

H	-2.389056	-5.182325	1.973678
H	-3.459425	-3.924986	0.130592

SIV.2. Photocatalytic experiments

Table SIV 1.2. The transitions which belong to the strong absorption band in the UV regions. Note that the OH and Cl group has the similar impact, which was in agreement with similar σ-electron withdrawing character.

Compound (transoid rotamer)	**Theoretical Λ_{abs} (nm)**	**transition**	**Intensity**
$[3,3'\text{-}Co(1,2\text{-}C_2B_9H_{11})_2]^-$	280	S0→S11	0.662
$[3,3'\text{-}Co(8\text{-}Cl\text{-}1,2\text{-}C_2B_9H_{10})(1,2\text{-}C_2B_9H_{11})]^-$	294	S0→S10	0.407
$[3,3'\text{-}Co(8\text{-}Cl\text{-}1,2\text{-}C_2B_9H_{10})_2]^-$	304	S0→S11	0.361
$[3,3'\text{-}Co(8\text{-}OH\text{-}1,2\text{-}C_2B_9H_{10})(1,2\text{-}C_2B_9H_{11})]^-$	296	S0→S10	0.339
$[3,3'\text{-}Co(8\text{-}OH\text{-}1,2\text{-}C_2B_9H_{10})_2]^-$	305	S0→S10	0.376

Figure SIV.2. a) Representative ^{1}H NMR spectrum ($CDCl_3$) of the product benzaldehyde and the substrate benzyl alcohol, using Na[3,3’-Co(1,2-$C_2B_9H_{11}$)$_2$] as catalyst in the photooxidation reaction after 8 hours. Conditions: catalyst (0.08 mM), substrate (20 mM), $Na_2S_2O_8$ (40 mM) 5 ml 0.1M phosphate buffer solution at pH=7.2 light at 8 h of irradiation. b) ^{1}H NMR spectrum of pure commercial benzyl alcohol. c) ^{1}H NMR spectrum of pure commercial benzaldehyde.

a)

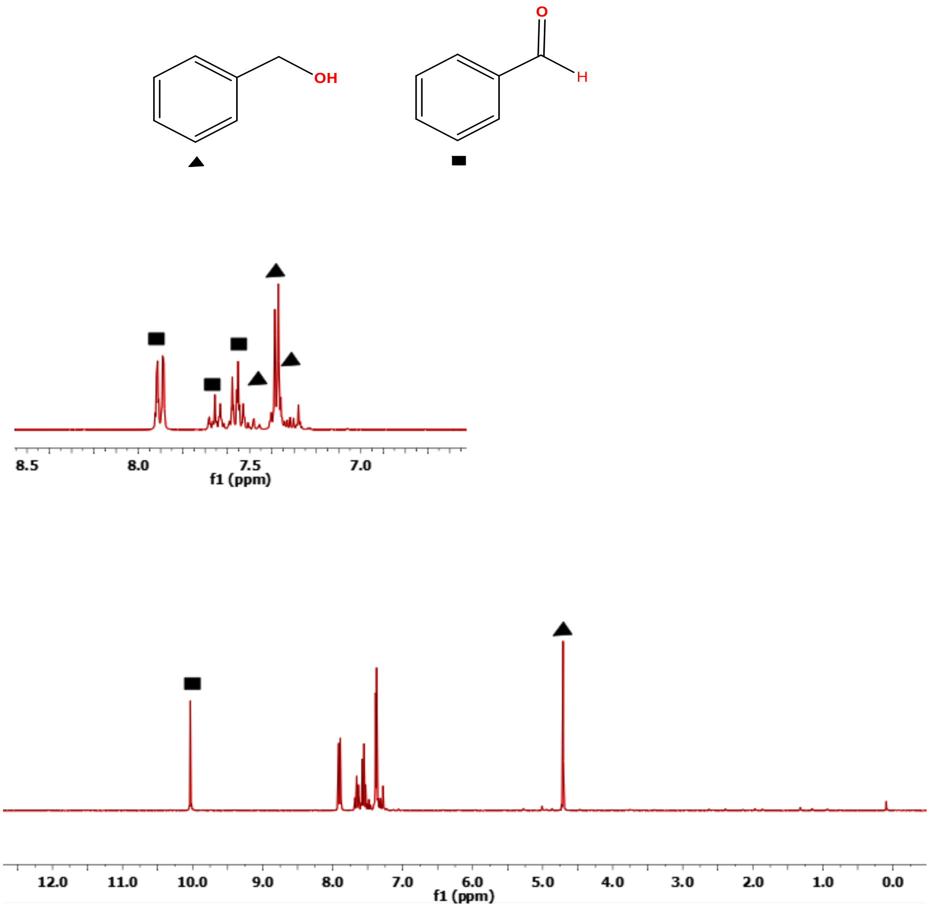

b)

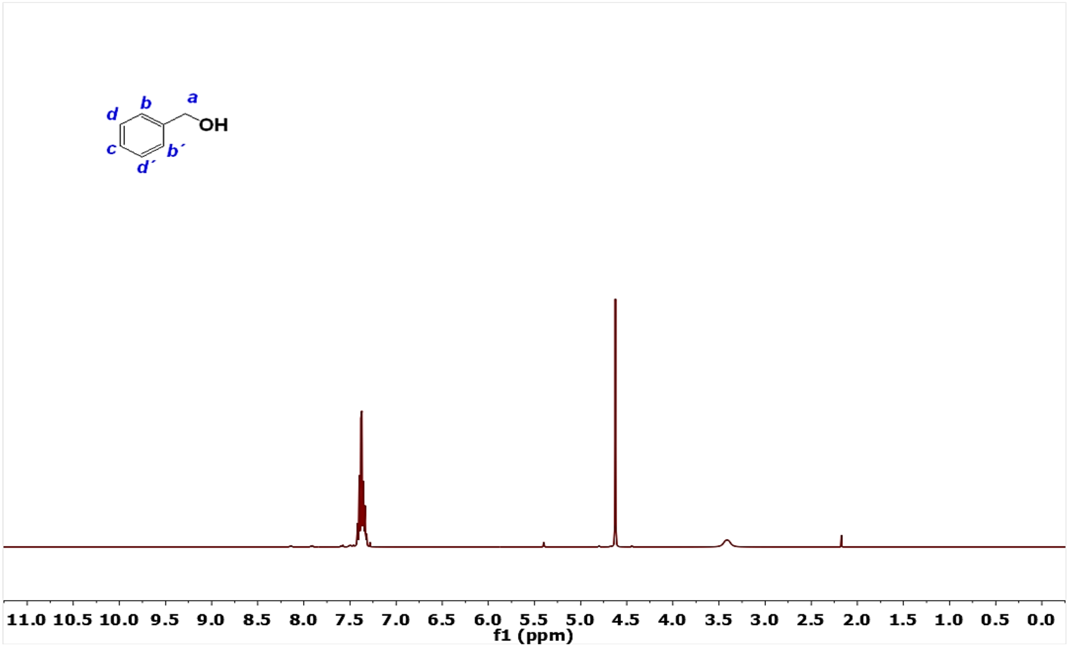

^{1}H NMR (400 MHz, $CDCl_3$) δ 7.46-7.29 (m, 5H), 4.62 (s, 1H).

c)

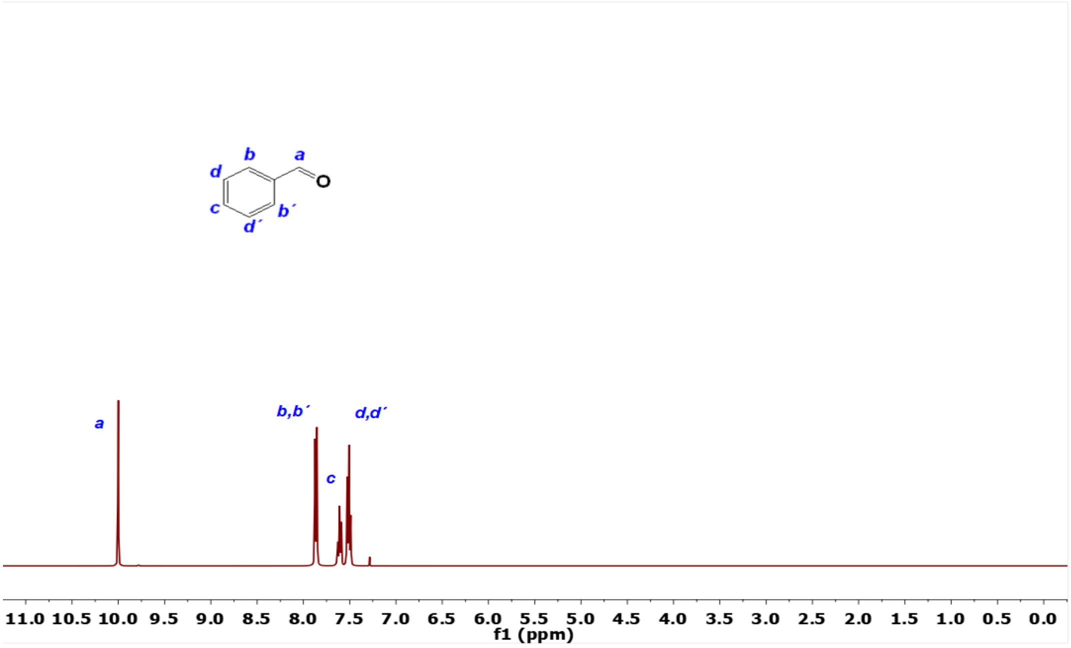

^{1}H NMR (400 MHz, CDCl$_3$) δ 10.00 (s, 1H), 7.86 (dt, *J* = 8.3, 1.0 Hz, 2H), 7.64 – 7.58 (m, 1H), 7.55 – 7.46 (m, 2H).

Figure SIV.3. a) Representative ^{1}H NMR spectrum ($CDCl_3$) of the product 4-methylbenzaldehyde and the substrate 4-methylbenzyl alcohol, using Na[3,3'-Co(1,2-$C_2B_9H_{11})_2$] as catalyst in the photooxidation reaction after 8 hours. Conditions: catalyst (0.08 mM), substrate (20 mM), $Na_2S_2O_8$ (40 mM) 5 ml 0.1M phosphate buffer solution at pH=7.2 light at 8 h of irradiation. b) ^{1}H NMR spectrum of pure commercial 4-methylbenzyl alcohol. c) ^{1}H NMR spectrum of pure commercial 4-methylbenzaldehyde.

a)

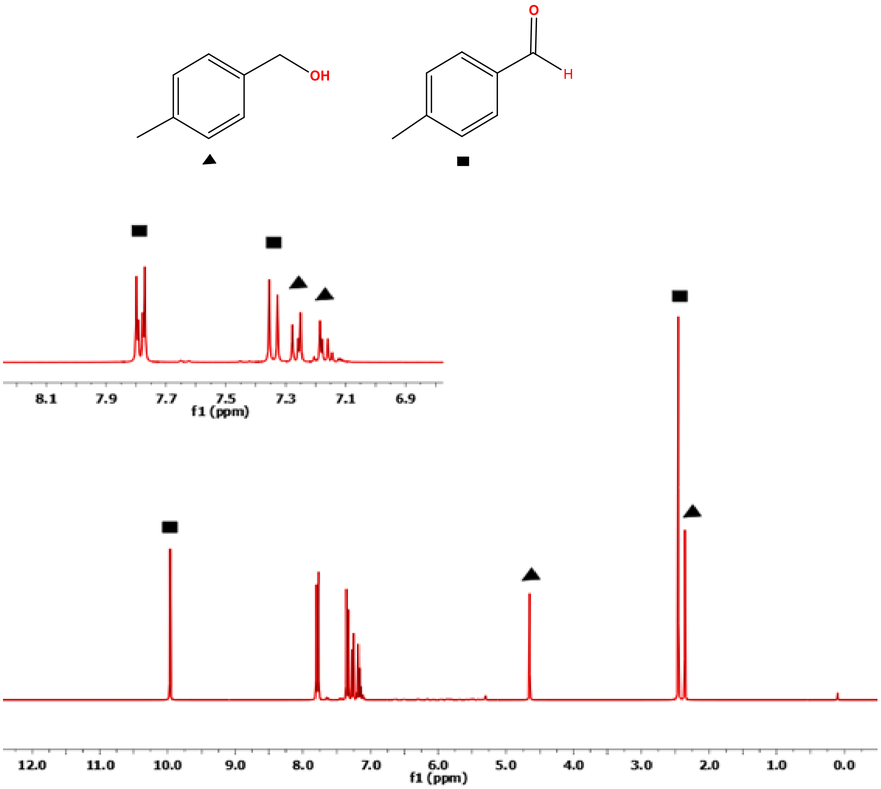

b)

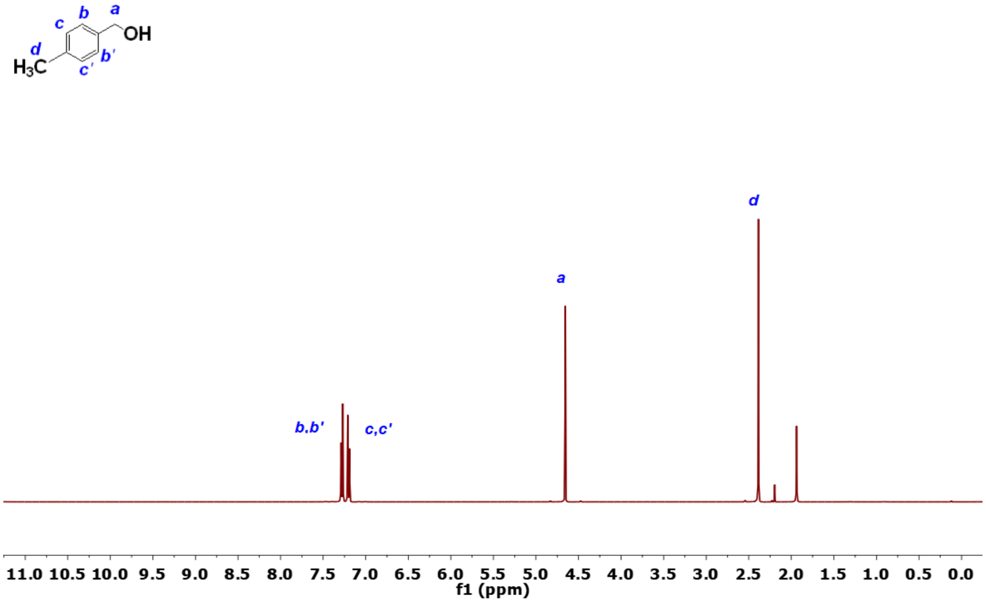

^{1}H NMR (400 MHz, $CDCl_3$) δ 7.27 (d, 2H, *J* = 8.1 Hz, 2H), 7.20 (d, *J* = 8.0, 2H), 4.65 (s, 2H), 2.39 (s, 3H).

c)

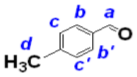
c
b
a
d
O
H3C
b'
c'

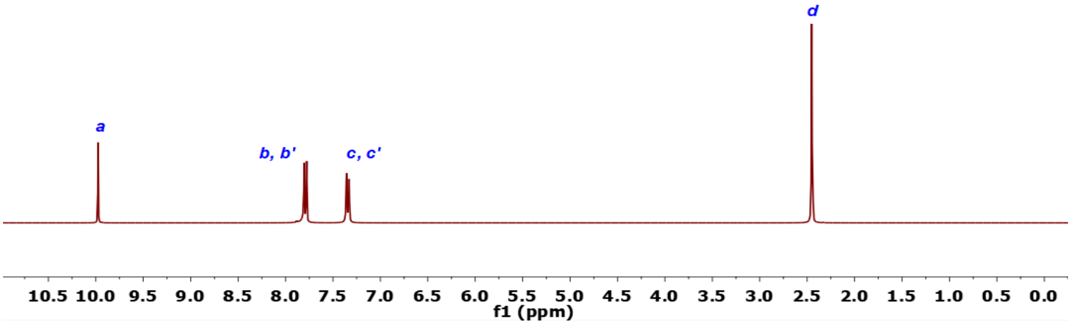

^{1}H NMR (400 MHz, $CDCl_3$) δ 9.98 (s, 1H), 7.79 (d, *J* = 8.1 Hz, 2H), 7.34 (d, *J* = 7.5 Hz, 2H), 2.45 (s, 3H).

Figure SIV.4. a) Representative ^{1}H NMR spectrum ($CDCl_3$) of 4-chlorobenzaldehyde and the substrate 4-chlorobenzyl alcohol, using Na[3,3'-Co(1,2-$C_2B_9H_{11}$)$_2$] as catalyst in the photooxidation reaction after 8 hours. Conditions: catalyst (0.08 mM), substrate (20 mM), $Na_2S_2O_8$ (40 mM) 5 ml 0.1M phosphate buffer solution at pH=7.2 light at 8 h of irradiation. b) ^{1}H NMR spectrum of pure commercial 4-chlorobenzyl alcohol. c) ^{1}H NMR spectrum of pure commercial 4-chlorobenzaldehyde.

a)

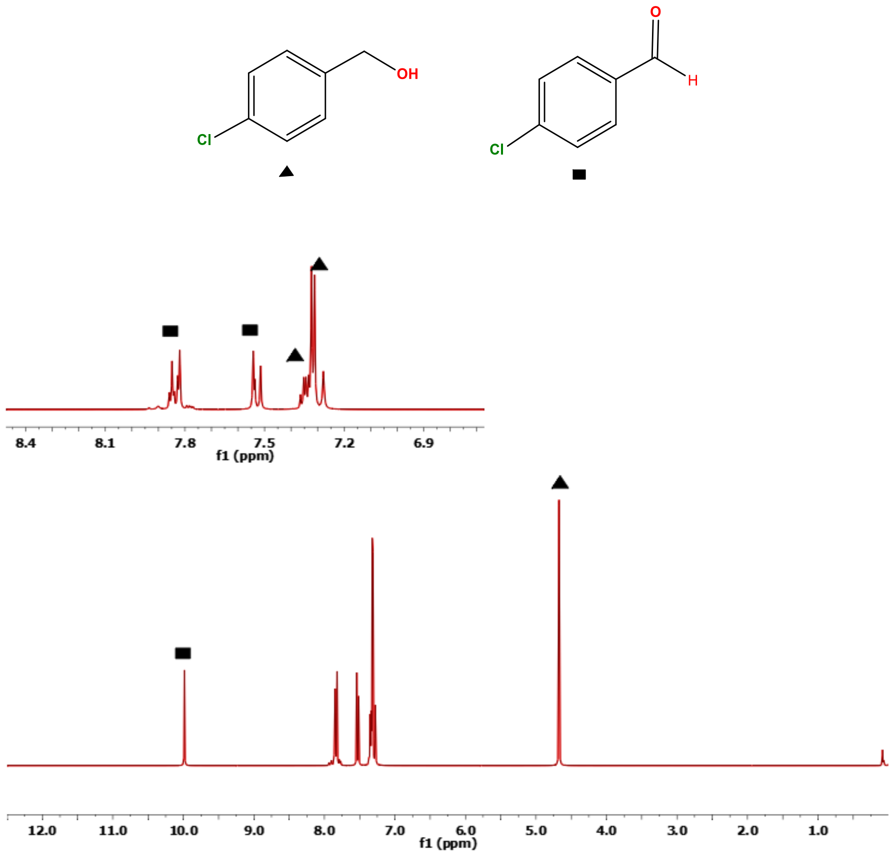

b)

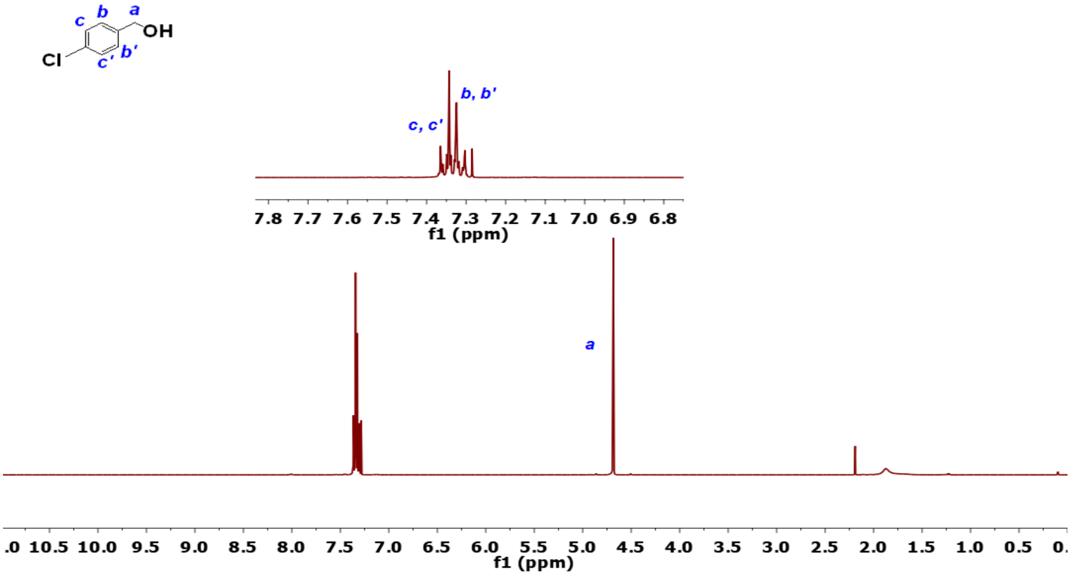

^{1}H NMR (400 MHz, $CDCl_3$) δ 7,39-7.29 (m, 4H), 4.68 (s, 2H, a).

c)

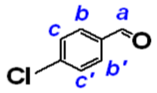

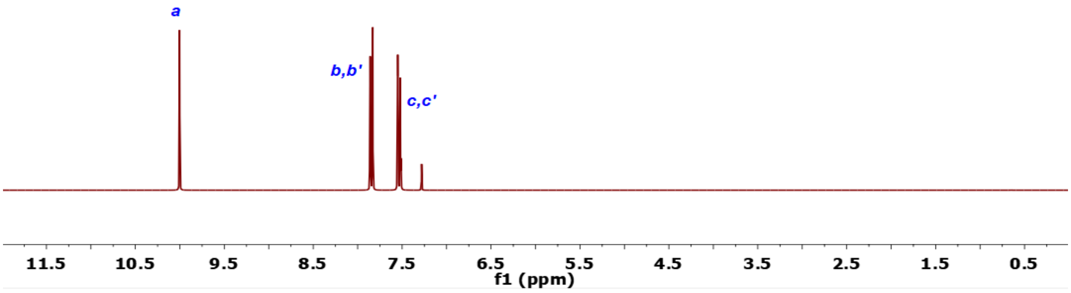

^{1}H NMR (360 MHz, $CDCl_3$) δ 10.00 (s, 1H), 7.88-7.81 (m, 2H), 7.57-7.50 (m, 2H).

Figure SIV.5. a) Representative ^{1}H NMR spectrum ($CDCl_3$) of the product benzophenone and the substrate diphenylmethanol, using $Na[3,3'-Co(1,2-C_2B_9H_{11})_2]$ as catalyst in the photooxidation reaction after 8 hours. Conditions: catalyst (0.08 mM), substrate (20 mM), $Na_2S_2O_8$ (40 mM) 5 ml 0.1M phosphate buffer solution at pH=7.2 light at 8 h of irradiation. b) ^{1}H NMR spectrum of pure commercial diphenylmethanol. c) ^{1}H NMR spectrum of pure commercial benzophenone.

a)

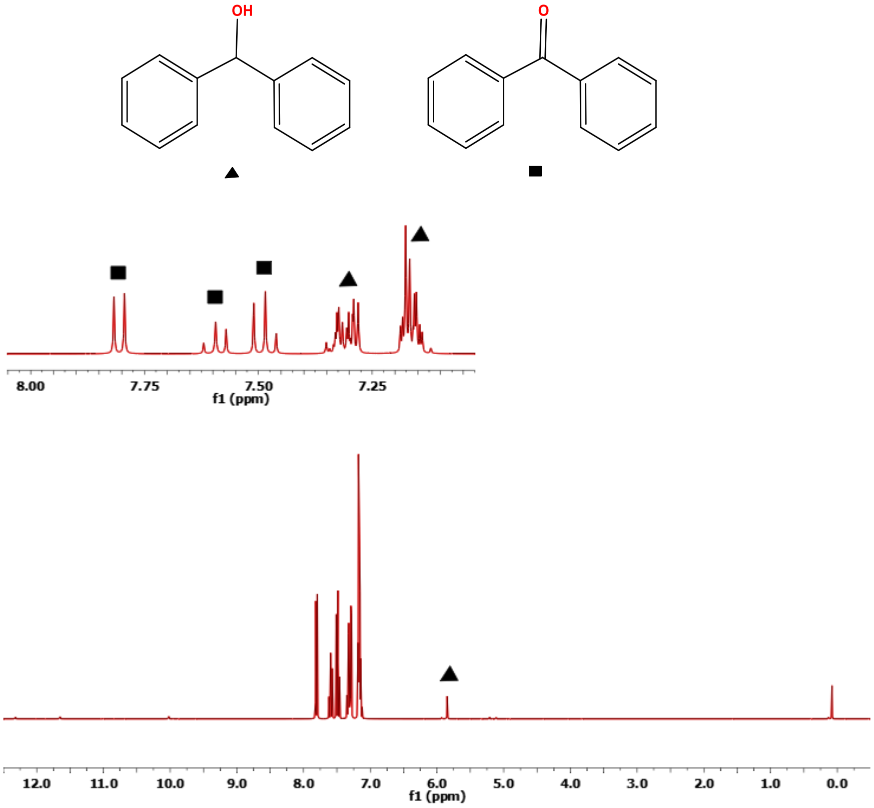

b)

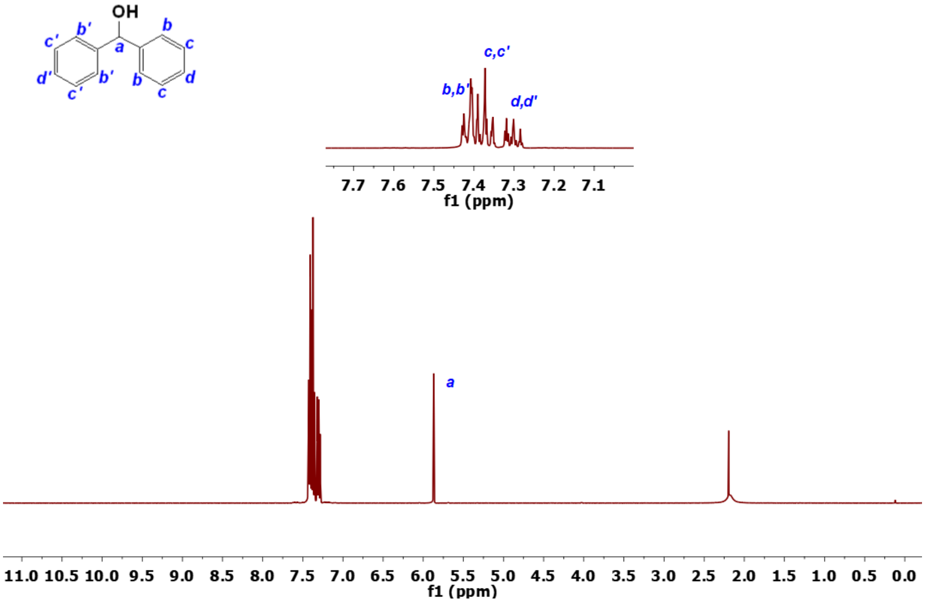

^{1}H NMR (400 MHz, $CDCl_3$) δ 7.45 – 7.34 (m, 8H), 7.33 – 7.27 (m, 2H), 5.87 (s, 1H).

c)

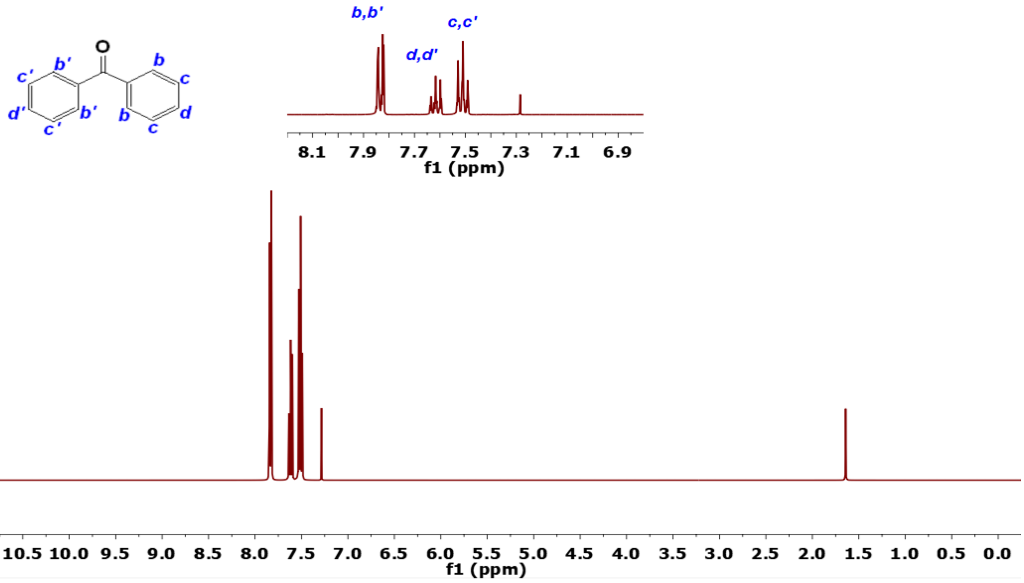

^{1}H NMR (400 MHz, $CDCl_3$) δ 7.87-7.80 (m, 4H), 7.65-7.58 (m, 2H), 7.51 (dddd, *J* = 8.2, 6.6, 1.5, 1.0 Hz, 4H).

Figure SIV.6. Representative chromatogram corresponding to the photooxidation tests of different alcohols performed with cobaltacarborane complex Na[3,3'-Co(1,2-$C_2B_9H_{11}$)$_2$]. Conditions: catalyst (0.08 mM), substrate (20 mM), $Na_2S_2O_8$ (40 mM) 5 ml 0.1M phosphate buffer solution at pH=7.2 light at 8 h of irradiation.

a) **1**:CH_2Cl_2, **2**: acetophenone, **3**: 1-phenylethanol, **4**: biphenyl (internal standard).

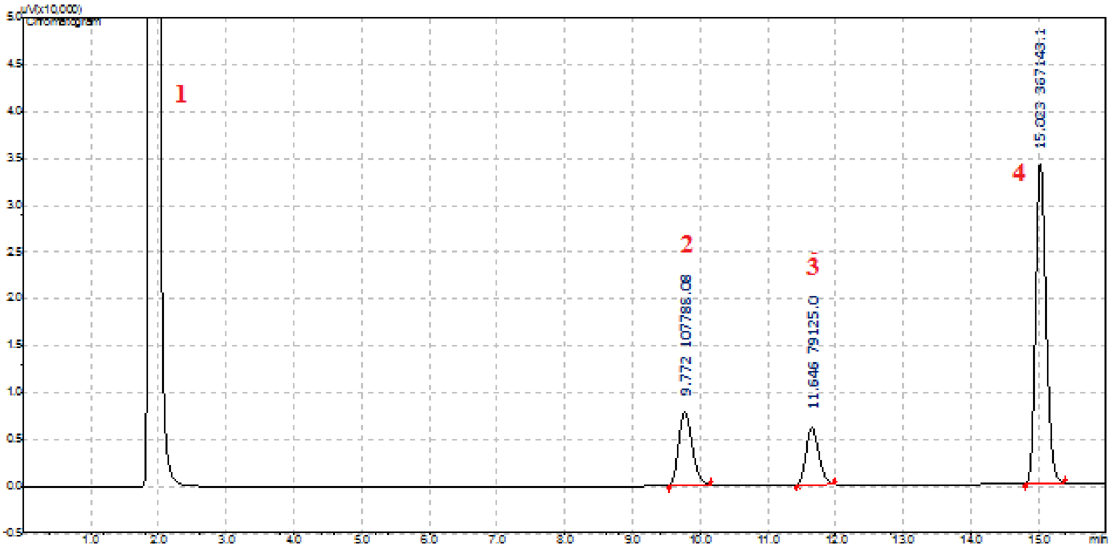

b) **1**:CH_2Cl_2, **2**: benzylaldehyde, **3**: benzyl alcohol, **4**: biphenyl (internal standard).

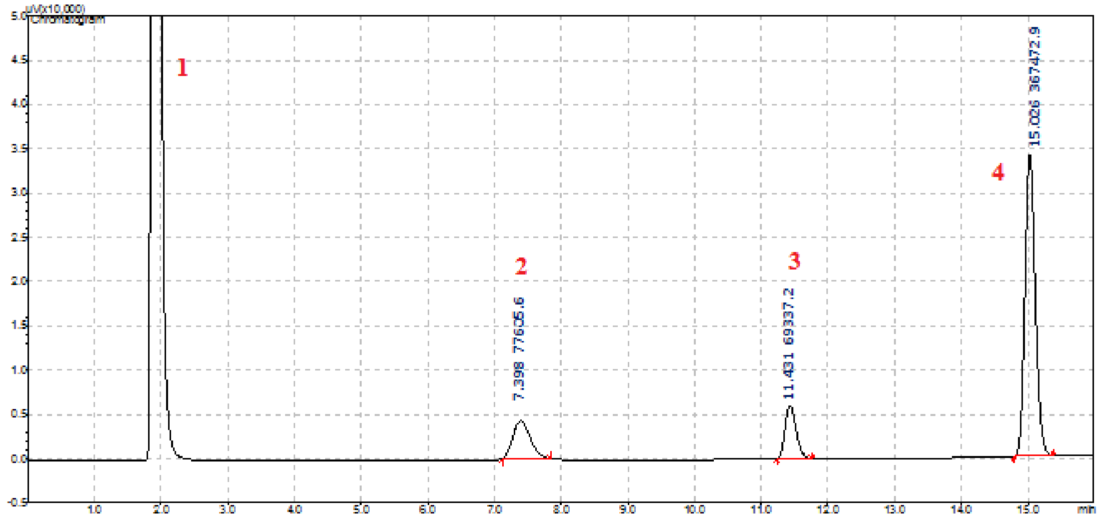

c) **1**:CH_2Cl_2, **2**: *p*-Toualdehyde, **3**: 4-Methylbenzyl alcohol, **4**: biphenyl (internal standard).

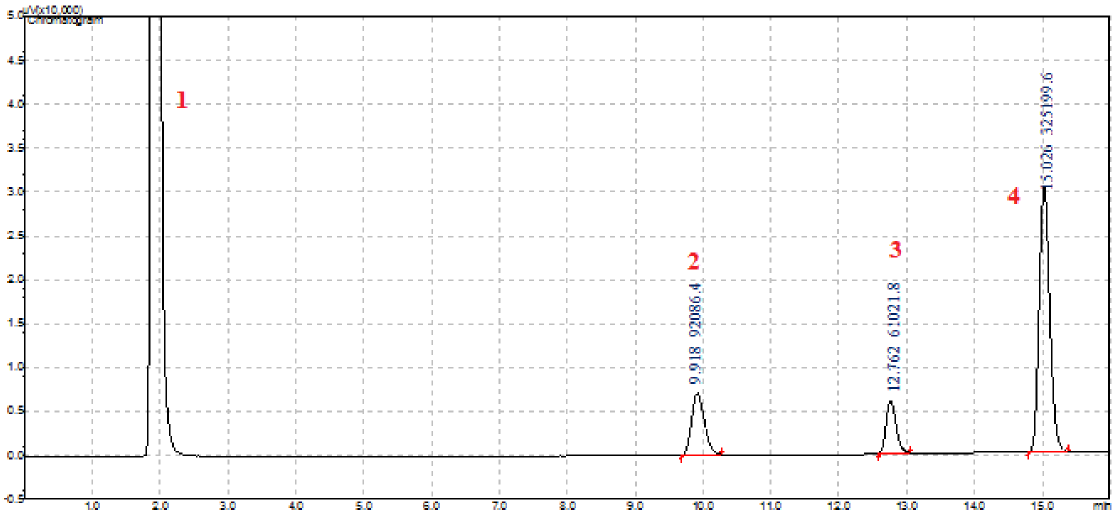

d) **1**:CH_2Cl_2, **2**: *4*-Chlorobenzaldehyde, **3**: naphtalene (internal standard), **4**: 4- Chlorobenzyl alcohol.

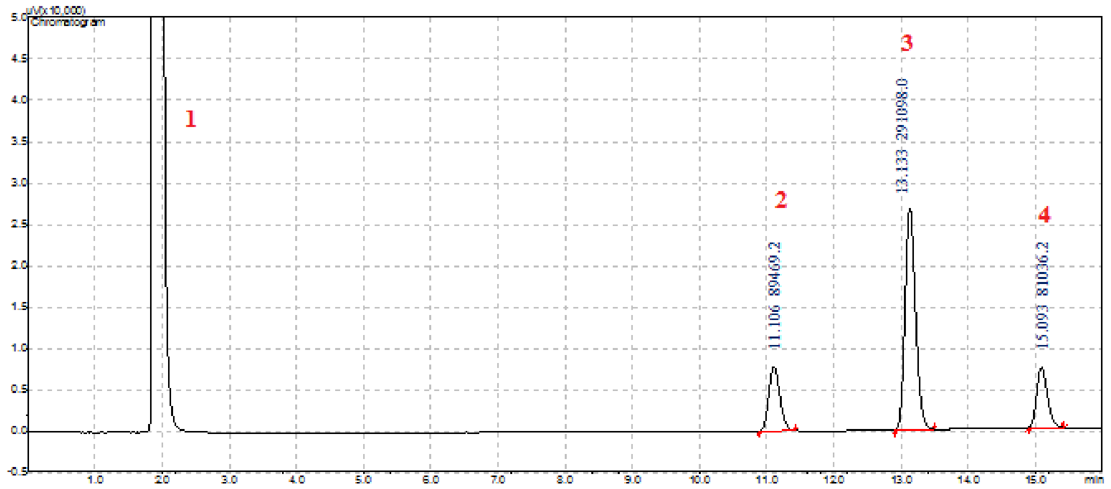

Figure SIV.7. Representative^{1}H NMR spectrum ($CDCl_3$) corresponding to the photooxidation of 1-phenylethanol, using Na[3,3'-Co(1,2-$C_2B_9H_{11})_2$] as catalyst. Conditions: Na[3,3'-Co(1,2-$C_2B_9H_{11})_2$] (0.002 mM), substrate (20 mM), $Na_2S_2O_8$ (40 mM), 5 mL potassium carbonate solution at pH=7. Light irradiation 8h.

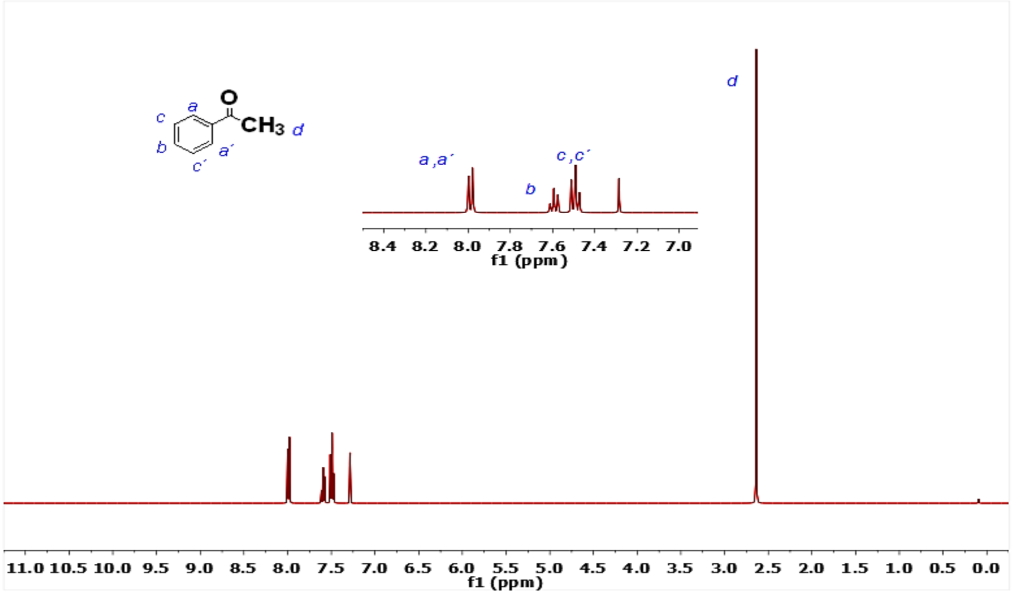

^{1}H NMR (360 MHz, $CDCl_3$) δ 8.07 – 7.90 (m, 2H), 7.59 (dd, *J* = 8.4, 6.5 Hz, 1H), 7.53 – 7.38 (m, 2H), 2.63 (s, 3H).

Figure SIV.8. ^{1}H NMR spectrum ($CDCl_3$) corresponding to the photooxidation of benzylalcohol, using Na[3,3'-Co(1,2-$C_2B_9H_{11})_2$] as catalyst. Conditions: Na[3,3'-Co(1,2-$C_2B_9H_{11})_2$] (0.02 mM), substrate (20 mM), $Na_2S_2O_8$ (40 mM), 5 mL potassium carbonate solution at pH=7. Light irradiation 8h.

a)

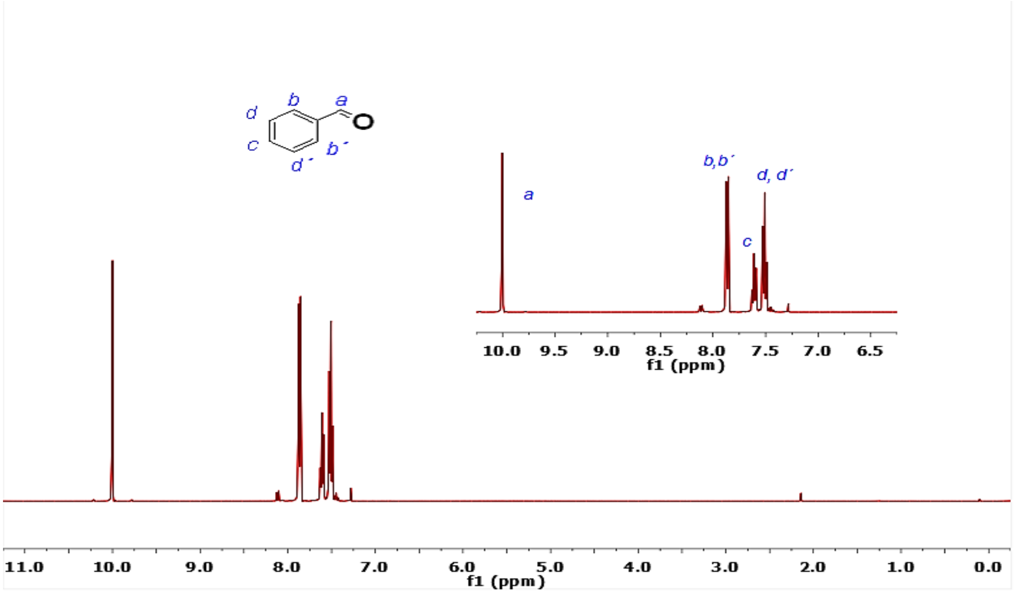

^{1}H NMR (400 MHz, $CDCl_3$) δ 10.00 (s, 1H), 7.92-7.83 (m, 2H), 7.65 – 7.56 (m, 1H), 7.54 – 7.47 (m, 2H).

Figure SIV.9. ^{1}H NMR spectrum ($CDCl_3$) corresponding to the photooxidation of 4-methylbenzylalcohol, using Na[3,3'-Co(1,2-$C_2B_9H_{11}$)$_2$] as catalyst. Conditions: Na[3,3'-Co(1,2-$C_2B_9H_{11}$)$_2$] (0.002 mM), substrate (20 mM), $Na_2S_2O_8$ (40 mM), 5 mL potassium carbonate solution at pH=7. Light irradiation 8h.

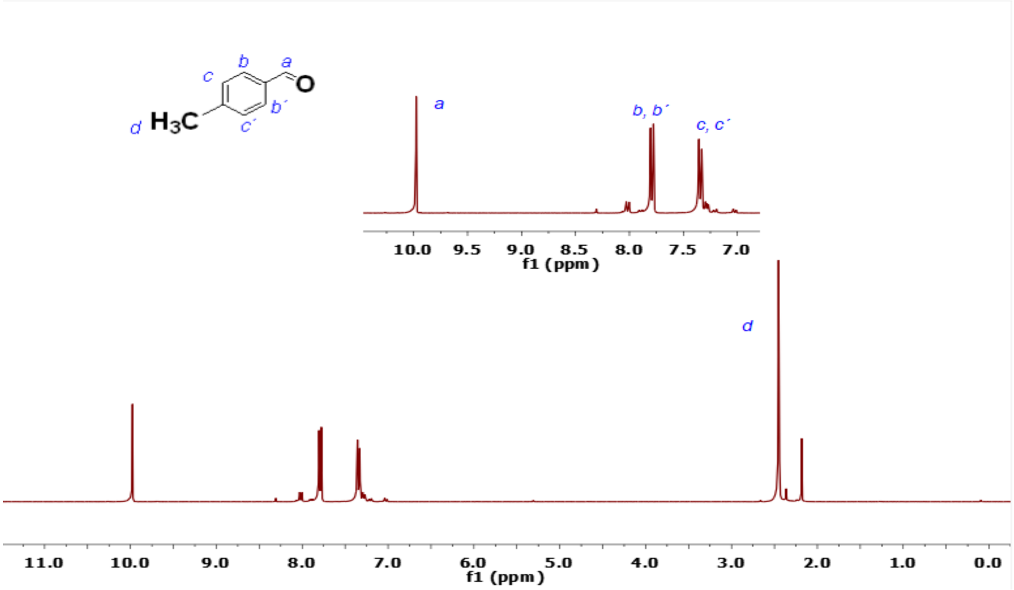

^{1}H NMR (300 MHz, $CDCl_3$) δ 9.98 (s, 1H), 7.85 – 7.72 (m, 2H), 7.34 (d, *J* = 7.6 Hz, 2H), 2.45 (s, 3H).

Figure SIV.10. ^{1}H NMR spectrum ($CDCl_3$) corresponding to the photooxidation of 4-chlorobenzylalcohol, using Na[3,3'-Co(1,2-$C_2B_9H_{11}$)$_2$] as catalyst. Conditions: Na[3,3'-Co(1,2-$C_2B_9H_{11}$)$_2$] (0.002 mM), substrate (20 mM), $Na_2S_2O_8$ (40 mM), 5 mL potassium carbonate solution at pH=7. Light irradiation 8h.

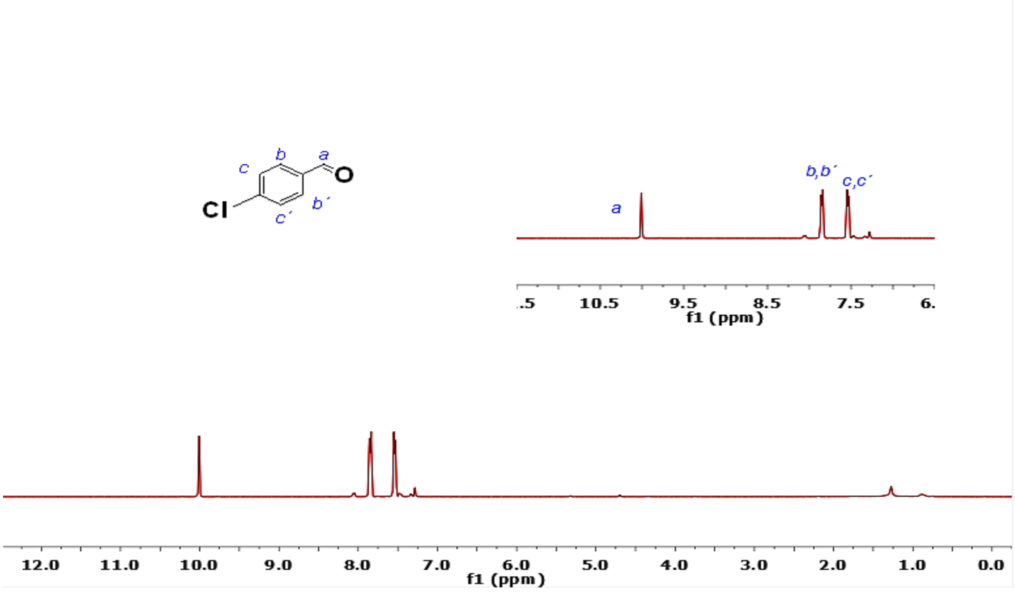

^{1}H NMR (400 MHz, $CDCl_3$) δ 10.01 (s, 1H), 7.85 (d, *J* = 7.9 Hz, 2H), 7.54 (d, *J* = 7.5 Hz, 2H).

Figure SIV.11. ^{1}H NMR spectrum ($CDCl_3$) corresponding to the photooxidation of diphenylmethanol, using $Na[3,3'\text{-}Co(1,2\text{-}C_2B_9H_{11})_2]$ as catalyst. Conditions: $Na[3,3'\text{-}Co(1,2\text{-}C_2B_9H_{11})_2]$ (0.002 mM), substrate (20 mM), $Na_2S_2O_8$ (40 mM), 5 mL potassium carbonate solution at pH=7. Light irradiation 8h.

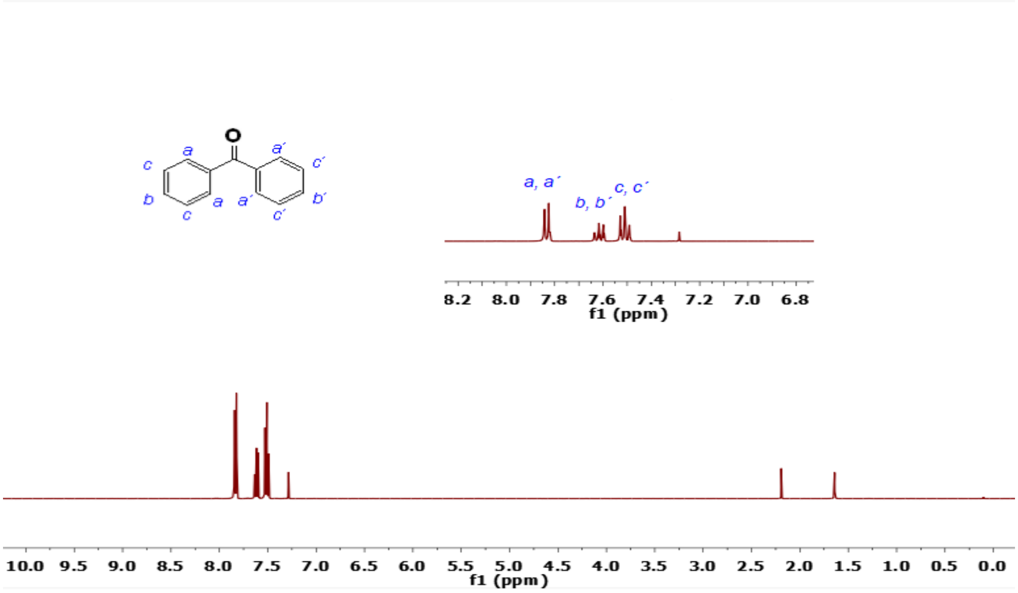

^{1}H NMR (400 MHz, $CDCl_3$) δ 7.87 – 7.81 (m, 4H), 7.66 – 7.58 (m, 2H), 7.51 (dddd, *J* = 8.2, 6.6, 1.5, 1.0 Hz, 4H).

Figure SIV.12. a) Representative ^{1}H NMR spectrum ($CDCl_3$) corresponding to the photooxidation of hexanol, using $Na[3,3'\text{-}Co(1,2\text{-}C_2B_9H_{11})_2]$ as catalyst. Conditions: $Na[3,3'\text{-}Co(1,2\text{-}C_2B_9H_{11})_2]$ (0.002 mM), substrate (20 mM), $Na_2S_2O_8$ (40 mM), 5 mL potassium carbonate solution at pH=7. Light irradiation 8h. b) ^{1}H NMR spectrum of pure commercial 1-hexanol. c) ^{1}H NMR spectrum of pure commercial Hexanoic acid.

a)

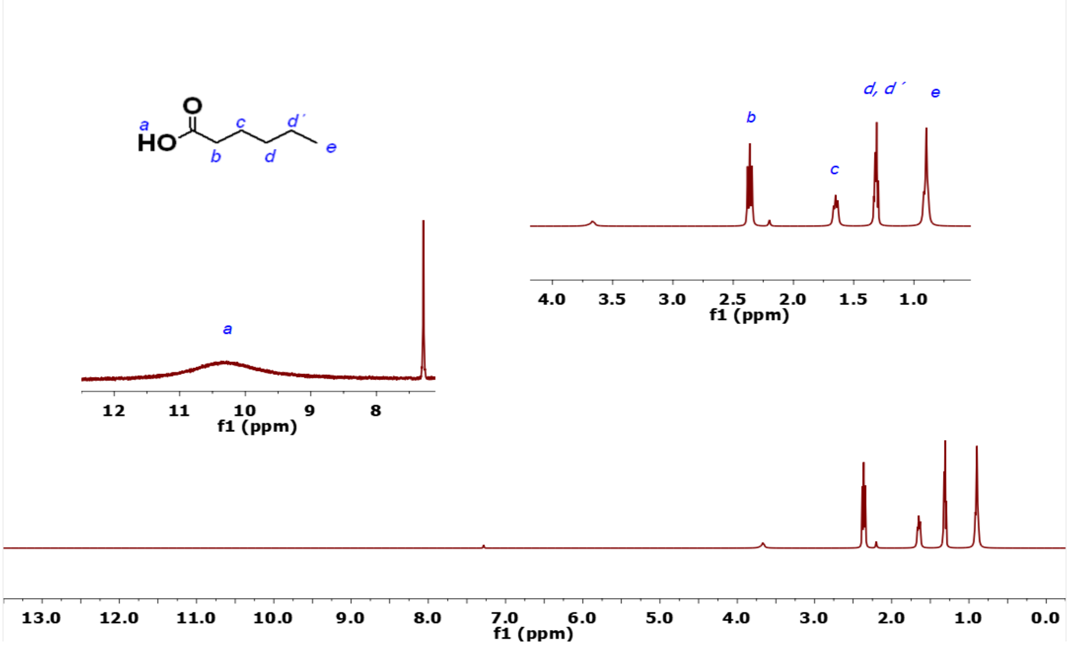

^{1}H NMR (400 MHz, $CDCl_3$) δ 10.34 (br, 1H, COOH), δ 2.36-2.29 (m, 2H), 1.67 (t, *J* = 8.1 Hz, 2H), 1.38 – 1.29 (m, 4H), 0.91 (t, *J* = 6.9 Hz, 3H).

b)

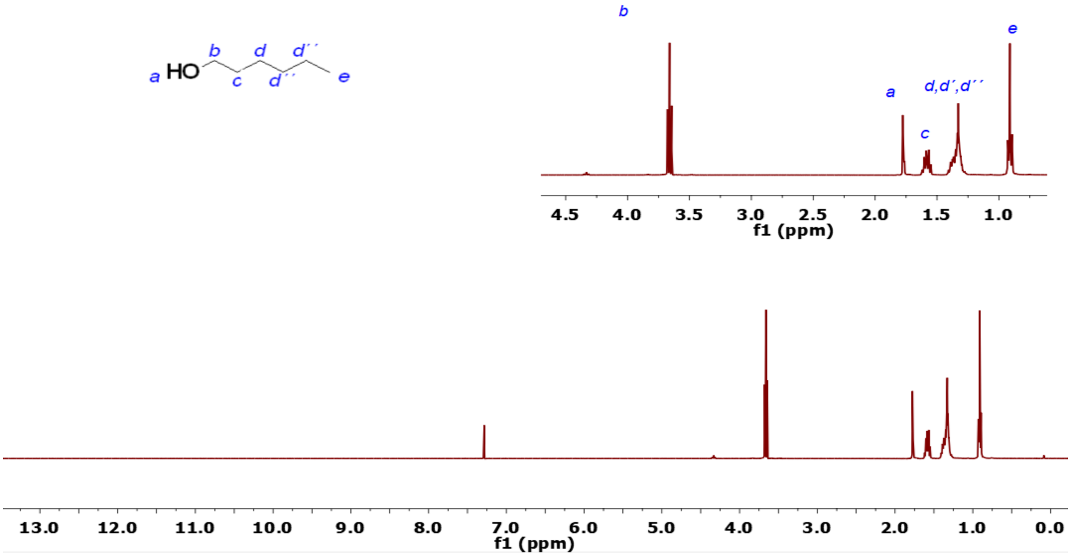

^{1}H NMR (400 MHz, CDCl$_3$) δ 3.66(t, *J* = 6.7 Hz, 2H), δ 1.78 (br, 1H, OH), 1.64-152 (m, 2H), 1.44 – 1.23 (m, 2H), 0.93-0.89 (m, 3H).

c)

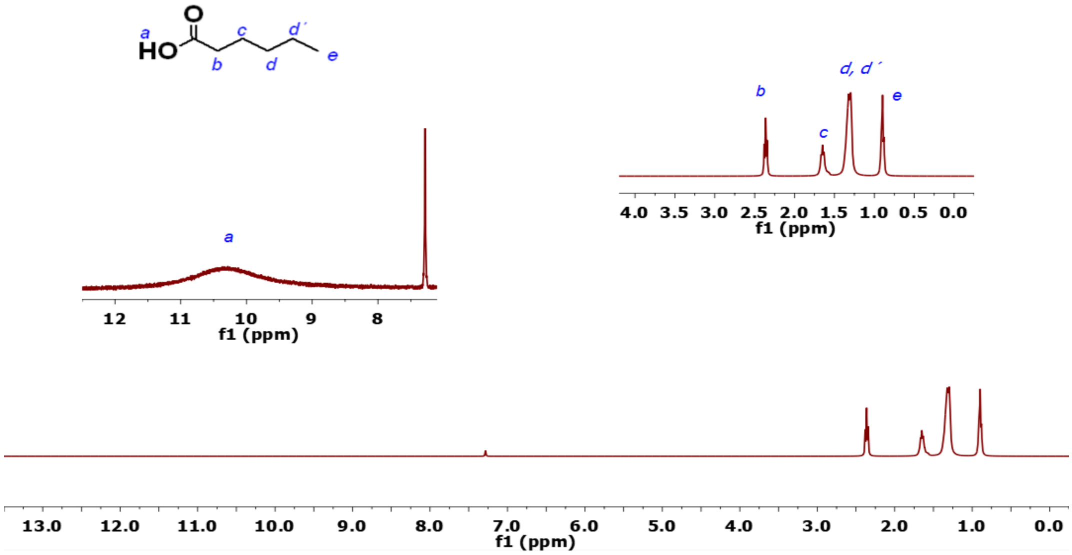

^{1}H NMR (400 MHz, CDCl$_3$) δ 10.34 (s, 1H, COOH), 2.36 (t, *J* = 7.5 Hz, 2H), 1.65 (t, *J* = 8.0 Hz, 3H), 1.41 – 1.23 (m, 4H), 0.90 (t, *J* = 6.9Hz, 3H).

Figure SIV.13. a) Representative ^{1}H NMR spectrum ($CDCl_3$) corresponding to the photooxidation of 2-ethoxyethanol, using $Na[3,3'\text{-}Co(1,2\text{-}C_2B_9H_{11})_2]$ as catalyst. Conditions: $Na[3,3'\text{-}Co(1,2\text{-}C_2B_9H_{11})_2]$ (0.002 mM), substrate (20 mM), $Na_2S_2O_8$ (40 mM), 5 mL potassium carbonate solution at pH=7. Light irradiation 8h. b) ^{1}H NMR spectrum of pure commercial 2-ethoxyethanol.

a)

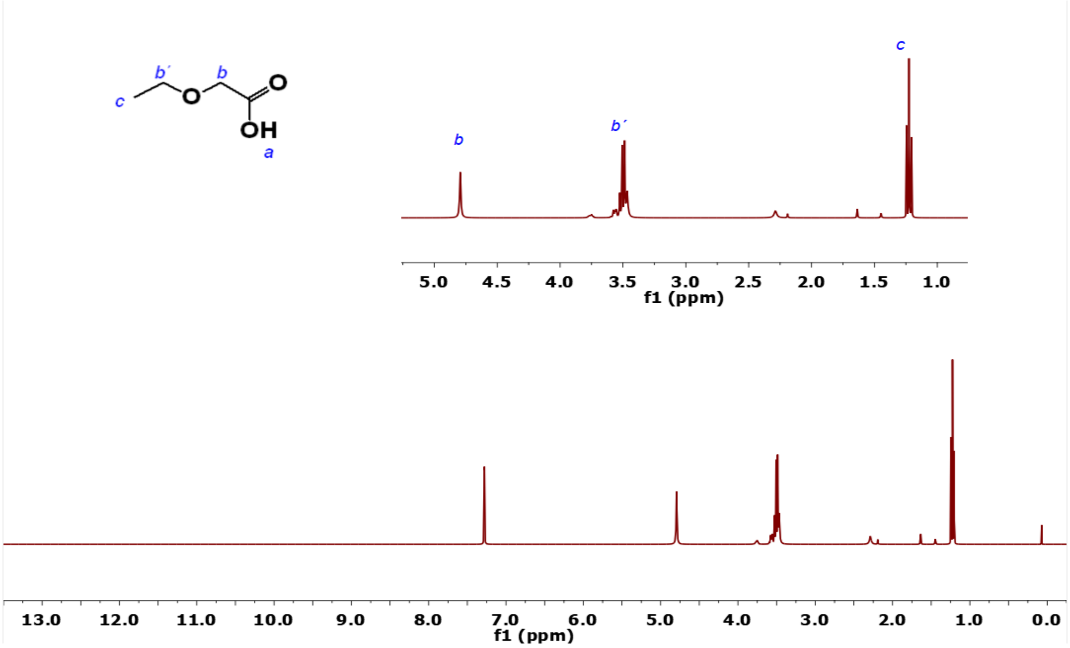

^{1}H NMR (360 MHz, $CDCl_3$) δ 4.79 (s, 2H), 3.50 (q, *J* = 7.0 Hz, 2H, 1.22 (t, *J* = 7.0 Hz, , *3H*).

b)

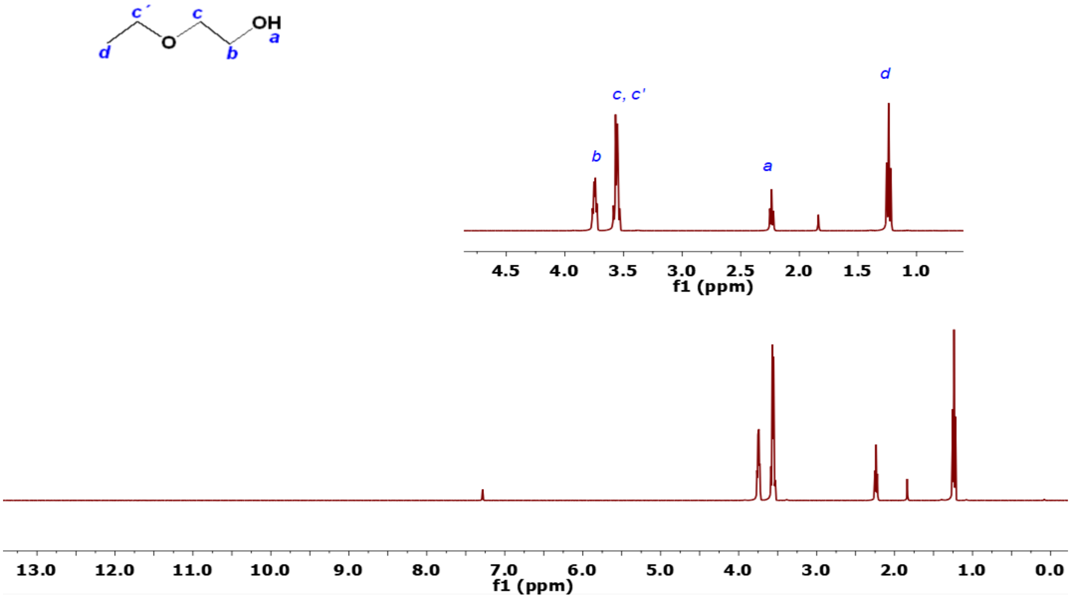

^{1}H NMR (400 MHz, $CDCl_3$) δ 3.79-3.71 (m, 2H), 3.61-3.51 (m, 4H), 2.24 (td, *J* = 6.1, 1.4 Hz, OH), 1.24 (td, *J* = 7.0, 1.4 Hz, 3H).

Figure SIV.14. a) Representative ^{1}H NMR spectrum ($CDCl_3$) corresponding to the photooxidation of cyclohexanol, using Na[3,3’-Co(1,2-$C_2B_9H_{11}$)$_2$] as catalyst. Conditions: Na[3,3’-Co(1,2-$C_2B_9H_{11}$)$_2$] (0.002 mM), substrate (20 mM), $Na_2S_2O_8$ (40 mM), 5 mL potassium carbonate solution at pH=7. Light irradiation 8h. b) ^{1}H NMR spectrum of pure commercial cyclohexanol.

a)

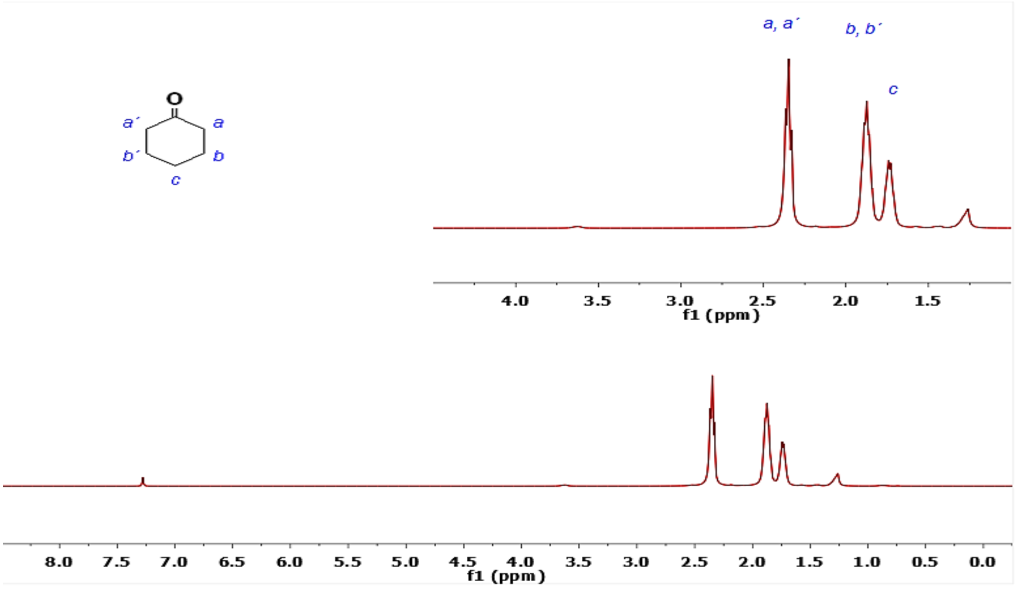

^{1}H NMR (360 MHz, $CDCl_3$) δ 2.35 (t, *J* = 6.6 Hz, 4H), 1.87 (p, *J* = 6.1 Hz, 4H), 1.74 (td, *J* = 7.0, 3.6 Hz, 2H).

b)

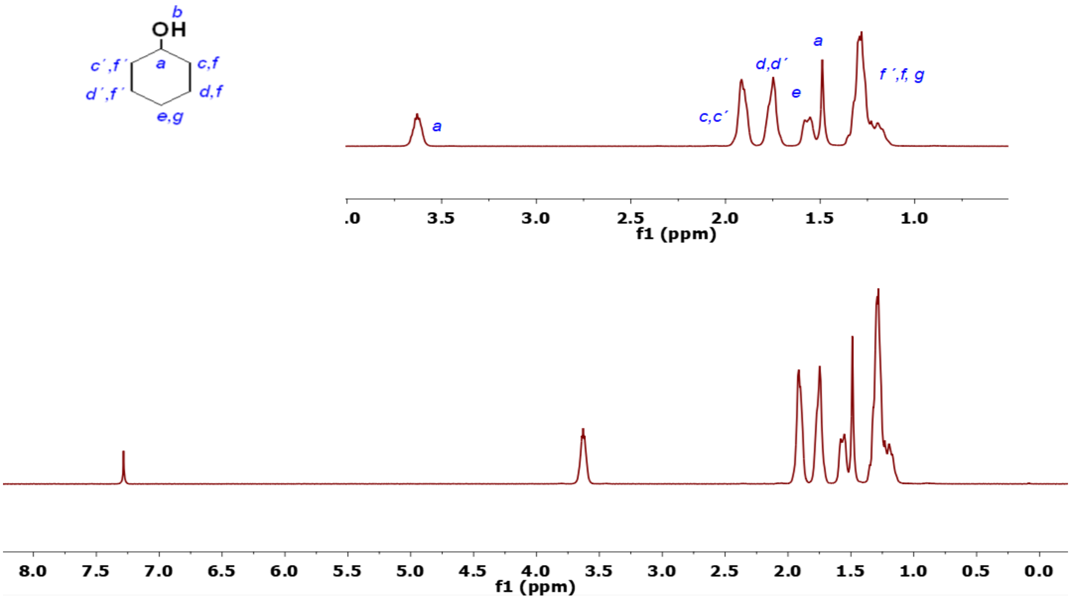

^{1}H NMR (400 MHz, $CDCl_3$) δ 3.63 (dt, *J* = 9.2, 4.8 Hz, 1H), 1.91 (dt, *J* = 10.9, 5.1 Hz, 2H), 1.84 – 1.66 (m, 2H), 1.64 – 1.41 (m, 2H), 1.40 – 1.11 (m, 5H).

c)

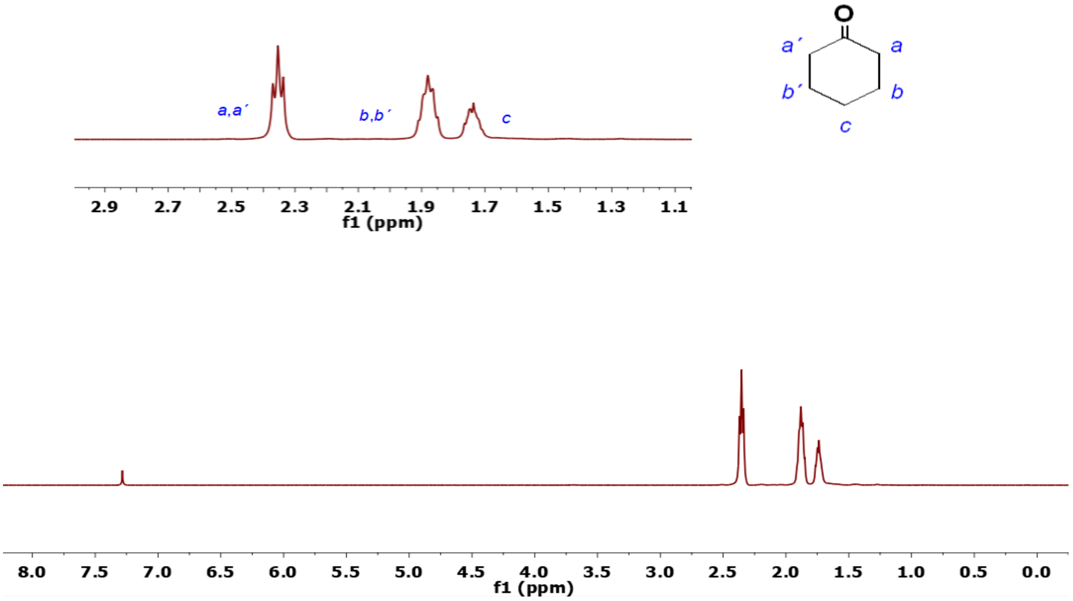

^{1}H NMR (400 MHz, $CDCl_3$) δ 2.35 (t, *J* = 6.6 Hz, 4H), 1.87 (p, *J* = 6.1 Hz, 4H), 1.79-1.68 (m, 2H).

ANNEX II. Supporting Information

Chapter IV.2

Figure SIV.15. a) Synthesis of Fe_3O_4 core (MNP) using co-precipitation method. b) Synthesis of Fe_3O_4 @SiO_2 core (MSNP) using co-precipitation method.

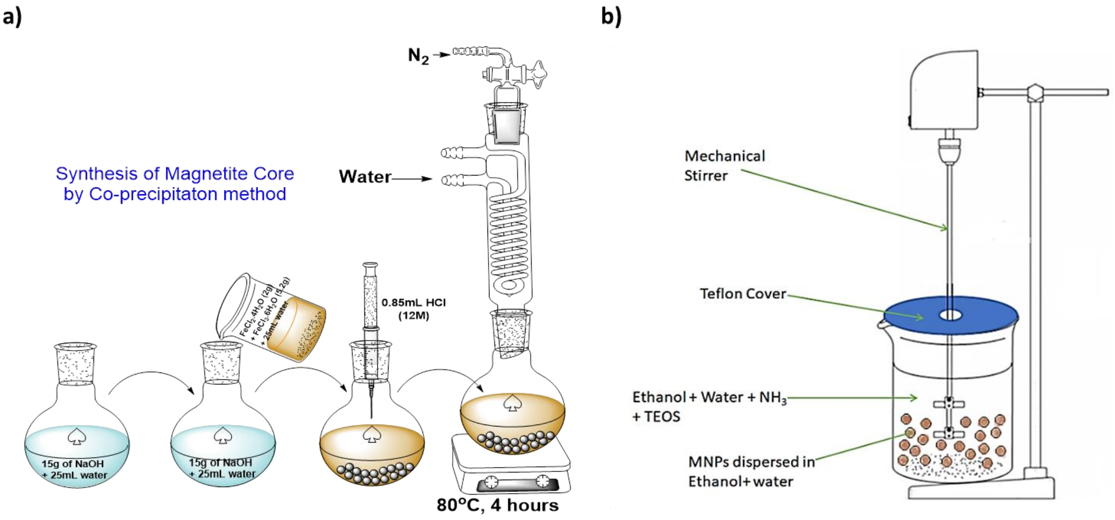
a)
b)
N2
Synthesis of Magnetite Core
by Co-precipitaton method
Water
$FeCl_2.4H_2O$ (2g)
+ $FeCl_3.6H_2O$ (5.2g)
+ 25mL water
0.85mL HCl
(12M)
15g of NaOH
+ 25mL water
15g of NaOH
+ 25mL water
80°C, 4 hours
Mechanical
Stirrer
Teflon Cover
Ethanol + Water + NH3
+ TEOS
MNPs dispersed in
Ethanol+water

Figure SIV.16. TEM images of a) MSNPs, b) Gaussian size graphs of MSNPs (9.34 nm), c) MSNPs-NH_2 (11.22 nm), and d) MSNPs-NH2@H**[1]** (14.17 nm)

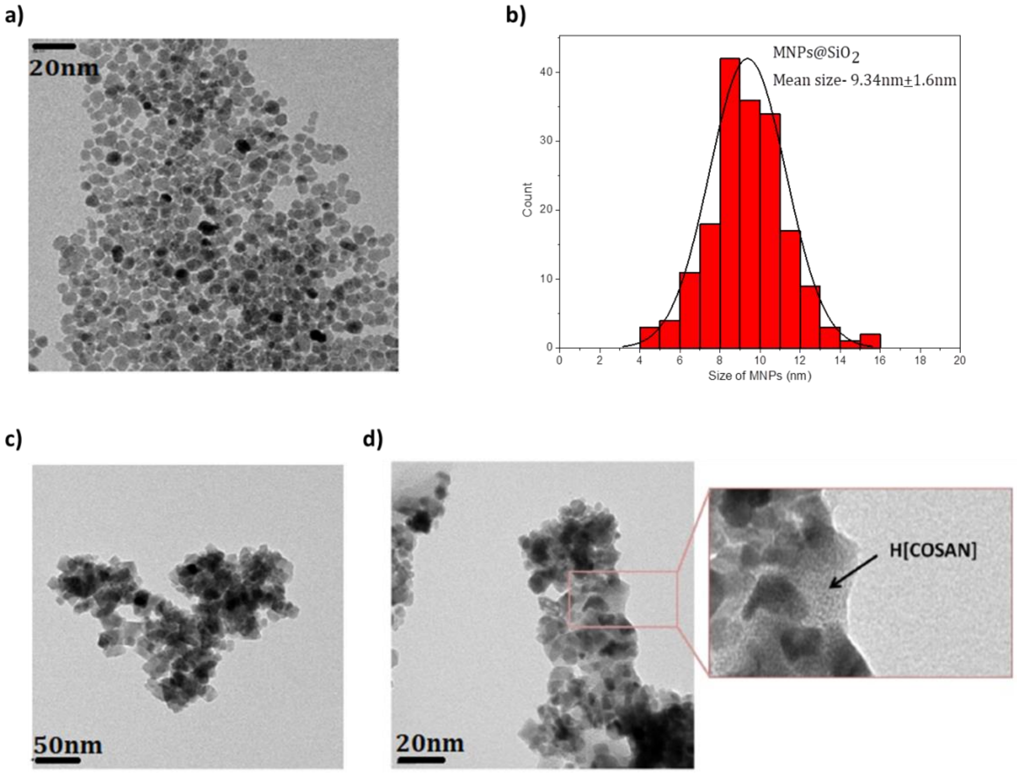

Figure SIV.17. Hysteresis cycles recorded at room temperature (300 K) for MSNPs-NH_2 and MSNPs-NH_2@**H[1].**

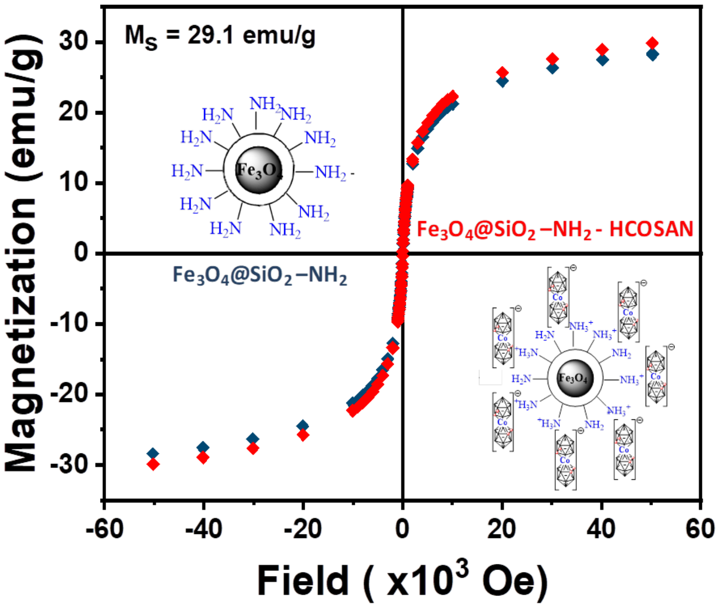

Table SIV 2.3. Stability of $Fe_3O_4@SiO_2$-NH_2 with different surfactants.

Surfactant	ζ-Potential
Citric acid	-15.6mV
Tricaprylyl methyl ammonium chloride	-26.8mV
Cetyl trimethyl ammonium chloride (CTAC)	-22.6mV
Tetrabutyl ammonium chloride	-36.9mV
Dimethyl di-n-octadecyl ammonium chloride	-54.2mV

Figure SIV.18. Stability of $Fe_3O_4@SiO_2-NH_2$ based on the measurement of the ζ-potential upon increasing amounts of dimethyl di-n-octadecyl ammonium chloride.

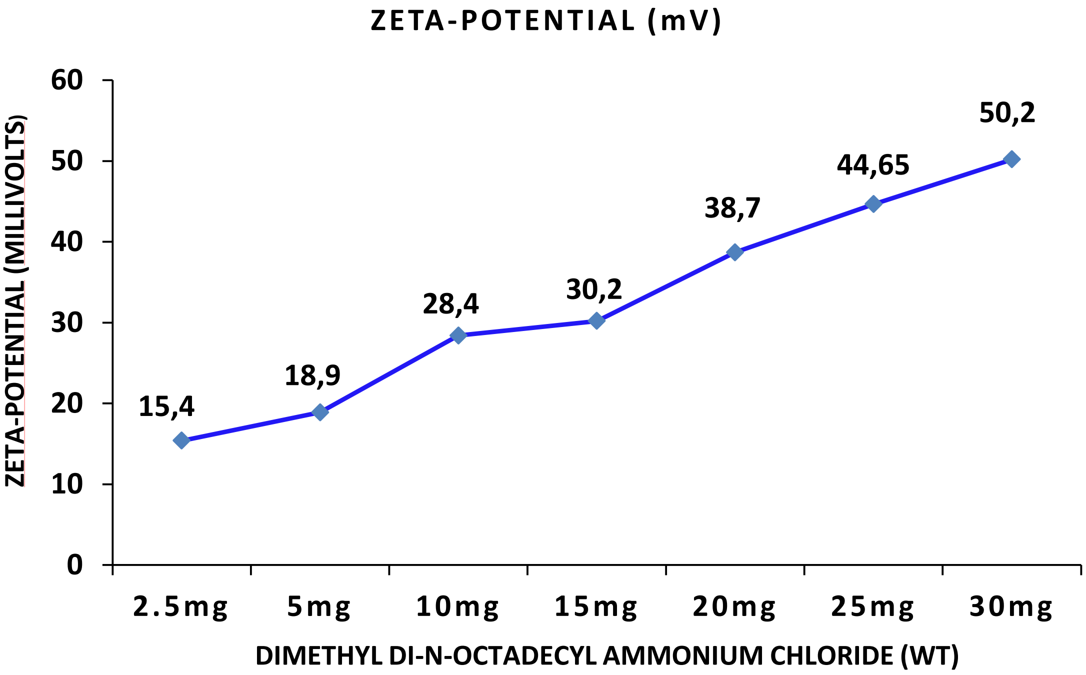

Figure SIV.19. SEM images of MSNP-NH_2@**H[1]**, a) before the photooxidation of 1-phenylethanol and b) after twelve reuses.

a)

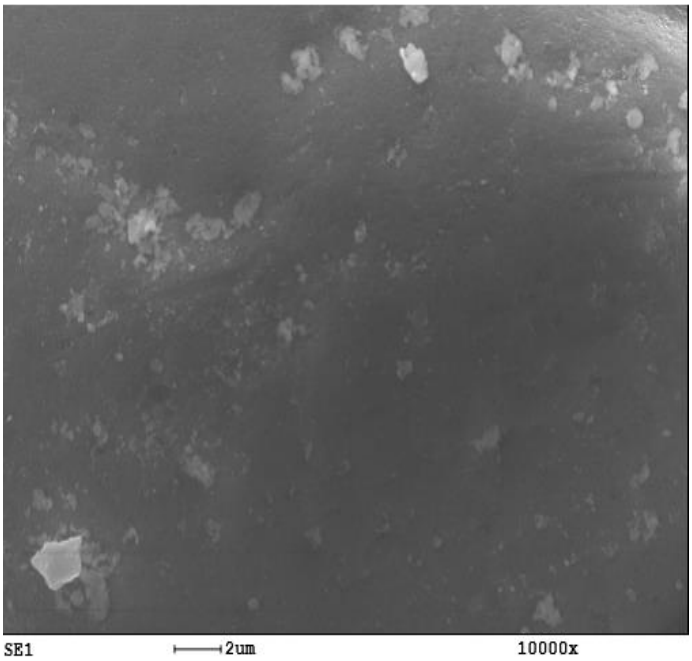
SE1
2um
10000x

b)

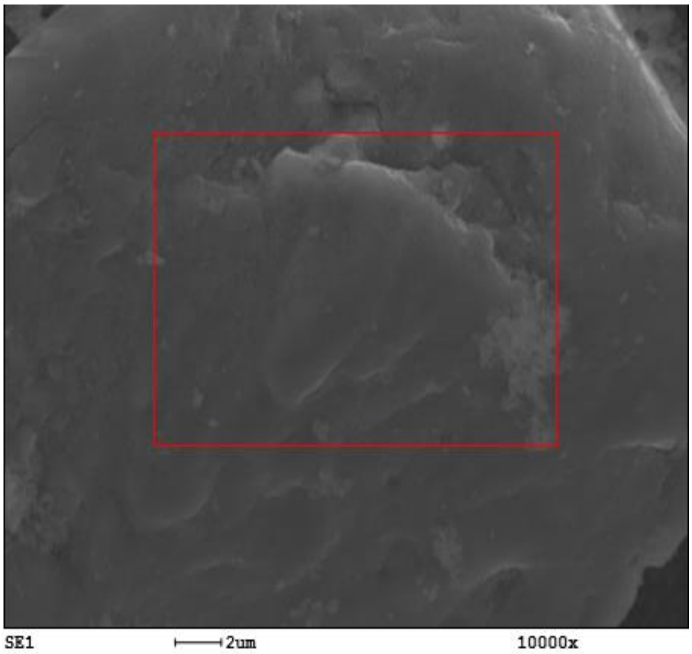
SE1
2um
10000x

Figure SIV.20. a) Representative ^{1}H NMR spectrum ($CDCl_3$) corresponding to the photooxidation of 1-butanol, using MSNPs-NH2@**H[1]** as catalyst. Conditions: **[1]** (0.02 mM), substrate (20 mM), $Na_2S_2O_8$ (40 mM), 5 mL potassium carbonate solution at pH=7. Light irradiation 8h. b) ^{1}H NMR spectrum of pure commercial 1-butanol**.** c) ^{1}H NMR spectrum of pure commercial butanoic acid.

a)

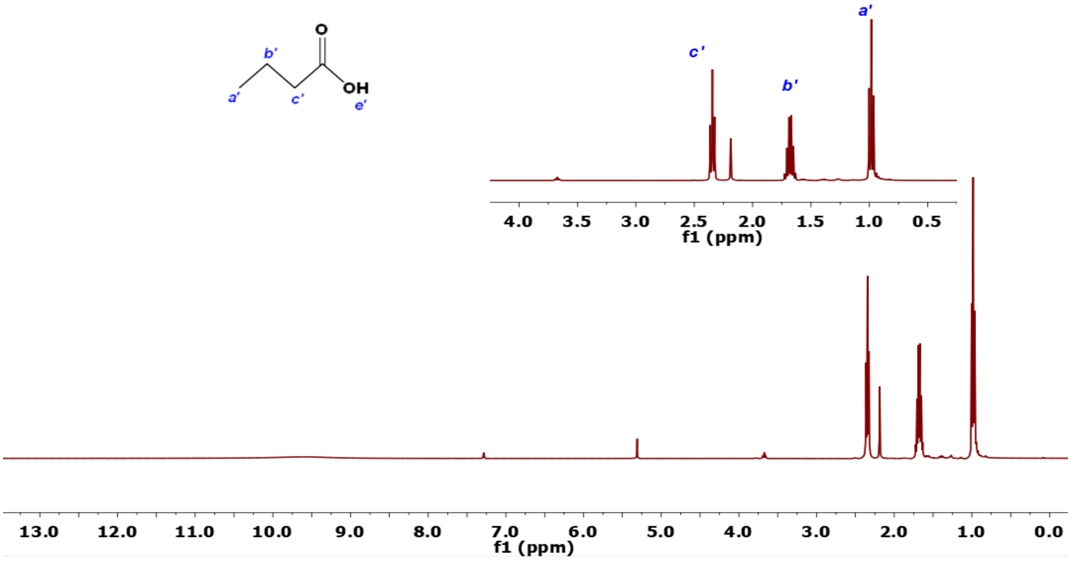

^{1}H NMR (400 MHz, $CDCl_3$) δ 9.60 (br, 1H), 2.34 (t, *J* = 7.4 Hz, 2H), 1.68 (h, *J* = 7.4 Hz, 2H), 1.02 – 0.96 (m, 3H).

b)

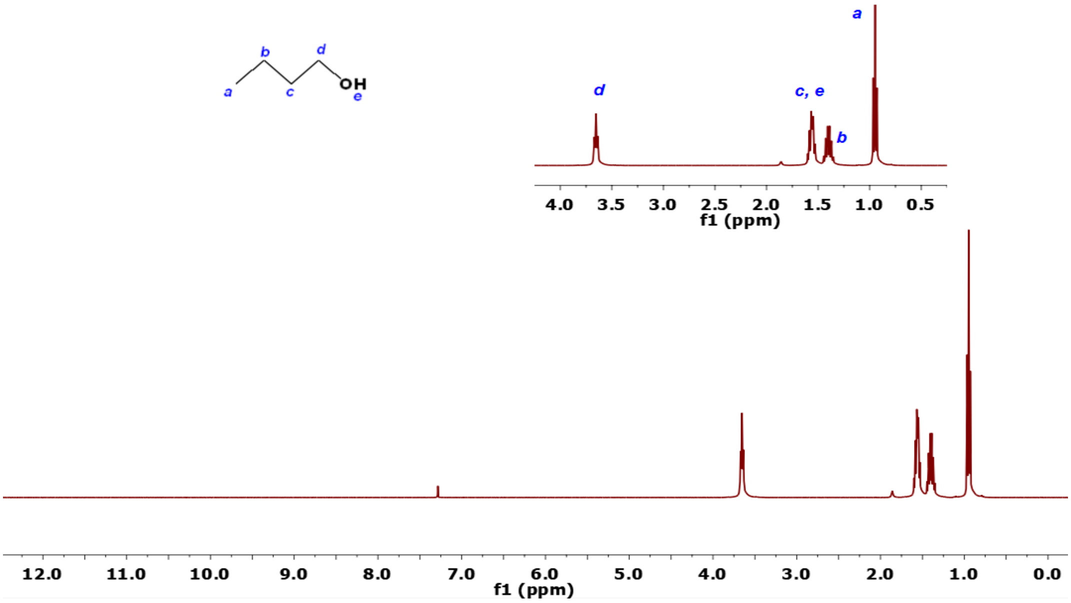

^{1}H NMR (400 MHz, $CDCl_3$) δ 3.65 (t, *J* = 6.6 Hz, 2H), 3.99 – 0.41 (m, 0H), 1.57 (tt, *J* = 8.6, 6.3 Hz, 3H), 1.44 – 1.29 (m, 2H), 0.95 (t, *J* = 7.4 Hz, 3H).

c)

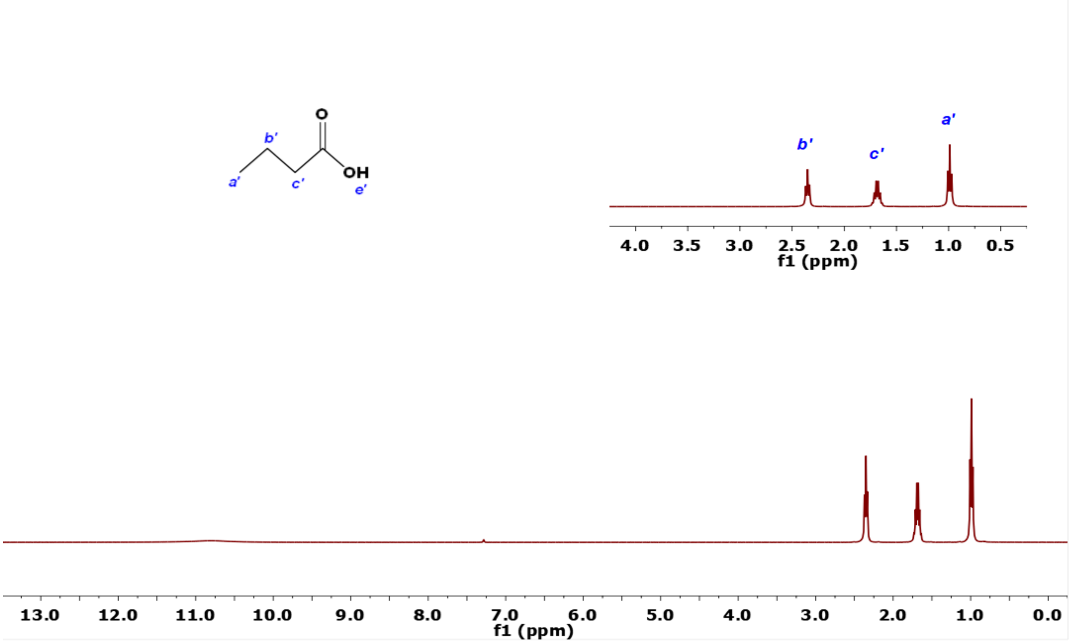

^{1}H NMR (400 MHz, CDCl$_3$) δ 10.79 (s, 1H), 2.35 (t, *J* = 7.4 Hz, 2H), 1.68 (h, *J* = 7.3 Hz, 2H), 0.99 (t, *J* = 7.4 Hz, 3H).

Figure SIV.21. a) Representative ^{1}H NMR spectrum (CDCl$_3$) corresponding to the photooxidation of Isobutyl alcohol, using MSNPs-NH2@**H[1]** as catalyst. Conditions: **[1]** (0.02 mM), substrate (20 mM), $Na_2S_2O_8$ (40 mM), 5 mL potassium carbonate solution at pH=7. Light irradiation 8h. b) ^{1}H NMR spectrum of pure commercial Isobutyl alcohol**.** c) ^{1}H NMR spectrum of pure commercial Isobutiric acid.

a)

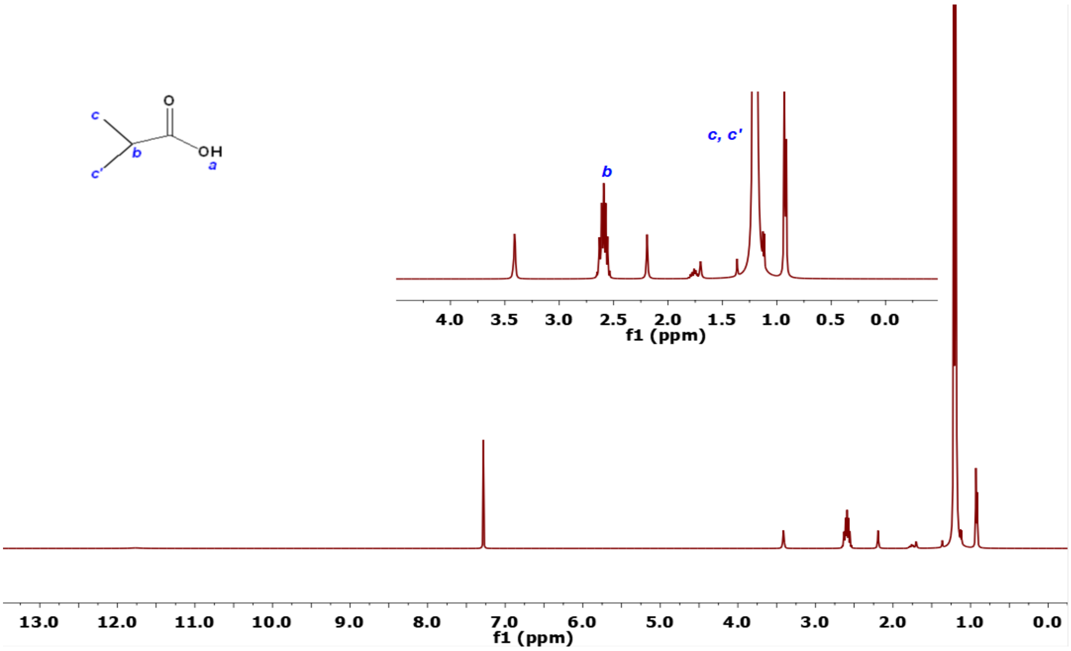

^{1}H NMR (360 MHz, CDCl$_3$) δ 2.58 (dq, *J* = 13.3, 7.2 Hz, 1H), 1.20 (d, *J* = 8.6 Hz, 6H).

b)

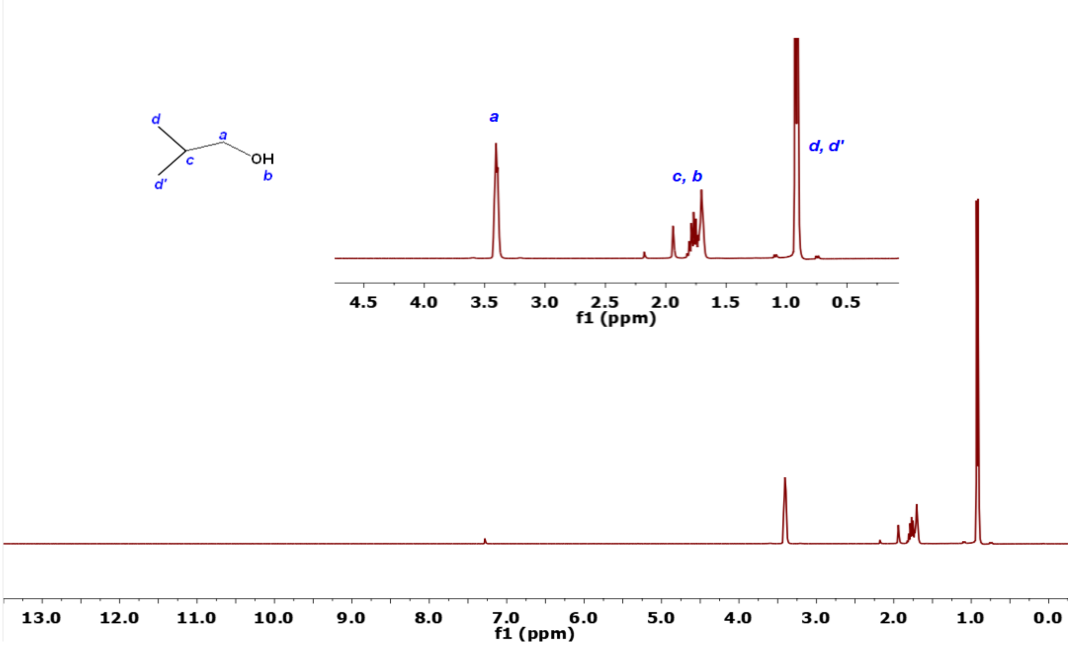

^{1}H NMR (360 MHz, CDCl$_3$) δ 3.40 (d, *J* = 5.6 Hz, 1H), 1.84 – 1.65 (m, 1H), 0.92 (d, *J* = 6.8 Hz, 1H).

c)

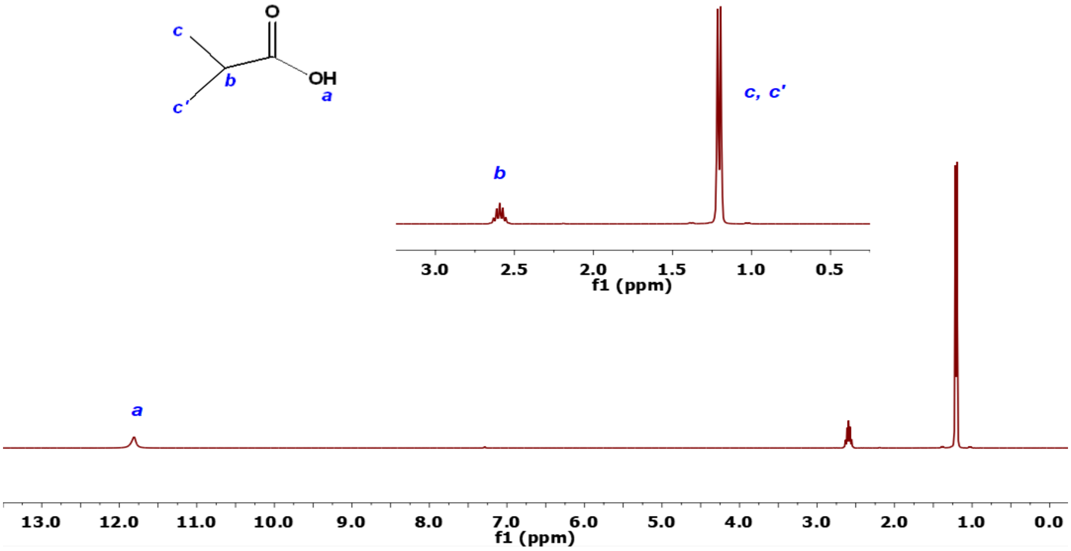

^{1}H NMR (360 MHz, CDCl$_3$) δ 2.59 (hept, *J* = 7.1 Hz, 1H), 1.21 (dd, *J* = 7.0, 1.5 Hz, 6H).

Figure SIV.22. a) Representative ^{1}H NMR spectrum (D_2O) corresponding to the photooxidation of diethylene glycol, using MSNPs-NH2@**H[1]** as catalyst. Conditions: **[1]**$^{-}$ (0.02 mM), substrate (20 mM), $Na_2S_2O_8$ (40 mM), 5 mL potassium carbonate solution at pH=7. Light irradiation 8h. b) ^{1}H NMR spectrum of pure commercial diethylene glycol**.** c) ^{1}H NMR spectrum of pure commercial diglycolic acid.

a)

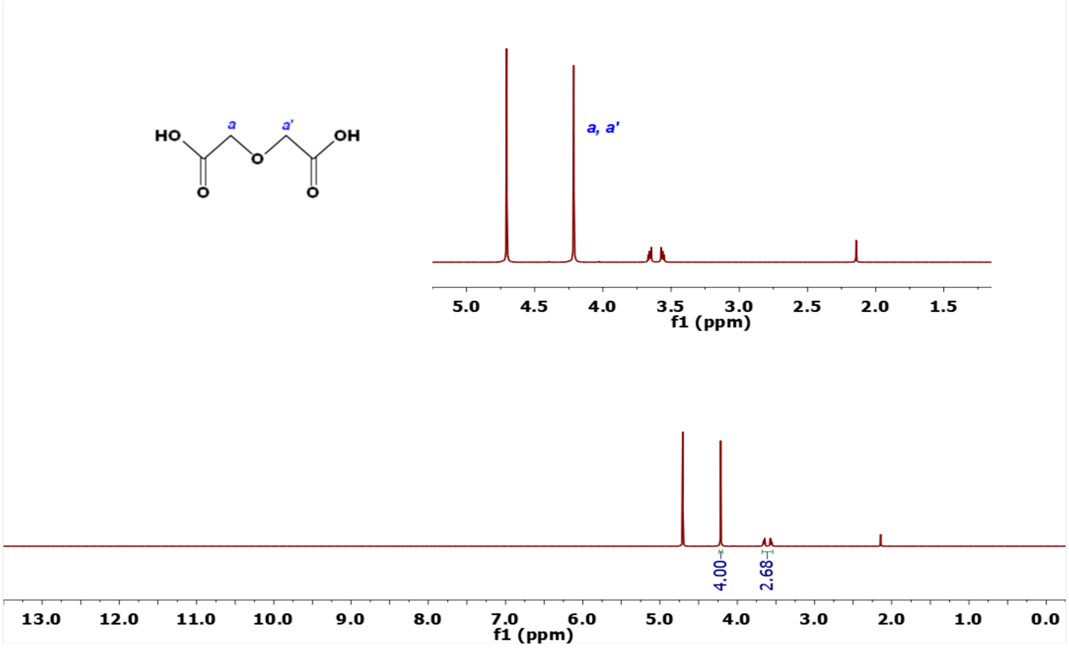

^{1}H NMR (360 MHz, D_2O) δ 4.20 (s, 4H).

b)

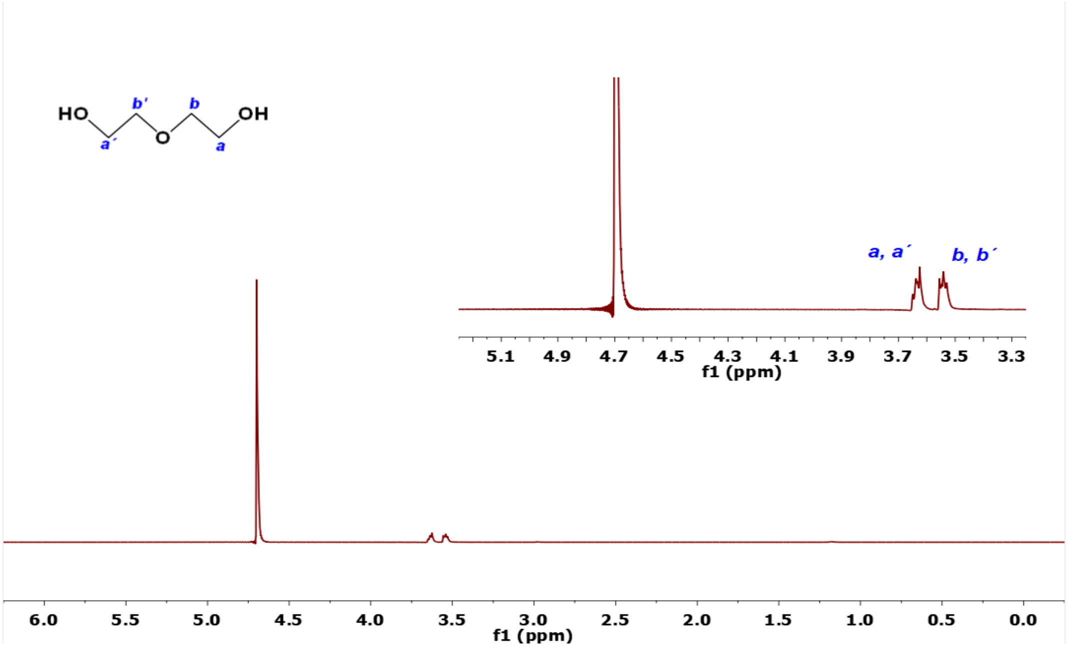

^{1}H NMR (360 MHz, D_2O) δ 3.67 – 3.59 (m, 4H), 3.57 – 3.50 (m, 4H).

c)

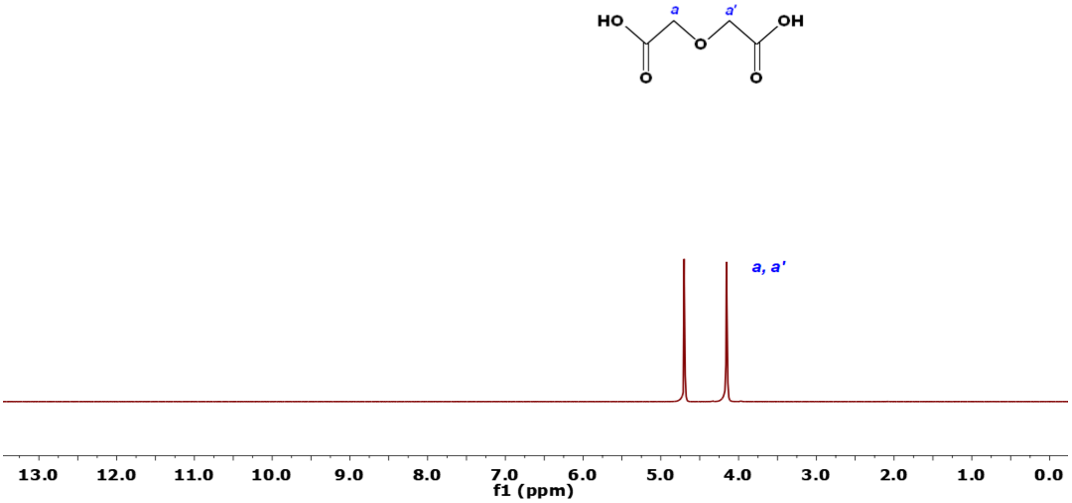

^{1}H NMR (360 MHz, D_2O) δ 4.16 (s, 4H).

Figure SIV.23. a) Representative ^{1}H NMR spectrum (acetone-d_6) corresponding to the photooxidation of 1,6-hexanediol, using MSNPs-NH2@**H[1]** as catalyst. Conditions: **[1]** (0.02 mM), substrate (20 mM), $Na_2S_2O_8$ (40 mM), 5 mL potassium carbonate solution at pH=7. Light irradiation 8h. b) ^{1}H NMR spectrum of pure commercial 1,6-hexanediol**.** c) ^{1}H NMR spectrum of pure commercial adipic acid.

a)

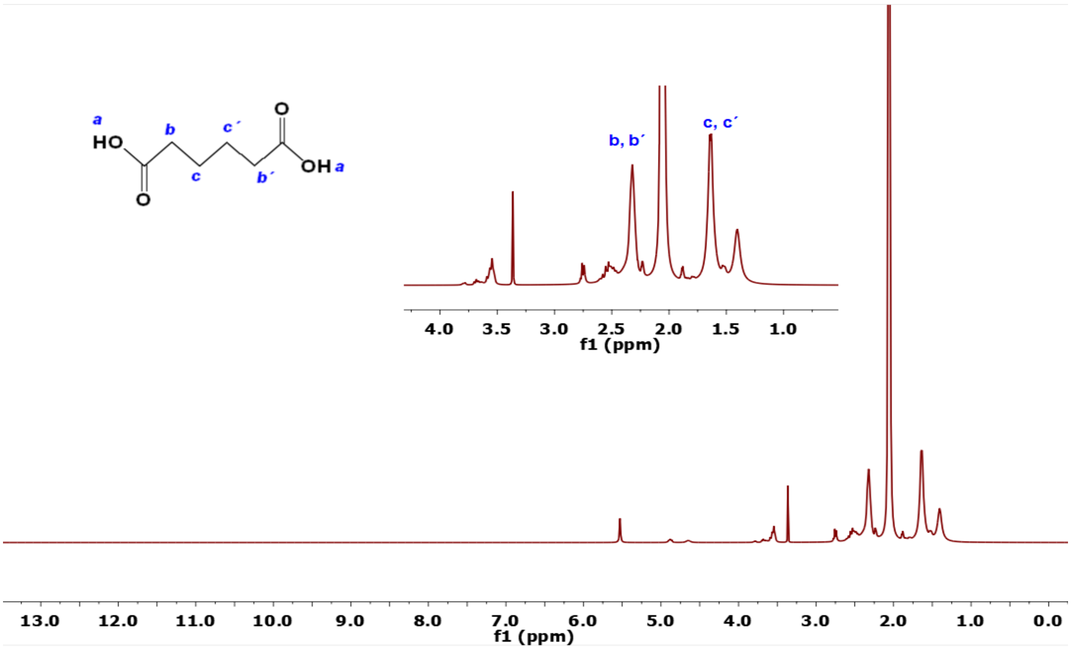

^{1}H NMR (360 MHz, acetone-d_6) δ 2.32 (m, 4H), 1.64 (d, *J* = 5.7 Hz, 4H).

b)

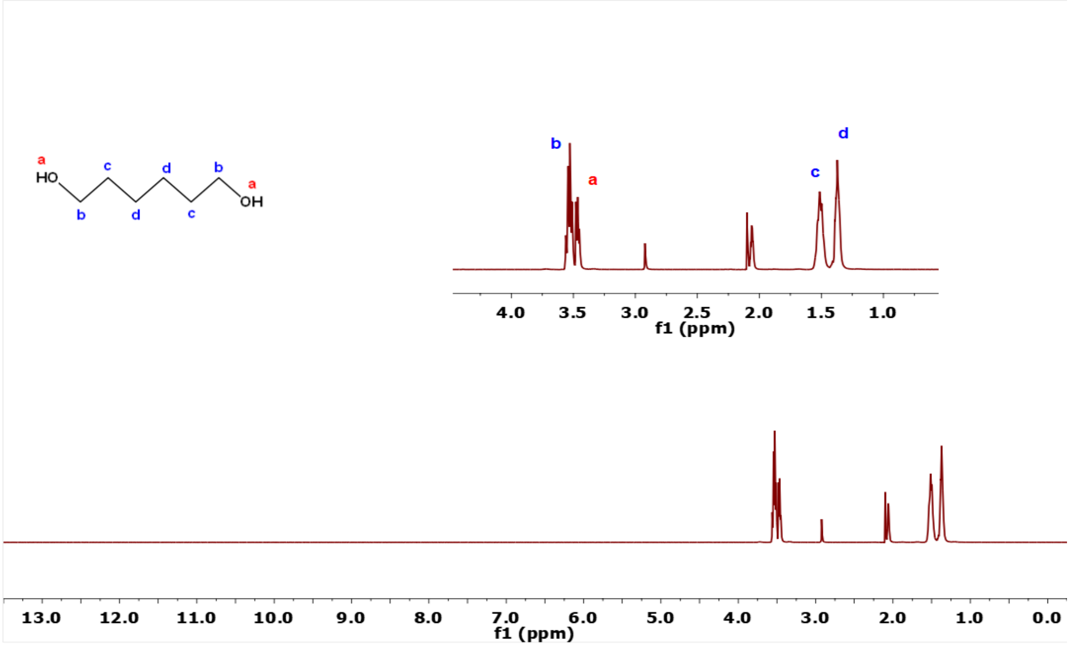

^{1}H NMR (360 MHz, acetone-d_6) δ 3.53 (dd, *J* = 6.6, 5.1 Hz, 4H), 3.47 (dd, *J* = 5.9, 4.6 Hz, 1H), 1.60 – 1.45 (m, 4H), 1.37 (dq, *J* = 7.4, 3.3 Hz, 4H).

c)

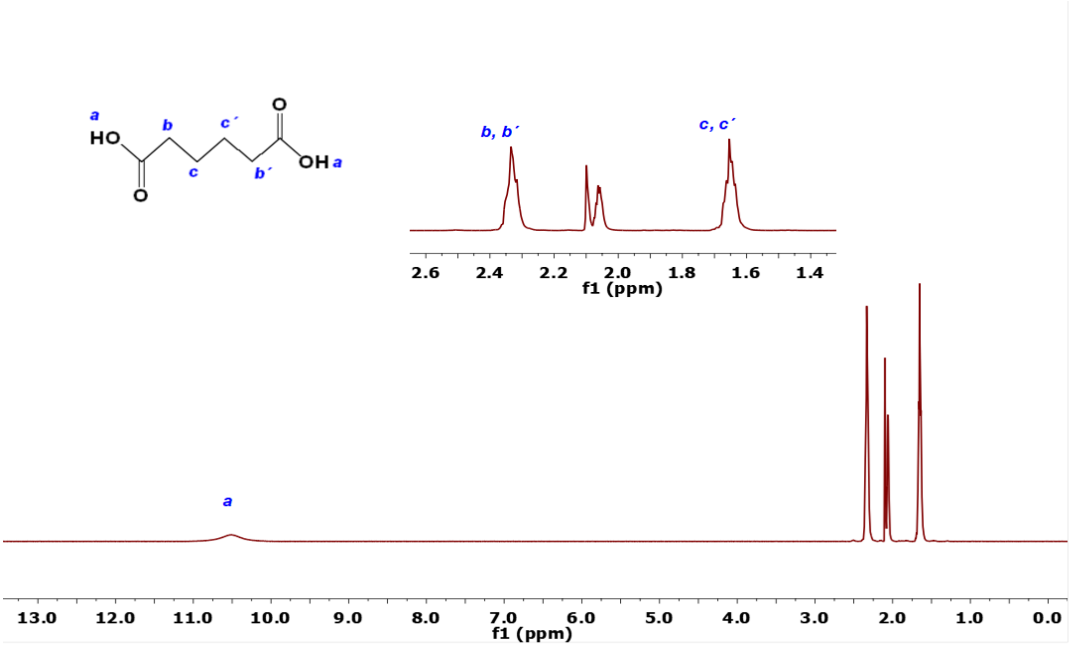

^{1}H NMR (360 MHz, Acetone-d6) δ 10.50 (br, 1H), 2.34 (dq, *J* = 7.1, 4.5, 3.1 Hz, 4H), 1.65 (h, *J* = 3.0 Hz, 4H).

ANNEX III. Supporting Information

Chapter IV.3

Table SIV 3.4. Crystal Data for X-ray structure of complex **C5**.

	[C5]
Empirical formula	$C_{35}H_{66}N_6B_{36}Co_2Ru$
Formula weight	1179.02
Crystal system	Triclinic
Space group	P-1
a [Å]	14.2721(17)
b [Å]	14.9427(17)
c [Å]	15.5782(19)
α [º]	114.464(2)
β [º]	106.404(2)
γ [º]	99.788(2)
V [Å^3]	2739.8(6)
Formula Units/Cell	2
$\rho_{calc.}$ [g cm^{-3}]	1.429
μ [mm^{-1}]	0.910
$R1$[a], [I > 2σ(I)]	0.0716
wR_2[b] [all data]	0.1639

[a] $R_1 = \Sigma||F_o| - |F_c||/\Sigma|F_o|$

[b] $wR_2 = [\Sigma\{w(F_o^2-F_c^2)^2\}/\Sigma\{w(F_o^2)^2\}]^{½}$,where $w = 1/[\sigma^2(Fo^2) + (0.0042P)^2]$ and $P=(F_o^2+2F_c^2)/3$

Table SIV 3.5. Selected bond lengths (Å) and angles (°) for **C5** complex.

Ru(1)-N(1)	2.034(6)	Co(3C)-C(2C)	2.049(7)	N(1)-Ru(1)-N(2)	78.9(2)
Ru(1)-N(2)	2.069(6)	Co(3C)-B(4C)	2.066(7)	N(1)-Ru(1)-N(3)	92.6(2)
Ru(1)-N(3)	2.067(5)	Co(3C)-C(1C)	2.022(7)	N(1)-Ru(1)-N(4)	92.3(2)
Ru(1)-N(4)	1.961(5)	Co(3C)-C(2C)_a	2.049(7)	N(1)-Ru(1)-N(5)	90.1 (2)
Ru(1)-N(5)	2.079(5)	Co(3C)-C(1C)_a	2.022(7)	N(1)-Ru(1)-N(6)	174.5(2)
Ru(1)-N(6)	2.035(6)	Co(3D)-B(4D)_b	2.070(8)	N(2)-Ru(1)-N(3)	97.4(2)
Co(3A)-C(2A)	2.046(7)	Co(3D)-B(7D)_b	2.077(8)	N(2)-Ru(1)-N(4)	170.7 (2)
Co(3A)-C(1A)	2.065(7)	Co(3D)-B(7D)	2.077(8)	N(2)-Ru(1)-N(5)	103.6(2)
Co(3A)-B(7A)	2.062(8)	Co(3D)-C(2D)_b	2.041(7)	N(2)-Ru(1)-N(6)	96.1(2)
Co(3A)-B(4B)	2.093(9)	Co(3D)-C(2D)	2.041(7)	N(3)-Ru(1)-N(4)	79.9(2)
Co(3A)-B(7B)	2.080(7)	Co(3D)-B(4D)	2.070(8)	N(3)-Ru(1)-N(5)	158.9(2)
Co(3A)-B(8A)	2.097(9)	Co(3D)-C(1D)	2.041(8)	N(3)-Ru(1)-N(6)	90.3(2)
Co(3A)-C(1B)	2.045(8)	Co(3D)-C(1D)_b	2.041(8)	N(4)-Ru(1)-N(5)	79.1(2)
Co(3A)-C(2B)	2.040(7)	Co(3D)-B(8D)_b	2.103(8)	N(4)-Ru(1)-N(6)	92.8(2)
Co(3A)-B(4A)	2.098(9)	Co(3D)-B(8D)	2.103(8)	N(5)-Ru(1)-N(6)	88.9(2)
Co(3C)-B(4C)_a	2.066(7)				

Figure SIV.24. Dihydrogen bonds C-H···H-B interactions between cationic and anionic moieties in **C5**.

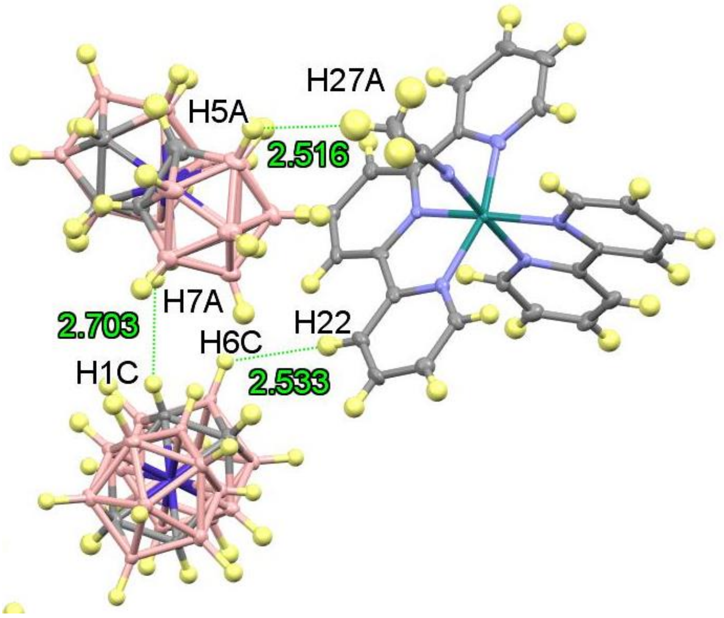
H27A
H5A
2.516
H7A
2.703
H6C
H22
H1C
2.533

Figure SIV.25. a) $^{1}H\{^{11}B\}$-NMR and b) $^{11}B\{^{1}H\}$-NMR spectra of Ag[1] **C3** compound in acetone-d_6.

a)

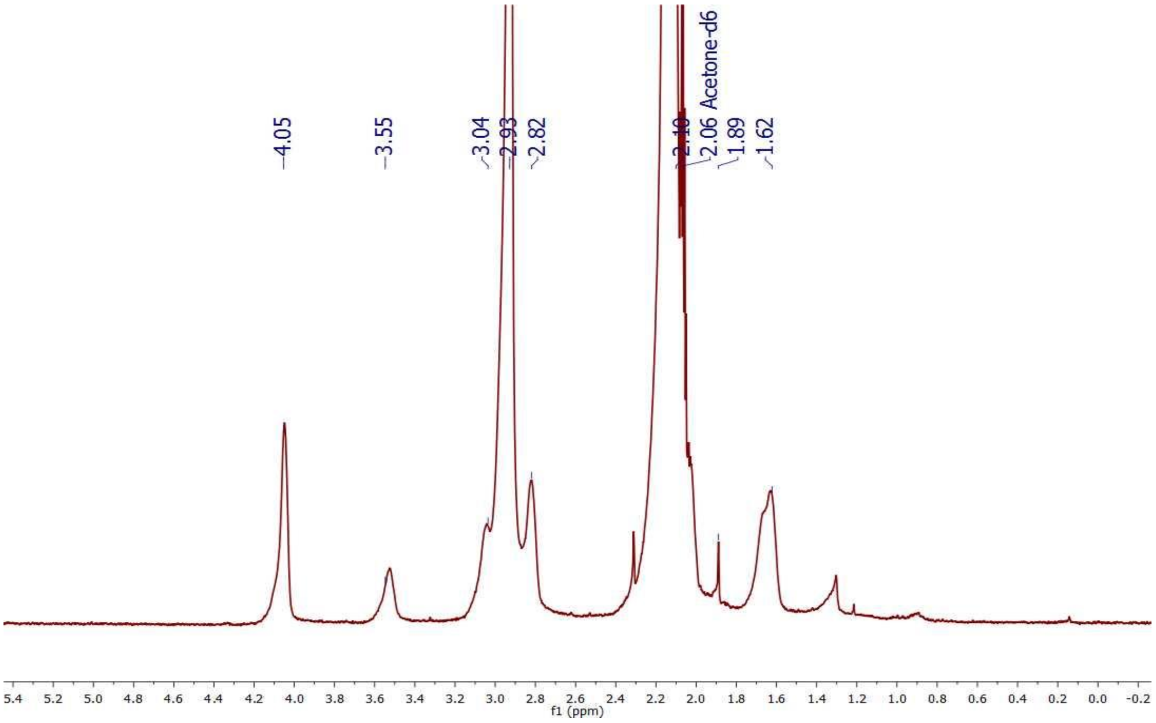

b)

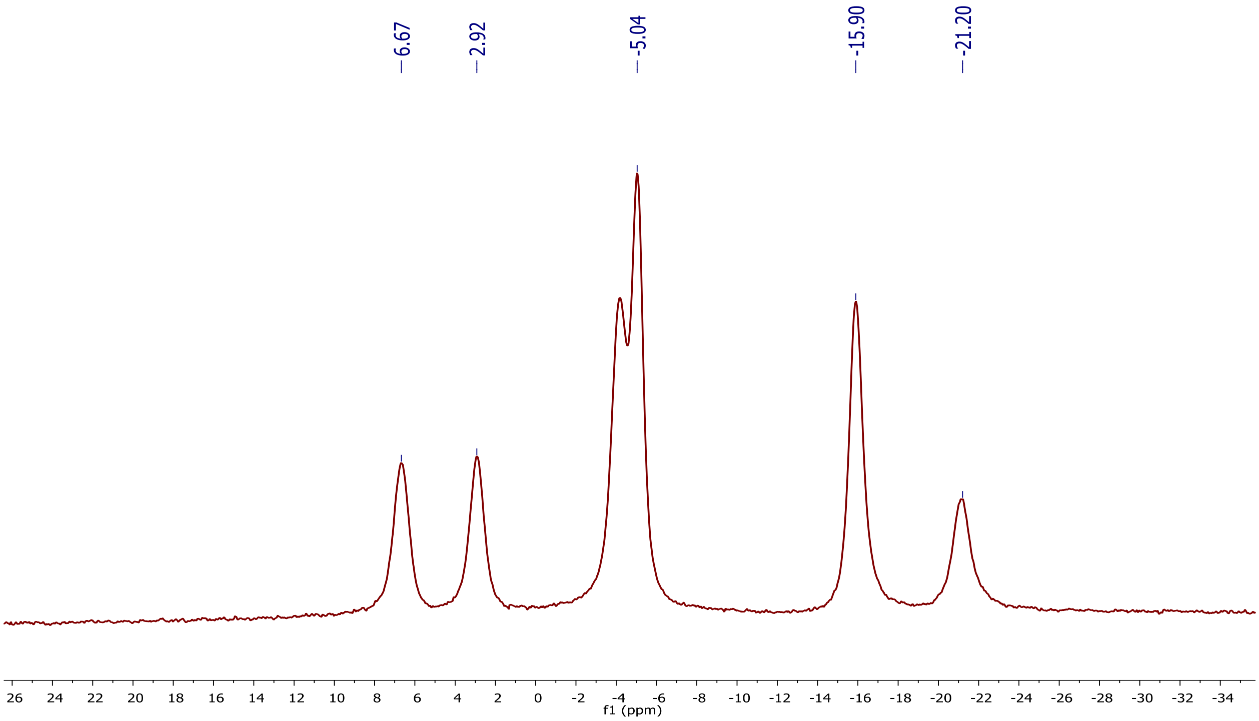

Figure SIV.26. COSY NMR spectra of cobaltabis(dicarbollide) **C4** compound in acetone-d_6.

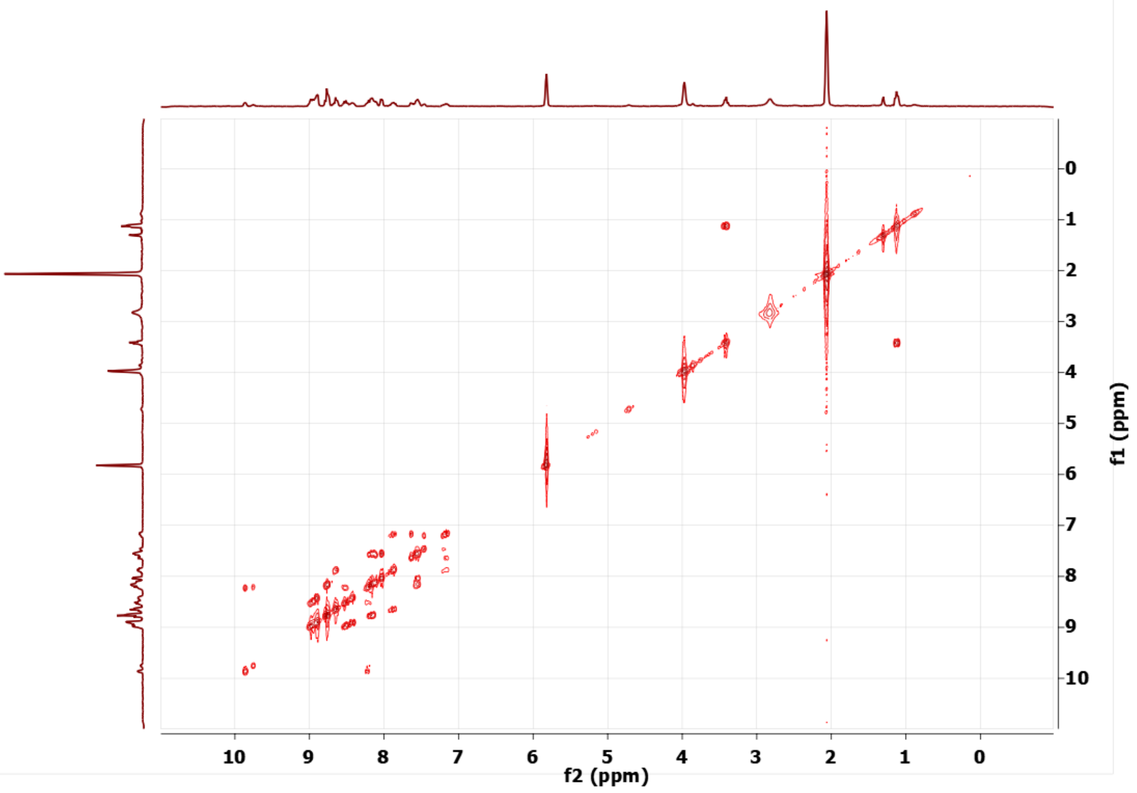

Figure SIV.27. UV-visible of **Ag[1]**, **C3**.

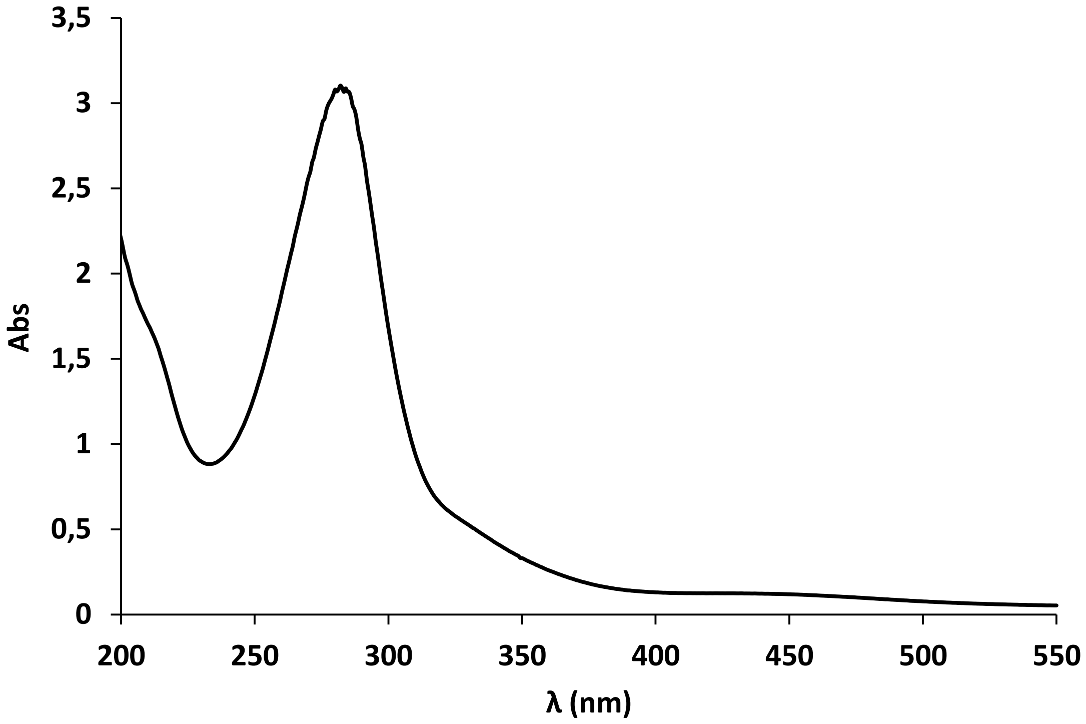

Figure SIV.28. CV of **Ag[1] C3** in CH_3CN + 0.1 M TBAH *vs* Ag.

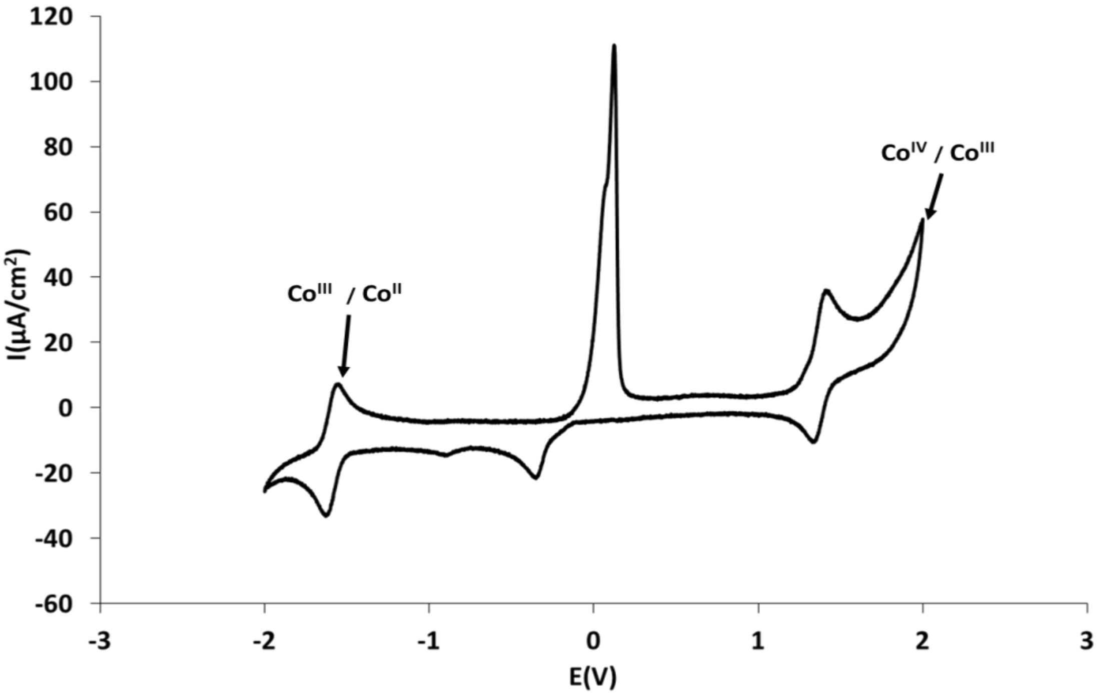

Figure SIV.29. CV for complex **Na[1]** registered in a phosphate buffer (pH= 7.12) *vs* Ag/AgCl.

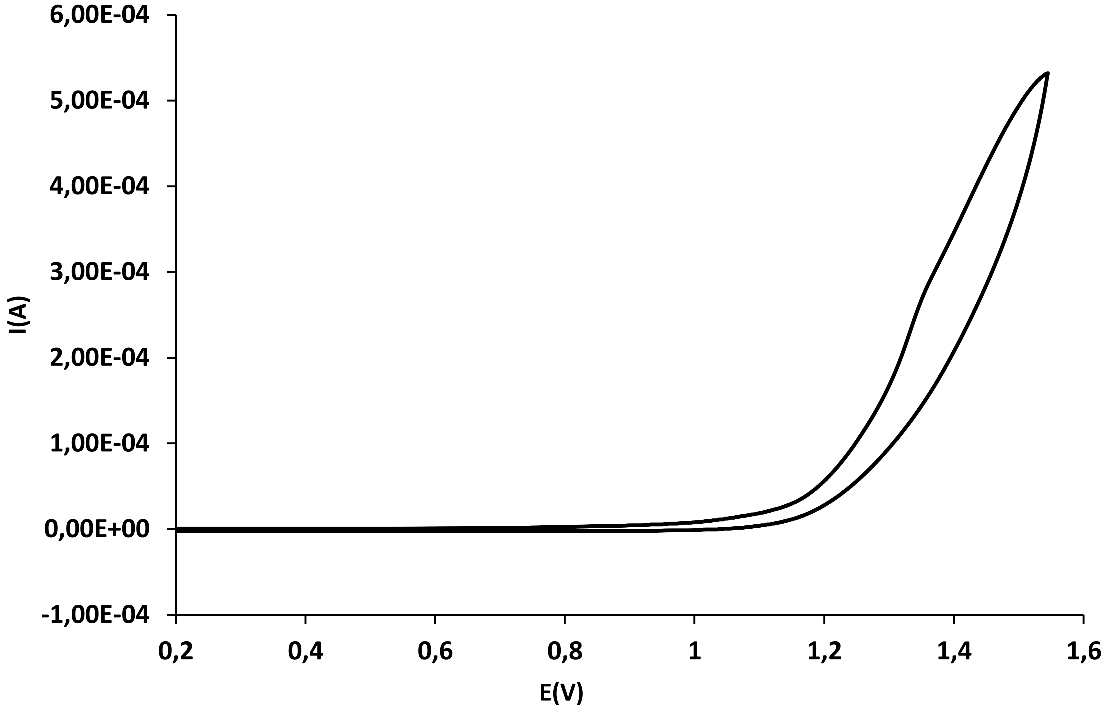

Figure SIV.30. CV of complex **Na[1]** (1 mM) registered in a phosphate buffer (pH= 7.12) *vs* Ag/AgCl, before and after the addition of 1 mM of a) $CaCl_2$ and b) $ZnCl_2$. The blue and purple inserts show dI/dE to better appreciate the position of the couple Co^{IV}/Co^{III}.

a)

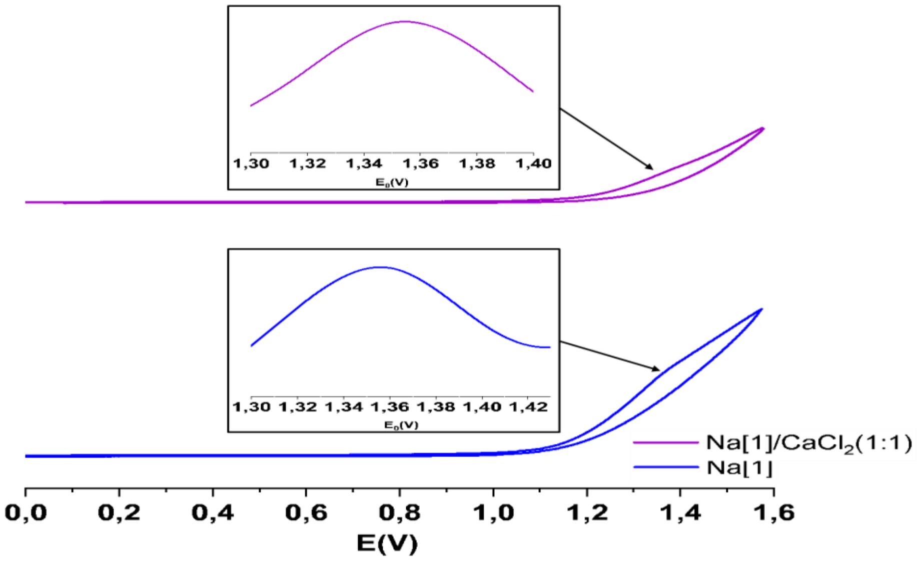

b)

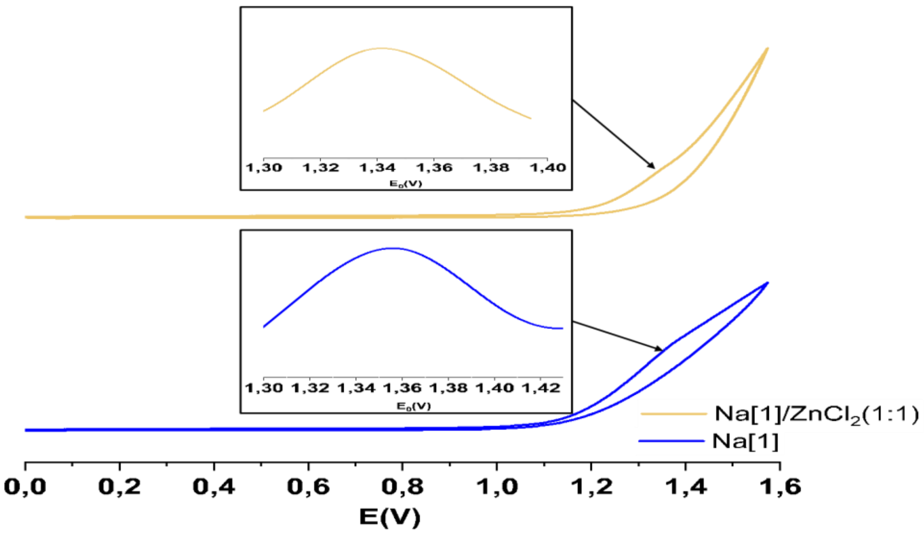

Figure SIV.31. MALDI of **C4** after the photooxidation of 1-phenylethanol. [3,3'-Co(1,2-$C_2B_9H_{11})_2]^-$=324.1 (m/z) and [3,3'Co(1,2-$C_2B_9H_{11}$)(1,2-$C_2B_9H_{11}$O)$]^-$ =340.1 (m/z).

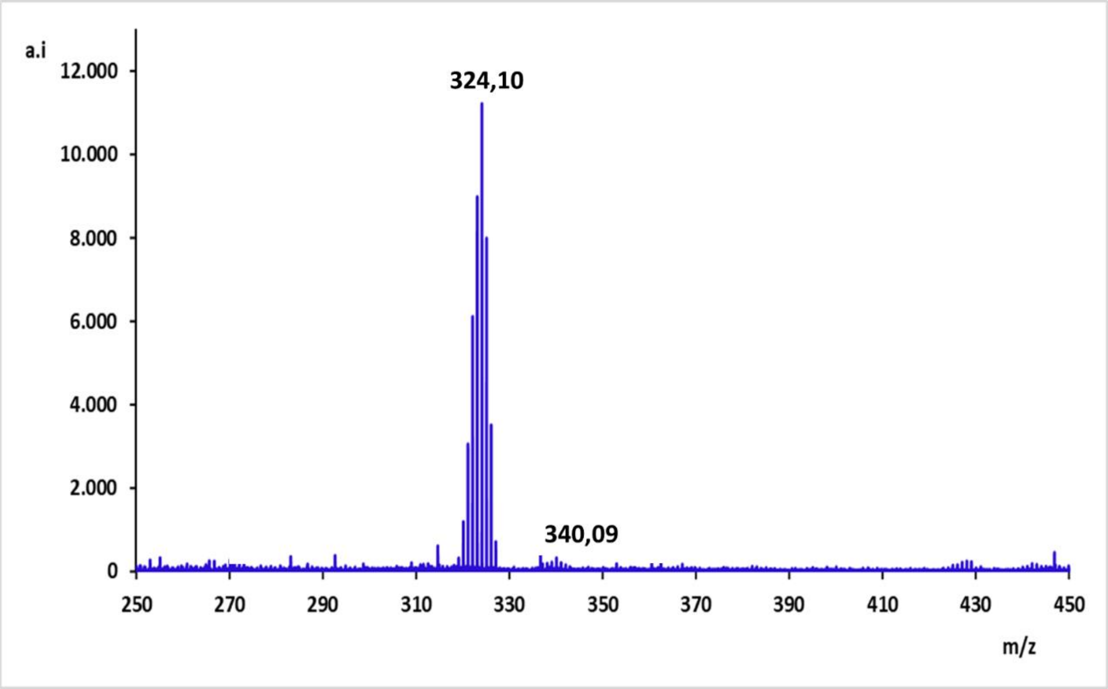

Figure SIV.32. UV-Visible spectra of mixtures of **C2':Na[1]** (1:1) (black line), (1:2) (dotted line) and **C4** (dash dotted line) at a) 3 x 10^{-6} and b) 0.33 x 10^{-6} M.

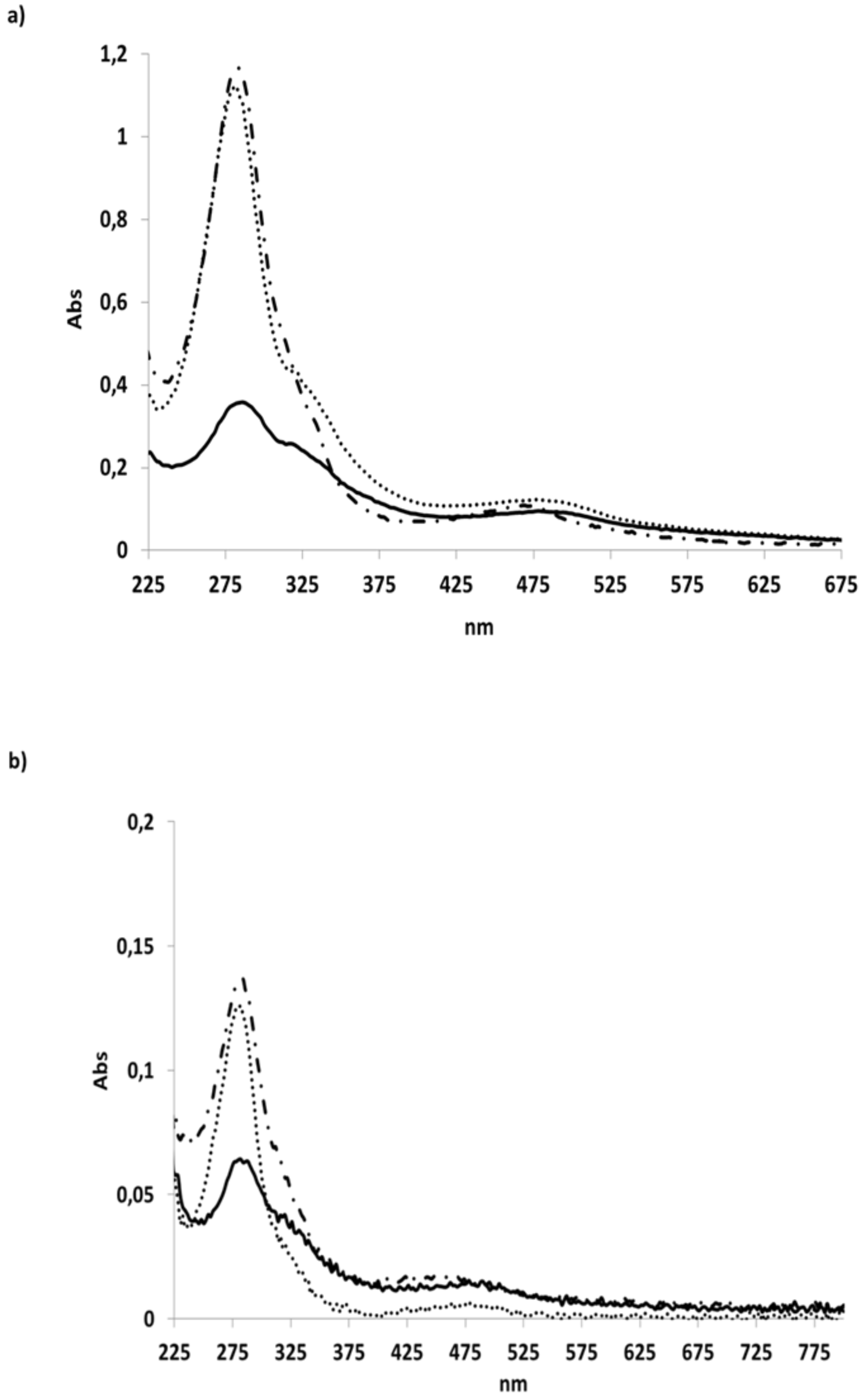

Figure SIV.33. DLS of catalytic mixture using a) **C4** as catalyst and b) **C2'** and **Na[1]** (1:2) as catalyst.

a)

Sample **Oxidant ($Na_2S_2O_8$)**

Without oxidant

D_H = 151nm; PDI = 0.34

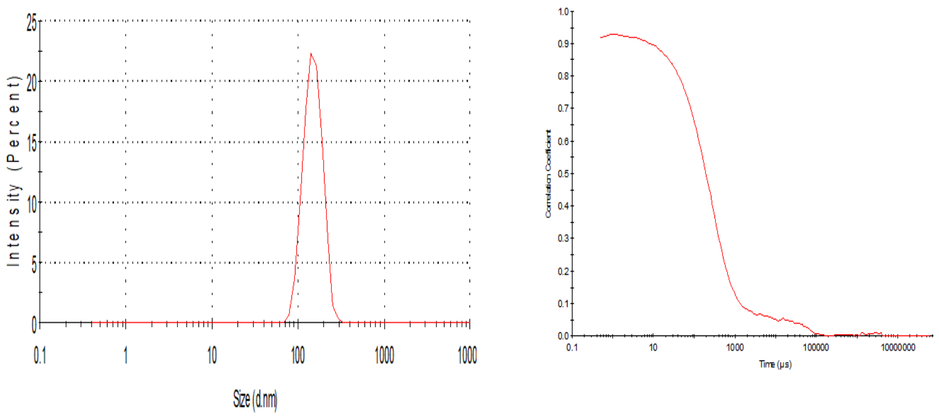

S1C4

With oxidant

D_H = 140.9nm; PDI = 0.48

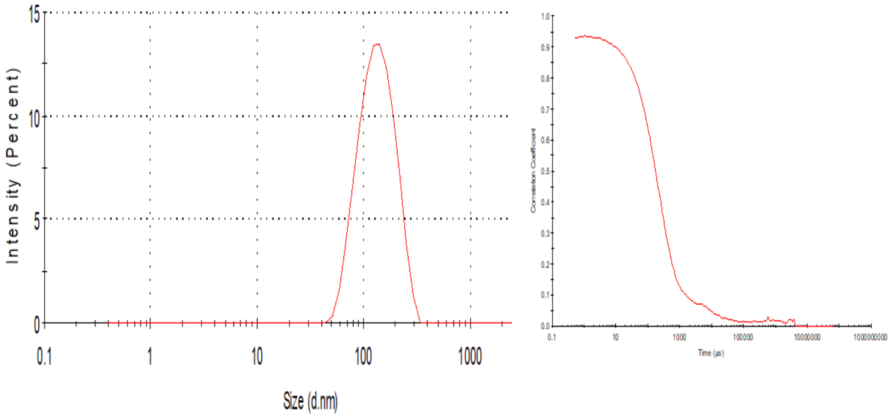

b)

Sample

Oxidant ($Na_2S_2O_8$)

Without oxidant

D_H = 116.1nm; PDI = 0.33

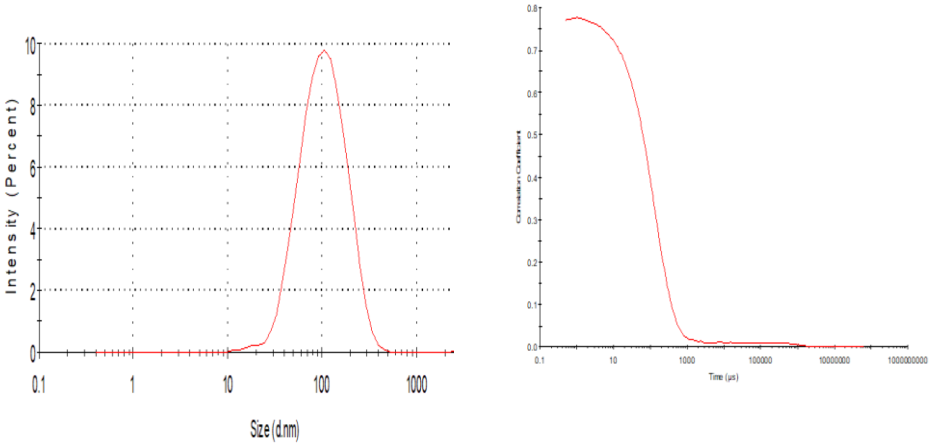

S2RuCo
1:2

With oxidant

D_H = 128.4nm; PDI = 0.34

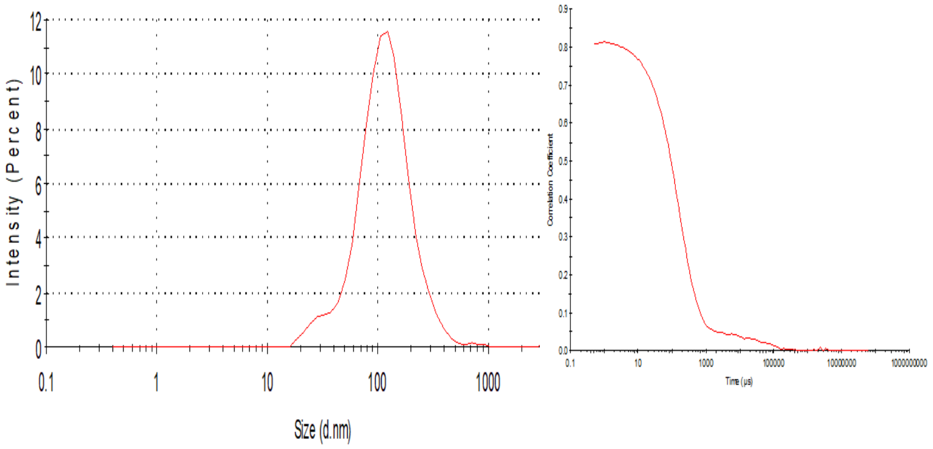

Figure SIV.34. ESI-MS spectra of **C4**.

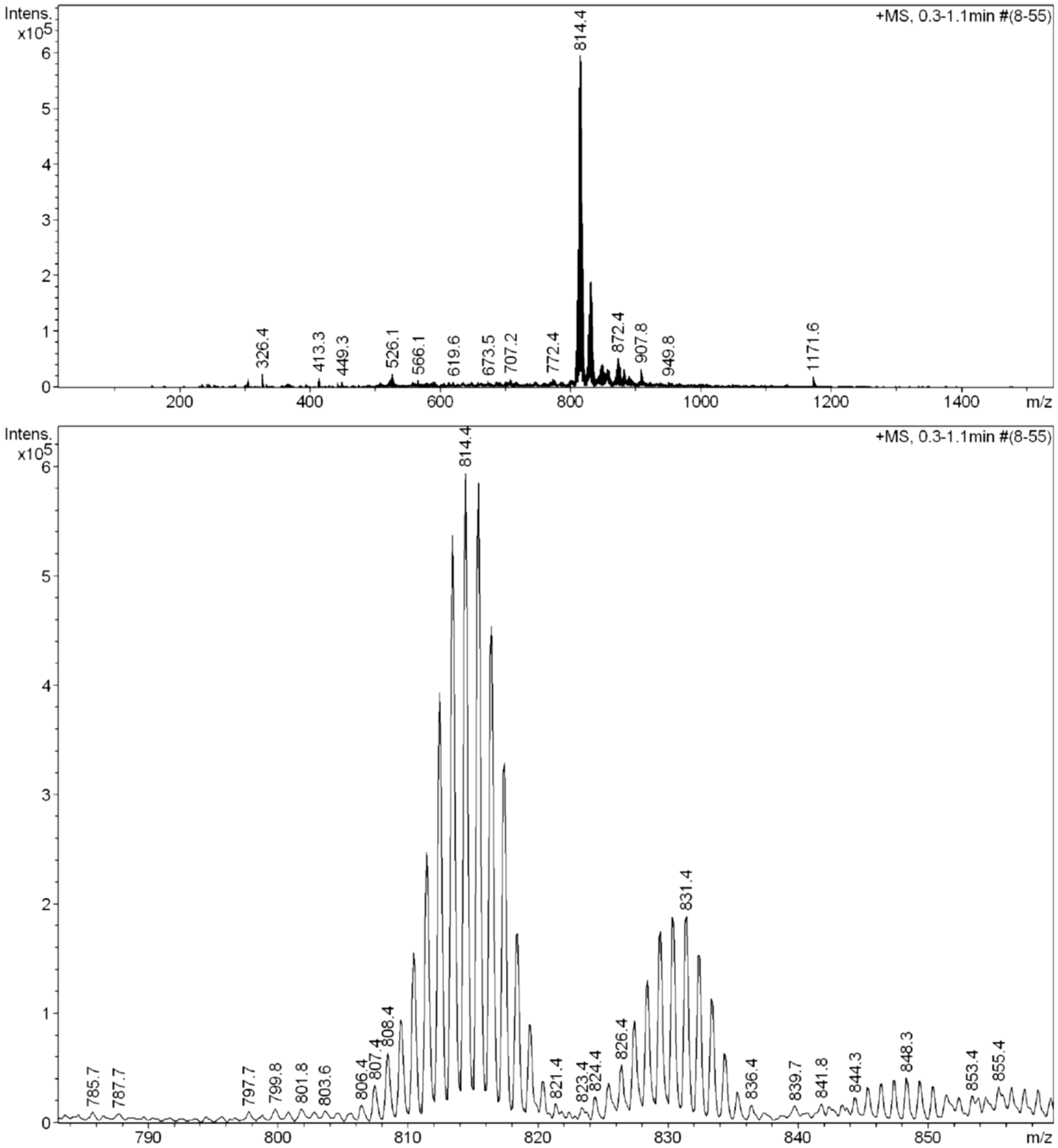

ANNEX IV. Supporting Information

Chapter IV.4

Table SIV 4.6. Photooxidation tests performed with **Na[1]** complex. Conditions: **Na[1]** (0.02 mM), substrate (20 mM), $Na_2S_2O_8$ (26 mM), 5 mL potassium carbonate solution at pH=7.

Entry	Substrate	Conv %	Product	Yield.(select.)%
1	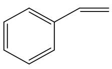	78[a][1] 80[b][1] 96[c][1]	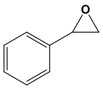	37(47)[a] 27(34)[b] 25(26)[c]
			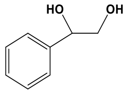	23(29)[a] 35(44)[b] 50(52)[c]
2	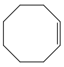	91[b] ≥99[c]	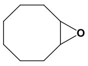	47(47)[b] 38(42)[c]
			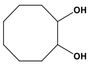	53(58)[b] 53(53)[c]
3	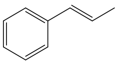	85[b] 91[c]	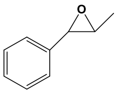	44(52)[b] 20(22)[c]
			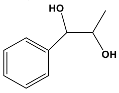	41(48)[b] 71(78)[c]
4	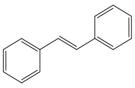	66 [b] 95 [c]	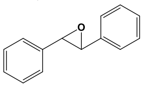	39(44)[b] 29(41)[c]
			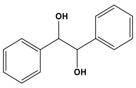	37(56)[b] 56(59)[c]
5	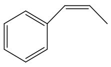	92[b] ≥99[c]	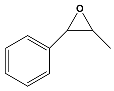	75[73/2, cis/trans](82[2])[b] 33[16/17, cis/trans](33[2])[c]
			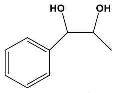	17(19)[b] 67(67)[c]
6	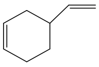	97[b] ≥99[c]	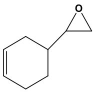	70(72)[b] 37(37)[c]
			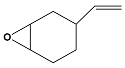	8(8)[b] 6(6)[c]
			Other products	19[3](19)[b] 57[3](57)[c]
7	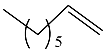	81[b] ≥99[c]	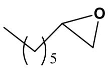	58(72)[b] 16(16)[c]
			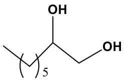	9(11)[b] 44(44)[c]
			Other products	14[4] (17)[b] 39[4] (39)[c]

Ratio 1:1000:1300: [a] 5 min of reaction [b] 15 min of reaction. [c] 30 min of reaction. [d] 60 min of reaction.[1] benzaldehyde and benzoic acid produced as another byproducts. [2]selectivity with respect the overall epoxide produced.[3]yield with diol and benzoic acid from vinyl produced. [4]octanal and octanoic produced.

Figure SIV.35. HPLC/ESI-MS spectra from Oxidation of methyl oleate by **Na[1]**.

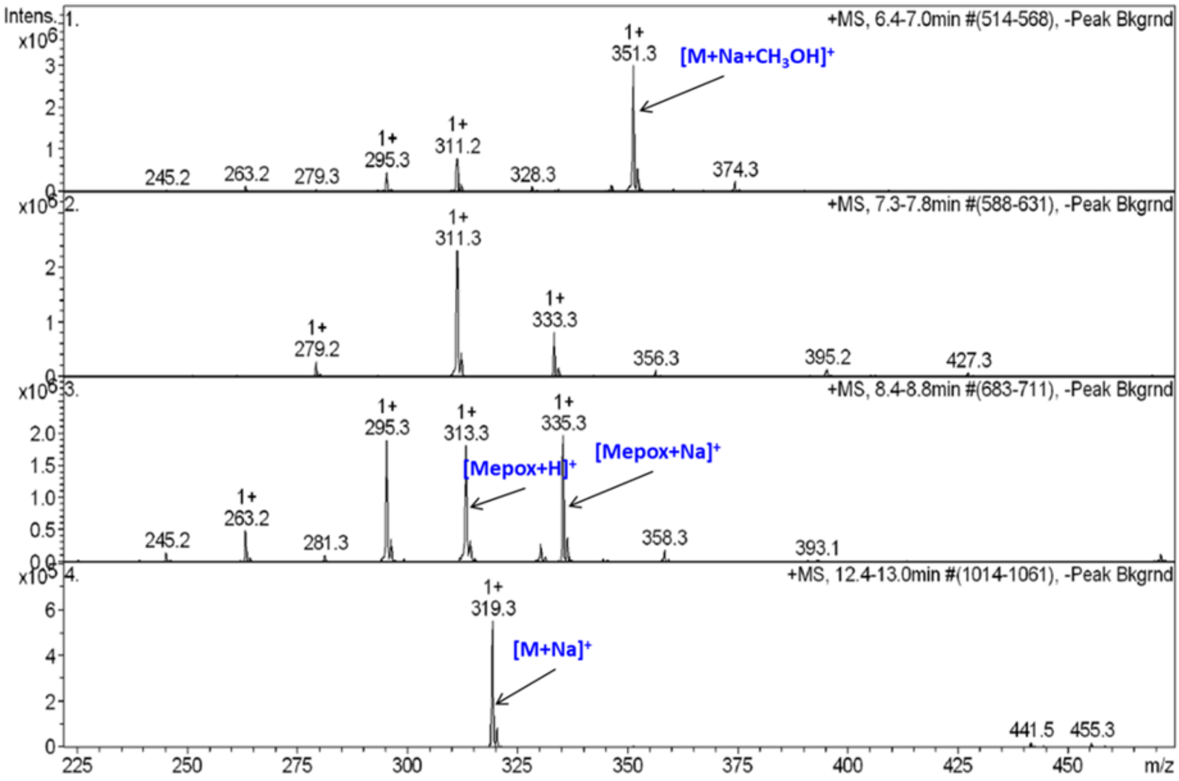

ANNEX V. Supporting Information

Chapter IV.5

Table SIV 5.1. Photooxidation tests performed with **Na[2]** complex. Conditions: **Na[2]** (0.02 mM), substrate (20 mM), $Na_2S_2O_8$ (26 mM), 5 mL potassium carbonate solution at pH=7.

Entry	Substrate	Conv %	Product	Yield.(sel.)%
1	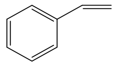	66[a]1 75[b]1 86[c]1	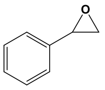	43(65)[a] 36(48)[b] 14(16)[c]
			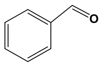	5(8)[a] 12(16)[b] 21(24)[c]
			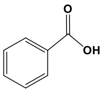	9(14)[a] 26(35)[b] 50(58)[c]
2	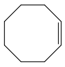	95[b] ≥99[c]	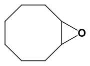	56(59)[b] 9(9)[c]
			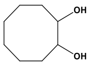	39(41)[b] 91(91)[c]
3	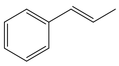	≥99[b] ≥99[c]	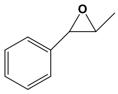	57(57)[b] 44(44)[c]
			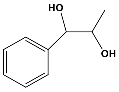	43(43)[b] 56(56)[c]
4	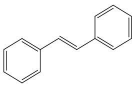	≥99 [b] ≥99 [c]	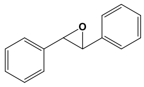	95(95)[b] 90(90)[c]
			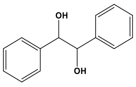	5(5)[b] 10(10)[c]
5	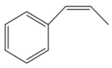	≥99[b]2 ≥99[c]2	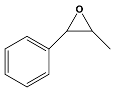	96[92/4, cis/trans](96[3])[b] 94[69/25, cis/trans](95[3])[c]
6	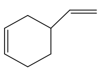	≥99[b]4 ≥99[c]4	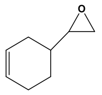	44(44)[b] 31(31)[c]
			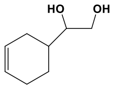	12(13)[b] 14(15)[c]
			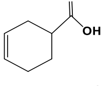	42(43)[b] 53(54)[c]
7	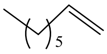	86[b]5 95[c]5	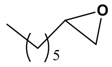	83(97)[b] 2(2)[c]
			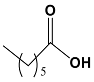	-(-)[b] 64 (67)[c]
			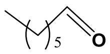	1(1)[b] 27 (28)[c]

Ratio 1:1000:1300: [a] 5 min of reaction [b] 15 min of reaction. [c] 30 min of reaction. [d] 60 min of reaction.[1] 1-phenylethane-1,2-diol as another byproduct. [2] 1-phenylpropane-1,2-diol as another byproduct. [3] selectivity with respect the overall epoxide produced. [4] 4-Vinyl-1-cyclohexene 1,2-epoxide as another byproduct. [5] octane-1,2-diol as another by product.